

# Letter from the Editors

**D**ear readers of *Acta Naturae*! We are delighted to bring you the 24<sup>th</sup> issue of the journal – the first one in 2015! Two dozen issues are on hand, and we are still alive and full of energy; our docket of papers is full, and our IF is growing! This is not being conceited, but, rather, the expression of our surprise and joy! In view of all these encouraging circumstances, the Editorial Council and Editorial Board will like to express their profound gratitude to all our enthusiastic colleagues who publish the journal, and, above all, our authors, who believed in us one day and, we hope, continue to believe in us now! Of course, we are facing a host of difficulties, but we are hopeful that we will overcome them with your help.

That said let us return to the current issue. The journal opens with four reviews that are more or less related to medicine. The first (P.V. Sergiev *et al.*) is devoted to a topic which, sooner or later, becomes everyone's preoccupation – the theories of aging. The second review (K.R. Valetdinova *et al.*) describes the cell and animal models of motor neuron diseases and also discusses is-

sues related to the use of cell technologies in biomedical applications. The third review (P.V. Panteleev *et al.*) dwells on antimicrobial peptides – molecular factors of the innate immune system that provide a versatile and evolutionarily ancient way of protecting higher organisms against infection and form the basis for the development of new drugs. Finally, the fourth review (D.V. Popov *et al.*) is dedicated to, at first glance, a more “academic” topic – the regulation of the expression of PGC-1 $\alpha$  isoforms in skeletal muscles – also has direct relevance to medicine; more specifically to physiology, since this expression directly depends on various physiological stimuli and pharmacological effects.

The scientific papers in this issue are devoted to a very wide range of subjects – from classical biochemistry to cell engineering. Yet, they share a common thread – all of them are dedicated to studies of topical issues of life science and are of high quality. We are delighted to see that most of the submitted papers meet these standards.

Until next time! ●

*Editorial Board*

# INNOVATION RUSSIA

Discussion club

We create a dialogue between all socially active groups of people: students, scientists, lecturers, businessmen, managers, innovators, investors, designers, art critics, architects, photographers.

Learn more  
at [WWW.STRF.RU](http://WWW.STRF.RU)

Everyone with something to say and  
ideas to share is welcome to visit  
our events

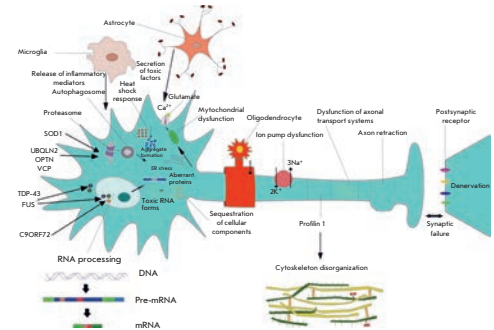


Tel.: +7 (495) 930-87-07, 930-88-50  
E-mail: seminar@strf.ru

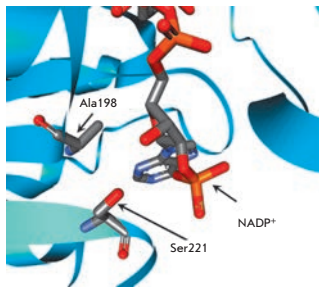
## Model Systems of Motor Neuron Diseases as a Platform for Studying Pathogenic Mechanisms and Searching for Therapeutic Agents

K.R. Valetdinova, S.P. Medvedev, S.M. Zakian

The review is devoted to recent advances in the development and investigation of cell and animal models of amyotrophic lateral sclerosis (ALS) and spinal muscular atrophy. The main problems concerning the use of cell technologies in biomedical applications are also considered.



A general scheme of ALS etiopathogenesis



Fragments of the structure of formate dehydrogenase from bacterium *Pseudomonas* sp. 101

## The Role of Ala198 in Stability and Coenzyme Specificity of Bacterial Formate Dehydrogenases

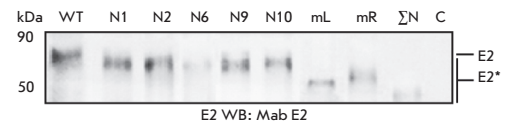
A.A. Alekseeva, V.V. Fedorchuk, S.A. Zarubina, E.G. Sadyhov, A.D. Matorin, S.S. Savin, V.I. Tishkov

The Ala198 residue in the NAD<sup>+</sup>-binding domain of formate dehydrogenases from *Pseudomonas* sp.101 and *Moraxella* sp. C-1 bacteria (PseFDH and MorFDH, respectively) has non-optimal values of the  $\psi$  and  $\phi$  angles. After introduction of the A198G substitution, the stability increased 2.5-fold, and the  $K_M$  values for NAD<sup>+</sup> increased 1.6-fold. An analysis of the kinetic properties of mutant NADP<sup>+</sup>-specific PseFDH D221S and PseFDH A198G/D221S suggests with a high probability that PseFDH was previously a NADP<sup>+</sup>-dependent rather than NAD<sup>+</sup>-dependent enzyme.

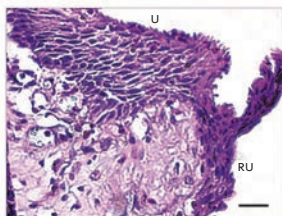
## The Role of HCV E2 Protein Glycosylation in Functioning of Virus Envelope Proteins in Insect and Mammalian Cells

O.V. Orlova, V.L. Druza, P.V. Spirin, A.V. Ivanov, V.S. Prasolov, P.M. Rubtsov, S.N. Kochetkov, S.N. Beljelarskaya

The effect of glycosylation of the hepatitis C virus E2 envelope protein on the formation of glycoprotein complexes and viral particles in insect and mammalian cells was studied. For this purpose, point mutations were introduced into N-glycosylation sites of E2, and mutant proteins were analyzed in insect Sf9 and human Hek293T cells. The E2 synthesis level in Hek293T, unlike Sf9, was dependent on glycosylation of the N1 and N8 sites. Removal of glycan in the N1, N2 and N10 sites resulted in accumulation of E1E2 dimers in the form of aggregates and suppression of productive assembly of virus-like particles.



Analysis of gene expression of mutant E2 proteins of HCV in Sf9 cells



A section of the reconstructed portion of rabbit urethra

## Reconstruction of Rabbit Urethral Epithelium with Skin Keratinocytes

O.S. Rogovaya, A.K. Fayzulin, A.V. Vasiliev, A.V. Kononov, V.V. Tersikh

The living skin equivalent was studied as an alternative source of plastic material for closing full-thickness epithelial-stromal urethral injuries. The possibility of transdifferentiation of epidermal keratinocytes, a component of 3D tissue constructs, was investigated *in vivo* in a model of the recovery of urethral injuries in laboratory rabbits. Skin keratinocytes placed in a specific *in vivo* microenvironment can be incorporated into the damaged area and function as urothelium.

## Founders

Ministry of Education and  
Science of the Russian Federation,  
Lomonosov Moscow State University,  
Park Media Ltd

## Editorial Council

*Chairman:* A.I. Grigoriev  
*Editors-in-Chief:* A.G. Gabibov, S.N. Kochetkov

V.V. Vlassov, P.G. Georgiev, M.P. Kirpichnikov,  
A.A. Makarov, A.I. Miroshnikov, V.A. Tkachuk,  
M.V. Ugryumov

## Editorial Board

*Managing Editor:* V.D. Knorre  
*Publisher:* K.V. Kiselev

K.V. Anokhin (Moscow, Russia)  
I. Bezprozvanny (Dallas, Texas, USA)  
I.P. Bilenkina (Moscow, Russia)  
M. Blackburn (Sheffield, England)  
S.M. Deyev (Moscow, Russia)  
V.M. Govorun (Moscow, Russia)  
O.A. Dontsova (Moscow, Russia)  
K. Drauz (Hanau-Wolfgang, Germany)  
A. Friboulet (Paris, France)  
M. Issagouliants (Stockholm, Sweden)  
A.L. Konov (Moscow, Russia)  
M. Lukic (Abu Dhabi, United Arab Emirates)  
P. Masson (La Tronche, France)  
K. Nierhaus (Berlin, Germany)  
V.O. Popov (Moscow, Russia)  
I.A. Tikhonovich (Moscow, Russia)  
A. Tramontano (Davis, California, USA)  
V.K. Švedas (Moscow, Russia)  
J.-R. Wu (Shanghai, China)  
N.K. Yankovsky (Moscow, Russia)  
M. Zouali (Paris, France)

*Project Head:* S.B. Nevskaya

*Editor:* N.Yu. Deeva

*Designer:* K.K. Oparin

*Art and Layout:* K. Shnaider

*Copy Chief:* Daniel M. Medjo

Address: 119234 Moscow, Russia, Leninskiye Gory, Nauchny  
Park MGU, vlad.1, stroeniye 75G.  
Phone/Fax: +7 (495) 930 88 50  
E-mail: vera.knorre@gmail.com, mmorozova@strf.ru,  
actanaturae@gmail.com

Reprinting is by permission only.

© ACTA NATURAE, 2015

Номер подписан в печать 11 марта 2015 г.

Тираж 200 экз. Цена свободная.

Отпечатано в типографии «МЕДИА-ГРАНД»

# CONTENTS

Letter from the Editors ..... 1

## FORUM

Milestones of World Life Science ..... 6

## REVIEWS

P. V. Sergiev, O. A. Dontsova, G. V. Berezkin  
**Theories of Aging: An Ever-Evolving Field ... 9**

K. R. Valetdinova, S. P. Medvedev, S. M. Zakian  
**Model Systems of Motor Neuron Diseases As a  
Platform for Studying Pathogenic Mechanisms  
and Searching for Therapeutic Agents ..... 19**

P. V. Panteleev, I. A. Bolosov, S. V. Balandin,  
T. V. Ovchinnikova

**Structure and Biological Functions  
of  $\beta$ -Hairpin Antimicrobial Peptides. .... 37**

D. V. Popov, E. A. Lysenko, I. V. Kuzmin,  
O. L. Vinogradova, A. I. Grigoriev

**Regulation of PGC-1 $\alpha$  Isoform Expression  
in Skeletal Muscles ..... 48**

## RESEARCH ARTICLES

A. A. Alekseeva, V. V. Fedorchuk,  
S. A. Zarubina, E. G. Sadykhov, A. D. Matorin,  
S. S. Savin, V. I. Tishkov

**The Role of Ala198 in the Stability and  
Coenzyme Specificity of Bacterial Formate  
Dehydrogenases. .... 60**

O. S. Rogovaya, A. K. Fayzulin, A. V. Vasiliev,  
A. V. Kononov, V. V. Terskikh

**Reconstruction of Rabbit Urethral Epithelium  
with Skin Keratinocytes .....70**

O. A. Shadrina, T. S. Zatsepin,  
Yu. Yu. Agapkina, M. G. Isaguliyants, M. B. Gottikh

**Influence of Drug Resistance Mutations  
on the Activity of HIV-1 Subtypes A and B  
Integrases: a Comparative Study .....78**

O. V. Orlova, V. L. Drutsa, P. V. Spirin,  
V. S. Prasolov, P. M. Rubtsov, S. N. Kochetkov,  
S. N. Beljelarskaya

**The Role of HCV E2 Protein Glycosylation  
in Functioning of Virus Envelope Proteins  
in Insect and Mammalian Cells. ....87**

D. V. Pankratov, E. González-Arribas,  
Yu. M. Parunova, M. A. Gorbacheva,  
Yu. S. Zeyfman, S. V. Kuznetsov, A. V. Lipkin,  
S. V. Shleev

**New Nanobiocomposite Materials  
for Bioelectronic Devices .....98**

S. V. Dentovskaya, S. A. Ivanov,  
P. Kh. Kopylov, R. Z. Shaikhtudinova,  
M. E. Platonov, T. I. Kombarova,  
T. V. Gapel'chenkova, S. V. Balakhonov,  
A. P. Anisimov

**Selective Protective Potency  
of *Yersinia pestis*  $\Delta nlpD$  Mutants. ....102**

A. V. Akimova, G. N. Rychkov, M. A. Grin,  
N. A. Filippova, G. V. Golovina, N. A. Durandin,  
A. M. Vinogradov, T. A. Kokrashvili,  
A. F. Mironov, A. A. Shtil, V. A. Kuzmin

**Interaction with Serum Albumin  
As a Factor of the Photodynamic Efficacy  
of Novel Bacteriopurpurinimide  
Derivatives. ....109**

L. A. Balabanova, V. A. Golotin,  
I. Y. Bakunina, L. V. Slepchenko, V. V. Isakov,  
A. B. Podvolotskaya, V. A. Rasskazov

**Recombinant  $\alpha$ -N-Acetylgalactosaminidase  
from Marine Bacterium-Modifying  
A Erythrocyte Antigens .....117**

**Guidelines for Authors. ....121**

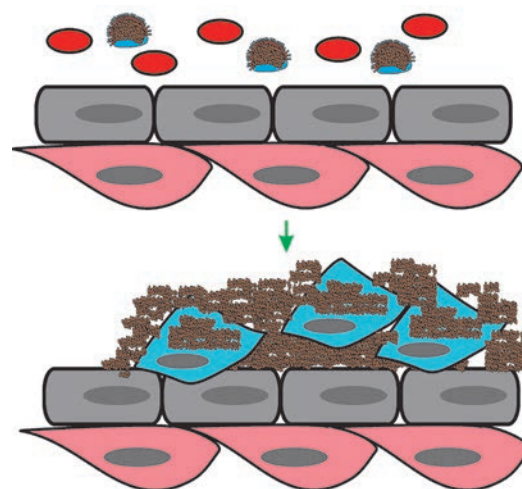


**IMAGE ON THE COVER PAGE**  
See the article by Sergiev *et al.*

# Milestones of World Life Science

## Mitochondriology and Cell Energy Supply

One of the most important aspects of modern biochemistry is the detailing of the mechanisms of cell energy supply. Mitochondria have for a long time been considered the “power plant” of cellular metabolism. In 1961, Peter Mitchell, who was later awarded the Nobel Prize for his discovery, published in *Nature* a revolutionary paper [1] that laid the groundwork for the chemiosmotic theory. According to this theory, the electrochemical potential of protons ( $\Delta\mu_{\text{H}^+}$ ) plays a critical role in energy production by mitochondria. During respiration, protons are transferred from the mitochondrial matrix to the intermembrane space to form a potential on the inner mitochondrial membrane. This respiration-generated potential is used by  $\text{H}^+$ -ATP synthase to convert ADP to ATP. Mitchell also assumed that uncoupling agents (such as dinitrophenol), which suppress the synthesis of ATP, do not inhibit ATP synthase directly, but their action is a result of the dissipation of the membrane potential - the driving force of ATP synthesis. This was a revolutionary interpretation of events at that time. It aroused great interest among leading scientists, many of whom expressed skepticism and offered their own hypotheses on mitochondrial ATP synthesis. A valuable contribution to the development of modern mitochondriology was made by the outstanding Russian biochemist V.P. Skulachev. In this issue, the Editorial Board has decided to devote the “Forum” section to a brief description of the major milestones in the development of this fascinating field of research.

**In** 1965, V.P. Skulachev established the world's first department of bioenergetics as a part of the Interdepartmental Laboratory of Molecular Biology and Bioorganic Chemistry of the Moscow State University (now the Belozersky Institute of Physico-Chemical Biology) organized by A.N. Belozersky. It was then that investigation of the coupling role of the proton potential in oxidative phosphorylation started on the basis of the chemiosmotic theory. In 1967, V.P. Skulachev, together with E.A. Lieberman, obtained one of the first experimental proofs for the Mitchell's theory [2]. Using various protonophores, the two found a correlation between stimulation of the respiration of mitochondria, oxidizing succinate, and the proton conductivity of the lipid bilayer membrane. To elucidate the molecular mechanisms coupling oxida-

tive phosphorylation with the mitochondrial membrane potential, an attempt was made to find ions capable of passing both through mitochondrial and through artificial planar lipid bilayer membranes. Such organic ions were found. The tetraphenylphosphonium cation ( $\text{TPP}^+$ ) and tetraphenylborate anion ( $\text{TPB}^-$ ), different in regard of a central atom that is positively charged in  $\text{TPP}^+$  and negatively charged in  $\text{TPB}^-$ , appeared to be the most effective.

Employing these compounds revealed that mitochondria, energized by ATP or substrate oxidation, can accumulate cations, and that submitochondrial particles can accumulate anions [3]. Besides the importance of the results obtained in that work, the term “protonophore” was introduced to the scientific literature for the first time, which is still successfully used

today. The publication generated great interest in the scientific community, and, in recognition of its importance, the developed ions were called, at the suggestion of the famous American biochemist Professor David Green, “Skulachev's ions” ( $\text{Sk}^+$  and  $\text{Sk}^-$ , cations and anions, respectively) [4]. For this work, V.P. Skulachev was awarded the State Prize of the USSR in 1975.

In the 1990s, X. Wang in a series of publications [5–7] demonstrated that mitochondria are involved in induction of apoptosis – programmed cell death that plays an important role in the development of the organism and the pathology of many diseases. Cytochrome *c*, a key molecule of the respiratory chain, was found to be able, under certain conditions, to leave the mitochondria and trigger apoptosis, upon association with other molecules into the apoptosome complex

in the cytosol. Long before Wang's publications, during the investigation of massive cell death under the influence of ionizing radiation, suppression of oxidative phosphorylation in mitochondria isolated from radiosensitive tissues (thymus and spleen) was established. However, in mitochondria isolated from radioresistant liver tissue oxidative phosphorylation was not altered by radiation [8, 9]. Such changes in oxidative phosphorylation could be detected as early as 30–60 min after total-body x-ray exposure of rats to relatively low doses (50–100 cGy) [10]. Suppression of oxidative phosphorylation in radiosensitive tissues correlated with the formation of the so-called pyknotic nuclei [11]. Furthermore, mitochondria isolated from radiosensitive tissues after irradiation contained a smaller amount of cytochrome *c* compared to mitochondria from radioresistant tissues [12]. Later, radiation damage was found to lead to reduced binding of cytochrome *c* to the inner mitochondrial membrane, and it was established that addition of exogenous cytochrome *c* can stimulate oxidative phosphorylation in mitochondria isolated from the radiosensitive tissues of irradiated rats [9, 13]. The mechanism underlying this phenomenon was established only in 2005 [14]. It is necessary to note that the mechanisms of radiation-induced cell death were extensively studied in the Soviet Union. Soviet researchers postulated and proved that radiation death of lymphoid cells is an example of a broader biological phenomenon – programmed cell death [15, 16] – which was recognized by the world community [17].

Simultaneously with Wang's studies, G. Kroemer demonstrated that a decline in the mitochondrial membrane potential is one of the key events that trigger cell death [18]. V.P. Skulachev became interested in this phenomenon, viewing

it from a different perspective. He decided to search for a relationship between programmed cell death and aging. Back in the late 19th century, A. Weismann suggested a hypothesis that in the heart of death caused by aging is the evolutionary-developed adaptive mechanism [19]. Based on this hypothesis, V.P. Skulachev proposed that the altruistic death of individuals, as an adaptive mechanism, could be beneficial to other groups of organisms in the environment. He first coined the term “phenoptosis” and explained it as a mechanism of ridding the community of undesirable elements [20]. The simplest example of phenoptosis can be observed in bacteria. Altruistic programmed death in these organisms is necessary for: (a) preventing the expansion of phage infection in the bacterial population; (b) eliminating cells whose genome or other key systems are damaged; and (c) optimizing the number of bacterial cells in the environment [21]. Later, the phenomenon of phenoptosis was described in yeast, where pheromone-dependent death was suppressed by protein synthesis inhibitors and was recognized as programmed death [22]. Phenoptosis examples were also described in some higher organisms [21, 23]. However, the molecular mechanisms that trigger the phenomenon remain unknown.

The aging process should be more important than acute phenoptosis in the evolution of permanently reproducing organisms, because the function of aging-dependent phenoptosis is to reduce the number of individuals in the population of long-living predecessors, thereby stimulating evolution. In other words, slow phenoptosis enhances this process [24]. What can be the regulators of age-dependent phenoptosis? V.P. Skulachev suggested that telomere shortening could underlie this mechanism (a similar mechanism was predicted by the

Russian researcher A.M. Olovnikov many years ago [25]). Unfortunately, it remains unknown whether telomere shortening determines the lifespan of a multicellular organism as a whole or whether it applies only to its specific cell systems.

In recent years, several fundamental observations have been published that have tried to establish a relationship between aging and death of the organism at the molecular level. For example, the lifespan of animals expressing and not expressing the p66<sup>shc</sup> protein, which is involved in the regulation of the level of reactive oxygen species, has been demonstrated to differ by 30% [26]. Furthermore, although no tumor growth has been observed in mutant mice with an increased activity of the tumor suppressor p53, their lifespan is shorter than that of wild-type mice [27]. These two proteins are actively involved in the regulation of apoptosis. Based on these observations, V.P. Skulachev suggested that the lifespan could be regulated through a coordinated activation of p53 and suppression of the p66<sup>shc</sup> protein. Time will tell whether it will be possible to reproduce this quite logical assumption in real life [23].

Based on the growing body of data on the mechanisms of programmed cell death and the phenoptosis phenomenon, V.P. Skulachev put forward the idea of the “samurai rule” in biology. This rule can briefly be formulated as follows: “it is better to die than to be wrong.” He wrote in one of his outstanding articles: “Any biological systems, ranging from organelles to the whole body, have a self-destruction program. This suicidal mechanism is activated when the system is dangerous to coexistence with other systems in the biological hierarchy” [21].

The development of science provides interesting examples of in-

terdisciplinary, pioneering breakthroughs based on the efforts of researchers from different countries who often only get to know each other personally after publishing their own seminal observations. The story told today is a clear example of this. V.P. Skulachev met with Peter Mitchell at the FEBS

Congress in Warsaw only in 1966. From then on, an enduring friendship developed between the two, based on common interest in mitochondriology. This area of knowledge remains far from exhausted, and it is particularly rewarding to know that Russian researchers were among its originators. ●

**B.D. Zhivotovsky<sup>1,2</sup>,  
V.G. Gogvadze<sup>1,2</sup>, V.A. Tkachuk<sup>1</sup>**

<sup>1</sup>*Faculty of Basic Medicine,  
Lomonosov Moscow State  
University, Moscow, Russia;*

<sup>2</sup>*Institute of Environmental  
Medicine, Karolinska Institutet,  
Stockholm, Sweden*

#### REFERENCES

- Mitchell P. // *Nature*. 1961. V. 191. P. 144–148.
- Skulachev V.P., Sharaf A.A., Liberman E.A. // *Nature*. 1967. V. 216. № 5116. P. 718–719.
- Liberman E.A., Topaly V.P., Tsofina L.M., Jasaitis A.A., Skulachev V.P. // *Nature*. 1969. V. 222. № 5198. P. 1076–1078.
- Green D.E. // *Biochim. Biophys. Acta*. 1974. V. 346. № 1. P. 27–78.
- Liu X., Kim C.N., Yang J., Jemmerson R., Wang X. // *Cell*. 1996. V. 86. № 1. P. 147–157.
- Zou H., Henzel W.J., Liu X., Lutschg A., Wang X. // *Cell*. 1997. V. 90. № 3. P. 405–413.
- Li P., Nijhawan D., Budihardjo I., Srinivasula S.M., Ahmad M., Alnemri E.S., Wang X. // *Cell*. 1997. V. 91. № 4. P. 479–489.
- Ashwell G., Hickman J. // *Proc. Soc. Exp. Biol. Med.* 1952. V. 80. № 3. P. 407–410.
- Khanson K.P., Ivanova L.V. // *Vopr. Med. Khim.* 1969. V. 15. № 1. P. 64–66.
- van Bekkum D.W. // *Biochim. Biophys. Acta*. 1957. V. 25. № 3. P. 487–492.
- van Bekkum D.W., de Vries M.J., Klouwen H.M. // *Int. J. Radiat. Biol. Relat. Stud. Phys. Chem. Med.* 1965. V. 9. № 5. P. 449–459.
- Scaife J.F. // *Can. J. Biochem.* 1964. V. 42. P. 431–434.
- Manoilov S.E., Khanson K.P. // *Vopr. Med. Khim.* 1964. V. 10. P. 410–413.
- Kuwana T., Bouchier-Hayes L., Chipuk J.E., Bonzon C., Sullivan B.A., Green D.R., Newmeyer D.D. // *Mol. Cell*. 2005. V. 17. № 4. P. 525–535.
- Khanson K.P. // *Radiobiologia*. 1979. V. 19. № 6. P. 814–820.
- Umansky S.R. // *J. Theor. Biol.* 1982. V. 97. № 4. P. 591–602.
- Wyllie A.H. // *ISI Atlas of Science: Immunology*. 1988. pp192–196.
- Zamzami N., Marchetti P., Castedo M., Zanin C., Vayssiere J.L., Petit P.X., Kroemer G. // *J. Exp. Med.* 1995. V. 181. № 5. P. 1661–1672.
- Weismann A., Wenderoth M., Lounis S., Zahn P., Quaas N., Ulbrich R.G., Dederichs P.H., Blugel S. // *Science*. 2009. V. 323. № 5918. P. 1190–1193.
- Skulachev V.P. // *Biochemistry (Moscow)*. 1997. V. 62. № 11. P. 1191–1195.
- Skulachev V.P. // *Exp. Gerontol.* 2001. V. 36. № 7. P. 995–1024.
- Severin F.F., Hyman A.A. // *Curr. Biol.* 2002. V. 12. № 7. P. R233–235.
- Skulachev V.P. // *Ann. N.Y. Acad. Sci.* 2002. V. 959. P. 214–237.
- Skulachev M.V., Severin F.F., Skulachev V.P. // *Biochemistry (Moscow)*. 2014. V. 79. № 10. P. 994–1003.
- Olovnikov A.M. // *J. Theor. Biol.* 1973. V. 41. № 1. P. 181–190.
- Migliaccio E., Giorgio M., Mele S., Pelicci G., Reboldi P., Pandolfi P.P., Lanfrancione L., Pelicci P.G. // *Nature*. 1999. V. 402. № 6759. P. 309–313.
- Tyner S.D., Venkatachalam S., Choi J., Jones S., Ghebranious N., Igelmann H., Lu X., Soron G., Cooper B., Brayton C., et al. // *Nature*. 2002. V. 415. № 6867. P. 45–53.

# Theories of Aging: An Ever-Evolving Field

P. V. Sergiev<sup>1,2\*</sup>, O. A. Dontsova<sup>1,2</sup>, G. V. Berezkin<sup>3</sup>

<sup>1</sup>Belozersky Institute of Physico-Chemical Biology, Moscow State University, Leninskie Gory 1, bld. 40, 119992, Moscow, Russia

<sup>2</sup>Chemistry Department, Moscow State University, Leninskie Gory, 1, bld. 3, 119992, Moscow, Russia

<sup>3</sup>ESN group, Rochdel'skaya Str., 11/5, bld. 2, 123100, Moscow, Russia

\*E-mail: petya@genebee.msu.ru

Received 29.08.2014

Copyright © 2015 Park-media, Ltd. This is an open access article distributed under the Creative Commons Attribution License, which permits unrestricted use, distribution, and reproduction in any medium, provided the original work is properly cited.

**ABSTRACT** Senescence has been the focus of research for many centuries. Despite significant progress in extending average human life expectancy, the process of aging remains largely elusive and, unfortunately, inevitable. In this review, we attempted to summarize the current theories of aging and the approaches to understanding it. **KEYWORDS** aging, life expectancy, reactive oxygen species, accumulation of damage, telomerase, advanced glycation end-product.

## INTRODUCTION

A number of theories, which fall into two main categories, have been proposed in an attempt to explain the process of aging. The first category is comprised of concepts holding that aging is programmed and those positing that aging is caused by the accumulation of damage. Conversely, the latter category of theories suggests various sources and targets of the damage. They are not necessarily mutually exclusive. Rather, aging could vary across different species, and programmed senescence can accelerate the buildup of damage or decrease the capacity for repair. What kinds of damage occur during aging?

## MITOCHONDRIA AND REACTIVE OXYGEN SPECIES

The primary function of mitochondria is respiration, which promotes energy production. Mitochondria break down organic compounds into water and carbon dioxide to release energy in the form of adenosine triphosphate (ATP). Each mitochondrion is contained in a double membrane. The outer membrane is relatively permeable to small molecules via transport proteins known as porins. The inner membrane forms folds (cristae) that increase the membrane area. Mitochondrial respiration generates a proton gradient across the inner membrane and a transmembrane potential through respiratory chain complexes (I–IV), enabling electron flow from the reduction equivalents NADH and FADH<sub>2</sub> to oxygen. Simultaneously, the energy released in the oxidation of NADH and FADH<sub>2</sub> is used to pump H<sup>+</sup> ions out of the matrix into the space between the outer and inner membranes (*Fig. 1*). Thus, the intermembrane space of mitochondria is charged

positively; and the matrix, negatively. Stored energy is used for ATP synthesis by the other membrane-bound protein complex – ATP synthase (*Fig. 2*).

A distinctive challenge for respiration is the release of excessive energy during the oxidation of organic molecules by oxygen (converted into the reduction equivalents NADH and FADH<sub>2</sub>). In this context, the respiratory chain is used to break the entire reaction into intermediate stages, the energy of which would be more efficiently saved (to establish a proton gradient). In addition, electrons could be transported one at a time or in pairs (as two reduction equivalents) in the respiratory chain. At the end of the catalytic cycle of oxygen reduction to two water molecules, four electrons are sequentially donated by reduced cytochrome c to cytochrome c oxidase.

During respiration, oxygen is reduced in several stages, producing a superoxide radical (O<sub>2</sub><sup>-</sup>) and hydrogen peroxide. Most commonly, these molecules, known as reactive oxygen species (ROS), remain bound to cytochrome c oxidase until the reduction of oxygen to water is completed. In contrast to the common sequence of oxygen reduction by cytochrome c oxidase, oxygen molecules can occasionally form superoxide species by reacting with the reduced components of the electron transport chain. This typically occurs at the level of complexes I and III in the respiratory chain. In addition, the p66Shc protein can generate ROS via cytochrome c [1, 2]. Short-lived ROS are potent inducers of oxidative damage to any biomolecule. In particular, mitochondrially produced ROS inflict detrimental mutations on mtDNA. Mitochondria carry their own genome inherited from a bacterial ancestor living within early eu-

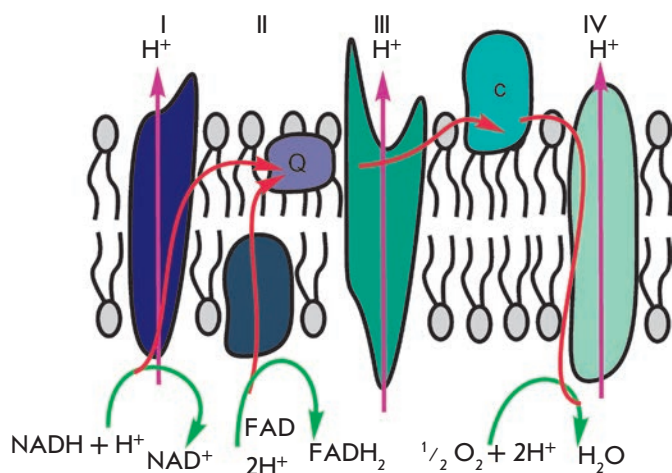


**Fig. 1.** The mitochondrial respiratory chain, illustrating electron transfer from NADH and FADH<sub>2</sub> to oxygen

karyotes. mtDNA encodes mainly the RNA molecules needed for the synthesis of mitochondrial proteins and subunits of respiratory chain enzymes. Human mtDNA codes for two ribosomal RNAs and 22 transport RNAs, seven proteins of respiratory complex I (ND1, ND2, ND3, ND4, ND4L, ND5, ND6), one protein of respiratory complex III (CYB), three proteins of respiratory complex IV (CO1, CO2, CO3), and two protein subunits of ATP synthase (ATP6, ATP8). The majority of the other proteins essential for mitochondrial function are encoded by the nuclear genome.

Mutations in mitochondrial DNA can affect longevity. The most dramatic example is deficiency in the COX5 gene coding for the fifth subunit of cytochrome c oxidase in the fungus *Podospira anserina* [3], manifesting as a tenfold increase in the lifespan. Given that, impairment of the normal respiratory pathway in *P. anserine* leads to the use of the alternative pathway, which is private only in a handful of taxonomic groups.

Cells possess their own ROS metabolizing enzymes. The superoxide radical is converted by superoxide dismutase (SOD) to a less reactive hydrogen peroxide. Human cells harbor mitochondrial manganese superoxide dismutase (MnSOD) and few cellular copper-zinc superoxide dismutases. Hydrogen peroxide, which is produced from the superoxide radical or in other pathways, is broken down by catalase (CAT), peroxiredoxin (Prx), and glutathione peroxidase (GPx). Hydrogen peroxide can spontaneously react with ferrous ion (II) by the Fenton reaction to yield highly reactive hydroxyl radicals (OH<sup>•</sup>), which can be detrimental to cellular functioning.

Viewing ROS as primary damaging molecules not only for mitochondria, but also for other cell compart-

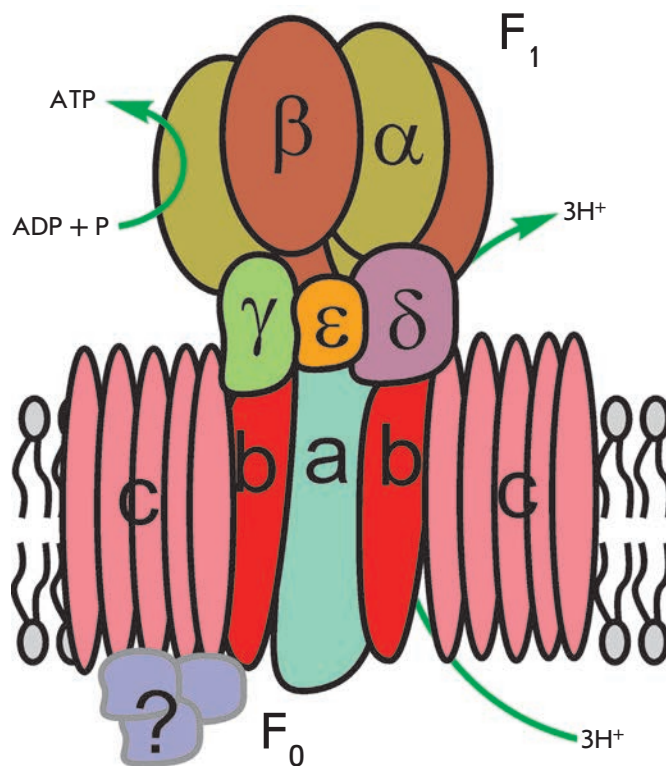


**Fig. 2.** A schematic representation of ATP synthase structure and function

ments in cell senescence was proposed by D. Harman in 1956 [4] and has remained entrenched to this day. A decline in ROS production using mitochondria-targeted rechargeable antioxidants provided the basis for the approach proposed by V.P Skulachev to prevent age-related disorders [5]. Importantly, the role of ROS in age-associated pathologies has undergone several revisions in the past years. Originally, it was believed that damaged mitochondria increase ROS generation and thus accelerate aging [6]. However, it was eventually proved that most mitochondrial deficiencies do not end up with an elevated ROS but completely inactivated mitochondria, which led to the hypothesis that cells lacking a mitochondrial function pose a threat to the entire organism [7].

A few studies have challenged the negative role assigned to ROS as the primary mediators of cell damage in aging. Endogenously produced ROS in a wide range of animal species inversely correlate with lifespan [8]; however, experimental evidence suggests that the naked mole-rats *Heterocephalus glaber*, which demonstrate exceptional longevity, tolerate much higher levels of ROS and oxidative damage with regard to short-lived mice (*Mus musculus*) [9]. ROS are known to play an essential role in immune functioning, cellu-

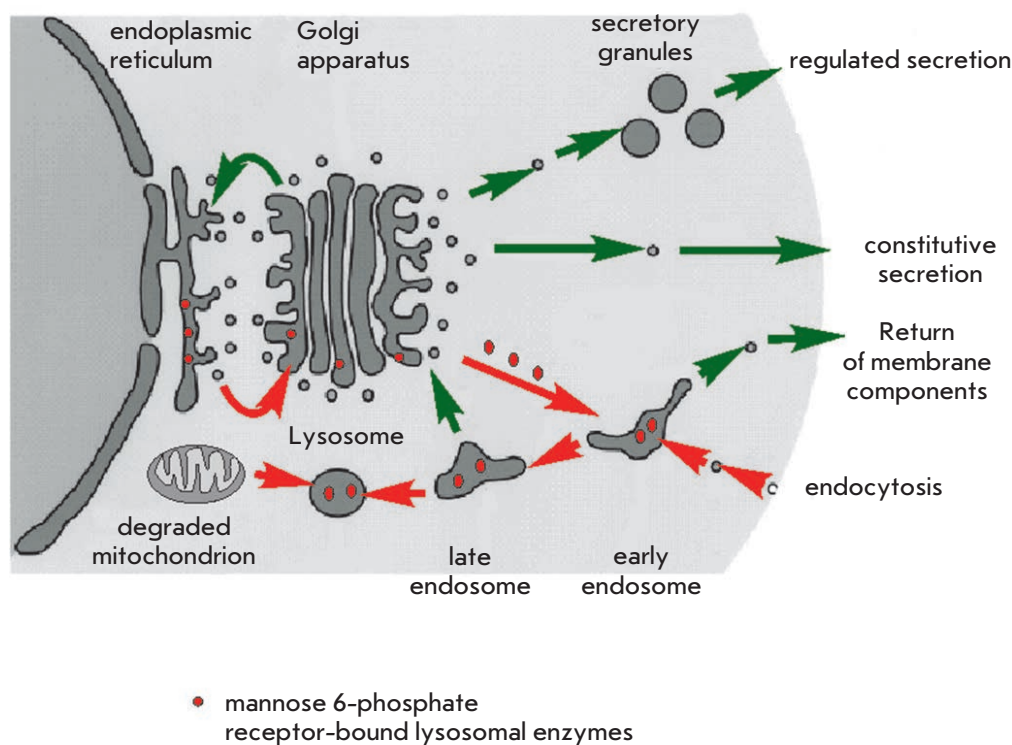


**Fig. 3.** Lysosomal transport. A schematic representation of vesicular transport in the cell. Red arrows indicate the flow of material from the cellular membrane (material absorbed by the cell), the cytoplasm (for example, defective mitochondria to be degraded), and from the endoplasmic reticulum (lysosomal enzymes) to lysosomes

lar signaling, and stress response (as reviewed in [10]). Special attention should be focused on the relationship between the ROS inactivation pathway and aging. Although it might appear that stronger protection against ROS extends the lifespan, in fact it does not. Conversely, a negative correlation has been established between the level of ROS metabolizing enzymes and longevity in mammals [8]. At the same time, exposure to the elevated enzyme concentrations involved in ROS inactivation results in lifespan extension. A positive impact was observed through genetic upregulation of catalase in mitochondria: not in the nuclei of murine cells [11]. Overexpression of CuZnSOD has been shown to increase the lifespan in adult *Drosophila melanogaster*. [12]. On the other hand, deletions in the genes implicated in ROS metabolizing pathways had no effect on the lifespan of the nematode *Caenorhabditis elegans*, while the deletion of the *sod-2* gene even extended it [13].

Overall, ROS seem to play a detrimental role in cellular functioning, in particular mitochondria, during aging, but yet a beneficial role in other pathways.

### ACCUMULATION OF UNDEGRADABLE BY-PRODUCTS OF METABOLISM

Another theory that attempts to explain the process of aging suggests that the accumulation of biological garbage that cannot be completely removed from the organism is responsible for cell senescence. In its ba-

sal form, this theory was described by V. Gladyshev [14, 15]. Its aspects were presented in detail in [16]. It holds that, due to the stochastic nature of biochemical reactions, including enzymatic pathways, side reactions have the potential to occur. The degree of complexity of a biochemical network contributes to the range of by-products formed. Some of them are readily eliminated by excretion or degradation. Each by-product is broken down by an appropriate enzyme or a series of enzymes, which in turns makes the metabolism more complex and increases the array of by-products. Enzymatic pathways for metabolizing by-products vary across species. These pathways, though not numerous, tend to be restricted to only the most commonly produced compounds with toxic properties, allowing other by-products to build up. The only mechanism by which these agents are diluted in the cells is cell division. This only applies to replicative cells. The challenge for multicellular organisms such as the human organism is that many cell types lose replicative capacity or divide slowly, even though they remain active throughout the lifespan. These cells, including cardiomyocytes and brain neurons, accumulate metabolic waste that eventually affects normal cell functioning. A common by-product of cellular metabolism seems to be lipofuscin, a substance composed of non-degradable material that accumulates in lysosomes. Lysosomes are intracellular organelles serving as degradative com-

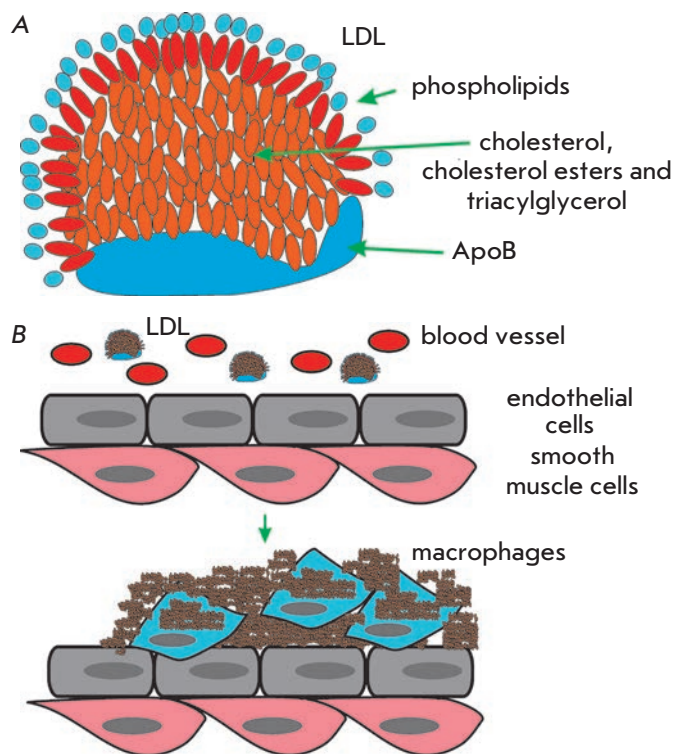


**Fig. 4.** Structure of the low-density lipoprotein (LDL), the major carrier of plasma lipids (A), and formation of the atherosclerotic plaque (B)

partments for intra- and extracellular components. In addition, the digestion enzyme hydrolases contained in lysosomes are transported in vesicles from the endoplasmic reticulum and the Golgi apparatus. Hydrolases are transferred to lysosomes after binding to mannose 6-phosphate residues (Fig. 3). Lysosomal enzymes are active at acidic lysosomal pH only. Lipofuscin deposition decreases enzyme levels and impairs lysosomal acidification, which ultimately affects hydrolase activity. Each organism displays species-specific groups of lysosomal enzymes and the enzymes responsible for the breakdown of metabolic debris in other cellular compartments.

The accumulation of non-degradable material can occur in the intra- and extracellular environments. Among the extracellular deposits found in humans, cholesterol-containing plaques and their oxidized derivatives in blood vessels are worth mentioning, as well as protein polymers, such as  $\beta$ -amyloid in the central nervous system. Atherosclerotic plaques contain lipids deposited in the walls of blood vessels. Firstly, there is oxidized and glycated cholesterol derivatives; however, other lipids may be present. Low-density lipoproteins (LDL) transport fat molecules around the body,

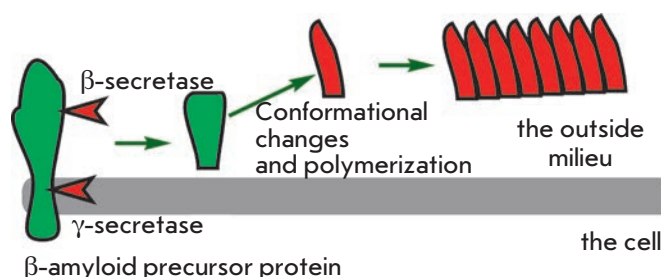


**Fig. 5.** Formation of  $\beta$ -amyloid and polymerization

from where they accumulate on the walls of arteries (Fig. 4A).

Atherosclerotic plaques serve as a site for the recruitment of monocytes, which eventually differentiate into macrophages. These immune cells absorb cholesterol and prove beneficial at some point. However, under certain conditions, macrophages accumulate in plaques and form lipid-loaded foam cells (Fig. 4B). A comparison of DNA polymorphisms in French centenarians with control individuals in a genome-wide association study (GWAS) demonstrated that one of the ApoE genotypes (E2 allele), a component of very low density lipoproteins, was significantly more frequent in the centenarian group, whereas the E4 allele, associated with a high risk of atherosclerosis, was significantly less frequently present [17]. Moreover, ApoB alleles, a major component of low density lipoproteins, had no association with longevity.

Amyloid proteins are another class of toxic waste accumulating mainly in the nervous system. The best-described amyloid protein is  $\beta$ -amyloid, which is known to cause Alzheimer's disease (reviewed in [18]). It is generated from a functionally important protein, the amyloid precursor protein, via cleavage of the precursor molecule at both termini by  $\beta$ - and  $\gamma$ -secretases (Fig. 5). The  $\beta$ -amyloid protein can exist in several forms, one of which, rich in  $\beta$ -sheets, is toxic. The toxicity is due to  $\beta$ -amyloid polymerization, which can induce other monomers to accept the misfolded structure. Amyloid  $\beta$ -peptide polymerization results in amyloid plaque formation in nerve cells, causing Alzheimer's disease. There is evidence suggesting that  $\beta$ -amyloid peptides can spontaneously undergo pyroglutamate modification and acquire a higher toxicity [19]. There is a wide array of compounds, other than  $\beta$ -amyloid peptides, capable of self-polymerization into toxic insoluble structures. It is likely that a spontaneous modification of proteins also plays a role in the formation of metabolic debris.

Finally, metabolic waste also includes, to a certain extent, spontaneously modified sugar-bound proteins,

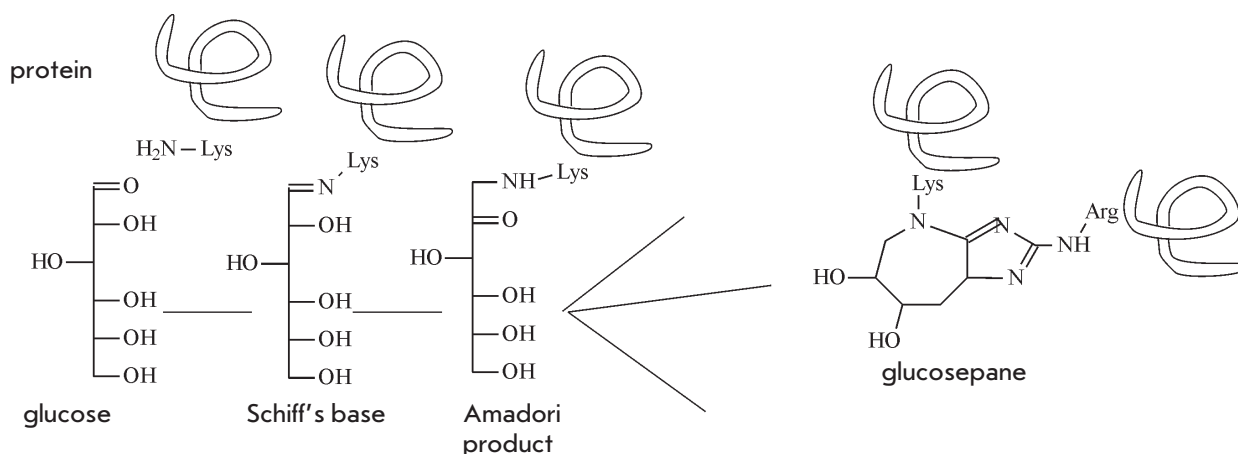


Fig. 6. Spontaneous glycation of proteins

mainly glucose molecules. Glycation involves interaction between the amino groups of lysine and the aldehyde groups of glucose (Fig. 6) via a Schiff base reaction. It is followed by rearrangement of the double C=N-bond, known as Amadori products, to yield a wide range of advanced glycation end-products such as glucosepane.

The main consequence of spontaneous glycation is impaired elasticity, which is essential to blood vessels [20]. In addition, spontaneous glycation affects protein functioning. This process well describes the concept of accumulation of metabolic waste that promotes aging. Until now, no enzyme has been discovered that is capable of metabolizing glycated products. Preventing spontaneous glycation seems to be impossible, because all proteins contain lysine residues and glucose is one of the important substances in all living organisms. FAD-dependent deglycating enzymes have been found in fungi (amadoriase) and bacteria (fructoselysine-6-kinase frlD and fructoselysine -6-phosphahte-deglycase frlB) [21], though they can only act on low-molecular weight molecules, such as amino acids conjugated to sugars, and have no activity towards glycated proteins. In vertebrates, fructosamine-3-kinase (FN3K) has been identified, together with a related protein (FN3K-RP), a breaker of glycation end products. It is an ATP-dependent enzyme that targets only intracellular, rather than extracellular, molecules.

### IMPAIRMENT OF REGULATORY PATHWAYS DURING AGING

Aging is associated not only with the buildup of metabolic by-products, but also with the dysregulation of regulatory pathways. For example, aging upsets the balance between pro- and anti-inflammatory components, promoting chronic inflammation. The causali-

ty between such inflammatory processes and age-related disorders has been stated in the inflamm-aging theory of Franceschi [22]. An elevated predisposition to inflammatory diseases in early age, as a protective barrier against infection, proves to be detrimental in the elderly.

Besides the imbalance in pro- and anti-inflammatory responsiveness, aging can also impair other important pathways. The Russian researcher V.M. Dilman conceptualized the neuroendocrinal theory (elevation hypothesis) of aging [23]. This theory involves the existence of self-regulatory mechanisms of homeostasis – negative feedback pathways. One of the essential systems is the hypothalamus-pituitary-adrenal axis. An elevation of the threshold of the hypothalamus to negative feedback signaling accounts for the unfavorable age-related changes in human health; in particular, reproductive decline [24]. The development and experimental verification of the elevation hypothesis represent an important achievement in aging research in Russia.

### TELOMERES ARE THE BIOLOGICAL CLOCKS OF THE CELL

Eukaryotic DNA is organized into linear, double-stranded chromosomes. The number of chromosomes varies from one to several hundred from species to species. Linear chromosomes are capped by repetitive nucleoprotein structures known as telomeres that protect the chromosome ends against degradation and fusion. Telomeres allow cells to distinguish the appropriate chromosome ends from the double-strand DNA breaks induced by exogenous factors like radiation. The linear arrangement is one cause of the end-replication problem first articulated by A.M. Olovnikov [25]. DNA replication requires an RNA primer to initiate synthesis, followed by its removal, which progressively short-

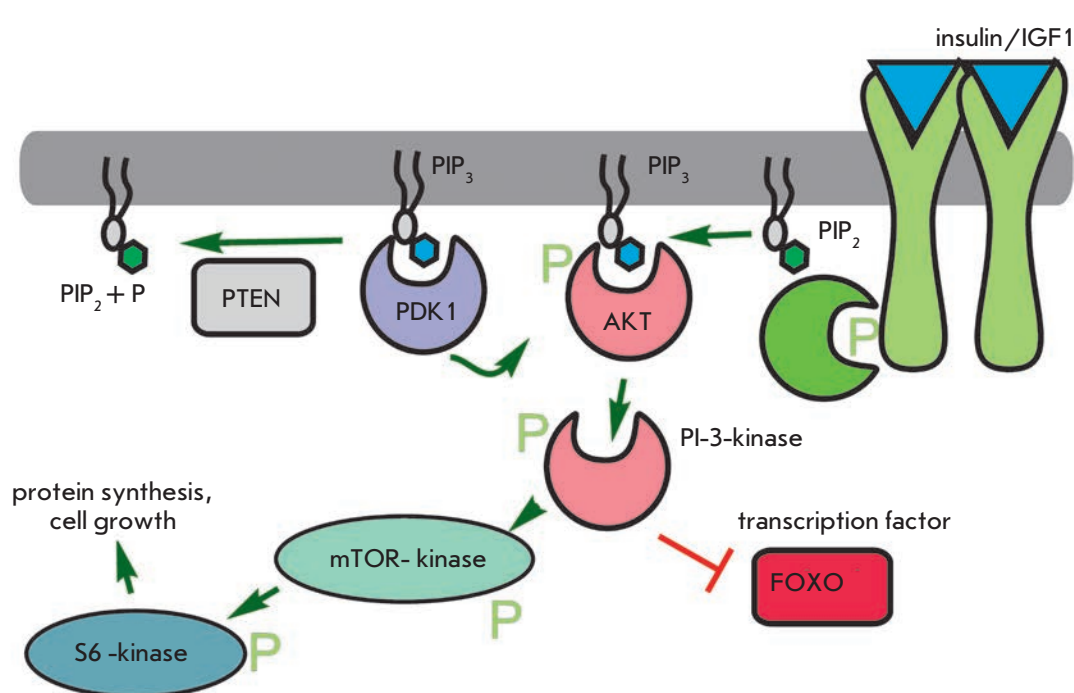


Fig. 7. Simplistic representation of the insulin/IGF-1 signal pathway

ens chromosome ends with each cell cycle. Olovnikov suggested the existence of an enzyme capable of elongating the ends. Long afterward, such an enzyme, called telomerase, was experimentally confirmed [26].

Telomerase activity was not shown in all cell types. Cells with unlimited proliferative potential such as germ and stem cells can extend telomeric DNA via telomerase. The majority of other cell types have a finite replicative capacity or are non-dividing. Such cells lack telomerase activity, thus suffering telomere attrition upon successive cell divisions [27]. This erosion provides an explanation for the observation of a limited lifespan in cultured somatic cells [28]. By and large, telomere shortening is a type of molecular clock that counts cell divisions. It is tempting to extrapolate this clock into the context of the entire organism, assuming that telomerase activation can confer replicative immortality to somatic (non-germ) cells. However, such a straightforward approach encounters serious challenges. The absence of telomerase activity in many cell types in a multicellular environment serves as a mechanism by which malignancy is suppressed [29]. Even in the event of mutations leading to uncontrolled growth regardless of cell-division pathways, such cells would have a finite lifespan anyway in the absence of telomerase activity. Many tumors carry mutations that upregulate telomerase and increase proliferative capacity in a small population of tumor cells with telomerase activity. Owing to this mechanism, malignancy rates are not high in contrast to the presence of telomerase in all cells. Overall, there is a trade-off between physiologi-

cal cell turnover and the occurrence of tumor cells. An insufficient amount of cells with telomerase activity would lead to poor tissue renewal, whereas an elevated number of telomerase-positive cells would increase malignancy rates.

### BIOLOGICAL CLOCKS AND METABOLISM RATES

It has been long known that dietary restrictions prolong the lifespan in various organisms. This observation was made by McCay *et al.* through studies of mice in the 1930s [30]. Since then, a wide array of mutations have been identified in genes that affect metabolic changes, which proved to increase the lifespan in the model animals. Extensive work has been performed on the nematode *C. elegans*, a favorable system for studying developmental biology. This tiny organism has a fixed number of cells, with each cell's fate predetermined. Some mutations lead to a twofold lifespan increase in *C. elegans* [31], while its normal life-span is 20 days. The mutations increasing the lifespan of *C. elegans* have been described in detail in [32]. Most of the mutations which positively affected the lifespan of the nematode had an effect on metabolic activity. Upon starvation, *C. elegans* can enter a state of dormancy.

This program, the dauer stage (enduring, persisting), involves a slowed metabolism and larval development, as well as decreased food intake, and of course reproductive arrest. In this state of dormancy, the worm can survive food deprivation by increasing its lifespan. Since the dauer stage is naturally triggered by larval

starvation, it is very similar to the lifespan extension in other organisms following dietary restrictions. The distinct difference is that highly organized organisms have no specific developmental strategies in the case of food deprivation.

The *daf-2 gene* mutation, which causes a two-fold lifespan increase in *C. elegans*, is related to the insulin receptor gene [33]. Other lifespan extension mutations also suggest a role for insulin-related pathways and the insulin-like growth factor (IGF1) (Fig. 7). These pathways, which are triggered by increased food intake, primarily glucose, elevate the metabolic rate, as well as promote growth and cell division. These mutations occur in genes encoding early and late components of the signaling cascade. Phosphoinositide-3-kinase (age-1) transmits a signal from the insulin-like receptor substrate (IRS) PDK and Akt kinases, which in turn mediate signaling to protein synthesis and alter transcriptional regulation through the FOXO transcription factor (*daf-16*). Another important component controlling metabolism and aging is histone deacetylase Sir2. Histone deacetylation results in transcriptional repression. Upregulation of Sir2 increased longevity, even though with deletion of this gene calorie restriction has no greater impact on the lifespan [34].

A handful of genes of the fruit fly *Drosophila melanogaster* have been mapped and implicated in lifespan extension [32]. Genetic analysis has shown that a significant increase in the lifespan is associated with mutations in the signal transduction pathways from the insulin and insulin-like growth factors and with mutations directly affecting the metabolic activity and the Krebs cycle. Nearly the same spectrum of cellular regulatory pathways is altered with lifespan extension mutations in mice [32]. Among these longevity genes are genes encoding elements from insulin and insulin-like growth factor signaling and those encoding stress response proteins.

Overall, the analysis of the mutations that cause lifespan increase in various model organisms brings us closer to understanding the concept of biological clocks, which behave as a function of time and the metabolic rate. In complete agreement with the concept by V. Gladyshev and other theories of aging, metabolic activity mainly accounts for the formation of by-products that fail to undergo elimination and accumulate. A higher metabolic rate contributes to a faster build-up of toxic metabolic waste and lesions. Conversely, a lowered metabolism either in the context of calorie restriction or mutations affecting metabolic pathways, triggered by increased food intake, promotes lifespan extension through a decline in the accumulation of toxic by-products.

Mechanisms whereby lesions occur in normal metabolism are also related. First and foremost, it is the formation of reactive oxygen species that damage cellular components and glycation of the cellular components induced by glucose, an essential macronutrient for cells. Glycation and oxidation products contribute to lipofuscin formation in lysosomes, reduced vessel elasticity, and deposition of insoluble aggregates on the walls of blood vessels and the nerve tissue.

### IS SENESCENCE PROGRAMED!

Although many molecular mechanisms of aging have been studied and are akin to an inevitable accumulation of toxic metabolic waste products or damage caused by them, there have been established theories claiming that aging is programmed. The theory of programmed senescence was first described by A. Weismann [35]. Later on, V. Skulachev extended this theory, which received much attention [36]. There is another theory of programmed aging by A. Boiko [37]. The theories of programmed aging and spontaneous senescence are often shared by molecular mechanisms.

What are the arguments to support the programmed aging theory? First, some species senesce abruptly, which undoubtedly appears to be programmed. Rapid senescence is nearly always initiated following reproduction. Bamboo reproduces vegetatively and can grow for 15–20 years without apparent senescence. After flowering and seed formation, it rapidly withers away, thus allowing seeds to germinate. The most salient example of accelerated aging is the salmon. Salmon migrate from the Pacific to the rivers, where they spawn eggs, followed by a marked elevation in the plasma levels of glucose, fatty acids, cholesterol, and adrenal secretion and death. An example of avoiding entering the state of accelerated aging was discovered by the Russian biologist V.V. Zyuganov [38]. The pearl mussel larvae parasitizing in the gills of salmon delay senescence in salmon for them to mature. The hypothesis of induced delay of senescence in the salmon was criticized [39], even though dying a programmed death cannot be doubted. There are a few other examples of apparent programmed death that are frequently linked to the reproductive function, such as death following copulation in males of the brown antechinus [40] and mayflies or post-copulatory decapitation by female mantises. These features are a clear indication of programmed death; however, its links to aging are often obscured. Yet, these examples show a potential for life-history strategies deleterious for an individual but beneficial to the entire population. The theory of V. Skulachev [36] holds that senescence of mammals is a deleterious program of the kind, though spread over an extended period and implemented through the formation of ROS in mitochondria.

Most obviously, the average lifespan within a given species is genetically programmed in one way or the other. Nevertheless, the current theories of aging differ in viewing aging as a consequence or a side effect of genetic pathways. According to the well-known disposable soma theory suggested by T. Kirkwood [41], aging is a trade-off in the allocation of limited energy resources between maintenance and restoration of tissue homeostasis and other traits needed for survival. This trade-off is demonstrated when comparing the mean lifespan of related animal species with different predation risks. When the risk is high, delayed senescence has no added benefit relative to, for example, rapid reproduction. According to A. Boiko [37], senescence is an acquired program. Ancestors of multicellular animals and many present-day taxa of multicellular species are devoid of such a program. Aging in itself is genetically programmed in ontogenesis, involving the formation of non-renewable tissues – the so-called post-mitotic tissues. The cells of such tissues are non-dividing and cannot be renewed by stem cell populations. The theory of Boiko thus incorporates the theory of by-product accumulation by V. Gladyshev [15] and seems to be well articulated.

### COMPARATIVE GENETICS OF LONGEVITY

The aging program is explicitly or implicitly encoded in the genome and, in theory, could be captured by comparing the genomes of aging and non-aging organisms. However, organisms should be related to avoid much variation in aging-unrelated genes across their genomes. Even genome wide association studies of long-lived and control individuals do not always provide unambiguous conclusions. There is a great body of work concerning a possible association between longevity and mutations (allelic polymorphisms); however, statistical significance has been a challenge. Current studies in this field involve several thousand DNA samples both from the control and long-lived individuals. Only a single gene, the *APOE* gene, has been statistically linked to longevity ( $p < 5 \times 10^{-8}$ ) [42]. Among the associations with a lower statistical significance are elements of the insulin/IGF-1 signal pathway (AKT1, AKT3, FOXO4, IGF2, INS, PIK3CA, SGK, SGK2, YWHAG) and telomerase (POT1) [43]. Lifespan extension mutations have been recently reviewed by Newman [44].

Genome-wide analysis of long-lived individuals within a given species with controls allows one to identify the genes affecting longevity, but there are specific aspects. The benefit of this approach is that individuals recruited to such a study possess highly related genomes, which enables a differentiation between relevant and non-relevant mutations with a high statistical significance. The human genome of  $3 \times 10^9$  bp carries

several million individual polymorphic sites [45]. Using such tools as microarrays, up to 1,000,000 loci could be analyzed per individual. Due to the high number of differences, statistical significance is set at  $p < 10^{-8}$ . Yet, the drawback of such studies is the low variation in life expectancy. Genome analysis of different species could theoretically reveal the genes affecting the lifespan to a higher extent (several-fold). The lifespan of animals can vary up to 10,000-fold. For example, rotifers live several days, and the great polar whale's lifespan is up to 200 years. Genome analysis of species with various lifespans poses additional challenges. Even representatives of a single species carry millions of differences. The genomes of different species differ to a degree that makes their comparison, if at all possible, infeasible.

The lifespan potential can vary up to 10,000-fold only in organisms that dramatically differ in morphology and body size range. There is no point in attempting to discover genes affecting longevity between rotifers and the great polar whale. In general, the lifespan is significantly governed by body size [46].

A feasible approach to unraveling the genetic background behind longevity is to compare genetically related similar-sized species with various lifespans. Among small mammals, flying bats have a longer lifespan and marsupials have a shorter lifespan than expected. Birds and bats have a longer mean lifespan as compared to similar-sized terrestrial animals. This is likely due to lower susceptibility to predation. Early death disfavors selection for individuals with long-lived genetic backgrounds, whereas the lack of predation risks favors selection for long-lived individuals.

There are a handful of mammals that are distinguishable as unusually long-lived species with short-lived counterparts. The best-known example is the naked mole rat *H. glaber* with a maximum lifespan of over 30 years, which is a 9-fold difference to the related mouse. The naked mole rat is a burrowing rodent native to Africa. It is the only truly eusocial mammal such as ants or bees. Each underground colony, which rodents never leave, has a reproductive queen that stops other females from breeding. The other naked mole rats, workers and soldiers, feed the queen and protect the colony against neighbor colonies or snakes – the main predator of naked mole-rats. The naked mole-rat is insensitive to pain and cold, tolerant to low-oxygen environments containing only 8% oxygen and 25% carbon dioxide. These rodents are known to show high resistance to cancer and their mortality rates do not increase with age without apparent aging. The genome of the naked mole-rat has been determined by the laboratory of V. Gladyshev [47] and comprises 22,561 genes, with 750 genes acquired and 320 genes lost during evolution. A total of 244 pseudogenes–non-functional

genes—have been identified. Among the pseudogenes are gene clusters with homology to the genes involved in ribosomal and nucleotide synthesis pathways, olfactory and vision systems, spermatogenesis and, possibly, ubiquitination – ubiquitin tagging of proteins for degradation. The putative telomere or the telomerase genes *TEP1* and *TERF1* have been found to be unique to the genome of the naked mole-rat. Forty-five amino acid substitutions were found in 39 naked mole rat proteins, not occurring at the same positions in other mammals. These proteins include components of replication and DNA integrity systems: CCNE1, APEX1, RFC1, TOP2A. In addition, unique substitutions were detected in the genes of body temperature maintenance (UCP1) and vision (CRYGS). The genome of *H. glaber* contains 1.87 million polymorphic loci. The frequency of polymorphic variants is more similar to that observed in humans than in rats and mice related to the naked mole rat. The analysis of the expression profiles of 33 genes affected by aging in the human brain revealed that 32 of the corresponding genes of the naked mole-rat were not affected. Among these are the *CYP46A1* gene regulating cholesterol metabolism and amyloid plaque formation and the *SMAD3* gene encoding a transcription factor that delays cell division and promotes tumor growth. The naked mole rat has impaired melatonin secretion, which, similarly to melatonin-deficient mice, is consistent with down-regulation of the insulin/IGF-1 signal pathway. A consequence of adaptation to oxygen deprivation seems to be mutations in the hypoxia-induced factor (HIF1 $\alpha$ ) and VHL, a protein regulating HIF1 $\alpha$ . The genome of *H. glaber* is an interesting model for studying longevity genes.

Another long-lived mammal whose genome has been recently annotated by V. Gladyshev's laboratory [48] is the Brandt's bat. In view of the above, bats display an exceptional longevity relative to similar-sized mammals. The lifespan of the Brandt's bat is over 40 years, which is the longest on record in the context of the positive relationship between longevity and body size, given the bat weight of 4–8 g. The genome of this nocturnal insectivorous mammal contains 22,256 genes and 194 pseudogenes, comprising  $2 \times 10^9$  nucleotides. A total of 67 gene families significantly expanded, and 44 gene families contracted. Immunity-related genes within the expanded gene families deserve a closer look. In the course of evolution, the Brandt's bat acquired 349 genes and lost 98 genes. Some genes are involved in echolocation, visual adaptation to low light conditions, and hibernation. Putative lifespan extension mutations are detected in growth hormone receptors (GHR) and insulin-like growth factors (IGF1R). Mutations in the *IGF1R* gene (*daf-2*) have been found in long-lived mutants of *C. elegans*. The expression pro-

files of the indulin/IGF1 pathway, like *FOXO1*, in the Brandt's bat were shown to change in a similar fashion to mutant long-lived mice and to be typical of a slowed metabolism.

### SEA URCHINS AS A MODEL FOR COMPARATIVE GENOMICS OF LONGEVITY

Sea urchins belong to the phylum Echinodermata, the superphylum Deuterostomia as vertebrates. They are closer relatives to vertebrate animals than to such protostomes as arthropods and mollusks. Adult sea urchins possess a five-fold symmetry. Sea urchins are enclosed in a calcareous globe-shaped shell, consisting of rows of plates with a pentameric symmetry as well. The mouth is located on the underside and the anus, on the top of the body. The body is covered with flexible spines moved by species muscles. Sea urchins have received attention as a model for developmental biology. Sperm and oocytes are released into the sea water and could be produced under laboratory conditions. Fertilization occurs externally in water, followed by immediate cell division. These creatures stirred another wave of interest as long-lived individuals. *Strongylocentrotus franciscanus*, or the red sea urchin, is found in the Pacific Ocean along the North American coast in the cold California current. The exceptional longevity of this species has been confirmed. Tetracycline injected into the red urchin is deposited in the calcareous shell. One-year-post-injection collection and analysis of sea urchins allows one to evaluate annual growth bands. It was shown that a period of accelerated growth is followed by a pronounced slowdown [49].

A statistical analysis of variation in the body size of *S. franciscanus* made it possible to estimate the maximum lifespan. Larger sized individuals can survive into old age, exceeding at least 100 years. Another confirmation was obtained with radiocarbon distribution ( $^{14}\text{C}$ ) in the calcareous teeth of *S. franciscanus*. An enhanced amount of radiocarbon in the world ocean, due to nuclear-bomb testing in the 1950s, was used as a marker for evaluating the mean tooth growth in the red sea urchin for a period of over several decades [50]. Both studies [49, 50] demonstrated that *S. franciscanus* lives over 100 years. Importantly, only few species of sea urchins show an extended longevity. Another sea urchin found in the Pacific Ocean, *S. purpuratus*, sharing the habitat with *S. franciscanus*, displays a long lifespan of 50 years, but not so much as that seen in the red sea urchin. At the same time, the variegated sea urchin, *Lytechinus variegates*, lives only 3–4 years [51]. The dramatic disparity in longevity among related species holds prospect in using these animals as models for gaining insight into the genetic background of longevity.

**CONCLUSIONS**

Nearly all current theories of aging have in common the fact that the fundamental cause of aging is the accumulation of molecular damage brought about mainly by ROS, but the role of amyloid protein, glycation end-products, and lipofuscin is acknowledged as well. The current theories differ in the extent to which the buildup of waste is encoded in the genome and whether it is programmed death or this accumulation that is deemed to bear the costs of evolutionary benefits. In addition to damage itself, the rate of accumulation is

also of concern, which results from overall metabolic activity. The most significant changes in the longevity of model organisms prove to be mutations in metabolic pathways. Alongside the analysis of model organisms, it is possible to extend to a genome-wide analysis of long-lived animals and short-lived counterpart species. ●

*The work was financially supported by the ESN group and the Russian Science Foundation (grant № 14-24-00061).*

**REFERENCES**

1. Giorgio M., Migliaccio E., Orsini F., Paolucci D., Moroni M., Contursi C., Pelliccia G., Luzi L., Minucci S., Marcaccio M., et al. // *Cell*. 2005. V. 122. P. 221–233.
2. Skulachev V.P. // *IUBMB Life*. 2000. V. 49. P. 177–180.
3. Dufour E., Boulay J., Rincheval V., Sainsard-Chanet A. // *Proc. Natl. Acad. Sci. USA*. 2000. V. 97. P. 4138–4143.
4. Harman D. // *J. Gerontol.* 1956. V. 11. P. 298–300.
5. Skulachev V.P. // *Biochemistry (Mosc)*. 2007. V. 72. P. 1385–1396.
6. Harman D. // *J. Am. Geriatr. Soc.* 1972. V. 20. P. 145–147.
7. de Grey A.D. // *Bioessays*. 1997. V. 19. P. 161–166.
8. Barja G. // *Free Radic. Biol. Med.* 2002. V. 33. P. 1167–1172.
9. Andziak B., O'Connor T.P., Qi W., DeWaal E.M., Pierce A., Chaudhuri A.R., van Remmen H., Buffenstein R. // *Ageing Cell*. 2006. V. 5. P. 463–471.
10. Labunskyy V.M., Gladyshev V.N. // *Antioxid. Redox Signal*. 2013. V. 19. P. 1362–1372.
11. Schriener S.E., Linford N.J., Martin G.M., Treuting P., Ogburn C.E., Emond M., Coskun P.E., Ladiges W., Wolf N., van Remmen H., et al. // *Science*. 2005. V. 308. P. 1909–1911.
12. Sun J., Tower J. // *Mol. Cell Biol.* 1999. V. 19. P. 216–228.
13. van Raamsdonk J.M., Hekimi S. // *PLoS Genet*. 2009. V. 5. P. e1000361.
14. Gladyshev V.N. // *Bioessays*. 2012. V. 34. P. 925–929.
15. Gladyshev V.N. // *Trends Genet*. 2013. V. 29. P. 506–512.
16. Brunk U.T., Terman A. // *Eur. J. Biochem.* 2002. V. 269. P. 1996–2002.
17. Schachter F., Faure-Delanef L., Guenot F., Rouger H., Froguel P., Lesueur-Ginot L., Cohen D. // *Nat. Genet.* 1994. V. 6. P. 29–32.
18. Huang Y., Mucke L. // *Cell*. 2012. V. 148. P. 1204–1222.
19. Russo C., Violani E., Salis S., Venezia V., Dolcini V., Damonte G., Benatti U., D'Arrigo C., Patrone E., Carlo P., et al. // *J. Neurochem.* 2002. V. 82. P. 1480–1489.
20. Sell D.R., Monnier V.M. // *Gerontology*. 2012. V. 58. P. 227–237.
21. Monnier V.M., Sell D.R. // *Rejuvenation Res.* 2006. V. 9. P. 264–273.
22. Franceschi C., Bonafe M., Valensin S. // *Vaccine*. 2000. V. 18. P. 1717–1720.
23. Dilman V.M. // *Lancet*. 1971. V. 1. P. 1211–1219.
24. Dilman V.M., Anisimov V.N. // *Exp. Gerontol.* 1979. V. 14. P. 161–174.
25. Olovnikov A.M. // *Dokl Akad Nauk SSSR*. 1971. V. 201. P. 1496–1499.
26. Greider C.W., Blackburn E.H. // *Cell*. 1985. V. 43. P. 405–413.
27. Harley C.B., Futcher A.B., Greider C.W. // *Nature*. 1990. V. 345. P. 458–460.
28. Hayflick L., Moorhead P.S. // *Exp. Cell Res.* 1961. V. 25. P. 585–621.
29. Kim N.W., Piatyszek M.A., Prowse K.R., Harley C.B., West M.D., Ho P.L., Coviello G.M., Wright W.E., Weinrich S.L., Shay J.W. // *Science*. 1994. V. 266. P. 2011–2015.
30. McCay C.M., Crowell M.F., Maynard L.A. // *Nutrition*. 1989. V. 5. P. 155–171. Discussion 172.
31. Kenyon C., Chang J., Gensch E., Rudner A., Tabtiang R. // *Nature*. 1993. V. 366. P. 461–464.
32. Anisimov V.N. *Molecular and Physiological Mechanisms of Aging*. St. Petersburg.: Nauka, 2008. 481 p.
33. Finch C.E., Ruvkun G. // *Annu. Rev. Genomics Hum. Genet.* 2001. V. 2. P. 435–462.
34. Tissenbaum H.A., Guarente L. // *Nature*. 2001. V. 410. P. 227–230.
35. Weismann A. *Ueber die Dauer des Lebens, ein Vortrag*. Jena: G. Fischer, 1882. 94 p.
36. Skulachev V.P. // *Biochemistry (Mosc)*. 2012. P. 77. P. 827–846.
37. Boiko A.G. // *Zh Obshch Biol.* 2007. V. 68. P. 35–51.
38. Ziuganov V.V. // *Izv Akad Nauk Ser Biol.* 2005. V. 4. P. 435–441.
39. Popov I.Yu. // *Adv. gerontol.* 2009. V. 22. P. 596–604.
40. Fisher D.O., Double M.C., Blomberg S.P., Jennions M.D., Cockburn A. // *Nature*. 2006. V. 444. P. 89–92.
41. Kirkwood T.B.L. // *Nature*. 1977. V. 270. P. 301–304.
42. Brooks-Wilson A.R. // *Hum. Genet.* 2013. V. 132. P. 1323–1338.
43. Deelen J., Uh H.W., Monajemi R., van Heemst D., Thijssen P.E., Bohringer S., van den Akker E.B., de Craen A.J., Rivadeneira F., Uitterlinden A.G., et al. // *Age (Dordr)*. 2013. V. 35. P. 235–249.
44. Newman A.B., Murabito J.M. // *Epidemiol. Rev.* 2013. V. 35. P. 181–197.
45. Venter J.C., Adams M.D., Myers E.W., Li P.W., Mural R.J., Sutton G.G., Smith H.O., Yandell M., Evans C.A., Holt R.A., et al. // *Science*. 2001. V. 291. P. 1304–1351.
46. Austad S.N. // *Mech. Ageing Dev.* 2005. V. 126. P. 43–49.
47. Kim E.B., Fang X., Fushan A.A., Huang Z., Lobanov A.V., Han L., Marino S.M., Sun X., Turanov A.A., Yang P., et al. // *Nature*. 2011. V. 479. P. 223–227.
48. Seim I., Fang X., Xiong Z., Lobanov A.V., Huang Z., Ma S., Feng Y., Turanov A.A., Zhu Y., Lenz T.L., et al. // *Nat. Commun.* 2013. V. 4. P. 2212.
49. Ebert T.A. // *Exp. Gerontol.* 2008. V. 43. P. 734–738.
50. Ebert T.A., Southon J.R. // *Fish. Bull.* 2003. V. 101. P. 915–922.
51. Francis N., Gregg T., Owen R., Ebert T., Bodnar A. // *FEBS Lett.* 2006. V. 580. P. 4713–4717.

# Model Systems of Motor Neuron Diseases As a Platform for Studying Pathogenic Mechanisms and Searching for Therapeutic Agents

K. R. Valetdinova<sup>1,2,3,4</sup>, S. P. Medvedev<sup>1,2,3,4</sup>, S. M. Zakian<sup>1,2,3,4\*</sup>

<sup>1</sup>Institute of Cytology and Genetics, Prospekt Lavrentyeva, 10, Novosibirsk, 630090, Russia

<sup>2</sup>Institute of Chemical Biology and Fundamental Medicine, Prospekt Lavrentyeva, 8, Novosibirsk, 630090, Russia

<sup>3</sup>Meshalkin Novosibirsk State Research Institute of Circulation Pathology, Rechkunovskaya Str., 15, Novosibirsk, 630055, Russia

<sup>4</sup>Novosibirsk State University, Pirogova Str., 2, Novosibirsk, 630090, Russia

\*E-mail: zakian@bionet.nsc.ru

Received 10.10.2014

After revision 01.19.2015

Copyright © 2015 Park-media, Ltd. This is an open access article distributed under the Creative Commons Attribution License, which permits unrestricted use, distribution, and reproduction in any medium, provided the original work is properly cited.

**ABSTRACT** Over the past 30 years, many molecular genetic mechanisms underlying motor neuron diseases (MNDs) have been discovered and studied. Among these diseases, amyotrophic lateral sclerosis (ALS), which causes the progressive degeneration and death of central and peripheral motor neurons, and spinal muscular atrophy (SMA), which is one of the inherited diseases that prevail among hereditary diseases in the pattern of child mortality, hold a special place. These diseases, like most nerve, neurodegenerative, and psychiatric diseases, cannot be treated appropriately at present. Artificial model systems, especially those that are based on the use of embryonic stem cells (ESCs) and induced pluripotent stem cells (iPSCs), are of paramount importance in searching for adequate therapeutic agents, as well as for a deep understanding of the MND pathogenesis. This review is mainly focused on the recent advance in the development of and research into cell and animal models of ALS and SMA. The main issues concerning the use of cellular technologies in biomedical applications are also described.

**KEYWORDS** amyotrophic lateral sclerosis; induced pluripotent stem cells; motor neurons; spinal muscular atrophy; embryonic stem cells.

**ABBREVIATIONS** MND – motor neuron disease; ALS – amyotrophic lateral sclerosis; FTD – frontotemporal dementia; iPSCs – induced pluripotent stem cells; SMA – spinal muscular atrophy; ESCs – embryonic stem cells; CNS – central nervous system.

## INTRODUCTION

In the central nervous system (CNS), motor neuron bodies are located in the motor cortex (upper or central motor neurons), in the nuclei of the cranial nerves of the brainstem, and in the anterior horns of the gray matter of the spinal cord (lower or peripheral motor neurons). The processes of these neurons (axons), being a part of the conduction tracts (pyramidal and extrapyramidal tracts), anterior roots of the spinal cord, and peripheral nerves reach the skeletal muscles to form the neuromuscular junction on muscle fibers that are innervated by these cells.

Neurodegenerative diseases that affect primarily this group of nerve cells are called motor neuron diseases (MNDs). These diseases are usually characterized

by muscle atrophy and palsy that result in the death of patients [1]. Degenerative processes associated with spinal muscular atrophy (SMA), progressive muscular atrophy, spinal and bulbar muscular atrophy (Kennedy's disease), and hereditary motor neuropathies affect lower motor neurons and their processes [2]. Upper motor neurons are mainly affected by primary lateral sclerosis, hereditary spastic paraplegia, progressive bulbar and pseudobulbar palsy, and spinal muscular atrophy with respiratory distress type I [2, 3]. Both the central and peripheral motor neurons are involved in the pathological process associated with amyotrophic lateral sclerosis (ALS) [1].

Of greatest interest are SMA, which is the most common inherited neurodegenerative disease, par-

ticularly in children, and ALS, which is an extremely heterogeneous disease whose molecular mechanisms are understudied. The challenging issue is to develop adequate model ALS and SMA systems, since investigation of pathological processes in CNS cells caused by motor neuron diseases is currently impossible due to the lack of non-invasive and safe intravital techniques, while a postmortem examination of patient tissues provides insight only into the terminal stages of the disease. The problem can be solved in two ways.

The first path is to generate animal models that express the human genes involved in the pathogenesis of these diseases. However, such model systems, for obvious reasons, do not have all the genotypic and phenotypic features typical of human MND. Therefore, the second approach is an actively developed one that is based on the production of motor neurons derived from human pluripotent cells possessing a particular phenotype of ALS or SMA.

So-called pluripotent cells have the capability of differentiating into derivatives of all three primitive germ layers (entoderm, mesoderm, and ectoderm), cells of the inner cell mass (ICM), and the epiblast of mammalian embryos before [4] and after implantation [5], as well as embryonic germ cells. Cells derived from ICM and the epiblast of preimplantation embryos, which are cultured *in vitro* and preserve the properties of their precursors for a long time, were called embryonic stem cells (ESCs). The first human ESC lines were produced in 1998 [6].

In 2006, a group of Japanese scientists led by S. Yamanaka developed a method for reprogramming somatic cells to a pluripotent state by the expression of four factors: Oct3/4, Sox2, c-Myc, and Klf4 [7]. The characteristics of the resulting cells were close to those of ESCs, and, therefore, the cells were called induced pluripotent stem cells (iPSCs).

ESC- or iPSC-derived motor neurons serve as a platform not only for modeling diseases, but also for screening drugs and developing therapy techniques for MNDs and spinal cord injuries [8, 9]. They can be used in cell replacement therapy for affected nerve cells, as well as microenvironment components producing neurotrophic factors and processing toxic metabolites. The therapeutic effect of the transplantation of neural stem cells, which exert a paracrine effect on the immediate cell environment, was observed in several models of neurodegenerative diseases [10, 11]. To enhance this effect, production of certain neurotrophic factors *in vitro* can artificially be modulated. In this case, the transplanted cells will secrete recovery-associated factors into damaged tissue, as it was demonstrated in an ALS model in rats (Gly93Ala) transplanted with human

neural progenitor cells expressing the glial-derived neurotrophic factor (GDNF) [12].

This review describes the main known model systems of ALS and SMA. Particular attention is focused on *in vitro* systems as well as on the application of cell technologies in practice.

## AMYOTROPHIC LATERAL SCLEROSIS

### General characteristics

Amyotrophic lateral sclerosis (ALS) (also known as Lou Gehrig's disease) was first described in detail by the prominent French doctor, a specialist in the field of neurological diseases, Jean-Martin Charcot in 1869. The very name reflects the distinctive features of the disease: muscle atrophy (amyotrophic) due to selective injury to peripheral motor neurons of the anterior horns of the spinal cord and the brainstem motor nuclei, as well as cortical motor neurons and the lateral columns of the spinal cord (lateral sclerosis) [13]. Patient death usually occurs due to complete failure of the respiratory muscles 2–5 years after the onset of the first symptoms [14].

ALS is an orphan disease whose rate in different populations ranges from one-two to four-six cases per 100,000 people per year [15–17]. Currently, about 25,000 patients with a mean age of 55 years are listed in the U.S. for ALS. In addition, ALS occurs in males more often than in females (3 : 2 ratio) [18].

Sporadic and familial (or inherited) forms of ALS can be distinguished, with the fraction of the sporadic form accounting for about 90% of all cases of the disease. The risk factors for ALS include the influence of heavy metals and toxins (e.g., the natural cyanobacteria toxin  $\beta$ -N-methylamino-L-alanine), smoking, severe traumatic brain injuries, increased motor activity, latent viral and non-viral infections, and autoimmune reactions [19–26].

According to modern concepts, the inherited form of ALS is linked to mutations in 12 genes [1]. In total, the development of ALS is associated with mutations in 116 genes, which are presented in the constantly updated Amyotrophic Lateral Sclerosis Online Database (ALSoD) [27]. These are mainly single nucleotide substitutions in the coding region of genes, deletions, insertions, and expansion of repetitive sequences. The most common genetic causes of ALS include expansion of the GGGGCC hexanucleotide repeats in the first intron/promoter of the *C9ORF72* gene [28–30], as well as mutations in the genes *SOD1* (*superoxide dismutase 1*, encodes Cu/Zn-binding superoxide dismutase 1) [31], *TDP-43* (*TAR DNA-binding protein 43*) [32], *FUS* (*fused in sarcoma*, RNA-binding protein FUS) [33, 34], *ANG* (*angiogenin*, ribonuclease) [35],

*OPTN* (*optineurin*) [36], and *VCP* (*valosin containing protein*) [37].

SOD1 is expressed in all cell types and localized in the cytoplasm. This protein catalyzes the conversion of the superoxide anion-radical into free oxygen and hydrogen peroxide. *SOD1* gene mutations are the most numerous ones (more than 160) [1], but not all of them lead to the formation of a non-functional protein product that would explain the key role of oxidative stress and mitochondrial dysfunction in the ALS pathogenesis. TDP-43 and FUS are multifunctional proteins involved in gene expression and regulation of expression, including transcription, RNA processing, transport and translation, as well as miRNA synthesis. Cytoplasmic aggregates of TDP-43 and FUS are detected in patients with frontotemporal dementia (FTD) [38, 39]. The protein product of *ANG* gene is involved in transcriptional regulation. ALS-associated mutations of *OPTN* activate the transcription factor NF- $\kappa$ B and also affect the distribution of optineurin in the cytoplasm. *VCP* is involved in a variety of cellular processes, including the cell cycle regulation, formation of the nuclear envelope, and Golgi biogenesis. It is also a component of the ubiquitin-dependent proteolytic system [40].

ALS affects not just motor, but also other types of neurons, and some ALS forms are combined with FTD or degeneration of the dopaminergic neurons located in the midbrain structures in the basal ganglia (striatum), limbic system (hippocampus), and hypothalamus. Histological changes in several types of neurons, including cells of the hippocampus and basal ganglia, are detected even in patients whose clinical picture is dominated by dysfunction of the motor system [41].

However, despite numerous studies, there are still no methods of effective therapy for ALS, and treatment is actually limited to relieving the symptoms. For example, the drug riluzole, a glutamate-release inhibitor exhibiting neuroprotective properties, can modulate the course of ALS, increasing the lifespan of patients by 2–3 months, but without relieving the symptoms [42]. The NeuRx Diaphragm Pacing System is approved for use in the USA. This system enables to extend, for several months, the time during which ALS patients can breathe independently without mechanical ventilation.

The development of appropriate model ALS systems should help search for effective drugs and answer the question of how these diverse molecular changes lead to selective death of motor neurons.

### Main laboratory ALS models

The generation of animal ALS model systems has made it possible to deepen our understanding of the disease and to identify a number of mechanisms leading to the

development of ALS, including mitochondrial dysfunction, protein misfolding (wrong packaging) and protein aggregation, oxidative stress, glutamate excitotoxicity, non-cell-autonomous effects, inflammatory processes in the nervous tissue, axonal transport dysfunction, RNA processing dysfunction, etc (*Fig. 1*).

Mice carrying mutations in the *SOD1* gene were generated in the early 1990s [31]. Mice and rats with various mutations in this gene are the most thoroughly studied animal model of ALS (*Table 1*). These animals have a lethal phenotype with a late onset. The phenotype is characterized by muscle denervation, activation of astrocytes and microglia, and loss of motor neurons in the spinal cord. This phenotype can be induced by overexpression of the mutant SOD1 protein; therefore, animals overexpressing the normal protein should serve as a control in these experiments.

The effects of TDP-43 insufficiency have been studied in different model organisms (*Table 1*). TDP-43 knockout in *Drosophila melanogaster* leads to a variety of neuromuscular defects [43], and TDP-43 knockdown in zebrafish (*Danio rerio*) causes decreased motor axons length and branching [44]. In mice, homozygous deletion of the *Tardbp* gene, which encodes TDP-43, is lethal, but only moderate motor defects are observed in heterozygous animals [45]. Overexpression of mutant TDP-43 in yeast, nematodes, and *D. rerio* induces more serious disturbances compared to normal protein overexpression [44–46]. An elevated expression of the normal or mutant TDP-43 protein in rodents led to the formation of a phenotype with cortical disorders with the involvement, in a number of cases, of peripheral motor neurons [47–51]. Overexpression of TDP-43 in the spinal cord of the cynomolgus monkey (*Macaca fascicularis*) induced a progressive loss of motor neurons [52].

Some deletions in the *Fus* gene in mice were demonstrated to be lethal or to induce a phenotype not associated with neurodegeneration [53, 54]. Mice with FUS knockout in hippocampal neurons have a reduced amount of dendrites and pronounced morphological defects of these processes [55]. Overexpression of the normal human FUS protein in transgenic mice caused active degeneration of motor neurons that was characterized by the formation of globular and “skein-like” FUS-positive inclusions in the motor neurons [56]. In rats, overexpression of FUS with an Arg521Cys mutation led to the death of cortical, hippocampal, and motor neurons, as well as to denervation and development of palsies [57].

Therefore, these ALS models demonstrate the important role of the proteins SOD1, TDP-43, and FUS in the functioning of different cells of the nervous system, including motor neurons.

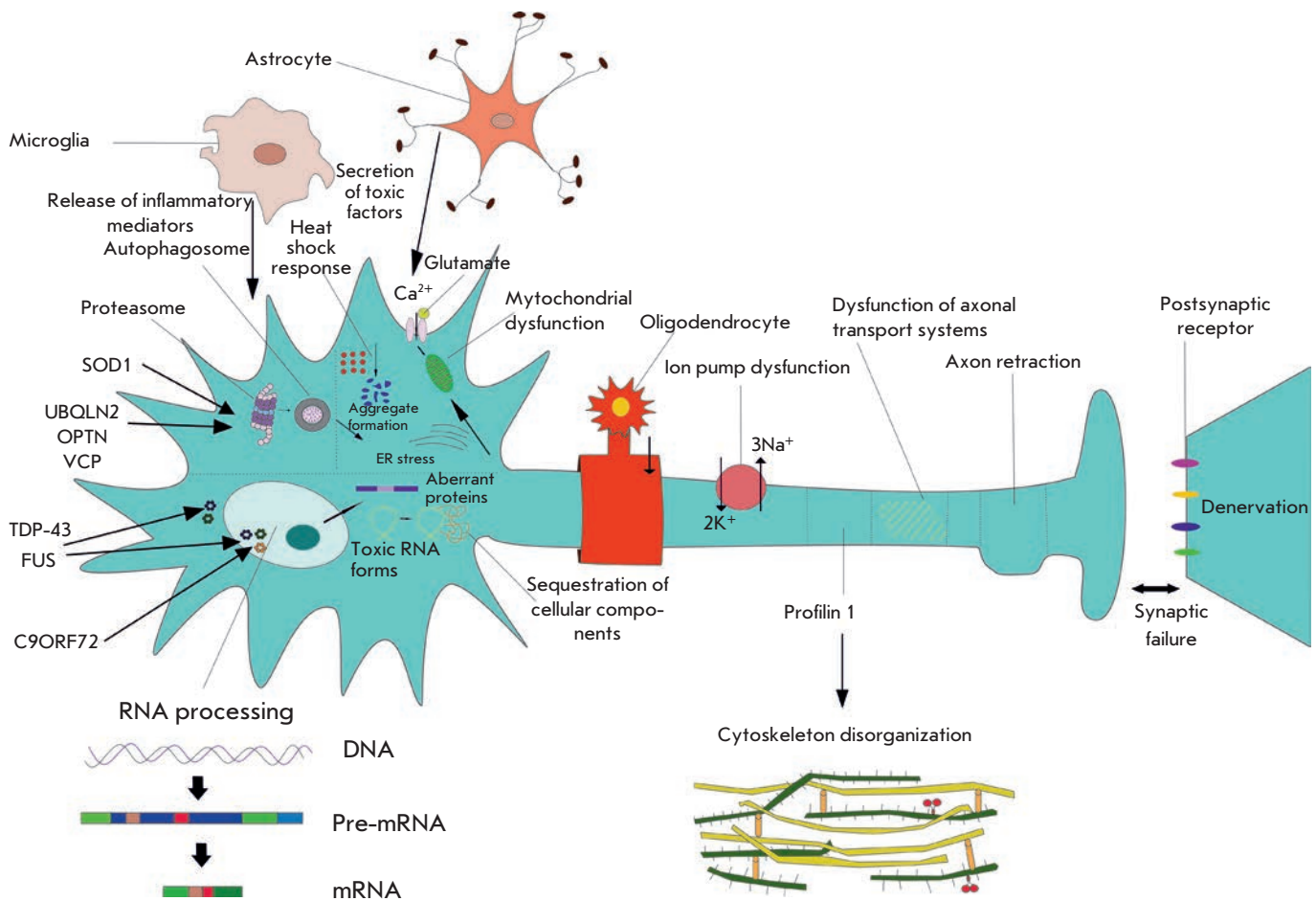


**Fig. 1.** A general scheme of ALS etiopathogenesis. Mutations in *SOD1*, *VCP*, *UBQLN2*, *OPTN*, *CHMP2B*, and, possibly, *TARDBP* cause changes in protein degradation systems, disrupting the normal proteasomal and autophagic disposal. Mutations in *C9ORF72*, *TARDBP*, and *FUS* disturb RNA processing that leads to the formation of a large number of aberrant (incorrectly assembled) proteins and toxic RNA forms. These changes lead to intracellular proteinopathy that is characterized by the development of clusters and granules, endoplasmic reticulum and Golgi stress, and mitochondrial dysfunction. Disorganization of the axonal cytoskeleton and dysfunction of the axonal transport systems lead to denervation of motor neurons located downstream in the signal transmission chain (peripheral motor neurons), or muscle fibers. Cells that do not belong to neurons, including astrocytes, microglia, and oligodendrocytes, modify this process, because they cannot provide normal functioning of nerve cells and, in addition, possess a toxic effect. Factors determining the level of sensitivity to damages, including factors that modulate the type of stress response (activation of heat shock proteins) and provide "predisposition" to excitotoxicity (features of glutamate receptors) define exactly which neurons will be affected by these processes to the greatest extent. The effect of proteins, such as profilin 1 and the neurofilament heavy chain (NFH), on this model is revealed at a considerable distance from the nerve cell body. They directly affect the cytoskeleton and *D*-amino acid oxidase, which plays an important role in excitotoxicity. The systems involved in the signaling processes of axonal "targeting" (e.g., semaphorin family proteins) as well as in determining the topography of connections in the nervous system (e.g., proteins of the ephrin and reticulon families) apparently trigger the processes of axon retraction and denervation

**ALS cell models**

To date, cell models of both the hereditary and sporadic forms of ALS have been generated (Table 2). However, technologies and approaches that use a patient's iPSCs

are mainly utilized not for a direct searching for therapy approaches, but for the identification and profound analysis of the pathogenic mechanisms of this neurodegenerative disease.

**Table 1.** Animal models of amyotrophic lateral sclerosis

| Model object  | Gene  | Phenotype   | Reference            |
|---|---|---|----------------------|
| <i>Saccharomyces cerevisiae</i>   | <i>SOD1</i> ,<br><i>TARDBP</i> , <i>FUS</i>                     | Damage of mitochondrial membrane integrity, TDP-43 and FUS aggregation.   | [155–158]            |
| <i>Caenorhabditis elegans</i>   | <i>SOD1</i> ,<br><i>TARDBP</i> , <i>FUS</i> ,<br><i>tdp-1</i>   | Uncoordinated movements and locomotor impairments, palsy, degeneration of motor neurons, synaptic transmission failure, nuclear accumulation of TDP-43 aggregates, SOD1 aggregation.  | [159–164]            |
| <i>Drosophila melanogaster</i>  | <i>SOD1</i> ,<br><i>TARDBP</i> , <i>FUS</i>                     | Motor defects, stress activation of glial cells, SOD1 aggregation, gliosis, axonal degeneration, neuronal atrophy. In general, the effects vary depending on the tissue that expresses normal/mutant SOD1, TARDBP and FUS proteins. | [165–173]            |
| <i>Danio rerio</i>  | <i>SOD1</i> ,<br><i>TARDBP</i> , <i>FUS</i> ,<br><i>Sod1</i>    | Motor defects, muscular atrophy, loss of motor neurons, reduced survival.   | [174–176]            |
| <i>Mus musculus</i><br><i>Rattus norvegicus</i>   | <i>TARDBP</i> ,<br><i>SOD1</i> , <i>Sod1</i> ,<br><i>Tardbp</i> | ALS phenotype: tremor, progressive motor disorders and palsy, gliosis, ubiquitinated SOD1 inclusions, degeneration of axons and motor neurons, vacuolization of mitochondria, rare cytoplasmic aggregates of phosphorylated TDP-43. | [48, 51,<br>177–192] |
| Dog breeds: Pembroke<br>Welsh corgi, Boxer,<br>Rhodesian ridgeback,<br>German Shepherd,<br>Chesapeake Bay | <i>SOD1</i>   | Degenerative myelopathy of dogs: inclusions capable of binding with SOD1 antibodies are observed in the cytoplasm of neurons; demyelination of the white matter of lateral cords and axonal loss.                                   | [193, 194]           |
| <i>Macaca fascicularis</i>  | <i>TDP-43</i>   | Accumulation of TDP-43 aggregates and cystatin C-positive granules in the cytoplasm; progressive motor weakness of the distal portions of the upper extremities, fasciculations and atrophy.  | [52]                 |

**Cell models of the inherited ALS form**

**SOD1.** Motor neurons containing the *SOD1* gene with an Asp90Ala mutation demonstrate signs of neurofilament aggregation that lead to the degeneration of neurites [58]. The mutant SOD1 protein was found to be capable of binding to the 3'-untranslated region of mRNA of one of the neurofilament components, NF-L, decreasing the mRNA stability. Thereby, the proportion of individual subunits of neurofilaments in motor neurons is disturbed. This is the interaction that can trigger a chain of events that lead to selective death of motor neurons [58].

Defects in the mitochondrial transport system and changes in the mitochondrial morphology have been found in motor neurons with an Ala4Val missense mutation in the *SOD1* gene. Manifestations of oxidative stress and endoplasmic reticulum stress, as well as activation of the unfolded protein response (UPR), were observed in these cells [59]. Furthermore, an analysis of high-throughput mRNA sequencing using the DAVID and GSEA platforms demonstrated that gene transcription in motor neurons with the *SOD1*<sup>+/A4V</sup> genotype is altered compared to the isogenic control without this mutation. Motor neurons with a *SOD1* mutation had an increased transcription level of genes encod-

ing contractile proteins, in particular kinesins, as well as the genes involved in cytoskeleton formation and transcription regulation. In this case, the transcription level of the genes involved in the functioning of mitochondria and translation was significantly decreased in these cells [59].

An electrophysiological study of iPSC-derived motor neurons with mutations in the *SOD1* gene, as well as in *C9ORF72* and *FUS*, revealed the hyperexcitability of their membranes that may be the main element of the ALS pathogenesis, leading to the death of motor neurons [60]. A decrease in the amplitude of the delayed-rectifier potassium current was observed in these cells, which might be the cause of the hyperexcitability of their membranes. The use of a potassium channel activator, retigabine, blocked the hyperexcitability and increased the degree of survival of motor neurons with mutations in the *SOD1* gene [60].

Screening of mouse ESCs with mutations in *SOD1* revealed a number of potential drugs [61]. A relationship between glycogen synthase kinase 3 (GSK-3) and ALS was previously identified [62]. Inhibition of the GSK-3 pathway was found to reduce neuronal apoptosis [63, 64]. One of the inhibitors of this pathway, kenpaullone, caused a significant increase in the viability of mouse motor neurons with mutations in *SOD1*, and

**Table 2.** Cell models of amyotrophic lateral sclerosis

| Gene           | Mutation  | Phenotype  | Reference               |
|----------------|---|--|-------------------------|
| <i>TDP-43</i>  | Met337Val<br>Gln343Arg<br>Gly298Ser   | Reduced survival, increased sensitivity to PI3K kinase inhibition, elevated level of the TDP-43 protein.   | [65, 68–70]             |
| <i>SOD1</i>    | Gly85Ser<br>Leu144Phe<br>Ala4Val<br>Asp90Ala<br>Asn87Ser<br>Ser106Leu       | Hyperexcitability of membranes, neurofilament aggregation, mitochondrial dysfunction, oxidative stress and endoplasmic reticulum stress.                                 | [58, 60, 146, 195, 196] |
| <i>FUS</i>     | His517Gln   | Hyperexcitability of membranes, FUS aggregates.  | [60]                    |
| <i>C9ORF72</i> | Expansion of the GGGGCC hexanucleotide repeat in the first intron/promoter. | Abnormal electrophysiologic indicators, hyperexcitability of membranes, formation of focal granules of <i>C9ORF72</i> RNA containing hnRNPA1 and Pur- $\alpha$ proteins. | [60, 71]                |
| Sporadic form  |   | Intranuclear aggregates of the hyperphosphorylated TDP-43 protein.   | [75]                    |

it also increased the degree of survival of the motor neurons produced after differentiation of these iPSCs of ALS patients [61].

In addition, the primary culture of mouse glial cells expressing a mutant (Gly93Ala) human SOD1 protein exerts an increased toxic effect on motor neurons. Most likely, the ALS pathogenesis occurs through a non-autonomous mechanism in the case of mutations in *SOD1* [65, 66].

**TDP-43.** TDP-43 protein aggregates in motor neurons are detected in 97% of ALS cases and in 45% of FTD cases [67]. Motor neurons derived from iPSCs with a Met337Val missense mutation in the *TDP-43* gene were found to have an increased level of the soluble and detergent-resistant TDP-43 protein, reduced survival in long-term cultivation, and also increased sensitivity to PI3K kinase inhibition [68].

Investigation of astrocytes produced from mutant iPSCs (Met337Val) demonstrated an increased level of the TDP-43 protein in astrocytes, same as in motor neurons, with protein aggregates being mainly found in the cytoplasm of the cells. These cells also showed reduced survival in the culture [65]. The co-culture of mutant astrocytes with control and mutant motor neurons demonstrated that the presence of astrocytes does not affect the viability of motor neurons. This indicates that the ALS pathogenesis occurs via the cell-autonomous pathway in the case of mutations in *TDP-43* [65].

Motor neurons differentiated from patient iPSCs carrying Met337Val, Gln343Arg, and Gly298Ser mutations in *TDP-43* had an increased amount of the insoluble TDP-43 protein bound to the SNRNP2 spliceosomal protein [69]. Furthermore, these cells had an increased

transcriptional level of the genes involved in the RNA metabolism and a reduced transcriptional level of the genes encoding cytoskeleton proteins. Four compounds that are inhibitors of the enzymes involved in covalent modification of chromatin and the proteins associated with RNA splicing were tested: trichostatin A (histone deacetyltransferase inhibitor), spliceostatin A (inhibitor of spliceosomal proteins), anacardic acid, and garcinol (histone acetyltransferase inhibitors). Anacardic acid appeared to be capable of increasing the chance of survival of mutant motor neurons, decreasing the transcriptional level of the *TDP-43* gene mRNA and the TDP-43 protein level in the insoluble fraction, as well as increasing the length of motor neuron neurites [69].

iPSCs can be used not only to search for new compounds as potential drugs for ALS, but also to explore alternative modes of therapy; e.g., via RNA interference. Based on the design of small interfering RNAs (siRNA) designated for allele-specific suppression of the translation of a mutant (Met337Val) TDP-43 protein [70], the use of siRNA was demonstrated to be capable of a 30% reduction in the cytoplasmic TDP-43 protein level in neural stem cells derived from patient iPSCs [70].

**C9ORF72.** RNA of the mutant *C9ORF72* gene with an abnormal number of GGGGCC hexanucleotides in the first intron/promoter can also initiate a pathological process associated with ALS. An increased transcriptional level of *C9ORF72*, as well as the formation of focal accumulations of *C9ORF72* RNA, containing, among other things, hnRNPA1 and Pur- $\alpha$  RNA-binding proteins, was observed in motor neurons produced after

the differentiation of iPSCs from patients with the C9-ALS familial form (hexanucleotide repeat expansion in the *C9ORF72* gene) [71]. hnRNPA1 is known to bind to TDP-43 molecules [72]. Therefore, the interaction of TDP-43 with its target RNAs probably changes upon removal of hnRNPA1 from focal accumulations. Therefore, there is a potential relationship between two ALS forms (C9-ALS and TDP-43-mediated ALS). Furthermore, mutations in the hnRNPA1 and hnRNPA2/B1 proteins were found to be one of the causes of MND in humans [73]. What is more, Pur- $\alpha$  was shown to interact with focal accumulations of RNAs containing the GGGGCC repeats and to modulate the toxic effect of similar structures in an ALS model in *D. melanogaster* [74]. Cells expressing mutant RNA of the *C9ORF72* gene had an altered expression level of the genes associated with the membrane excitability, in particular *DPP6*, and had abnormal electrophysiological indicators. The use of antisense oligonucleotides complementary to RNA of the *C9ORF72* gene enabled the suppression of the formation of focal accumulations and recovery of the normal level of gene transcription in motor neurons [71]. These studies exemplify the fact that differentiated derivatives of iPSCs can be used to search for and explore potential drugs [61, 69].

### Cell models of the sporadic ALS form

Using patients with the sporadic ALS form, Burkhardt *et al.* [75] produced iPSC lines with a unique genetic and epigenetic background. The formation of hyperphosphorylated aggregates of the TDP-43 protein was observed in the nuclei of motor neurons differentiated from these cells after 2 months of cultivation [75], but no accumulation of ubiquitin-labeled TDP-43 granules was found. This suggests that TDP-43 is exposed to ubiquitination at the later stages of proteinopathy compared to hyperphosphorylation. The authors note that it is important to differentiate iPSCs derived from different patients not only into motor neurons, but also into other cell types in order to investigate the causes behind the wide variety of sporadic ALS cases. This model is of particular interest for the search for therapeutic agents and factors that modify ALS.

## SPINAL MUSCULAR ATROPHY

### General characteristics

Spinal muscular atrophy (SMA) is a neurodegenerative disorder with an autosomal recessive mode of inheritance that is characterized by degeneration of motor neurons in the anterior horns of the spinal cord that leads to muscle atrophy, palsy, and death of the patient [76–78]. Spinal muscular atrophy in children was first described by G. Werdnig in 1891. The disease's fre-

quency in European populations is 1 per 10,000 newborns, and the carrier frequency of the mutant gene is 1 per 40–50 [79].

Over 95% of SMA patients have a homozygous deletion in the *SMN1* (*Survival Motor Neuron 1*) gene located on chromosome 5, while inversions, reading frame shift mutations, missense mutations, nonsense mutations, and splicing site changes occur only in a few cases [80, 81]. A full list of known mutations of the *SMN1* gene is available in the Leiden Open Variation Database ([http://www.dmd.nl/nmdb2/home.php?select\\_db=SMN](http://www.dmd.nl/nmdb2/home.php?select_db=SMN)). The *SMN2* pseudogene, which differs from *SMN1* only in eight single nucleotide substitutions by one in the seventh and eighth exons, and the other substitutions occurring in introns, is located on the same chromosome [82]. A C/T transition in exon 7 leads to a change in the splicing of the *SMN2* transcript, such that 90% of translated RNAs do not contain exon 7, and the protein product is unstable and shortened [83, 84] (Fig. 2). In this case, the number of pseudogene copies in the genome of different individuals can vary from 0 to 6. The larger the number of *SMN2* copies, the lesser the severity of SMA symptoms [85–87]. The *SMN2* gene significance for the development of a more mild form of spinal muscular atrophy is confirmed by asymptomatic cases when the number of *SMN2* gene copies is sufficiently large (four or more) in individuals homozygous for deletion of the *SMN1* gene [88].

Depending on the age of onset, severity, and lifespan, the following disease types are distinguished [89]:

Type I (Werdnig-Hoffmann disease) is the most severe form that manifests itself during the first 6 months of life and is characterized by pronounced signs of palsy of the limb and trunk muscles, as well as the respiratory muscles; children are unable to sit and to keep their head independently. The lifespan for this disease form does not exceed 2 years.

Type II is an intermediate form that has a later onset, usually at the age of 7–18 months. Sick children are capable of sitting independently but do not achieve the ability to walk. The lifespan is more than 2 years.

Type III (Kugelberg-Welander disease) is a mild/moderate form. The first symptoms emerge after 18 months. Patients are able to achieve independent standing and walking.

Type IV is an adult form. In most cases, it starts after 20–30 years and does not significantly affect the lifespan. It manifests itself in weakness of the proximal muscles, fasciculations (involuntary, chaotic contractions of individual groups of muscle fibers), as well as reduced tendon reflexes.

A *SMN1* gene protein product performs several functions in the cell: it is involved in pre-mRNA splicing, mature mRNA transport, and axonal growth

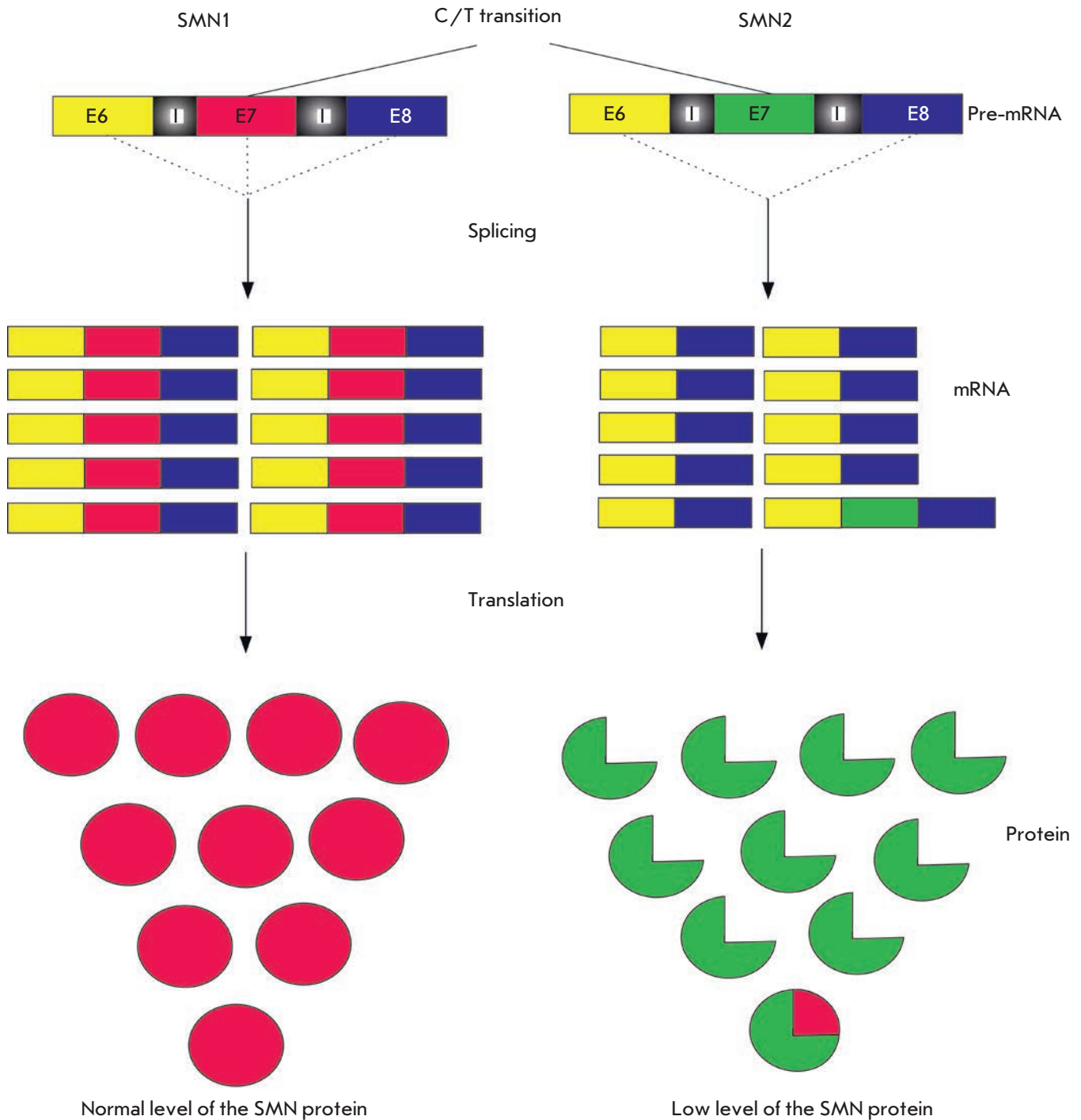


Fig. 2. Expression of the SMN1 and SMN2 genes (see the text for the description)

[90–94]. SMN is a central component of the complex required for assembly of spliceosomal small nuclear ribonucleic particles (snRNPs) [95]. An association of spliceosomal components with each other in every splicing cycle is known to occur *ex novo* each time through stepwise assembly, which means that mutant SMN

cannot provide effective assembly of snRNPs. Therefore, one of the hypotheses used to explain the SMA mechanism is based on the assumption that impaired snRNP formation affects the splicing of a specific group of genes that are important for the functioning of a motor neuron chain [95–97].

An axonal isoform of a protein product of the *SMN1* gene (a-SMN) was discovered in 2006 [98]. The axonal SMN transcript differs from the full-length transcript by the inclusion of the intron 3 sequence, but the protein translated from this transcript is shorter than the SMN protein because of the stop codon located on the boundary of exon 3 and intron 3. Therefore, the SMN and a-SMN proteins have an identical N-terminal region and a different C-terminal region. The a-SMN-protein was found to be selectively expressed in the critical phase of motoneuron development and to be localized mainly in axons, stimulating axonogenesis. Expression of this protein is reduced in adults [98]. However, the existence of the specific neuronal a-SMN isoform does not explain the important fact of a lacking exon 7 in the *SMN2* gene mRNA in most SMA cases, because only the first four exons in a-SMN are encoding ones [99]. Therefore, the second hypothesis suggests that SMA is associated with impairment of the important function that is performed by SMN in the axons of motor neurons [91, 94–97, 99, 100]. Therefore, what is the cause of the selective death of a motor neuron in the presence of *SMN1* mutations? And how can we help SMA patients? Artificial model systems should help answer these questions.

**Main animal SMA models**

The SMN protein deficiency has been studied in several model organisms (Table 3). However, working with animals is complicated by the fact that their genomes contain only one *Smn* gene that is equivalent to the human *SMN1* gene, and they do not have the *SMN2* gene. For this reason all *Smn* knockout animals die, and the time of death is determined by the *SMN1* mRNA level inherited by a new organism from the mother. For ex-

ample, death in mice occurs at the early stages of development [101], and death in egg-laying organisms, e.g. in *D. melanogaster*, occurs later, when the SMN protein level inherited from the mother decreases to a critical point [102]. As expected, *Smn* knockout in a specific tissue leads to the maldevelopment of this tissue and loss of a larger portion of its cellular component [103–105]. Additional copies of *SMN2* are usually inserted into the genome of transgenic mice with SMA. Two copies of this gene ensure a greater chance of survival of embryos, while eight copies result in mice with a normal phenotype [106, 107]. Two *SMN2* copies were shown to be sufficient for the normal functioning of most tissues; however, motor neurons require a higher SMN level, at least in mice [108].

To conduct laborious experiments, invertebrates and vertebrates are usually used that do not belong to the class of mammals. For example, full-scale molecular genetic screening of chemical agents, potential drugs, is easier to conduct in *C. elegans* and *D. melanogaster*. So, a nematode with a *smn-1(cb131)* mutation was used for selection of three substances that most effectively alter a mutant phenotype: 4-AP (potassium channel blocker), gaboxadol hydrochloride (GABA<sub>A</sub> receptor agonist), and Neu5Ac monosaccharide [109]. Therefore, this model can serve as a basis for the screening of compounds that modify the functions of the *Smn* protein.

The influence of the most effective substances is further studied in more complex objects: in particular in *D. rerio* and mice. There are data indicating that the RhoA GTP-ase and its effector, Rho-kinase (ROCK), involved in cytoskeleton formation are of great importance upon diseases of motor neurons. Introduction of ROCK inhibitors into mice with SMA increased their lifespan and improved the state of their neuromuscular

**Table 3.** Animal models of spinal muscular atrophy

| Object                           | Manipulations with the <i>SMN (Smn)</i> gene   | Phenotype   | Reference           |
|----------------------------------|--|---|---------------------|
| <i>Schizosaccharomyces pombe</i> | Knockout   | Death   | [197–199]           |
| <i>Caenorhabditis elegans</i>    | Knockout, knockdown, point mutations.  | Embryonic death, developmental defects, motor defects, decreased life span.   | [109, 200, 201]     |
| <i>Drosophila melanogaster</i>   | Point mutations equivalent to silent alleles, mutations disorganized <i>Smn</i> protein in adult flies, knockdown.   | Embryonic death, loss of the ability to fly and jump.   | [102, 112, 202]     |
| <i>Danio rerio</i>               | Knockdown  | Death, defects of axon development.   | [91]                |
| <i>Mus musculus</i>              | Knockout, directed alteration of expression in specific tissues at a specific period of time, introduction of transgenes of the human <i>SMN1</i> gene with known missense mutations, introduction of additional copies of <i>SMN2</i> . | Embryonic death, apoptosis of a cellular component of the tissue that does not express <i>Smn</i> , a phenotype varies depending on the mutation type and the presence of additional transgenes, two copies increase the life span of embryos up to 5 days. | [101, 103–107, 203] |

synapses and skeletal muscle fibers [110]. These findings have been confirmed in humans. For example, a genome-wide methylation analysis revealed significant differences in the DNA methylation level of two genes, *CHML* and *ARHGAP22*, in SMA patients and healthy individuals. The products of these genes regulate the function of the Rho and Rab GTP-ases that are regulators of actin dynamics, and, therefore, they can affect initiation, growth, direction, and branching of axons [111].

The results obtained in various animal SMA models should be interpreted with caution. For example, survival of the SMN-deficient flies *D. melanogaster* can be achieved by expression of this protein in the muscle tissue [102, 112]. But, there is no such effect in SMA mice with expression of SMN in muscles [108]. However, it can be noted that SMN in these experiments was expressed in the mesodermal progenitors of muscle fibers in *D. melanogaster* and in already formed muscle fibers, which no longer divided, in mice.

### Cell SMA models

To date, iPSCs of type I SMA patients have been produced [113–115]. These cells differentiate into motor neurons *in vitro* with the same initial efficiency as control cells without mutations of *SMN1* in the genome [113, 114]. However, the number and size of motor neurons derived from SMA patients is significantly reduced during prolonged cultivation compared to those of motor neuron cultures from healthy donors [113]. This reduction is caused by an elevated level of apoptosis, mediated by the Fas-ligand, and activation of caspase-8 and caspase-3. In this case, the addition of antibodies specific to the Fas-ligand and use of a caspase-3 inhibitor decrease the level of motoneuron apoptosis [114].

In neurons and astrocytes, the SMN protein is located in the cytoplasm, while in the nucleus of nerve cells it is located in special structures, gems (gemini of coiled (Cajal) bodies), so named because of the similarity of their structure, functions, and proximity. The Cajal bodies, similar to the gems associated with them, are involved in the maturation, assembly, and transport of snRNAs [116]. The amount of gems in the nucleus was demonstrated to correlate with the SMA form [117]. The number of gems in healthy people corresponded to the number of Cajal bodies and they were easily detected. Only Cajal bodies, and no gems, were found in type I SMA patients, whereas gems were detected only in some nuclei in type III SMA patients [118, 119]. There were no gems in the nuclei of the neurons and astrocytes derived from the iPSCs of SMA patients. Addition of valproic acid and tobramycin, which are used in SMA therapy, significantly increased the num-

ber of gems in cell nuclei and the SMN protein level. However, both the total level of the SMN protein and the number of gems still remained significantly lower than those in cells from healthy donors [113].

In a study by Corti *et al.*, iPSCs were obtained from SMA patients using nonviral, nonintegrated episomal vectors [115]. Then, the resulting cells were transfected with short single-stranded oligonucleotides complementary to 75 nucleotides of the coding strand of the gene. The central part of these oligonucleotides contained a substitution (the same as in exon 7 that prevents full protein formation). After recombination with this donor molecule, the *SMN2* gene in some cells became the “SMN1-like gene”; i.e. it was translated to the normal full-length SMN protein. Motor neurons derived from these cells with the corrected phenotype were transplanted into the spinal cord of mice with SMA. As a result, some changes in the pathological phenotype, as well as an increased lifespan of sick mice, were observed. However, the positive dynamics was apparently due to the production of neurotrophic factors by the transplanted cells [115].

SMA-associated pathological changes are known to occur also in other cell types, including astrocytes, sensory neurons, Schwann cells, and skeletal muscle fibers [120–124]. Do sensory neurons with a mutation in the *SMN1* gene affect the progressive degeneration of motor neurons? The use of iPSCs from type I SMA patients helps answer this question.

iPSC lines with the SMA genotype were differentiated into sensory neurons. In this case, a decrease in the calcium response to depolarizing stimuli was observed, but the survival of these cells did not differ from that of the control group cells [125]. The co-culture of sensory neurons from SMA patients and motor neurons from healthy donors revealed no significant reduction in the number of motor neurons, as well as the formation of clusters of glutamate transport vesicles near the bodies of the motor neurons and neurites. Therefore, in this system, sensory neurons carrying a mutation in *SMN1* was demonstrated not to contribute significantly to the death of motor neurons with the normal *SMN1* gene.

### The use of modern methods of genomic engineering to generate artificial model systems

Modern methods of genome editing that are based on the technologies ZFN (Zinc-Finger Nuclease), TALEN (Transcription Activator-Like Effector Nucleases), and CRISPR/Cas9 (Clustered Regularly Interspaced Short Palindromic Repeats/Cas9) enable one to produce artificial model systems both *in vitro* and *in vivo*. They can be used not only to introduce a certain mutation in the genome of the study subject, but also to repair mutations [126–134].

At present, the TALEN and CRISPR/Cas9 technologies can be used in basic and translational biomedical research and experiments to test hypotheses and principles of gene and cell therapy. Artificial nucleases can be used, apart from the generation of models for developing approaches to treatment, directly for therapeutic purposes. One such area is treatment of chronic viral infections [135–138].

It became possible to correct a mutation of the Ala-4Val substitution in the *SOD1* gene in iPSCs using a pair of ZFNs [59]. In this case, homozygous and heterozygous cell clones ( $SOD1^{+/A4V}$  and  $SOD1^{+/+}$ ) were generated. These cells were used to further investigate the functions of the mutant *SOD1* protein and for the purpose of isogenic control.

### Cell therapy of MND

Cell therapy for neurodegenerative diseases involves the replacement of the affected nervous tissue with new healthy cells and recovery of the disrupted functions. For example, motor neurons derived from human ESCs were transplanted into chick embryos, where they survived and retained their cell specificity. Furthermore, their axons extended beyond CNS and reached their peripheral muscle targets [139]. Similar cells transplanted into the spinal cord of adult rats also survived in a foreign tissue. A number of cells expressing a marker of motoneurons, choline acetyltransferase, were found 6 months after the operation. A stronger effect can be achieved by co-transplantation of neural stem cells secreting a glial-derived neurotrophic factor into the affected area and additional administration of a phosphodiesterase-4 inhibitor and dibutyryl cyclic adenosine monophosphate, substances that stimulate peripheral axonal outgrowth, to these animals [140]. Transplantation of motor neurons into the distal ends of the peripheral nerves in mice stimulated the formation of neuromuscular synapses [141–143]. In this case, the formation of functional synapses that persisted for 6–18 months after the surgery was observed. And additional electrical stimulation of the surviving cells resulted in re-innervation of the atrophied muscle fibers [143].

Surgery for motor neuron transplantation is still associated with technical difficulties and immunological responses. However, transplantation of differentiated iPSC derivatives avoids the problems of tissue incompatibility observed upon using ESC derivatives. In addition, issues of co-transplantation of microenvironment cells, formation of peripheral functional neuromuscular synapses, and increase in the survival and time of the transplanted cell activity require further research.

### The problem of directed differentiation of motor neurons and experiment scaling in pharmacological studies

Currently, motor neurons can be produced using three sources (*Fig. 3*):

- ESCs;
- iPSCs; and
- fibroblasts.

The development of protocols for fast and efficient differentiation of ESCs and iPSCs is extremely important, because differentiated derivatives of these cells are required for large-scale use in pharmacological and toxicological studies and cell replacement therapy. Currently, there is a large number of protocols for directed differentiation of cultured pluripotent human and mouse cells into motor neurons [71, 75, 115, 144–153]. This procedure includes two stages. The first stage is neuronal differentiation with the formation of embryoid bodies or neural rosettes. This stage is carried out in a ESC medium supplemented with specific factors that guide the differentiation towards neurons. The second step is differentiation of the resulting neural progenitors towards motor neurons by means of addition in the medium of factors such as RA (retinoic acid) and Shh (sonic hedgehog). The procedure efficiency is evaluated based on the expression of specific markers, morphology of the cells, their electrophysiological activity, as well as by xenotransplantation to animals. The resulting cells are a mixed population. It can be enriched with motor neurons by using gradient centrifugation [115] or protocols with a higher yield of the desired cells.

Protocols that use induction of the embryoid bodies followed by treatment with RA/Shh are quite laborious; they take a total of about 2 months, with a relatively low yield of motor neurons (10–40%). The method of directed programming that is based on adenoviral delivery of three motoneuron-specific transcription factors (*Ngn2*, *ISL1*, and *Lhx3*) is faster (formation of motor neurons from neural progenitors takes 11 days) and more efficient (motoneuron population amounts to about 60%). The disadvantages of this method are as follows:

- manipulations, which are based on the use of adenoviruses, with genomes that are relatively unsafe for further use of these cells; and
- considerable variations in the amount of produced motoneurons, as well as the variability of their survival.

However, protocols have already been developed for a fairly quick (within 20 days) and highly efficient (over 70%) production of motor neurons without the use of adenoviruses [154].

Further efforts should be aimed not only at searching for new, more effective methods of differentiation,

## Sources of motor neurons

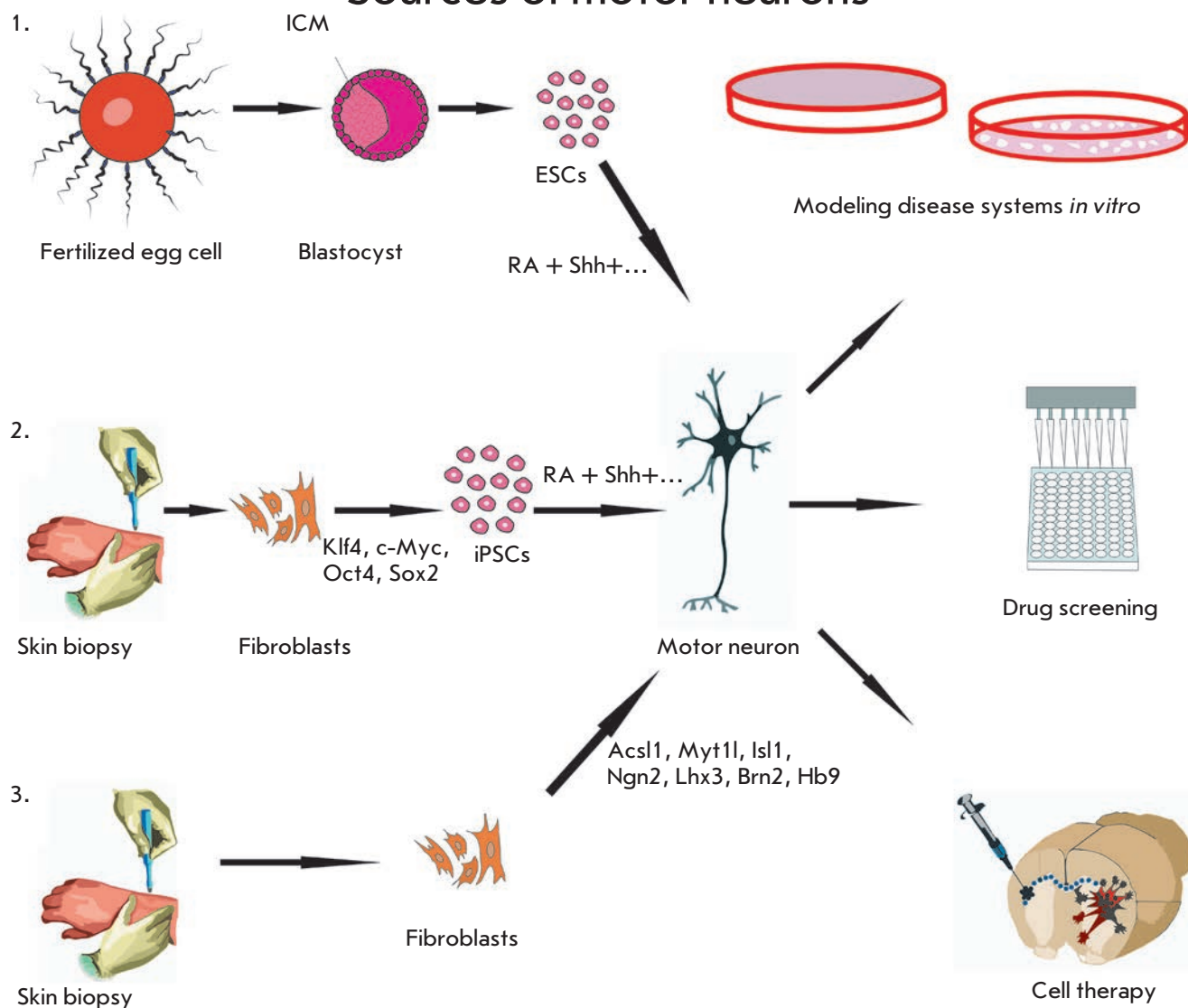


**Fig. 3.** Sources of motor neurons. 1 – ESCs derived from the inner cell mass of a blastocyst can be differentiated into motor neurons. Compounds like RA and Shh play a key role in this process. 2 – human fibroblasts obtained from a skin biopsy material can be reprogrammed into iPSCs by expression of factors such as Klf-4, c-Myc, Oct4, and Sox2. iPSCs differentiation into motor neurons is performed by the method described for ESCs. 3 – motor neurons can directly be produced from fibroblasts by expressing seven factors (Acs11, Mt11, Isl1, Ngn2, Lhx3, Brn2, Hb9)

but also at standardizing the parameters of cell passaging and culturing according to existing methods, as well as at studying procedures of direct differentiation of cells into specific motor neuron subtypes.

### The problem of generating cell model biobanks

The essential requirement in performing pharmacological and toxicological studies and cell therapy is the availability of cell samples obtained from patients with

rare diseases. This gives rise to an urgent need for the generation of banks of human ESC and iPSC lines. This task requires employees with a high level of competence, the development of a specialized infrastructure, and strict quality control of samples. The world scientific community has long been concerned about this issue. The criteria to be met by banks of human ESC and iPSC lines are addressed in new programs such as CCRM (<http://ccrm.ca/>), CIRM ([30 | ACTA NATURAE | VOL. 7 № 1 \(24\) 2015](http://www.</a></p>
</div>
<div data-bbox=)

coriell.org/media-center/coriell-in-the-news/coriell-awarded-10mm-for-induced-pluripotent-stem-cell-program), HiPSCi (<http://www.hipsci.org>), and StemBANCC (<http://www.stembancc.org/>).

One of the possible ways to achieve this important goal may be to use a crowdsourcing platform as, for example, is already the case in resources such as the Zebrafish Gene Collection, ADDGENE, PubMed, and the Drosophila “Red Book”. In the USA, there is already a prototype of a similar organization based on NIH (the National Institutes of Health, in particular NCATS (National Center for Advanced Translational Science) and NIHCRM (the NIH Center for Regenerative Medicine)). The collections of three organizations, RUCDR Infinite Biologics (Rutgers), the Coriell Institute for Medical Research (Coriell), and Wisconsin Stem Cell Bank (WISC), already include hundreds of ESC and iPSC lines received from various institutions.

Therefore, a number of issues need to be addressed in order to generate biobanks of cell models. The first issue is related to joining the efforts of the international community to ensure that researchers around the world can enjoy unfettered access to this biobank. The problem of biosafety and compliance of a biobank with the legislation of different countries is no less important. The second issue is the generation of a single database, where all the necessary characteristics of cell lines should be spelled out. The third issue is related to the rapid progress in the field of cell technologies. Less than 10 years after its creation, the iPSC technology has reached a level of development that already allows the use of these cells in preclinical trials of drugs, as well as their application in the field of regenerative and personalized medicine.

## CONCLUSION

The problem of neurodegenerative diseases and finding ways to treat them becomes the most urgent ones due to the increased lifespan in developed countries, since most of these diseases develop in old and senile age. Motor neuron diseases do not prevail in the overall pattern of mortality from neurodegenerative diseases, but they are the absolute leaders in the severity

of progression and rate of death. Amyotrophic lateral sclerosis (ALS) causes progressive muscular atrophy and death due to respiratory failure within 2–5 years, and the most severe form of spinal muscular atrophy (SMA), the Werdnig-Hoffmann disease, leads to muscle atrophy, palsy, and death of sick children within the first 2 years of life.

MND modeling in *in vivo* systems using organisms, such as nematodes, drosophila, laboratory mice, and rats, has significantly expanded our understanding of the causes and mechanisms of MND pathogenesis and revealed a number of chemical compounds that could be used as treatment for these diseases. However, at the genotypic and phenotypic level, these models are very different from that which is observed upon MND in humans. Therefore, differentiated derivatives of ESCs and iPSCs are extensively used at present to develop relevant model systems. They can be used not only to study the disease features at the molecular, subcellular, and cellular levels, but also to exploit these cells in the future for replacement therapy and screening of new drugs. The highest prospects are associated with the possibility of transplantation of iPSC derivatives, because these cells are autologous to an intended donor that allows one to avoid immunological rejection reactions and promotes the development and implementation of a new phase of modern medicine, the era of personalized medicine.

The major problem that needs to be solved to reach this stage is the development of open-access banks of ESC and iPSC lines containing full information on each cell line. Today, the National Institutes of Health in the USA and a number of organizations in some developed countries are the most active ones in this area. However, combining the efforts of the world scientific community, including the scientific organizations and institutions of the Russian Federation, is required to create a more complete bank of ESC and iPSC lines. ●

*This work was funded under the program of the Russian Academy of Sciences “Basic Sciences to Medicine” 2.1.7.*

## REFERENCES

1. Andersen P.M., Al-Chalabi A. // Nat. Rev. Neurol. 2011. V. 7. № 11. P. 603–615.
2. Faravelli I., Bucchia M., Rinchetti P., Nizzardo M., Simone C., Frattini E., Corti S. // Stem Cell Res. Ther. 2014. V. 5. № 4. P. 87.
3. Simone C., Nizzardo M., Rizzo F., Ruggieri M., Riboldi G., Salani S., Bucchia M., Bresolin N., Comi G.P., Corti S. // Stem Cell Repts. 2014. V. 3. № 2. P. 297–311.
4. Boiani M., Scholer H.R. // Nat. Rev. Mol. Cell Biol. 2005. V. 6. № 11. P. 872–884.
5. Tesar P.J., Chenoweth J.G., Brook F.A., Davies T.J., Evans E.P., Mack D.L., Gardner R.L., Mckay R.D. // Nature. 2007. V. 448. № 7150. P. 196–199.
6. Thomson J.A., Itskovitz-Eldor J., Shapiro S.S., Waknitz M.A., Swiergiel J.J., Marshall V.S., Jones J.M. // Science. 1998. V. 282. № 5391. P. 1145–1147.
7. Takahashi K., Yamanaka S. // Cell. 2006. V. 126. № 4. P. 663–676.
8. Lunn J.S., Sakowski S.A., Federici T., Glass J.D., Boullis N.M., Feldman E.L. // Regen. Med. 2011. V. 6. № 2. P. 201–213.

9. Amemori T, Romanyuk N, Jendelova P, Herynek V, Turnovcova K, Prochazka P, Kapcalova M, Cocks G, Price J, Sykova E. // *Stem Cell Res. Ther.* 2013. V. 4. № 3. P. 68.
10. Rossi F, Cattaneo E. // *Nat. Rev. Neurosci.* 2002. V. 3. № 5. P. 401–409.
11. Rosser A.E., Zietlow R., Dunnett S.B. // *Curr. Opin. Neurol.* 2007. V. 20. № 6. P. 688–692.
12. Klein S.M., Behrstock S., Mchugh J., Hoffmann K., Wallace K., Suzuki M., Aebischer P., Svendsen C.N. // *Hum. Gene Ther.* 2005. V. 16. № 4. P. 509–521.
13. Mulder D.W. // *Adv. Neurol.* 1982. V. 36. P. 15–22.
14. Gordon P.H. // *Aging Dis.* 2013. V. 4. № 5. P. 295–310.
15. Mcguire V., Longstreth W.T., Jr., Koepsell T.D., van Belle G. // *Neurology.* 1996. V. 47. № 2. P. 571–573.
16. Logroscino G., Traynor B.J., Hardiman O., Chio A., Mitchell D., Swingler R.J., Millul A., Benn E., Beghi E. // *J. Neurol. Neurosurg. Psychiatry.* 2010. V. 81. № 4. P. 385–390.
17. Marin B., Hamidou B., Couratier P., Nicol M., Delzor A., Raymondeau M., Druet-Cabanac M., Lautrette G., Boumediene F., Preux P.M. // *Eur. J. Neurol.* 2014. V. 21. № 10. P. 1292–300. e1278–9.
18. Kurtzke J.F. // *Adv. Neurol.* 1991. V. 56. P. 245–270.
19. Papapetropoulos S. // *Neurochem. Int.* 2007. V. 50. № 7–8. P. 998–1003.
20. Caller T.A., Field N.C., Chipman J.W., Shi X., Harris B.T., Stommel E.W. // *Amyotroph. Lateral Scler.* 2012. V. 13. № 1. P. 25–32.
21. Vinceti M., Bottecchi I., Fan A., Finkelstein Y., Mandrioli J. // *Rev. Environ. Health.* 2012. V. 27. № 1. P. 19–41.
22. Wang H., O'reilly E.J., Weisskopf M.G., Logroscino G., McCullough M.L., Thun M.J., Schatzkin A., Kolonel L.N., Ascherio A. // *Arch. Neurol.* 2011. V. 68. № 2. P. 207–213.
23. Pupillo E., Messina P., Logroscino G., Zoccolella S., Chio A., Calvo A., Corbo M., Lunetta C., Micheli A., Millul A., et al. // *Eur. J. Neurol.* 2012. V. 19. № 12. P. 1509–1517.
24. Huisman M.H., Seelen M., De Jong S.W., Dorresteyn K.R., van Doormaal P.T., van Der Kooi A.J., De Visser M., Schelhaas H.J., van Den Berg L.H., Veldink J.H. // *J. Neurol. Neurosurg. Psychiatry.* 2013. V. 84. № 9. P. 976–981.
25. Macgowan D.J., Scelsa S.N., Waldron M. // *Neurology.* 2001. V. 57. № 6. P. 1094–1097.
26. Steele A.J., Al-Chalabi A., Ferrante K., Cudkowicz M.E., Brown R.H., Jr., Garson J.A. // *Neurology.* 2005. V. 64. № 3. P. 454–458.
27. Abel O., Powell J.F., Andersen P.M., Al-Chalabi A. // *Hum. Mutat.* 2012. V. 33. № 9. P. 1345–1351.
28. Dejesus-Hernandez M., Mackenzie I.R., Boeve B.F., Boxer A.L., Baker M., Rutherford N.J., Nicholson A.M., Finch N.A., Flynn H., Adamson J., et al. // *Neuron.* 2011. V. 72. № 2. P. 245–256.
29. Majounie E., Renton A.E., Mok K., Dopfer E.G., Waite A., Rollinson S., Chio A., Restagno G., Nicolaou N., Simon-Sanchez J., et al. // *Lancet Neurol.* 2012. V. 11. № 4. P. 323–330.
30. Renton A.E., Majounie E., Waite A., Simon-Sanchez J., Rollinson S., Gibbs J.R., Schymick J.C., Laaksovirta H., van Swieten J.C., Myllykangas L., et al. // *Neuron.* 2011. V. 72. № 2. P. 257–268.
31. Rosen D.R. // *Nature.* 1993. V. 364. № 6435. P. 362.
32. Sreedharan J., Blair I.P., Tripathi V.B., Hu X., Vance C., Rogelj B., Ackerley S., Durnall J.C., Williams K.L., Buratti E., et al. // *Science.* 2008. V. 319. № 5870. P. 1668–1672.
33. Vance C., Rogelj B., Hortobagyi T., De Vos K.J., Nishimura A.L., Sreedharan J., Hu X., Smith B., Ruddy D., Wright P., et al. // *Science.* 2009. V. 323. № 5918. P. 1208–1211.
34. Kwiatkowski T.J., Jr., Bosco D.A., Leclerc A.L., Tamrazian E., Vanderburg C.R., Russ C., Davis A., Gilchrist J., Kasarskis E.J., Munsat T., et al. // *Science.* 2009. V. 323. № 5918. P. 1205–1208.
35. Greenway M.J., Andersen P.M., Russ C., Ennis S., Cashman S., Donaghy C., Patterson V., Swingler R., Kieran D., Prehn J., et al. // *Nat. Genet.* 2006. V. 38. № 4. P. 411–413.
36. Maruyama H., Morino H., Ito H., Izumi Y., Kato H., Watanabe Y., Kinoshita Y., Kamada M., Nodera H., Suzuki H., et al. // *Nature.* 2010. V. 465. № 7295. P. 223–226.
37. Johnson J.O., Mandrioli J., Benatar M., Abramzon Y., van Deerlin V.M., Trojanowski J.Q., Gibbs J.R., Brunetti M., Gronka S., Wu J., et al. // *Neuron.* 2010. V. 68. № 5. P. 857–864.
38. Mackenzie I.R., Rademakers R., Neumann M. // *Lancet Neurol.* 2010. V. 9. № 10. P. 995–1007.
39. Lagier-Tourenne C., Polymenidou M., Cleveland D.W. // *Hum. Mol. Genet.* 2010. V. 19. № R1. P. R46–64.
40. Halawani D., Latterich M. // *Mol. Cell.* 2006. V. 22. № 6. P. 713–717.
41. Al-Sarraj S., King A., Troakes C., Smith B., Maekawa S., Bodi I., Rogelj B., Al-Chalabi A., Hortobagyi T., Shaw C.E. // *Acta Neuropathol.* 2011. V. 122. № 6. P. 691–702.
42. Miller R.G., Mitchell J.D., Lyon M., Moore D.H. // *Cochrane Database Syst Rev.* 2007. № 1. P. CD001447.
43. Feiguin F., Godena V.K., Romano G., D'ambrogio A., Klima R., Baralle F.E. // *FEBS Lett.* 2009. V. 583. № 10. P. 1586–1592.
44. Laird A.S., van Hoecke A., De Muyenck L., Timmers M., van Den Bosch L., van Damme P., Robberecht W. // *PLoS One.* 2010. V. 5. № 10. P. e13368.
45. Kraemer B.C., Schuck T., Wheeler J.M., Robinson L.C., Trojanowski J.Q., Lee V.M., Schellenberg G.D. // *Acta Neuropathol.* 2010. V. 119. № 4. P. 409–419.
46. Johnson B.S., Snead D., Lee J.J., Mcaffery J.M., Shorter J., Gitler A.D. // *J. Biol. Chem.* 2009. V. 284. № 30. P. 20329–20339.
47. Arnold E.S., Ling S.C., Huelga S.C., Lagier-Tourenne C., Polymenidou M., Ditsworth D., Kordasiewicz H.B., Mcalonis-Downes M., Platoshyn O., Parone P.A., et al. // *Proc. Natl. Acad. Sci. USA.* 2013. V. 110. № 8. P. E736–745.
48. Stallings N.R., Puttapparthi K., Luther C.M., Burns D.K., Elliott J.L. // *Neurobiol. Dis.* 2010. V. 40. № 2. P. 404–414.
49. Wegorzewska I., Bell S., Cairns N.J., Miller T.M., Bahloh R.H. // *Proc. Natl. Acad. Sci. USA.* 2009. V. 106. № 44. P. 18809–18814.
50. Wils H., Kleinberger G., Janssens J., Pereson S., Joris G., Cuijt I., Smits V., Ceuterick-De Groote C., Van Broeckhoven C., Kumar-Singh S. // *Proc. Natl. Acad. Sci. USA.* 2010. V. 107. № 8. P. 3858–3863.
51. Zhou H., Huang C., Chen H., Wang D., Landel C.P., Xia P.Y., Bowser R., Liu Y.J., Xia X.G. // *PLoS Genet.* 2010. V. 6. № 3. P. e1000887.
52. Uchida A., Sasaguri H., Kimura N., Tajiri M., Ohkubo T., Ono F., Sakaue F., Kanai K., Hirai T., Sano T., et al. // *Brain.* 2012. V. 135. Pt 3. P. 833–846.
53. Hicks G.G., Singh N., Nashabi A., Mai S., Bozek G., Klewes L., Arapovic D., White E.K., Koury M.J., Oltz E.M., et al. // *Nat. Genet.* 2000. V. 24. № 2. P. 175–179.
54. Kuroda M., Sok J., Webb L., Baechtold H., Urano F., Yin Y., Chung P., De Rooij D.G., Akhmedov A., Ashley T., et al. // *EMBO J.* 2000. V. 19. № 3. P. 453–462.
55. Fujii R., Okabe S., Urushido T., Inoue K., Yoshimura A., Tachibana T., Nishikawa T., Hicks G.G., Takumi T. // *Curr. Biol.* 2005. V. 15. № 6. P. 587–593.

56. Mitchell J.C., Mcgoldrick P., Vance C., Hortobagyi T., Sreedharan J., Rogelj B., Tudor E.L., Smith B.N., Klasen C., Miller C.C., et al. // *Acta Neuropathol.* 2013. V. 125. № 2. P. 273–288.
57. Huang C., Zhou H., Tong J., Chen H., Liu Y.J., Wang D., Wei X., Xia X.G. // *PLoS Genet.* 2011. V. 7. № 3. P. e1002011.
58. Chen H., Qian K., Du Z., Cao J., Petersen A., Liu H., Blackburn L.W.T., Huang C.L., Errigo A., Yin Y., et al. // *Cell Stem Cell.* 2014. V. 14. № 6. P. 796–809.
59. Kiskinis E., Sandoe J., Williams L.A., Boulting G.L., Moccia R., Wainger B.J., Han S., Peng T., Thams S., Mikkilineni S., et al. // *Cell Stem Cell.* 2014. V. 14. № 6. P. 781–795.
60. Wainger B.J., Kiskinis E., Mellin C., Wiskow O., Han S.S., Sandoe J., Perez N.P., Williams L.A., Lee S., Boulting G., et al. // *Cell Rep.* 2014. V. 7. № 1. P. 1–11.
61. Yang Y.M., Gupta S.K., Kim K.J., Powers B.E., Cerqueira A., Wainger B.J., Ngo H.D., Rosowski K.A., Schein P.A., Ackeifi C.A., et al. // *Cell Stem Cell.* 2013. V. 12. № 6. P. 713–726.
62. Koh S.H., Baek W., Kim S.H. // *Neurol. Res. Int.* 2011. V. 2011. P. 205761.
63. Hetman M., Xia Z. // *Acta Neurobiol. Exp. (Wars).* 2000. V. 60. № 4. P. 531–545.
64. Linseman D.A., Butts B.D., Precht T.A., Phelps R.A., Le S.S., Laessig T.A., Bouchard R.J., Florez-Mcclure M.L., Heidenreich K.A. // *J. Neurosci.* 2004. V. 24. № 44. P. 9993–10002.
65. Serio A., Bilican B., Barmada S.J., Ando D.M., Zhao C., Siller R., Burr K., Haghi G., Story D., Nishimura A.L., et al. // *Proc. Natl. Acad. Sci. USA.* 2013. V. 110. № 12. P. 4697–4702.
66. Di Giorgio F.P., Carrasco M.A., Siao M.C., Maniatis T., Egan K. // *Nat. Neurosci.* 2007. V. 10. № 5. P. 608–614.
67. Ling S.C., Polymenidou M., Cleveland D.W. // *Neuron.* 2013. V. 79. № 3. P. 416–438.
68. Bilican B., Serio A., Barmada S.J., Nishimura A.L., Sullivan G.J., Carrasco M., Phatnani H.P., Puddifoot C.A., Story D., Fletcher J., et al. // *Proc. Natl. Acad. Sci. USA.* 2012. V. 109. № 15. P. 5803–5808.
69. Egawa N., Kitaoka S., Tsukita K., Naitoh M., Takahashi K., Yamamoto T., Adachi F., Kondo T., Okita K., Asaka I., et al. // *Sci. Transl. Med.* 2012. V. 4. № 145. P. 145ra104.
70. Nishimura A.L., Shum C., Scotter E.L., Abdelgany A., Sardone V., Wright J., Lee Y.B., Chen H.J., Bilican B., Carrasco M., et al. // *PLoS One.* 2014. V. 9. № 3. P. e91269.
71. Sareen D., O'Rourke J.G., Meera P., Muhammad A.K., Grant S., Simpkinson M., Bell S., Carmona S., Ornelas L., Sahabian A., et al. // *Sci. Transl. Med.* 2013. V. 5. № 208. P. 208ra149.
72. Buratti E., Brindisi A., Giombi M., Tisminetzky S., Ayala Y.M., Baralle F.E. // *J. Biol. Chem.* 2005. V. 280. № 45. P. 37572–37584.
73. Kim H.J., Kim N.C., Wang Y.D., Scarborough E.A., Moore J., Diaz Z., Maclea K.S., Freibaum B., Li S., Molliex A., et al. // *Nature.* 2013. V. 495. № 7442. P. 467–473.
74. Xu Z., Poidevin M., Li X., Li Y., Shu L., Nelson D.L., Li H., Hales C.M., Gearing M., Wingo T.S., et al. // *Proc. Natl. Acad. Sci. USA.* 2013. V. 110. № 19. P. 7778–7783.
75. Burkhardt M.F., Martinez F.J., Wright S., Ramos C., Volfson D., Mason M., Garnes J., Dang V., Lievers J., Shoukat-Mumtaz U., et al. // *Mol. Cell Neurosci.* 2013. V. 56. P. 355–364.
76. Burghes A.H., Beattie C.E. // *Nat. Rev. Neurosci.* 2009. V. 10. № 8. P. 597–609.
77. Lunn M.R., Wang C.H. // *Lancet.* 2008. V. 371. № 9630. P. 2120–2133.
78. Monani U.R. // *Neuron.* 2005. V. 48. № 6. P. 885–896.
79. Emery A.E. // *J. Med. Genet.* 1971. V. 8. № 4. P. 481–495.
80. Hahnen E., Forkert R., Marke C., Rudnik-Schoneborn S., Schonling J., Zerres K., Wirth B. // *Hum. Mol. Genet.* 1995. V. 4. № 10. P. 1927–1933.
81. Lefebvre S., Burglen L., Reboullet S., Clermont O., Burlet P., Viollet L., Benichou B., Cruaud C., Millasseau P., Zeviani M., et al. // *Cell.* 1995. V. 80. № 1. P. 155–165.
82. Burglen L., Lefebvre S., Clermont O., Burlet P., Viollet L., Cruaud C., Munnich A., Melki J. // *Genomics.* 1996. V. 32. № 3. P. 479–482.
83. Cartegni L., Hastings M.L., Calarco J.A., De Stanchina E., Krainer A.R. // *Am. J. Hum. Genet.* 2006. V. 78. № 1. P. 63–77.
84. Kashima T., Manley J.L. // *Nat. Genet.* 2003. V. 34. № 4. P. 460–463.
85. Campbell L., Potter A., Ignatius J., Dubowitz V., Davies K. // *Am. J. Hum. Genet.* 1997. V. 61. № 1. P. 40–50.
86. Mailman M.D., Heinz J.W., Papp A.C., Snyder P.J., Sedra M.S., Wirth B., Burghes A.H., Prior T.W. // *Genet. Med.* 2002. V. 4. № 1. P. 20–26.
87. Rodrigues N.R., Owen N., Talbot K., Patel S., Muntoni F., Ignatius J., Dubowitz V., Davies K.E. // *J. Med. Genet.* 1996. V. 33. № 2. P. 93–96.
88. Zheleznyakova G.Y., Kiselev A.V., Vakharlovsky V.G., Rask-Andersen M., Chavan R., Egorova A.A., Schioth H.B., Baranov V.S. // *BMC Med. Genet.* 2011. V. 12. P. 96.
89. Munsat T.L., Davies K.E. // *Neuromuscul. Disord.* 1992. V. 2. № 5–6. P. 423–428.
90. Akten B., Kye M.J., Hao Le T., Wertz M.H., Singh S., Nie D., Huang J., Merianda T.T., Twiss J.L., Beattie C.E., et al. // *Proc. Natl. Acad. Sci. USA.* 2011. V. 108. № 25. P. 10337–10342.
91. Mcwhorter M.L., Monani U.R., Burghes A.H., Beattie C.E. // *J. Cell Biol.* 2003. V. 162. № 5. P. 919–931.
92. Meister G., Buhler D., Pillai R., Lottspeich F., Fischer U. // *Nat. Cell Biol.* 2001. V. 3. № 11. P. 945–949.
93. Pellizzoni L., Yong J., Dreyfuss G. // *Science.* 2002. V. 298. № 5599. P. 1775–1779.
94. Rossoll W., Jablonka S., Andreassi C., Kroning A.K., Karle K., Monani U.R., Sendtner M. // *J. Cell Biol.* 2003. V. 163. № 4. P. 801–812.
95. Pellizzoni L. // *EMBO Rep.* 2007. V. 8. № 4. P. 340–345.
96. Eggert C., Chari A., Lagerbauer B., Fischer U. // *Trends Mol. Med.* 2006. V. 12. № 3. P. 113–121.
97. Gabanella F., Butchbach M.E., Saieva L., Carissimi C., Burghes A.H., Pellizzoni L. // *PLoS One.* 2007. V. 2. № 9. P. e921.
98. Giavazzi A., Setola V., Simonati A., Battaglia G. // *J. Neuropathol. Exp. Neurol.* 2006. V. 65. № 3. P. 267–277.
99. Carrel T.L., Mcwhorter M.L., Workman E., Zhang H., Wolstencroft E.C., Lorson C., Bassell G.J., Burghes A.H., Beattie C.E. // *J. Neurosci.* 2006. V. 26. № 43. P. 11014–11022.
100. Fan L., Simard L.R. // *Hum. Mol. Genet.* 2002. V. 11. № 14. P. 1605–1614.
101. Schrank B., Gotz R., Gunnensen J.M., Ure J.M., Toyka K.V., Smith A.G., Sendtner M. // *Proc. Natl. Acad. Sci. USA.* 1997. V. 94. № 18. P. 9920–9925.
102. Chan Y.B., Miguel-Aliaga I., Franks C., Thomas N., Trulzsch B., Sattelle D.B., Davies K.E., van Den Heuvel M. // *Hum. Mol. Genet.* 2003. V. 12. № 12. P. 1367–1376.
103. Frugier T., Tiziano F.D., Cifuentes-Diaz C., Miniou P., Roblot N., Dierich A., Le Meur M., Melki J. // *Hum. Mol. Genet.* 2000. V. 9. № 5. P. 849–858.
104. Cifuentes-Diaz C., Frugier T., Tiziano F.D., Lacene E.,

- Roblot N., Joshi V., Moreau M.H., Melki J. // *J. Cell Biol.* 2001. V. 152. № 5. P. 1107–1114.
105. Vitte J.M., Davoult B., Roblot N., Mayer M., Joshi V., Courageot S., Tronche F., Vadrot J., Moreau M.H., Kemeny F., et al. // *Am. J. Pathol.* 2004. V. 165. № 5. P. 1731–1741.
106. Hsieh-Li H.M., Chang J.G., Jong Y.J., Wu M.H., Wang N.M., Tsai C.H., Li H. // *Nat. Genet.* 2000. V. 24. № 1. P. 66–70.
107. Monani U.R., Sendtner M., Coovert D.D., Parsons D.W., Andreassi C., Le T.T., Jablonka S., Schrank B., Rossoll W., Prior T.W., et al. // *Hum. Mol. Genet.* 2000. V. 9. № 3. P. 333–339.
108. Gavrilina T.O., Mcgovern V.L., Workman E., Crawford T.O., Gogliotti R.G., Didonato C.J., Monani U.R., Morris G.E., Burghes A.H. // *Hum. Mol. Genet.* 2008. V. 17. № 8. P. 1063–1075.
109. Sleigh J.N., Buckingham S.D., Esmaeili B., Viswanathan M., Cuppen E., Westlund B.M., Sattelle D.B. // *Hum. Mol. Genet.* 2011. V. 20. № 2. P. 245–260.
110. Coque E., Raoul C., Bowerman M. // *Front Neurosci.* 2014. V. 8. P. 271.
111. Zheleznyakova G.Y., Voisin S., Kiselev A.V., Sallman Almen M., Xavier M.J., Maretina M.A., Tishchenko L.I., Fredriksson R., Baranov V.S., Schioth H.B. // *Eur. J. Hum. Genet.* 2013. V. 21. № 9. P. 988–993.
112. Chang H.C., Dimlich D.N., Yokokura T., Mukherjee A., Kankel M.W., Sen A., Sridhar V., Fulga T.A., Hart A.C., van Vactor D., et al. // *PLoS One.* 2008. V. 3. № 9. P. e3209.
113. Ebert A.D., Yu J., Rose F.F., Jr., Mattis V.B., Lorson C.L., Thomson J.A., Svendsen C.N. // *Nature.* 2009. V. 457. № 7227. P. 277–280.
114. Sareen D., Ebert A.D., Heins B.M., Mcgovern J.V., Ornelas L., Svendsen C.N. // *PLoS One.* 2012. V. 7. № 6. P. e39113.
115. Corti S., Nizzardo M., Simone C., Falcone M., Nardini M., Ronchi D., Donadoni C., Salani S., Riboldi G., Magri F., et al. // *Sci. Transl. Med.* 2012. V. 4. № 165. P. 165ra162.
116. Liu Q., Dreyfuss G. // *EMBO J.* 1996. V. 15. № 14. P. 3555–3565.
117. Coovert D.D., Le T.T., Mcandrew P.E., Strasswimmer J., Crawford T.O., Mendell J.R., Coulson S.E., Androphy E.J., Prior T.W., Burghes A.H. // *Hum. Mol. Genet.* 1997. V. 6. № 8. P. 1205–1214.
118. Lefebvre S., Burlet P., Liu Q., Bertrand S., Clermont O., Munnich A., Dreyfuss G., Melki J. // *Nat. Genet.* 1997. V. 16. № 3. P. 265–269.
119. Young P.J., Le T.T., Thi Man N., Burghes A.H., Morris G.E. // *Exp. Cell Res.* 2000. V. 256. № 2. P. 365–374.
120. Gogliotti R.G., Quinlan K.A., Barlow C.B., Heier C.R., Heckman C.J., Didonato C.J. // *J. Neurosci.* 2012. V. 32. № 11. P. 3818–3829.
121. Jablonka S., Karle K., Sandner B., Andreassi C., Von Au K., Sendtner M. // *Hum. Mol. Genet.* 2006. V. 15. № 3. P. 511–518.
122. Ling K.K., Lin M.Y., Zingg B., Feng Z., Ko C.P. // *PLoS One.* 2010. V. 5. № 11. P. e15457.
123. Voigt T., Meyer K., Baum O., Schumperli D. // *Neuromuscul Disord.* 2010. V. 20. № 11. P. 744–752.
124. Murray L.M., Beauvais A., Bhanot K., Kothary R. // *Neurobiol. Dis.* 2012. V. 49C. P. 57–67.
125. Schwab A.J., Ebert A.D. // *PLoS One.* 2014. V. 9. № 7. P. e103112.
126. Cermak T., Doyle E.L., Christian M., Wang L., Zhang Y., Schmidt C., Baller J.A., Somia N.V., Bogdanove A.J., Voytas D.F. // *Nucl. Acids Res.* 2011. V. 39. № 12. P. e82.
127. Horii T., Tamura D., Morita S., Kimura M., Hatada I. // *Int. J. Mol. Sci.* 2013. V. 14. № 10. P. 19774–19781.
128. Schwank G., Koo B.K., Sasselli V., Dekkers J.F., Heo I., Demircan T., Sasaki N., Boymans S., Cuppen E., van Der Ent C.K., et al. // *Cell Stem Cell.* 2013. V. 13. № 6. P. 653–658.
129. Bassett A.R., Tibbit C., Ponting C.P., Liu J.L. // *Cell Rep.* 2013. V. 4. № 1. P. 220–228.
130. Chang N., Sun C., Gao L., Zhu D., Xu X., Zhu X., Xiong J.W., Xi J.J. // *Cell Res.* 2013. V. 23. № 4. P. 465–472.
131. Cong L., Ran F.A., Cox D., Lin S., Barretto R., Habib N., Hsu P.D., Wu X., Jiang W., Marraffini L.A., et al. // *Science.* 2013. V. 339. № 6121. P. 819–823.
132. Li D., Qiu Z., Shao Y., Chen Y., Guan Y., Liu M., Li Y., Gao N., Wang L., Lu X., et al. // *Nat. Biotechnol.* 2013. V. 31. № 8. P. 681–683.
133. Mali P., Yang L., Esvelt K.M., Aach J., Guell M., Dicarlo J.E., Norville J.E., Church G.M. // *Science.* 2013. V. 339. № 6121. P. 823–826.
134. Shan Q., Wang Y., Li J., Zhang Y., Chen K., Liang Z., Zhang K., Liu J., Xi J.J., Qiu J.L., et al. // *Nat. Biotechnol.* 2013. V. 31. № 8. P. 686–688.
135. Moehle E.A., Rock J.M., Lee Y.L., Jouvenot Y., Dekelver R.C., Gregory P.D., Urnov F.D., Holmes M.C. // *Proc. Natl. Acad. Sci. USA.* 2007. V. 104. № 9. P. 3055–3060.
136. Bloom K., Ely A., Mussolino C., Cathomen T., Arbuthnot P. // *Mol. Ther.* 2013. V. 21. № 10. P. 1889–1897.
137. Schiffer J.T., Aubert M., Weber N.D., Mintzer E., Stone D., Jerome K.R. // *J. Virol.* 2012. V. 86. № 17. P. 8920–8936.
138. Holt N., Wang J., Kim K., Friedman G., Wang X., Taupin V., Crooks G.M., Kohn D.B., Gregory P.D., Holmes M.C., et al. // *Nat. Biotechnol.* 2010. V. 28. № 8. P. 839–847.
139. Lee H., Shamy G.A., Elkabetz Y., Schofield C.M., Harrison N.L., Panagiotakos G., Succi N.D., Tabar V., Studer L. // *Stem Cells.* 2007. V. 25. № 8. P. 1931–1939.
140. Deshpande D.M., Kim Y.S., Martinez T., Carmen J., Dike S., Shats I., Rubin L.L., Drummond J., Krishnan C., Hoke A., et al. // *Ann. Neurol.* 2006. V. 60. № 1. P. 32–44.
141. Craff M.N., Zeballos J.L., Johnson T.S., Ranka M.P., Howard R., Motarjem P., Randolph M.A., Winograd J.M. // *Plast Reconstr. Surg.* 2007. V. 119. № 1. P. 235–245.
142. Kubo T., Randolph M.A., Groger A., Winograd J.M. // *Plast Reconstr. Surg.* 2009. V. 123. № 2 Suppl. P. 139S–148S.
143. Yohn D.C., Miles G.B., Rafuse V.F., Brownstone R.M. // *J. Neurosci.* 2008. V. 28. № 47. P. 12409–12418.
144. Reinhardt P., Glatza M., Hemmer K., Tsytsyura Y., Thiel C.S., Hoing S., Moritz S., Parga J.A., Wagner L., Bruder J.M., et al. // *PLoS One.* 2013. V. 8. № 3. P. e59252.
145. Amoroso M.W., Croft G.F., Williams D.J., O'keeffe S., Carrasco M.A., Davis A.R., Roybon L., Oakley D.H., Maniatis T., Henderson C.E., et al. // *J. Neurosci.* 2013. V. 33. № 2. P. 574–586.
146. Boulting G.L., Kiskinis E., Croft G.F., Amoroso M.W., Oakley D.H., Wainger B.J., Williams D.J., Kahler D.J., Yamaki M., Davidow L., et al. // *Nat. Biotechnol.* 2011. V. 29. № 3. P. 279–286.
147. Hester M.E., Murtha M.J., Song S., Rao M., Miranda C.J., Meyer K., Tian J., Boulting G., Schaffer D.V., Zhu M.X., et al. // *Mol. Ther.* 2011. V. 19. № 10. P. 1905–1912.
148. Hu B.Y., Du Z.W., Zhang S.C. // *Nat-Protoc.* 2009. V. 4. № 11. P. 1614–1622.
149. Karumbayaram S., Novitch B.G., Patterson M., Umbach J.A., Richter L., Lindgren A., Conway A.E., Clark A.T., Goldman S.A., Plath K., et al. // *Stem Cells.* 2009. V. 27. № 4. P. 806–811.
150. Wichterle H., Lieberam I., Porter J.A., Jessell T.M. // *Cell.* 2002. V. 110. № 3. P. 385–397.

151. Takazawa T., Croft G.F., Amoroso M.W., Studer L., Wichterle H., Macdermott A.B. // *PLoS One*. 2012. V. 7. № 7. P. e40154.
152. Wada T., Honda M., Minami I., Tooi N., Amagai Y., Nakatsuji N., Aiba K. // *PLoS One*. 2009. V. 4. № 8. P. e6722.
153. Zeng H., Guo M., Martins-Taylor K., Wang X., Zhang Z., Park J.W., Zhan S., Kronenberg M.S., Lichtler A., Liu H.X., et al. // *PLoS One*. 2010. V. 5. № 7. P. e11853.
154. Qu Q., Li D., Louis K.R., Li X., Yang H., Sun Q., Crandall S.R., Tsang S., Zhou J., Cox C.L., et al. // *Nat. Commun.* 2014. V. 5. P. 3449.
155. Lu L., Li Y., Kim S.M., Bossuyt W., Liu P., Qiu Q., Wang Y., Halder G., Finegold M.J., Lee J.S., et al. // *Proc. Natl. Acad. Sci. USA*. 2010. V. 107. № 4. P. 1437–1442.
156. Bastow E.L., Gourlay C.W., Tuite M.F. // *Biochem. Soc. Trans.* 2011. V. 39. № 5. P. 1482–1487.
157. Couthouis J., Hart M.P., Shorter J., Dejesus-Hernandez M., Erion R., Oristano R., Liu A.X., Ramos D., Jethava N., Hosangadi D., et al. // *Proc. Natl. Acad. Sci. USA*. 2011. V. 108. № 52. P. 20881–20890.
158. Martins D., English A.M. // *Redox Biol.* 2014. V. 2. P. 632–639.
159. Oeda T., Shimohama S., Kitagawa N., Kohno R., Imura T., Shibasaki H., Ishii N. // *Hum. Mol. Genet.* 2001. V. 10. № 19. P. 2013–2023.
160. Vaccaro A., Tauffenberger A., Aggad D., Rouleau G., Drapeau P., Parker J.A. // *PLoS One*. 2012. V. 7. № 2. P. e31321.
161. Gidalevitz T., Krupinski T., Garcia S., Morimoto R.I. // *PLoS Genet.* 2009. V. 5. № 3. P. e1000399.
162. Wang J., Farr G.W., Hall D.H., Li F., Furtak K., Dreier L., Horwich A.L. // *PLoS Genet.* 2009. V. 5. № 1. P. e1000350.
163. Ash P.E., Zhang Y.J., Roberts C.M., Saldi T., Hutter H., Buratti E., Petrucelli L., Link C.D. // *Hum. Mol. Genet.* 2010. V. 19. № 16. P. 3206–3218.
164. Liachko N.F., Guthrie C.R., Kraemer B.C. // *J. Neurosci.* 2010. V. 30. № 48. P. 16208–16219.
165. Watson M.R., Lagow R.D., Xu K., Zhang B., Bonini N.M. // *J. Biol. Chem.* 2008. V. 283. № 36. P. 24972–24981.
166. Lanson N.A., Jr., Maltare A., King H., Smith R., Kim J.H., Taylor J.P., Lloyd T.E., Pandey U.B. // *Hum. Mol. Genet.* 2011. V. 20. № 13. P. 2510–2523.
167. Wang J.W., Brent J.R., Tomlinson A., Shneider N.A., McCabe B.D. // *J. Clin. Invest.* 2011. V. 121. № 10. P. 4118–4126.
168. Xia R., Liu Y., Yang L., Gal J., Zhu H., Jia J. // *Mol. Neurodegener.* 2012. V. 7. P. 10.
169. Miguel L., Avequin T., Delarue M., Feuillet S., Frebourg T., Champion D., Lecourtois M. // *Neurobiol. Aging*. 2012. V. 33. № 5. P. 1008. e1–15.
170. Li Y., Ray P., Rao E.J., Shi C., Guo W., Chen X., Woodruff E.A., 3rd, Fushimi K., Wu J.Y. // *Proc. Natl. Acad. Sci. USA*. 2010. V. 107. № 7. P. 3169–3174.
171. Lu Y., Ferris J., Gao F.B. // *Mol. Brain*. 2009. V. 2. P. 30.
172. Hanson K.A., Kim S.H., Wassarman D.A., Tibbetts R.S. // *J. Biol. Chem.* 2010. V. 285. № 15. P. 11068–11072.
173. Elden A.C., Kim H.J., Hart M.P., Chen-Plotkin A.S., Johnson B.S., Fang X., Armarkola M., Geser F., Greene R., Lu M.M., et al. // *Nature*. 2010. V. 466. № 7310. P. 1069–1075.
174. Ramesh T., Lyon A.N., Pineda R.H., Wang C., Janssen P.M., Canan B.D., Burghes A.H., Beattie C.E. // *Dis. Model Mech.* 2010. V. 3. № 9–10. P. 652–662.
175. Bosco D.A., Lemay N., Ko H.K., Zhou H., Burke C., Kwiatkowski T.J., Jr., Sapp P., Mckenna-Yasek D., Brown R.H., Jr., Hayward L.J. // *Hum. Mol. Genet.* 2010. V. 19. № 21. P. 4160–4175.
176. Kabashi E., Bercier V., Lissouba A., Liao M., Brustein E., Rouleau G.A., Drapeau P. // *PLoS Genet.* 2011. V. 7. № 8. P. e1002214.
177. Gurney M.E., Pu H., Chiu A.Y., Dal Canto M.C., Polchow C.Y., Alexander D.D., Caliendo J., Hentati A., Kwon Y.W., Deng H.X., et al. // *Science*. 1994. V. 264. № 5166. P. 1772–1775.
178. Deng H.X., Shi Y., Furukawa Y., Zhai H., Fu R., Liu E., Gorrie G.H., Khan M.S., Hung W.Y., Bigio E.H., et al. // *Proc. Natl. Acad. Sci. USA*. 2006. V. 103. № 18. P. 7142–7147.
179. Wong P.C., Pardo C.A., Borchelt D.R., Lee M.K., Copeland N.G., Jenkins N.A., Sisodia S.S., Cleveland D.W., Price D.L. // *Neuron*. 1995. V. 14. № 6. P. 1105–1116.
180. Chang-Hong R., Wada M., Koyama S., Kimura H., Arawaka S., Kawanami T., Kurita K., Kadoya T., Aoki M., Itoyama Y., et al. // *Exp. Neurol.* 2005. V. 194. № 1. P. 203–211.
181. Wang J., Xu G., Gonzales V., Coonfield M., Fromholt D., Copeland N.G., Jenkins N.A., Borchelt D.R. // *Neurobiol. Dis.* 2002. V. 10. № 2. P. 128–138.
182. Wang J., Slunt H., Gonzales V., Fromholt D., Coonfield M., Copeland N.G., Jenkins N.A., Borchelt D.R. // *Hum. Mol. Genet.* 2003. V. 12. № 21. P. 2753–2764.
183. Wang L., Deng H.X., Grisotti G., Zhai H., Siddique T., Roos R.P. // *Hum. Mol. Genet.* 2009. V. 18. № 9. P. 1642–1651.
184. Wang J., Ma J.H., Giffard R.G. // *Free Radic. Biol. Med.* 2005. V. 38. № 8. P. 1112–1118.
185. Deng H.X., Jiang H., Fu R., Zhai H., Shi Y., Liu E., Hirano M., Dal Canto M.C., Siddique T. // *Hum. Mol. Genet.* 2008. V. 17. № 15. P. 2310–2319.
186. Jonsson P.A., Graffmo K.S., Andersen P.M., Brannstrom T., Lindberg M., Oliveberg M., Marklund S.L. // *Brain*. 2006. V. 129. Pt 2. P. 451–464.
187. Watanabe Y., Yasui K., Nakano T., Doi K., Fukada Y., Kitayama M., Ishimoto M., Kurihara S., Kawashima M., Fukuda H., et al. // *Brain Res. Mol. Brain Res.* 2005. V. 135. № 1–2. P. 12–20.
188. Nagai M., Aoki M., Miyoshi I., Kato M., Pasinelli P., Kasai N., Brown R.H., Jr., Itoyama Y. // *J. Neurosci.* 2001. V. 21. № 23. P. 9246–9254.
189. Howland D.S., Liu J., She Y., Goad B., Maragakis N.J., Kim B., Erickson J., Kulik J., Devito L., Psaltis G., et al. // *Proc. Natl. Acad. Sci. USA*. 2002. V. 99. № 3. P. 1604–1609.
190. Xu Y.F., Gendron T.F., Zhang Y.J., Lin W.L., Dalton S., Sheng H., Casey M.C., Tong J., Knight J., Yu X., et al. // *J. Neurosci.* 2010. V. 30. № 32. P. 10851–10859.
191. Shan X., Chiang P.M., Price D.L., Wong P.C. // *Proc. Natl. Acad. Sci. USA*. 2010. V. 107. № 37. P. 16325–16330.
192. Igaz L.M., Kwong L.K., Lee E.B., Chen-Plotkin A., Swanson E., Unger T., Malunda J., Xu Y., Winton M.J., Trojanowski J.Q., et al. // *J. Clin. Invest.* 2011. V. 121. № 2. P. 726–738.
193. Awano T., Johnson G.S., Wade C.M., Katz M.L., Johnson G.C., Taylor J.F., Perloski M., Biagi T., Baranowska I., Long S., et al. // *Proc. Natl. Acad. Sci. USA*. 2009. V. 106. № 8. P. 2794–2799.
194. Coates J.R., Winger F.A. // *Vet. Clin. North Am. Small Anim. Pract.* 2010. V. 40. № 5. P. 929–950.
195. Dimos J.T., Rodolfa K.T., Niakan K.K., Weisenthal L.M., Mitsumoto H., Chung W., Croft G.F., Saphier G., Leibel R., Goland R., et al. // *Science*. 2008. V. 321. № 5893. P. 1218–1221.
196. Chestkov I.V., Vasilieva E.A., Illarioshkin S.N., Lagarkova M.A., Kiselev S.L. // *Acta Naturae*. 2014. V. 6. № 1. P. 54–60.

## REVIEWS

197. Owen N., Doe C.L., Mellor J., Davies K.E. // *Hum. Mol. Genet.* 2000. V. 9. № 5. P. 675–684.
198. Paushkin S., Charroux B., Abel L., Perkinson R.A., Pellizzoni L., Dreyfuss G. // *J. Biol. Chem.* 2000. V. 275. № 31. P. 23841–23846.
199. Hannus S., Buhler D., Romano M., Seraphin B., Fischer U. // *Hum. Mol. Genet.* 2000. V. 9. № 5. P. 663–674.
200. Miguel-Aliaga I., Culetto E., Walker D.S., Baylis H.A., Sattelle D.B., Davies K.E. // *Hum. Mol. Genet.* 1999. V. 8. № 12. P. 2133–2143.
201. Briese M., Esmaeili B., Fraboulet S., Burt E.C., Christodoulou S., Towers P.R., Davies K.E., Sattelle D.B. // *Hum. Mol. Genet.* 2009. V. 18. № 1. P. 97–104.
202. Rajendra T.K., Gonsalvez G.B., Walker M.P., Shpargel K.B., Salz H.K., Matera A.G. // *J. Cell Biol.* 2007. V. 176. № 6. P. 831–841.
203. Workman E., Saieva L., Carrel T.L., Crawford T.O., Liu D., Lutz C., Beattie C.E., Pellizzoni L., Burghes A.H. // *Hum. Mol. Genet.* 2009. V. 18. № 12. P. 2215–2229.

# Structure and Biological Functions of $\beta$ -Hairpin Antimicrobial Peptides

P. V. Panteleev, I. A. Bolosov, S. V. Balandin, T. V. Ovchinnikova\*

M.M. Shemyakin and Yu.A. Ovchinnikov Institute of Bioorganic Chemistry of the Russian Academy of Sciences, Miklukho-Maklaya Str., 16/10, Moscow, 117997, Russia

\*E-mail: ovch@ibch.ru

Received 12.11.2014

Copyright © 2015 Park-media, Ltd. This is an open access article distributed under the Creative Commons Attribution License, which permits unrestricted use, distribution, and reproduction in any medium, provided the original work is properly cited.

**ABSTRACT** Antimicrobial peptides (AMPs) are evolutionarily ancient factors of the innate immune system that serve as a crucial first line of defense for humans, animals, and plants against infection. This review focuses on the structural organization, biosynthesis, and biological functions of AMPs that possess a  $\beta$ -hairpin spatial structure. Representatives of this class of AMPs are among the most active antibiotic molecules of animal origin. Due to their wide spectrum of activity and resistance to internal environmental factors, natural  $\beta$ -hairpin AMP-based compounds might become the most promising drug candidates.

**KEYWORDS** antimicrobial peptides, innate immunity,  $\beta$ -hairpin structure.

**ABBREVIATIONS** AMP – antimicrobial peptide; LPS – lipopolysaccharide; MIC – minimum inhibitory concentration; HIV – human immunodeficiency virus; LEAP-1 – liver-expressed antimicrobial peptide-1 (hepcidin); MRSA – methicillin-resistant *Staphylococcus Aureus*.

## INTRODUCTION

The innate immune system provides immediate protection for an organism in response to pathogen introduction through a variety of molecular factors that implement the recognizing and effector mechanisms of its function: cell adhesion molecules, pattern recognition (including Toll-like) receptors, scavenger receptors, peptidoglycan recognition proteins, lectins, pentraxins, components of the complement system, LPS-binding protein, lysozyme, lactoferrin, cytokines, chemokines, and many others responsible for the regulation of the initiation and course of protective reactions [1]. Along with the aforementioned protein factors of innate immunity, endogenous antimicrobial peptides (AMPs), produced in vertebrates, invertebrates, plants, fungi and bacteria, play a special role in the protection of an organism against infection. AMPs are mainly synthesized on ribosomes within precursor proteins and might be subjected to post-translational modifications during the maturation process. Mature AMPs contain several to several dozen amino acid residues and usually have basic properties due to their high content of lysine and arginine [2]. Initially, AMPs isolated from insect hemolymph, amphibian skin secretions, and mammalian phagocytes attracted the attention of researchers due to their ability to inhibit the growth of various microorganisms. As novel AMPs began to appear, it became evident that these are universal and evolutionarily ancient elements of the innate immune system. Later, along with facts indicating a direct effector (an-

tibiotic) action, the new ability of most AMPs to play a regulatory (immunomodulatory) role and participate in the functioning of both the innate and acquired immunity has been revealed [3]. In this regard, two terms can be found in the literature: antimicrobial peptides and host defense peptides; the latter is more often applied in relation to the peptides that coordinate immune processes within the host organism.

Acquired immunity appeared during the process of evolution only with the emergence of jawed fish about 500 million years ago. Since invertebrate organisms lack acquired immunity, they can only rely on their innate immune system when coming into contact with pathogens. It is worth noting that the vast majority (98%) of animal species on Earth are invertebrates, with some representatives having a life cycle of more than 100 years [4]. Taking into account the “evolutionary success” of invertebrates, one can speak of the high performance of their immune defense system. In multicellular organisms, AMPs can be distributed systemically, for example, through hemolymph in insects or expressed by immune cells in the blood of vertebrates, or localize in epithelial tissues, which more often come into contact with pathogens (mucous membranes, skin). The wide range of antibiotic characteristics of AMPs, including those directed against resistant strains of pathogens, a relatively low probability to select AMP-resistant infectious agents, and fast and effective destruction of target cells allow one to tap these peptide compounds as a basis for developing a new generation of drugs [5].

About 4,000 natural AMPs have been isolated and characterized thus far [6]. Such physicochemical and biological characteristics as origin, molecular size, primary structure, type of biological activity, mechanism of action, etc. can be used for a classification of AMPs. However, the spatial structure of peptides has turned out to be the most convenient criterion for such classification. The first classification based on the spatial structure was proposed in 1995 [7]. The presence and the number of disulfide bonds in a peptide molecule play a central role in this system. The most widespread classification divides all AMPs into three structural classes. The first class includes peptides that share the  $\alpha$ -helical conformation. The second class combines linear peptides that do not form  $\alpha$ -helices and can be distinguished by the abundant presence of certain amino acid residues (Gly, Pro, His, Trp). The third class is comprised of peptides that exhibit antiparallel  $\beta$ -strands in their structure. Among the latter group of AMPs are also molecules with a  $\beta$ -sheet structure consisting of three strands (most vertebrate defensins), two strands with a  $\beta$ -hairpin structure, or a mixed structure that includes both  $\beta$ -sheets and  $\alpha$ -helices. This review focuses on  $\beta$ -hairpin antimicrobial peptides of animal origin stabilized by disulfide bonds. *Figure 1* presents data on the multifunctional properties of the main representatives of  $\beta$ -hairpin AMPs, as well as their primary and spatial structures.

The molecular mechanism of the antibiotic action of AMPs in most cases involves a disruption of the cytoplasmic membrane. Three basic models have been proposed to describe the mechanisms of impairment of the barrier function of the cell membrane in the presence of AMPs. The first one, the “barrel-stave” model [8], suggests that AMP molecules, which usually possess a net positive charge, are hydrophobic and amphiphilic in nature, are incorporated into the membrane to form oligomeric ion channels or pores with their inner surface formed by hydrophilic amino acid residues. This model has been proposed particularly for  $\beta$ -hairpin AMP tachyplesin isolated from horseshoe crab hemocytes [9]. Taking into account the high content of basic amino acid residues in the structure of most AMPs, the resulting channels are expected to possess a positively charged inner surface and be anion-selective, which is usually not the case. However, the channels formed by  $\beta$ -hairpin AMP tachyplesin turned out to be anion-selective. The second model is based on the description of the toroidal pore formation (the toroidal pore model) and applicable to a wider range of AMPs [10]. The main difference between the abovementioned models is that the second one suggests that the inner hydrophilic surface of the channels includes not only AMP cationic sites, but anionic heads of phospholipids as well. The

advantage of this model consists in the higher stability of the complex due to the electrostatic interactions between the AMP and lipids. The third model known as the “carpet model” is based on the detergent-like action of AMPs at high peptide concentrations [11]. The membrane gradually loses its stability as the AMP concentration increases, thus leading to the formation of toroidal gaps and lipid-peptide micelles and finally resulting in cell lysis. The scope of these models for application is conditional, and the final result of AMP action through any of the aforementioned mechanisms is the disruption of the cell membrane barrier function. The selectivity of AMP action is due to the differences in the biochemical composition and electrophysiological properties of the microbial membranes and host cells [12].

Along with the extensive data on the membranotropic properties of AMPs there has been an increasing number of reports on their intracellular targets. In particular, tachyplesin was shown to bind to DNA in the minor groove [13]. When binding to DNA, AMPs can inhibit the replication and transcription processes. Aside from the cytoplasmic membrane and intracellular targets, some AMPs exhibit affinity to the components of bacterial and fungal cell walls. The antibiotic action of such AMPs is thought to be ensured through the inhibition of cell wall biosynthesis. Many AMPs that exhibit antifungal activity (including tachyplesin) are capable of binding to chitin [14].

Besides the inactivation of microorganisms, including bacteria, fungi, protozoa and viruses, AMPs as molecular factors of the innate immune system participate in the regulation of immune reactions. In particular, AMPs possess the ability to opsonize microbes [15]; exhibit chemotactic activity against macrophages, neutrophils, and immature dendritic cells [16]; cause the degranulation of mast cells [17]; modulate dendritic cell differentiation [18]; and they are also involved in the regulation of angiogenesis [19] and possess corticostatic activity [20]. Specific examples of the involvement of  $\beta$ -hairpin AMPs in the regulation of immune reactions are shown below.

Further, we consider the structural and functional characteristics of the main representatives of the  $\beta$ -hairpin AMP family divided into four subgroups, depending on the number of disulfide bonds.

## 1. $\beta$ -HAIRPIN AMPs STABILIZED BY A SINGLE DISULFIDE BOND

### Lactoferricins

Lactoferricins are the fragments of the functional N-terminal domain of lactoferrin that are produced by limited proteolysis of the protein by pepsin under acid-

## REVIEWS

| Name            | Source   | Activity            | Amino acid sequence               | Spatial structure   | References      |
|-----------------|--|---------------------|-----------------------------------|---|-----------------|
| Tigerinin-1     | <i>Rana tigrina</i><br>(frog skin secretion)                   | B, M                | <b>FCTMIPIPRCY*</b>               | -   | [37]            |
| Bactenecin      | <i>Bos taurus</i><br>(bovine neutrophils)                      | B, V                | <b>RLCRIVVIRVCR</b>               | -   | [34]            |
| Thanatin        | <i>Podisus maculiventris</i><br>(spined soldier bug hemolymph) | B, F                | <b>GSKKPVPPIIYCNRRTGKCRQM</b>     |    | [40, 42]        |
| Arenicin-2      | <i>Arenicola marina</i> (lugworm coelomocytes)                 | B, F, H             | <b>RWCVYAYVRIRGVLVRYRRCW</b>      |    | [50, 54]        |
| Lactoferricin B | <i>Bos taurus taurus</i><br>(bovine milk)                      | B, F, V, C, E, I    | <b>FKCRRWQWRMKKLGAPSIITCVRRAF</b> |    | [22, 23]        |
| Tachyplesin-1   | <i>Tachyplesus tridentatus</i><br>(horseshoe crab hemocytes)   | B, F, V, C, H, E, I | <b>KWCFRVCYRGICYRRCR*</b>         |    | [62, 63]        |
| Gomesin         | <i>Acanthoscurria gomesiana</i><br>(spider hemocytes)          | B, F, P, C, H       | <b>ZCRRLCYKQRCVTYCRGR*</b>        |    | [72, 73]        |
| Androctonin     | <i>Androctonus australis</i><br>(scorpion hemolymph)           | B, F, T             | <b>RSVCRQIKICRRRGGCYKCTNRPY</b>   |  | [76, 77]        |
| Protegrin-1     | <i>Sus scrofa</i><br>(porcine leukocytes)                      | B, F, V, C, H       | <b>RGGRLCYCRRRFCVCGVR*</b>        |  | [79, 80]        |
| θ-defensin-1    | <i>Macaca mulatta</i><br>(rhesus monkey leukocytes)            | B, F, V, E, I       | <b>GFCRCLCRRGVCRICCTR</b>         |  | [89, 93]        |
| Hepcidin        | <i>Homo sapiens</i><br>(human hepatocytes)                     | B, M                | <b>DTHFPICIFCCGCHRSKCGMCKT</b>    |  | [100, 101, 103] |

**Fig. 1.** Structure and biological activities of  $\beta$ -hairpin antimicrobial peptides. The disulfide bonds are marked with thin lines. The bold line denotes the peptide bond that forms a  $\theta$ -defensin cycle. (\*) – C-terminal amidation, Z – N-terminal pyroglutamic acid. The biological activities are indicated as follows: B – antibacterial, F – antifungal, V – antiviral, P – antiparasitic, C – anticancer, H – cytotoxic and hemolytic, E – exo- and endotoxin binding, I – immunomodulatory, T – neurotoxic, M – metabolic ones.

ic conditions (Fig. 2). Lactoferrin is a multifunctional iron-binding glycoprotein now regarded as one of the essential elements of the defense system against infections in humans and animals. The possible involvement of lactoferrin in resistance against infection was first

noticed by Japanese scientists [21]. They isolated two peptides that were the fragments 1–54 and 17–41 of the N-terminal region of bovine lactoferrin and exhibited significantly greater antimicrobial activity than the parent protein. Fragment 17–41, which was later

called lactoferricin B [22], is a cationic peptide with a single disulfide bond forming an 18-membered ring between residues Cys2 and Cys20 [23]. Lactoferricin family members have a number of the protective properties intrinsic to lactoferrins isolated from human and bovine milk, with some of these properties being more potent than in the case of the parent protein. Lactoferricins exhibit antimicrobial activity against a broad range of microorganisms, acting both through bactericidal and bacteriostatic mechanisms [24]. The antiviral effect of lactoferricin B is less potent than that of native bovine lactoferrin. Nevertheless, it has an inhibitory effect against a number of viruses [25]. Along with suppression of pathogenic bacteria, lactoferricin B exhibits inhibitory activity against several fungal pathogens, including *Candida albicans* and some dermatophytes [26], *in vitro* antitumor activity against a variety of malignant cell types produced in leukemia, fibrosarcoma and neuroblastoma at concentrations non-toxic to fibroblasts and erythrocytes [27]. It is worth noting that lactoferricin B causes tumor cell death both through necrosis and apoptosis [28, 29]. In addition to that, the peptide exhibits immunomodulatory activity, acting as an anti-inflammatory agent [30]. This effect is explained by the ability of lactoferricin B to bind unmethylated CpG-containing oligonucleotides that are released during bacterial cell death or proliferation and activate inflammatory processes in the organism [31]. Lactoferricin B is also able to actively bind bacterial LPSs, thereby inhibiting the activity of immune system cells [32]. To date, the human lactoferrin-derived fragment hLF1-11, which possesses anti-inflammatory activity, has passed phase I of clinical trials as an immunomodulator [33].

### Bactenecin

Bactenecin is a small antimicrobial peptide isolated from the neutrophilic granulocytes of cattle that consists of 12 amino acid residues. Cysteine residues at positions 3 and 11 form a disulfide bond resulting in a 9-membered ring [34]. Native bactenecin exhibits a pronounced antibacterial activity against a broad spectrum of both Gram-positive and Gram-negative bacteria, while its hemolytic activity is negligible [35]. A number of bactenecin analogs that have an increased therapeutic index have been obtained. Some of these peptides possess antiviral activity against the herpes virus [36].

### Tigerinin-1

Tigerinin-1 is a short peptide consisting of 12 amino acid residues. Isolated from the skin of the frog *Rana tigerina*, this peptide is rather different from other amphibian AMPs. The cysteines at positions 2 and 10

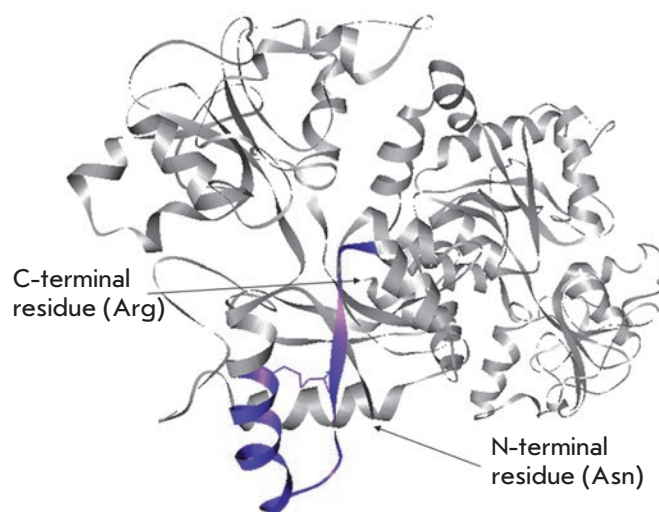


**Fig. 2.** Crystal structure of bovine lactoferrin. The region of the amino acid sequence corresponding to lactoferricin B (residues 17–41) is highlighted in purple

form a disulfide bond, which leaves a large portion of the molecule within the 9-membered ring. This structural feature is common to both tigerinin and bactenecin [37]. The similarity is also reflected in the spectra of the peptides' activity. Tigerinin exhibits antimicrobial activity against a broad range of pathogenic microorganisms [38]. One of tigerinin analogs, tigerinin-1R, is to be mentioned separately, since it is capable of stimulating insulin production. It has been shown that the peptide can cause membrane depolarization and increase intracellular  $\text{Ca}^{2+}$  concentration in pancreatic  $\beta$ -cells, thus stimulating insulin release. The course of experiments conducted in mice with type II diabetes showed that injection of tigerinin-1R leads to a significant acceleration in glucose decomposition. Furthermore, the peptide does not exert any toxic effect on the organism. The possible development of tigerinin-1R-based drug effective in type II diabetes is currently being discussed [39].

### Thanatin

Among the numerous AMPs isolated from insects, thanatin from the spined soldier bug *Podisus maculiventris* is the only peptide molecule with a  $\beta$ -hairpin conformation. Mature thanatin consists of 21 amino acid residues and bears a significant positive charge (+6) at physiological pH [40]. The peptide shares no significant homology with other protective peptides in insects [41]. However, its primary and secondary structures are close to those of the AMPs from the skin secretions of the frog *Rana* [41]. The degree of homol-

ogy between thanatin and brevenin-1 isolated from the skin of the Japanese frog *R. brevipoda* approaches 50%, with both peptides containing a small loop at the C-terminal part of the molecule, which is formed by a disulfide bond and comprises eight (thanatin) or seven (brevenin) amino acid residues (Fig. 3).

The motif typical of brevenins and known as “Rana box” was found in many amphibian AMPs: esculentins, gaegurins, and ranalexins. In all of these molecules, the cycle contains positively charged residues separated by a threonine residue. In thanatin, such a region forms a rigid  $\beta$ -hairpin structure, while the N-terminal fragment of the peptide retains mobility [42].

Thanatin was found to be produced in an insect’s fat body upon experimental infection with pathogenic microorganisms. The peptide is characterized by a wide spectrum of antibacterial and antifungal activities; it is capable of suppressing the growth of Gram-positive and Gram-negative bacteria, as well as filamentous fungi and yeasts at concentrations in most cases not exceeding 10  $\mu$ M. Furthermore, thanatin shows no hemolytic activity even at concentrations one order of magnitude higher than MIC against bacteria, indicating the high selectivity of its action. Thanatin can inhibit the growth of several multidrug-resistant bacteria, including antibiotic-resistant strains of *Enterobacter aerogenes* and *Klebsiella pneumoniae*. Native thanatin promotes the efficacy of a number of classical antibiotics against clinical isolates expressing the efflux pumps that provide multidrug resistance [43]. In the course of structural and functional studies of thanatin, a series of analogs with improved therapeutic indices were found [44]. A truncated analog of thanatin, R-thanatin, can effectively suppress the growth and formation of biofilms in various MRSA strains both *in vitro* and *in vivo* [45]. Of most interest among the analogs is the more active S-thanatin, wherein the threonine at position 15 has been replaced by serine. This analog has demonstrated high safety and efficacy against a multiresistant strain of *K. pneumoniae* both *in vitro* and in the case of intravenous administration in mice [46, 47]. The ability of thanatin to effectively suppress the growth of fungal pathogens has been applied in the field of plant biotechnology. Thus, transgenic rice and Arabidopsis cultures containing the thanatin gene have demonstrated high resistance to a number of phytopathogens [48, 49].

### Arenicins

Arenicins are cationic peptides isolated from coelomocytes of the lugworm *Arenicola marina* [50]. Arenicin molecules consist of 21 amino acid residues, six of which are positively charged arginine residues, and stabilized with a disulfide bond forming an 18-membered macrocycle (Fig. 4). Natural arenicins show high

Thanatin  
Brevenin-1

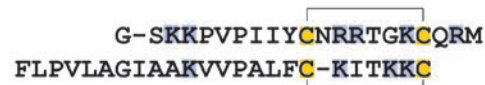


Fig. 3. Amino acid sequences of thanatin from *P. maculiventris* and brevenin-1 from *R. brevipoda*. Cysteine residues are highlighted in yellow. Basic amino acid residues are highlighted in blue. The disulfide bonds are marked with thin lines

Arenicin-1  
Arenicin-2  
Arenicin-3



Fig. 4. Amino acid structures of arenicin isoforms from *A. marina*. Cysteine residues are highlighted in yellow. Basic amino acid residues are highlighted in blue. The disulfide bonds are marked with thin lines

activity against Gram-positive and Gram-negative bacteria, as well as pathogenic fungi and yeasts even under high ionic strength conditions [51]. Studies by a variety of methods have demonstrated the ability of arenicins to disrupt the integrity of bacterial membranes. Obtained experimental data suggest a bactericidal, but not bacteriostatic, mechanism of arenicin action. The study of the antifungal activity of arenicin-1 showed its involvement in the induction of apoptosis [52]. Furthermore, natural isoforms of arenicin exhibit high hemolytic activity. The results of *in vivo* experiments on the assessment of the recombinant arenicin total toxicity have shown that the peptide can be referred to as a Class III toxicity ( $20 > LD_{50} > 700$  mg/kg) for CD-1 mice [53]. The spatial structure of arenicin-2 in aqueous solutions is a twisted  $\beta$ -hairpin stabilized by nine hydrogen bonds and one disulfide bond [54, 55]. When surrounded by a membrane, conformational changes and peptide dimerization take place, leading to the lipid-mediated formation of oligomeric pores [56–58]. A similar mechanism of membrane depolarization resulting in the formation of toroidal pores has been described earlier for  $\beta$ -hairpin AMP protegrin [59].

## 2. $\beta$ - HAIRPIN AMPs STABILIZED BY TWO DISULFIDE BONDS

### Arenicin-3

In 2005, the Danish pharmaceutical company Adenium Biotech patented the antimicrobial peptide arenicin-3

isolated from lugworm *A. marina* [60]. The spectrum of its biological activity is similar to the spectra of the earlier discovered arenicin-1 and arenicin-2 [50] (Fig. 4). Arenicin-3 differs significantly in structure from the other two members of the family: the homology degrees constitute only 57% and 44% at the nucleotide and amino acid levels of the precursor proteins, respectively. Arenicin-3 consists of 21 amino acid residues, has a net positive charge of +4 and is biologically active at concentrations of less than 1  $\mu\text{M}$  against a broad spectrum of Gram-positive and Gram-negative bacteria, including clinical isolates with multidrug resistance. Unlike arenicin-1 and arenicin-2, this molecule is stabilized by two disulfide bonds and causes almost no lysis of erythrocytes at concentrations of up to 400  $\mu\text{M}$ . High-throughput screening of combinatorial libraries has allowed researchers to create a wide range of arenicin-3 analogs, the structures of which have been patented. The study of the antimicrobial action of arenicin-3 *in vivo* revealed their high therapeutic potential, since the effective doses turned out to be one order of magnitude lower than the maximum-tolerated dose in mouse models of pneumonia and urinary tract infection. One of the arenicin-3 analogs (NZ17074) is currently undergoing preclinical studies as a therapeutic agent against infections caused by multidrug-resistant Gram-negative bacteria [61].

### Tachyplesins and polyphemusins

Tachyplesins were isolated from the hemocytes of horseshoe crab *Tachyplesus tridentatus* [62]. Similar peptides, called polyphemusins, were found in a closely related species: *Limulus polyphemus* [63]. Along with other antimicrobial factors, tachyplesins and polyphemusins are deposited in small-granule hemocytes [64]. Tachyplesins and polyphemusins consist of 17–18 amino acid residues, have a net positive charge of +6 or +7, and are stabilized by two disulfide bonds. Among the notable features of their structure is the presence of an amidated C-terminal arginine residue. Positively charged and hydrophobic residues provide pronounced amphiphilic properties, when in contact with a lipid bilayer [65]. Tachyplesins exhibit marked activity against a broad spectrum of bacteria and yeasts. Polyphemusins show a similar spectrum of antimicrobial activity. However, the MIC values are generally lower, which provides ground for considering the members of this subfamily to be the most active AMPs of animal origin, along with protegrins and arenicins [66]. Moreover, the activity of these peptides is not limited to direct membranotropic action. In addition to the ability to form stable pores and cause depolarization of bacterial membranes, tachyplesin can also bind to intracellular targets, particularly genomic and plasmid

DNAs [13]. Moreover, tachyplesin can bind bacterial endotoxins and likewise exhibit immunomodulatory function, participating in the activation of the complement system and regulating the proliferation of cells responsible for the innate immune response [67]. The discovery of polyphemusin antiviral activity against human immunodeficiency (HIV) and influenza viruses led to the development of several therapeutically useful analogs with the appropriate direction of action [68]. Another target for tachyplesins and polyphemusins is tumor cells. Despite the pronounced membranotropic activity, including that in relation to erythrocytes, the antitumor properties of these molecules are associated with such processes as activation of apoptosis [69], inhibition of tumor cell proliferation [70], and activation of the classical complement pathway [71].

### Gomesin

Gomesin is an AMP isolated from the hemocytes of the spider *Acanthoscurria gomesiana* [72]. The protein is structurally closer to tachyplesins and polyphemusins [73]. The homology level between these AMPs is about 50%. Gomesin contains 18 amino acid residues, including four cysteines that form two disulfide bonds, N-terminal pyroglutamic acid, and a C-terminal amidated arginine residue. Similar modifications of the N- and C-terminal residues are found among peptide hormones. The spectrum of the antimicrobial activity of gomesin is as wide as that of its homologs, and it includes Gram-negative and Gram-positive bacteria, parasitic protozoa, as well as yeast and filamentous fungi. For example, gomesin is capable of binding to the membrane surface and inhibiting the growth of the yeast-like fungus *Cryptococcus neoforma* [74]. Similar to tachyplesins, gomesin exhibits antitumor activity both *in vitro* in relation to melanoma and malignant breast and colon cells, and *in vivo* in melanoma-grafted mice [75]. It is important to note that gomesin has moderate hemolytic activity and toxicity in relation to normal cells.

### Androctonin

Androctonin is a 25-membered peptide from the hemolymph of the scorpion *Androctonus australis* that contains four cysteine residues forming two disulfide bonds [76]. The synthesis of androctonin occurs constitutively in scorpion hemocytes. An androctonin molecule has a large net positive charge (+8) and contains the RRRGG motif, which is also found in scorpion defensins. The amino acid sequences of androctonins, tachyplesins, and polyphemusins are characterized by a moderate level of homology, but their spatial structures differ in the type of  $\beta$ -turn [77]. In addition, the location of cysteine residues and the position of di-

sulfide bonds in the peptide resemble those of  $\alpha$ -conotoxin SII, a blocker of n-acetylcholine receptors isolated from the venom of the marine mollusk *Conus striatus* (Fig. 5). Moreover, androctonin was reported to share a comparable with  $\alpha$ -conotoxin SII affinity to the nicotinic receptors in *Torpedo* [76], thus suggesting a basis for the development of analgesic drugs.

Androctonin does not cause lysis of mammalian erythrocytes even at high concentrations, up to 150  $\mu$ M, which may be due to its greater hydrophilicity and mild amphiphilic properties [78]. However, despite the low content (about 30%) of hydrophobic residues as compared with other  $\beta$ -hairpin AMPs, androctonin is able to disrupt the integrity of bacterial membranes. Androctonin is active against Gram-positive and Gram-negative bacteria, yeast and filamentous fungi, while its linear analog, which does not contain any disulfide bonds, exhibits activity only against Gram-positive bacteria.

### Protegrins

The family of protegrins, first isolated from porcine neutrophils more than 20 years ago [79], includes four isoforms consisting of 16–18 amino acid residues. The stability of the protegrin spatial structure is provided by two intramolecular disulfide bonds [80]. Protegrins belong to the family of cathelicidins, AMPs synthesized as the C-terminal region of the precursor protein containing a conserved cathelin domain. Mature protegrins are formed in the extracellular space during proteolytic processing by elastase [81]. As mentioned earlier, protegrins are among the most active AMPs. The MIC of protegrin-1 against the majority of bacterial strains is less than 0.5  $\mu$ M [82]. For comparison, MSI-78 is a highly potent analog of one of the best known  $\alpha$ -helical AMPs, magainin, which was isolated from the skin of the frog *Xenopus laevis* and acts through a membranotropic mechanism similar to that of protegrins, and exhibits activity against a broad spectrum of bacterial strains at concentrations ~2–4  $\mu$ M and higher [83]. Aside from its antibacterial action, protegrin can also exhibit activity against yeast and tumor cells [84, 85], as well as viruses [86]. One of the protegrin analogs, the synthetic 17-membered peptide iseganan (IB-367), selected by screening of several hundred analogs with various amino acid substitutions and deletions, should be noted separately [87]. Iseganan exhibits pronounced activity against a broad spectrum of bacteria and fungi, sometimes even exceeding that of natural peptides. The protein preserves its bactericidal activity in a 150 mM NaCl solution, which is equal to the physiological concentration of Na<sup>+</sup> in human blood plasma. Iseganan is regarded as a promising agent for treating patients with oral mucositis, patients undergoing anticancer

Androctonin  
 $\alpha$ -Conotoxin SII

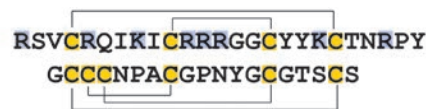


Fig. 5. Amino acid sequences of androctonin from *A. australis* and  $\alpha$ -conotoxin SII from *C. striatus*. Cysteine residues are highlighted in yellow. Basic amino acid residues are highlighted in blue. The disulfide bonds are marked with thin lines

| Source                                    | Gene/Pseudogene   | Nonapeptide + 3 a.a. |
|---|-------------------|----------------------|
| <i>Homo sapiens</i><br>(human)            | DEFT-1 ( $\psi$ ) | RCICGRGIC RLL        |
|   | DEFT-4 ( $\psi$ ) | RCICGRRIC RLL        |
| <i>Gorilla gorilla</i><br>(gorilla)       | DEFT-1 ( $\psi$ ) | RCICGRGIC RLL        |
| <i>Macaca mulatta</i><br>(rhesus monkey)  | DEFT-1            | RCLCRRGVC QLL        |
|   | DEFT-2            | RCICTRGFC RLL        |
|   | DEFT-3            | RCICVLGIC RLL        |
|   | DEFT-4            | RCICTRGVC QLL        |
| <i>Hylobates syndactylus</i><br>(siamang) | DEFT-1            | RCICGRGVC RLL        |

Fig. 6. Comparison of primate DEFT genes/pseudogenes expression products [91]. Only the first nine amino acid residues (nonapeptide) in each sequence are incorporated into a mature circular  $\theta$ -defensin. The other three amino acid residues are eliminated during processing. Cysteine residues are highlighted in yellow. Basic amino acid residues are highlighted in blue

therapy, as well as for treating ventilator-associated pneumonia, cystic fibrosis, and preventing various sexually transmitted diseases [88].

### 3. $\beta$ -HAIRPIN AMPs STABILIZED BY THREE DISULFIDE BONDS

#### $\theta$ -defensins

Vertebrate defensins are usually subdivided into three subfamilies:  $\alpha$ -,  $\beta$ -, and  $\theta$ -defensins. All of them share cationic properties, the presence of  $\beta$ -structural regions and six cysteine residues that form three intramolecular disulfide bonds. The subfamilies differ in molecular size, structure and properties, as well as the location of the disulfide bonds.  $\theta$ -defensins were isolated from the leukocytes of *Catarrhini*, rhesus monkeys and baboons, and are the only example of covalently linked cyclic peptides of animal origin [89, 90].  $\theta$ -Defensins have not been found in humans and other most evolutionarily “advanced” primates. It was shown later that human leukocytes produce mRNA encoding precursor proteins of  $\theta$ -defensins, but the presence of a stop codon

in the signal sequence prevents its biosynthesis [91]. Human  $\theta$ -defensins, known as retrocyclins, have been synthesized using transcript sequence data [92]. Simian  $\theta$ -defensins are formed by “head-to-tail” splicing of the two nonapeptides, which are the fragments of two independent precursor proteins (Fig. 6). Thus, mature  $\theta$ -defensins consist of 18 amino acid residues and form a  $\beta$ -hairpin structure stabilized by three disulfide bonds [93] (Fig. 7). It is worth noting that due to the independent homo- or heterodimeric splicing the number of genes expressing precursor proteins (*DEFT*) defines the finite number of  $\theta$ -defensin isoforms in a species. Thus, in *Papio anubis* baboon the expression of four *DEFT* genes should theoretically lead to the formation of ten isoforms; however, there were only five peptides found [94]. *DEFT* is a mutated gene of the  $\alpha$ -defensin precursor with a stop codon in the region encoding for the mature peptide.

By disrupting the structural integrity of the membrane,  $\theta$ -defensins and retrocyclins exhibit high antibacterial and antifungal activity at concentrations of about 1  $\mu$ M. However, unlike the other AMPs described above, they show a one-order decrease in activity following a considerable increase in ionic strength.  $\theta$ -defensins possess the ability to bind bacterial exotoxins, in particular the anthrax lethal factor from *Bacillus anthracis* [95] and listeriolysin O from *Listeria monocytogenes* [96]. As in androctonins, the spatial structure of  $\theta$ -defensins is characterized by low amphiphilicity, which is rather unusual for  $\beta$ -hairpin AMPs and results in a low hemolytic activity of the molecules. Due to its low toxicity and the discovery that they exhibit the properties of lectines,  $\theta$ -defensins are regarded as the prototype of antiviral agents. Numerous studies have demonstrated the ability of retrocyclins to prevent human immunodeficiency [92], influenza [97], and herpes [98] viruses. It is worth noting that the antiviral effect of  $\theta$ -defensins is not associated with the virotoxic or cytotoxic effect against infected cells.  $\theta$ -defensins are believed to prevent the spread of enveloped viruses by binding to the surface glycoproteins responsible for the interaction between the virus and the cell during infection. The immunomodulatory activity of  $\theta$ -defensins, which manifests itself through the ability to inhibit biosynthesis of proinflammatory cytokines, has been demonstrated [99].

#### 4. $\beta$ -HAIRPIN AMPs STABILIZED BY FOUR DISULFIDE BONDS

##### Hepcidins

Hepcidins are a family of  $\beta$ -hairpin AMPs stabilized by four disulfide bonds. Hepcidins are found in many vertebrates at the transcriptome level, but the mature peptides were isolated only from human and fish flu-

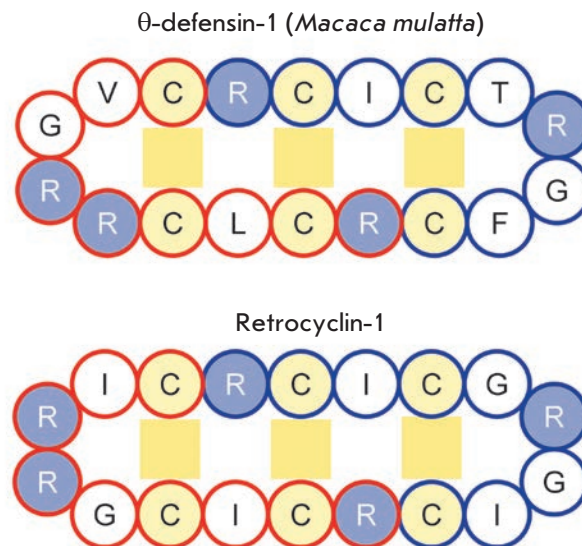


Fig. 7. Amino acid sequences of  $\theta$ -defensin-1 from *Macaca mulatta* and retrocyclin-1. The amino acid residues of the first and second nonapeptides coupling in the cyclic structure are circled in red and blue, respectively. Cysteine residues are highlighted in yellow. Basic amino acid residues are highlighted in blue

ids and tissues [100–102]. Human hepcidin, sometimes referred to as liver-expressed AMP-1 (LEAP-1), was isolated from urine, blood, and the liver. The nucleotide sequence encoding hepcidin is rather conserved between different species, which is especially apparent in mammals. Hepcidins are characterized by the following order of disulfide bonds: Cys1–Cys8, Cys2–Cys7, Cys3–Cys6, Cys4–Cys5, with three of them involved in the interaction of  $\beta$ -strands, whereas the disulfide bridge Cys4–Cys5 causes the deformation typical of molecules of this family in the region of the  $\beta$ -turn and formation of a groove with basic amino acid residues in the inner side and hydrophobic amino acid residues in the outer side [103]. Due to their amphiphilic structure, hepcidins possess a wide spectrum of antimicrobial activity inhibiting the growth of bacteria, filamentous fungi, and yeasts. It is worth noting that mature hepcidins have been detected in fish and isolated from the gills, although the gene is primarily expressed in hepatocytes. Biosynthesis of hepcidin is induced in fish when subjected to pathogenic bacteria. A similar situation was observed in humans: mature peptides were present in urine and blood serum, while the mRNA is predominantly synthesized in the liver.

It has been established that the antimicrobial effect of hepcidin is not due to its direct influence on the bac-

terial membrane [104], but to its ability to bind nucleic acids [105] and free iron deprivation of the microorganisms [106] necessary for the functioning of superoxide dismutase; i.e. protection against reactive oxygen species. That is why, in spite of the typical properties of AMPs, regulation of the iron metabolism is considered to be its main physiological function in the organism. A series of experiments on knockout mice suggested that hepcidin plays a key role in maintaining iron homeostasis [107]. The lack of hepcidin in the organism leads to metabolic disorders characterized by iron overload. Hepcidin excess is associated with chronic renal failure, anemia, inflammation, and a number of other diseases [108].

### CONCLUSIONS

The data presented above indicate that, despite the relatively small number of known  $\beta$ -hairpin AMPs, their biological functions are very diverse. Summarizing the findings, a conclusion can be drawn that  $\beta$ -hairpin AMPs share a series of essential structural and functional features in terms of the possibility of developing new antibiotics based on their structure, namely: small size (up to 25 amino acid residues), net positive charge and amphiphilic properties sufficient for the manifestation of membranotropic activity against a broad spectrum of bacterial targets, and compact structure stabilized by disulfide bonds providing enhanced proteolytic resistance. The key role of disulfide bonds as a factor that provides the resistance of  $\beta$ -hairpin AMPs to biodegradation has been shown in a number of papers on

the example of the analogs of lactoferricin, bactenecin, gomesin, and  $\theta$ -defensin [109–112]. Thus, all  $\beta$ -hairpin AMPs described in this review share both a similarity in their spatial structures and the ability to effectively destroy target bacterial cells. Their main advantage compared to conventional antibiotics is that bacteria are not yet able to develop effective mechanisms to resist these substances, as this would require significant changes in the structure and electrophysiological properties of the cell membrane [113].

The search for and study of the structural and functional features of  $\beta$ -hairpin AMPs provide exclusively abundant material for developing next-generation drugs. The key objective for researchers laboring on developing new peptide antibiotics is currently the problem of toxicity and increasing the longevity of these molecules in the bloodstream. Due to their structural and functional features,  $\beta$ -hairpin AMPs can be used to develop antibiotics for systemic and surface application, immunomodulators, blockers of exo- and endotoxins, drugs for treating metabolic disorders, anticancer and antiviral drugs, and analgesics. An alternative area of application for  $\beta$ -hairpin AMPs is agricultural biotechnology: namely, the development of transgenic lines of plants that constitutively express AMP genes and, therefore, exhibit high resistance to phytopathogenic microorganisms and other stressful environmental factors. ●

*This work was supported by the Russian Science Foundation (grant № 14-14-01036).*

### REFERENCES

- Kokryakov V.N. Ocherki o vrozhdennom immunitete (Essays on innate immunity). St. Petersburg: Nauka, 2006. 261 p.
- Zasloff M. // *Nature*. 2002. V. 415. № 6870. P. 389–395.
- Oppenheim J.J., Biragyn A., Kwak L.W., Yang D. // *Ann. Rheum. Dis*. 2003. V. 62 (Suppl 2). P. ii17–ii21.
- Bergquist D.C., Williams F.M., Fisher C.R. // *Nature*. 2000. V. 403. № 6769. P. 499–500.
- Roscia G., Falciani C., Bracci L., Pini A. // *Curr. Protein Pept. Sci*. 2013. V. 14. № 8. P. 641–649.
- Zhao X., Wu H., Lu H., Li G., Huang Q. // *PLoS One*. 2013. V. 8. № 6. P. e66557.
- Boman H.G. // *Annu. Rev. Immunol*. 1995. V. 13. P. 61–92.
- Baumann G., Mueller P. J. // *Supramol. Struct*. 1974. V. 2. № 5–6. P. 538–557.
- Matsuzaki K., Yoneyama S., Fujii N., Miyajima K., Yamada K., Kirino Y., Anzai K. // *Biochemistry*. 1997. V. 36. № 32. P. 9799–9806.
- Yang L., Harroun T.A., Weiss T.M., Ding L., Huang H.W. // *Biophys. J*. 2001. V. 81. № 3. P. 1475–1485.
- Shai Y. // *Biochim. Biophys. Acta*. 1999. V. 1462. № 1–2. P. 55–70.
- Matsuzaki K. // *Biochim. Biophys. Acta*. 1999. V. 1462. № 1–2. P. 1–10.
- Yonezawa A., Kuwahara J., Fujii N., Sugiura Y. // *Biochemistry*. 1992. V. 31. № 11. P. 2998–3004.
- Osaki T., Omotezako M., Nagayama R., Hirata M., Iwanaga S., Kasahara J., Hattori J., Ito I., Sugiyama H., Kawabata S.J. // *Biol. Chem*. 1999. V. 274. № 37. P. 26172–26178.
- Fleischmann J., Selsted M., Lehrer R.I. // *Diagn. Microbiol. Dis*. 1985. V. 3. № 3. P. 233–242.
- Biragyn A., Surenhu M., Yang D., Ruffini P.A., Haines B.A., Klyushnenkova E., Oppenheim J.J., Kwak L.W. // *J. Immunol*. 2001. V. 167. № 11. P. 6644–6653.
- Niyonsaba F., Someya A., Hirata M., Ogawa H., Nagaoka I. // *Eur. J. Immunol*. 2001. V. 31. № 4. P. 1066–1075.
- Davidson D.J., Currie A.J., Reid G.S., Bowdish D.M., MacDonald K.L., Ma R.C., Hancock R.E., Speert D.P. // *Immunol*. 2004. V. 172. № 2. P. 1146–1156.
- Li J., Post M., Volk R., Gao Y., Li M., Metais C., Sato K., Tsai J., Aird W., Rosenberg R., et al. // *Nat. Med*. 2000. V. 6. № 1. P. 49–55.
- Zhu Q.Z., Hu J., Mulay S., Esch F., Shimasaki S., Solomon S. // *Proc. Natl. Acad. Sci. USA*. 1988. V. 85. № 2. P. 592–596.
- Saito T., Miyakawa H., Tamura Y.J. // *Dairy Sci*. 1991. V. 74. № 11. P. 3724–3730.
- Bellamy W., Takase M., Yamauchi K., Wakabayashi H., Kawase K., Tomita M. // *Biochem. Biophys. Acta*. 1992. V. 1121. № 1–2. P. 130–136.

## REVIEWS

23. Hwang P.M., Zhou N., Shan X., Arrowsmith C.H., Vogel H.J. // *Biochemistry*. 1998. V. 37. № 12. P. 4288–4298.
24. Yamauchi K., Tomita M., Giehl T.J., Ellison R.T. // *Infect. Immunol.* 1993. V. 61. № 2. P. 719–728.
25. Jenssen H., Andersen J.H., Uhlin-Hansen L., Gutteberg T.J., Rekdal O. // *Antiviral Res.* 2004. V. 61. № 2. P. 101–109.
26. Bellamy W., Yamauchi K., Wakabayashi H., Takase M., Takakura N., Shimamura S., Tomita M. // *Lett. Appl. Microbiol.* 2008. V. 18. P. 230–233.
27. Yoo Y., Watanabe S., Watanabe R., Hata K., Shimazaki K., Azuma I. // *Jpn. J. Cancer Res.* 1997. V. 88. № 2. P. 184–190.
28. Eliassen L.T., Berge G., Leknessund A., Wikman M., Lindin I., Løkke C., Ponthan F., Johnsen J.I., Sveinbjørnsson B., Kogner P., et al. // *Int. J. Cancer*. 2006. V. 119. № 3. P. 493–500.
29. Mader J.S., Salsman J., Conrad D.M., Hoskin D.W. // *Mol. Cancer. Ther.* 2005. V. 4. № 4. P. 612–624.
30. Mattsby-Baltzer I., Roseanu A., Motas C., Elverfors J., Engberg I., Hanson L.A. // *Pediatr. Res.* 1996. V. 40. № 2. P. 257–262.
31. Britigan B.E., Lewis T.S., Waldshemidt M., McCormick M.L., Krieg A.M. // *J. Immunol.* 2001. V. 167. № 5. P. 2921–2928.
32. Ellison R., 3rd, Giehl T. // *J. Clin. Invest.* 1991. V. 88. № 8. P. 1080–1091.
33. Velden W.J., van Iersel T.M., Blijlevens N.M., Donnelly J.P. // *BMC Med.* 2009. V. 7. P. 44.
34. Romeo D., Skerlavaj B., Bolognesi M., Gennaro R. // *J. Biol. Chem.* 1988. V. 263. № 20. P. 9573–9575.
35. Wu M., Hancock R. // *Antimicrob. Agents Chemother.* 1999. V. 43. № 5. P. 1274–1276.
36. Shestakov A., Jenssen H., Hancock R.E., Nordström I., Eriksson K. // *Antiviral Res.* Nov. 2013. V. 100. № 2. P. 455–459.
37. Sai K.P., Jagannadham M.V., Vairamani M., Raju N.P., Devi A.S., Nagaraj R., Sitaram N. // *J. Biol. Chem.* 2001. V. 276. № 4. P. 2701–2707.
38. Sitaram N., Purna Sai K., Singh S., Sankaran K., Nagaraj R. // *Antimicrob. Agents Chemother.* 2002. V. 46. № 7. P. 2279–2283.
39. Ojo O., Abdel-Wahab Y., Flatt P., Mechkarska M., Conlon J. // *Diabetes Obes. Metab.* 2011. V. 13. № 12. P. 1114–1122.
40. Fehlbaum P., Bulet P., Chernysh S., Briand J.P., Rousssel J.P., Letellier L., Hetru C., Hoffmann J.A. // *Proc. Natl. Acad. Sci.* 1996. V. 93. № 3. P. 1221–1225.
41. Morikawa N., Hagiwara K., Nakajima T. // *Biochem. Biophys. Res. Commun.* 1992. V. 189. № 1. P. 184–190.
42. Mandard N., Sodano P., Labbe H., Bonmatin J.M., Bulet P., Hetru C., Ptak M., Vovelle F. // *Eur. J. Biochem.* 1998. V. 256. № 2. P. 404–410.
43. Pages J.M., Dimarcq J.L., Quenin S., Hetru C. // *Int. J. Antimicrob. Agents.* 2003. V. 22. № 3. P. 265–269.
44. Lee M.K., Cha L., Lee S.H., Hahm K.S. // *J. Biochem. Mol. Biol.* 2002. V. 35. № 3. P. 291–296.
45. Hou Z., Da F., Liu B., Xue X., Xu X., Zhou Y., Li M., Li Z., Ma X., Meng J., et al. // *Antimicrob. Agents Chemother.* 2013. V. 57. № 10. P. 5045–5052.
46. Wu G., Deng X., Wu P., Shen Z., Xu H. // *Peptides*. 2012. V. 36. № 1. P. 109–113.
47. Wu G., Wu P., Xue X., Yan X., Liu S., Zhang C., Shen Z., Xi T. // *Peptides*. 2013. V. 45. P. 73–77.
48. Wu T., Tang D., Chen W., Huang H., Wang R., Chen Y. // *Gene*. 2013. V. 527. № 1. P. 235–242.
49. Imamura T., Yasuda M., Kusano H., Nakashita H., Ohno Y., Kamakura T., Taguchi S., Shimada H. // *Transgenic Res.* 2010. V. 19. № 3. P. 415–424.
50. Ovchinnikova T.V., Aleshina G.M., Balandin S.V., Krasnodembskaya A.D., Markelov M.L., Frolova E.I., Leonova Y.F., Tagaev A.A., Krasnodembsky E.G., Kokryakov V.N. // *FEBS Lett.* 2004. V. 577. № 1–2. P. 209–214.
51. Andrä J., Jakovkin I., Grötzinger J., Hecht O., Krasnodembskaya A.D., Goldmann T., Gutschmann T., Leippe M. // *Biochem. J.* 2008. V. 410. № 1. P. 113–122.
52. Cho J., Lee D.G. // *Biochim. Biophys. Acta.* 2011. V. 1810. № 12. P. 1246–1251.
53. Diachenko I.A., Murashev A.N., Yakimenko Z.A., Balandin S.V., Ovchinnikova T.V. // *Toksikologicheskii vestnik. (Toxicological review)*. 2012. V. 112. № 1. P. 40–43. In Russian.
54. Ovchinnikova T.V., Shenkarev Z.O., Nadezhdin K.D., Balandin S.V., Zhmak M.N., Kudelina I.A., Finkina E.I., Kokryakov V.N., Arseniev A.S. // *Biochem. Biophys. Res. Commun.* 2007. V. 360. № 1. P. 156–162.
55. Stavrakoudis A., Tsoulos I.G., Shenkarev Z.O., Ovchinnikova T.V. // *Biopolymers*. 2009. V. 92. № 3. P. 143–155.
56. Ovchinnikova T.V., Shenkarev Z.O., Balandin S.V., Nadezhdin K.D., Paramonov A.S., Kokryakov V.N., Arseniev A.S. // *Biopolymers*. 2008. V. 89. № 5. P. 455–464.
57. Salnikov E.S., Aisenbrey C., Balandin S.V., Zhmak M.N., Ovchinnikova T.V., Bechinger B. // *Biochemistry*. 2011. V. 50. № 18. P. 3784–3795.
58. Shenkarev Z.O., Balandin S.V., Trunov K.I., Paramonov A.S., Sukhanov S.V., Barsukov L.I., Arseniev A.S., Ovchinnikova T.V. // *Biochemistry*. 2011. V. 50. № 28. P. 6255–6265.
59. Mani R., Cady S.D., Tang M., Waring A.J., Lehrer R.I., Hong M. // *Proc. Natl. Acad. Sci. USA*. 2006. V. 103. № 44. P. 16242–16247.
60. Hoegenhaug H.H.K., Mygind P.H., Kruse T., Segura D.R., Sandvang D., Neve S. // *WO Patent App.* 2011 PCT/EP2011/059,6896.
61. Fox J.L. // *Nat. Biotechnol.* 2013. V. 31. № 5. P. 379–382.
62. Nakamura T., Furunaka H., Miyata T., Tokunaga F., Muta T., Iwanaga S., Niwa M., Takao T., Shimonishi Y. // *J. Biol. Chem.* 1988. V. 263. № 32. P. 16709–16713.
63. Miyata T., Tokunaga F., Yoneya T., Yoshikawa K., Iwanaga S., Niwa M., Takao T., Shimonishi Y. // *J. Biochem.* 1989. V. 106. № 4. P. 663–668.
64. Shigenaga T., Takayenoki Y., Kawasaki S., Seki N., Muta T., Toh Y., Ito A., Iwanaga S. // *J. Biochem.* 1993. V. 114. № 3. P. 307–316.
65. Oishi O., Yamashita S., Nishimoto E., Lee S., Sugihara G., Ohno M. // *Biochemistry*. 1997. V. 36. № 14. P. 4352–4359.
66. Fjell C.D., Hiss J.A., Hancock R.E., Schneider G. // *Nat. Rev. Drug. Discov.* 2011. V. 11. № 1. P. 37–51.
67. Ozaki A., Ariki S., Kawabata S. // *FEBS J.* 2005. V. 272. № 15. P. 3863–3871.
68. Tamamura H., Kuroda M., Masuda M., Otaka A., Funakoshi S., Nakashima H., Yamamoto N., Waki M., Matsumoto A., Lancelin J.M., et al. // *Biochim. Biophys. Acta.* 1993. V. 1163. № 2. P. 209–216.
69. Chen Y., Xu X., Hong S., Chen J., Liu N., Underhill C.B., Creswell K., Zhang L. // *Cancer Res.* 2001. V. 61. № 6. P. 2434–2438.
70. Shi S.L., Wang Y.Y., Liang Y., Li Q.F. // *World J. Gastroenterol.* 2006. V. 12. № 11. P. 1694–1698.
71. Chen J., Xu X.M., Underhill C.B., Yang S., Wang L., Chen Y., Hong S., Creswell K., Zhang L. // *Cancer Res.* 2005. V. 65. № 11. P. 4614–4622.
72. Silva P. Jr., Daffre S., Bulet P. // *J. Biol. Chem.* 2000. V. 275. № 43. P. 33464–33470.

## REVIEWS

73. Mandard N., Bulet P., Caille A., Daffre S., Vovelle F. // *Eur. J. Biochem.* 2002. V. 269. № 4. P. 1190–1198.
74. Barbosa F.M., Daffre S., Maldonado R.A., Miranda A., Nimrichter L., Rodrigues M.L. // *FEMS Microbiol Lett.* 2007. V. 274. № 2. P. 279–286.
75. Rodrigues E.G., Dobroff A.S., Cavarsan C.F., Paschoalin T., Nimrichter L., Mortara R.A., Santos E.L., Fázio M.A., Miranda A., Daffre S., et al. // *Neoplasia.* 2008. V. 10. № 1. P. 61–68.
76. Ehret-Sabatier L., Loew D., Goyffon M., Fehlbaum P., Hoffmann J.A., van Dorsseleer A., Bulet P. // *J. Biol. Chem.* 1996. V. 271. № 47. P. 29537–29544.
77. Mandard N., Sy D., Maufrais C., Bonmatin J.M., Bulet P., Hetru C., Vovelle F. // *J. Biomol. Struct. Dyn.* 1999. V. 17. № 2. P. 367–380.
78. Hetru C., Letellier L., Oren Z., Hoffmann J.A., Shai Y. // *Biochem J.* 2000. V. 345 (Pt 3). P. 653–664.
79. Kokryakov V.N., Harwig S.S.L., Panyutich E.A., Shevchenko A.A., Aleshina G.M., Shamova O.V., Korneva H.A., Lehrer R.I. // *FEBS Lett.* 1993. V. 327. № 2. P. 231–236.
80. Fahrner R.L., Dieckmann T., Harwig S.S., Lehrer R.I., Eisenberg D., Feigon J. // *Chem. Biol.* 1996. V. 3. № 7. P. 543–550.
81. Panyutich A., Shi J., Boutz P.L., Zhao C., Ganz T. // *Infect Immun.* 1997. V. 65. № 3. P. 978–985.
82. Steinberg D.A., Hurst M.A., Fujii C.A., Kung A.H., Ho J.F., Cheng F.C., Loury D.J., Fiddes J.C. // *Antimicrob. Agents Chemother.* 1997. V. 41. № 8. P. 1738–1742.
83. Ge Y.G., MacDonald D.L., Holroyd K.J., Thornsberry C., Wexler H., Zasloff M. // *Antimicrob. Agents Chemother.* 1999. V. 43. № 4. P. 782–788.
84. Shamova O.V., Sakuta G.A., Orlov D.S., Zenin V.V., Shtein G.I., Kolodkin N.I., Afonina I.V., Kokriakov V.N. // *Cell Tissue Biology.* 2007. V. 1. № 6. P. 524–533.
85. Paredes-Gamero E.J., Martins M.N., Cappabianco F.A., Ide J.S., Miranda A. // *Biochim. Biophys. Acta.* 2012. V. 1820. № 7. P. 1062–1072.
86. Rothan H.A., Abdulrahman A.Y., Sasikumer P.G., Othman S., Rahman N.A., Yusof R. // *J. Biomed. Biotechnol.* 2012. V. 2012. P. ID 251482.
87. Chen J., Falla T.J., Liu H., Hurst M.A., Fujii C.A., Mosca D.A., Embree J.R., Loury D.J., Radcliff P.A., Cheng Chang C., et al. // *Biopolymers.* 2000. V. 55. № 1. P. 88–98.
88. Giles F.J., Redman R., Yazji S., Bellm L. // *Expert Opin. Investig. Drugs.* 2002. V. 11. № 8. P. 1161–1170.
89. Tang Y.Q., Yuan J., Osapay G., Osapay K., Tran D., Miller C.J., Ouellette A.J., Selsted M.E. // *Science.* 1999. V. 286. № 5439. P. 498–502.
90. Lehrer R.I., Cole A.M., Selsted M.E. // *J. Biol. Chem.* 2012. V. 287. № 32. P. 27014–27019.
91. Nguyen T.X., Cole A.M., Lehrer R.I. // *Peptides.* 2003. V. 24. № 11. P. 1647–1654.
92. Cole A.M., Hong T., Boo L.M., Nguyen T., Zhao C., Bristol G., Zack J.A., Waring A.J., Yang O.O., Lehrer R.I. // *Proc. Natl. Acad. Sci. USA.* 2002. V. 99. № 4. P. 1813–1818.
93. Trabi M., Schirra H.J., Craik D.J. // *Biochemistry.* 2001. V. 40. № 14. P. 4211–4221.
94. Garcia A.E., Osapay G., Tran P.A., Yuan J., Selsted M.E. // *Infect. Immun.* 2008. V. 76. № 12. P. 5883–5891.
95. Wang W., Mulakala C., Ward S.C., Jung G., Luong H., Pham D., Waring A.J., Kaznessis Y., Lu W., Bradley K.A., et al. // *J. Biol. Chem.* 2006. V. 281. № 43. P. 32755–32764.
96. Arnett E., Lehrer R.I., Pratikhya P., Lu W., Seveau S. // *Cell Microbiol.* 2011. V. 13. № 4. P. 635–651.
97. Doss M., White M.R., Teclé T., Gantz D., Crouch E.C., Jung G., Ruchala P., Waring A.J., Lehrer R.I., Hartshorn K.L. // *J. Immunol.* 2009. V. 182. № 12. P. 7878–7887.
98. Yasin B., Wang W., Pang M., Cheshenko N., Hong T., Waring A.J., Herold B.C., Wagar E.A., Lehrer R.I. // *J. Virol.* 2004. V. 78. № 10. P. 5147–5156.
99. Schaal J.B., Tran D., Tran P., Osapay G., Trinh K., Roberts K.D., Brasky K.M., Tongaonkar P., Ouellette A.J., Selsted M.E. // *PLoS One.* 2012. V. 7. № 12. P. e51337.
100. Krause A., Neitz S., Mägert H.J., Schulz A., Forssmann W.G., Schulz-Knappe P., Adermann K. // *FEBS Lett.* 2000. V. 480. № 2–3. P. 147–150.
101. Park C.H., Valore E.V., Waring A.J., Ganz T. // *Biol. Chem.* 2001. V. 276. № 11. P. 7806–7810.
102. Shike H., Lauth X., Westerman M.E., Ostland V.E., Carlberg J.M., van Olst J.C., Shimizu C., Bulet P., Burns J.C. // *Eur. J. Biochem.* 2002. V. 269. № 8. P. 2232–2237.
103. Hunter H.N., Fulton D.B., Ganz T., Vogel H.J. // *J. Biol. Chem.* 2002. V. 277. № 40. P. 37597–37603.
104. Hocquellet A., Odaert B., Cabanne C., Noubhani A., Dieryck W., Joucla G., Le Senechal C., Milenkovic M., Chaignepain S., Schmitter J.M. // *Peptides.* 2010. V. 31. № 1. P. 58–66.
105. Hocquellet A., Le Senechal C., Garbay B. // *Peptides.* 2012. V. 36. № 2. P. 303–307.
106. Ganz T. // *Blood.* 2003. V. 102. № 3. P. 783–788.
107. Nicolas G., Bennoun M., Devaux I., Beaumont C., Grandchamp B., Kahn A., Vaulont S. // *Proc. Natl. Acad. Sci. USA.* 2001. V. 98. № 15. P. 8780–8785.
108. Ganz T., Nemeth E. // *Annu. Rev. Med.* 2011. V. 62. P. 347–360.
109. Nguyen L.T., Chau J.K., Perry N.A., de Boer L., Zaat S.A.J., Vogel H.J. // *PLoS One.* 2010. V. 5. № 9. P. e12684.
110. Nan Y., Jacob B., Kim Y., Shin S. // *J. Pept. Sci.* 2012. V. 18. № 12. P. 740–747.
111. Fazio M.A., Oliveira V.X., Bulet P., Miranda M.T.M., Daffre S., Miranda A. // *Biopolymers.* 2006. V. 84. № 2. P. 205–218.
112. Conibear A.C., Rosengren K.J., Daly N.L., Henriques S.T., Craik D.J. // *J. Biol. Chem.* 2013. V. 188. № 15. P. 10830–10840.
113. Peschel A., Sahl H.G. // *Nat. Rev. Microbiol.* 2006. V. 4. № 7. P. 529–536.

# Regulation of PGC-1 $\alpha$ Isoform Expression in Skeletal Muscles

D. V. Popov<sup>1,2\*</sup>, E. A. Lysenko<sup>1</sup>, I. V. Kuzmin<sup>1,3</sup>, O. L. Vinogradova<sup>1,2</sup>, A. I. Grigoriev<sup>1,2</sup>

<sup>1</sup>Institute of Biomedical problems, Russian Academy of Sciences, Khoroshevskoye shosse, 76A, Moscow, 123007, Russia

<sup>2</sup>Faculty of Fundamental Medicine, M.V. Lomonosov Moscow State University, Lomonosovskiy prospect, 26B–10, Moscow, 119192, Russia

<sup>3</sup>Department of Genetics, Faculty of Biology, M.V. Lomonosov Moscow State University, Leninskie Gory, 1–12, Moscow, 119991, Russia

\*E-mail: danil-popov@yandex.ru

Received 26.11.2014

Copyright © 2015 Park-media, Ltd. This is an open access article distributed under the Creative Commons Attribution License, which permits unrestricted use, distribution, and reproduction in any medium, provided the original work is properly cited.

**ABSTRACT** The coactivator PGC-1 $\alpha$  is the key regulator of mitochondrial biogenesis in skeletal muscle. Skeletal muscle expresses several PGC-1 $\alpha$  isoforms. This review covers the functional role of PGC-1 $\alpha$  isoforms and the regulation of their exercise-associated expression in skeletal muscle. The patterns of PGC-1 $\alpha$  mRNA expression may markedly differ at rest and after muscle activity. Different signaling pathways are activated by different physiological stimuli, which regulate the expression of the *PGC-1 $\alpha$*  gene from the canonical and alternative promoters: expression from a canonical (proximal) promoter is regulated by activation of the AMPK; expression from an alternative promoter, via a  $\beta$ 2-adrenergic receptor. All transcripts from both promoters are subject to alternative splicing. As a result, truncated isoforms that possess different properties are translated: truncated isoforms are more stable and predominantly activate angiogenesis, whereas full-length isoforms mainly regulate mitochondrial biogenesis. The existence of several isoforms partially explains the broad-spectrum function of this protein and allows the organism to adapt to different physiological stimuli. Regulation of the *PGC-1 $\alpha$*  gene expression by different signaling pathways provides ample opportunity for pharmacological influence on the expression of this gene. Those opportunities might be important for the treatment and prevention of various diseases, such as metabolic syndrome and diabetes mellitus. Elucidation of the regulatory mechanisms of the *PGC-1 $\alpha$*  gene expression and their functional role may provide an opportunity to control the expression of different isoforms through exercise and/or pharmacological intervention.

**KEYWORDS** alternative splicing, alternative promoter, skeletal muscle, PGC-1 $\alpha$ , gene expression.

**ABBREVIATIONS** AICAR – 5-aminoimidazole-4-carboxamide-1- $\beta$ -D-ribofuranosyl 5'-monophosphate; AMPK – AMP-activated protein kinase; ATF – activating transcription factor; CaMK – Ca<sup>2+</sup>/calmodulin-dependent protein kinase; CREB – cAMP response element-binding protein; ERR – estrogen-related receptor; HDAC – class IIa histone deacetylase; HIF – hypoxia inducible factor; IGF-1 – insulin-like growth factor 1; MEF – myocyte enhancer factor; OXPHOS – oxidative phosphorylation; p38 MAPK – p38 mitogen-activated protein kinases; PGC – peroxisome proliferator-activated receptor gamma, coactivator; PKA – protein kinase A; PPAR – peroxisome proliferator-activated receptor; UCP – uncoupling protein; VEGFA – vascular endothelial growth factor A;  $\dot{V}O_{2max}$  – maximal oxygen consumption rate.

## INTRODUCTION

Skeletal muscle constitutes more than 30% of body mass in adults. As skeletal muscles have high levels of metabolic and secretory activity, they are identified as secretory organs that have an influence on other organs [1]. Blood flow and the consumption of oxygen and substrates (glucose, fatty acids, etc.) increase significantly as active skeletal muscles contract. The pronounced accumulation of calcium ions and other metabolites occurs simultaneously in muscle fibers; a

decrease in energy charge and redox potential may also occur. Aerobic training induces the following marked adaptive changes in skeletal muscles: capillarization, changes in mitochondrial density, and an increase in the activity of oxidative enzymes. Maximum oxygen consumption and aerobic performance of muscles improve due to these changes. These adaptive changes are tightly connected to the functioning of coactivators belonging to the PGC-1 family (peroxisome proliferator-activated receptor (PPAR) gamma coactivator 1).

This family includes PGC-1 $\alpha$ , PGC-1 $\beta$ , and PGC-related coactivators. One of these proteins, PGC-1 $\alpha$ , plays the most important role in regulation of mitochondrial biogenesis in skeletal muscle.

Several isoforms of PGC-1 $\alpha$  exist [2,3]; this partially explains the broad-spectrum function of this protein. Over the past decade, many studies have focused on PGC-1 $\alpha$  function, the molecular mechanisms of its activation, and the regulation of *PGC-1 $\alpha$*  gene expression. Skeletal muscle expresses several PGC-1 $\alpha$  isoforms. This review is devoted to the functional role of PGC-1 $\alpha$  isoforms and to the regulation of their expression in skeletal muscle at rest and during recovery after exercise.

### FULL-LENGTH PGC-1 $\alpha$ ISOFORMS

#### Functional role of PGC-1 $\alpha$

Several signaling kinases, such as AMPK, CaMK, and p38 MAPK [4] and the NAD-dependent deacetylase sirtuin-1 (Sirt-1) [5], are activated in skeletal muscle during and immediately after acute endurance exercise. This activation results in an increase in *PGC-1 $\alpha$*  (*PPARGC1A*) gene expression (see below); an increase in the phosphorylation and acetylation of existing PGC-1 $\alpha$  also occurs (i.e., PGC-1 $\alpha$  activation) (*Fig. 1*). In rodents [6,7] and humans [8,9], activated PGC-1 $\alpha$  translocates from skeletal muscle to the nucleus and coactivates many transcription factors and nuclear receptors. Exercise-induced activation of PGC-1 $\alpha$  may occur without increasing the level of this protein in the nucleus. In human skeletal muscle, acute endurance exercise leads to increased AMPK $\alpha$ 2 [10] and phosphorylated p38 MAPK [11] levels in the nucleus. The authors assumed that the nuclear translocation of these kinases promotes activation of PGC-1 $\alpha$  in the nucleus.

Activated PGC-1 $\alpha$  regulates the expression of its own gene via the feedforward mechanism [12]. The activated protein also co-activates the nuclear respiratory factors (NRF) -1 and -2, estrogen-related receptor (ERR)  $\alpha$ , and peroxisome proliferator-activated receptors (PPAR)  $\alpha$  and  $\gamma$ . The activation of these nuclear receptors and transcription factors induces the expression of many genes involved in the regulation of oxidative phosphorylation (OXPHOS) and fat and carbohydrate metabolism [13-15]. NRF-1 and NRF-2 induce the expression of the mitochondrial transcription factors A (*TFAM*), B1 (*TFB1M*), and B2 (*TFB2M*) genes. These transcription factors, primarily TFAM and TFB2M, translocate to the mitochondria and initiate the expression of genes from mitochondrial DNA [16]. The PGC-1 $\alpha$ -TFAM complex has been found in mitochondria [7,17,18], where it most likely initiates mitochondrial DNA transcription (*Fig. 1*). PGC-1 $\alpha$  also induces the

expression of the hypoxia-inducible factor (HIF), independent of the vascular endothelial growth factor A (*VEGFA*) gene [19,20]. It has recently been demonstrated that skeletal muscle angiogenesis is connected to the PGC-1 $\alpha$ -dependent activation of macrophages [21].

Acute endurance exercise induces a pronounced increase in the expression of the *PGC-1 $\alpha$*  gene, the activation of PGC-1 $\alpha$  present in the cell, and changes in the intracellular localization of the protein. PGC-1 $\alpha$  has a complex effect on nuclear and mitochondrial DNA gene expression. This protein is one of the most important regulators of mitochondrial biogenesis, fat and carbohydrate metabolism, and angiogenesis in skeletal muscle (*Fig. 1*).

#### Regulation of PGC-1 $\alpha$ gene expression derived from the canonical promoter

Over a decade ago, Puigserver and coworkers cloned the *PGC-1 $\alpha$*  gene from mice [22]. The human *PGC-1 $\alpha$*  gene contains 13 exons; this gene encodes a protein composed of 798 a.a. with a calculated mass of ~91 kDa. The promoter of this gene contains two major transcription initiation sites 90 and 119 bp upstream of the initiation transcription codon ATG [23]. The *PGC-1 $\alpha$*  canonical (proximal) promoter contains two conservative binding sites for myocyte enhancer factor 2 (MEF2) and one CRE-binding site for the cAMP response element-binding protein (CREB) [23]. The regulation of *PGC-1 $\alpha$*  gene expression derived from the canonical promoter was investigated in detail (see below and *Fig. 1*). Cellular models and mice were investigated [12,24]; *in vivo* study of mice skeletal muscle by means of optical bioluminescence was performed [25] and the results confirmed the essential role of MEF2 and CREB in activation of *PGC-1 $\alpha$*  gene expression derived from the canonical promoter.

Activated PGC-1 $\alpha$  can coactivate MEF2, thereby upregulating its own gene expression [11,12]. Acute cycling exercise increases the phosphorylation level of nuclear p38 MAPK<sup>Thr180/Tyr182</sup>, increases the amount of the p38 MAPK<sup>Thr180/Tyr182</sup>-MEF2 complex in human skeletal muscle [11], and apparently activates MEF2. MEF2 activity is inhibited by class IIa histone deacetylases (HDAC) [26], primarily HDAC5 [25]. Acute endurance exercise increases the phosphorylation level of HDAC5; in turn, this phosphorylation leads to the dissociation of the MEF2-HDAC5 complex and the nuclear export of HDAC5 [11,27]. Endurance exercise-induced phosphorylation of HDACs is regulated by the kinases CAMKII and AMPK [27]; these kinases respond to intracellular levels of AMP and calcium ions [28,29]. The phosphorylation level and/or the activation of CAMKII and AMPK are positively correlated with the intensity of the endurance exercise [4,30-34].

The CRE transcription factor family includes CREB and the activating transcription factor (ATF)-2. Phosphorylation of CREB<sup>Ser133</sup> and its subsequent activation is regulated by several signaling kinases, including CAMKII and AMPK [35,36]. The activation of CAMKII and AMPK induced by acute endurance exercise increases the phosphorylation level of CREB<sup>Ser133</sup>; the phosphorylation of this protein upregulates *PGC-1 $\alpha$*  gene expression [4,37]. The phosphorylation level of CREB<sup>Ser133</sup> during latter recovery depends on the intensity of the endurance exercise [4].

Stress-mediated activation of p38 MAPK upregulates *PGC-1 $\alpha$*  gene expression via phosphorylation of ATF-2<sup>Thr71</sup> and its subsequent activation [37-39]. Several factors may activate p38 MAPK, including calcium ions and reactive oxygen species [37,39]. Endurance exercise leads to an intensity-independent increase in the p38 MAPK<sup>Thr180/Tyr182</sup> phosphorylation level [4]. Phosphorylation of p38 MAPK<sup>Thr180/Tyr182</sup> may be determined by a systemic factor; the p38 MAPK<sup>Thr180/Tyr182</sup> phosphorylation level increases after acute endurance exercise even in inactive muscle [40]. The phosphorylation level of ATF-2<sup>Thr71</sup> depends on the intensity of the endurance exercise. This finding indirectly indicates that another signaling pathway may be involved in exercise-mediated phosphorylation of ATF-2<sup>Thr71</sup> [4].

The exercise-induced activation of various signaling kinases and their targets, including HDACs, MEF2, ATF-2, and CREB, upregulates the transcriptional activity of the *PGC-1 $\alpha$*  promoter. Moreover, total *PGC-1 $\alpha$*  mRNA expression is associated with exercise of moderate to maximal aerobic power [4,41-43].

### Regulation of expression of the *PGC-1 $\alpha$* gene derived from an alternative promoter

Two groups of researchers have recently independently described an alternative promoter of *PGC-1 $\alpha$*  in skeletal muscle, which is located ~14 kb upstream of the canonical (proximal) promoter (*Fig. 2A*) [2,44]. An additional promoter located 587 kb upstream of the canonical promoter has been described in human nerve tissue. This promoter gives rise to several isoforms of *PGC-1 $\alpha$*  mRNA. However, these transcripts were not detected in skeletal muscle [45]. A tissue-specific isoform of *PGC-1 $\alpha$*  was also found in liver (L-*PGC-1 $\alpha$* ) [46]. In this review, the focus will be mainly directed at the mechanisms behind the regulation of *PGC-1 $\alpha$*  gene expression in skeletal muscle.

Miura *et al.* investigated the effect of  $\beta$ -adrenergic receptor activation on *PGC-1 $\alpha$*  gene expression. The  $\beta$ 2-agonist clenbuterol substantially increased *PGC-1 $\alpha$*  gene expression in mice skeletal muscle. The increase was not observed in knockout animals without  $\beta$ 1-,  $\beta$ 2-, and  $\beta$ 3-adrenergic receptors. The  $\beta$ 2-blockers propran-

olol and ICI 118551 tempered the exercise-induced (45 min running, 15 m/min) increase in *PGC-1 $\alpha$*  gene expression in the skeletal muscle of wild-type mice [47]. These findings suggest that *PGC-1 $\alpha$*  gene expression is regulated at least in part via  $\beta$ -adrenergic receptor activation. The authors also found that different *PGC-1 $\alpha$*  mRNA isoforms are expressed in skeletal muscle [2].

It has been demonstrated [2,20,44] that new transcripts originate from an alternative promoter located 14 kb upstream of the canonical promoter. The canonical promoter originates at the first exon (1a) of the canonical *PGC-1 $\alpha$* -a mRNA isoform. Due to alternative splicing, the alternative promoter directs the transcription of two different first exons (1b and 1c), which results in the *PGC-1 $\alpha$* -b and *PGC-1 $\alpha$* -c mRNA isoforms, respectively. The nucleotide sequence from the second exon to the 13<sup>th</sup> exon is identical in the isoforms *PGC-1 $\alpha$* -a, *PGC-1 $\alpha$* -b, and *PGC-1 $\alpha$* -c. The amino acid sequences encoded by the first exons of *PGC-1 $\alpha$* -b and *PGC-1 $\alpha$* -c mRNAs differ and are shorter than that of *PGC-1 $\alpha$* -a mRNA by 4 and 13 a.a., respectively (*Fig. 2A*). At rest, the mRNA abundance of transcripts derived from the alternative promoter in the skeletal muscle of mice [2,20,48] and humans [49-51] are much lower than that of transcripts derived from the canonical promoter. However, one study demonstrated that the levels of *PGC-1 $\alpha$* -a, *PGC-1 $\alpha$* -b, and *PGC-1 $\alpha$* -c mRNAs were similar in resting skeletal muscles in mice [52].

The proteins encoded by the new transcripts are found to be functionally active. The functional activity of these isoforms was evaluated by transfecting HEK 293 cells with plasmids encoding different nuclear receptor PPAR ( $\alpha$ , - $\delta$ , and - $\gamma$ ) and *PGC-1 $\alpha$*  isoforms. The proteins *PGC-1 $\alpha$* -b, *PGC-1 $\alpha$* -c, and *PGC-1 $\alpha$* -a activated PPARs [2]. The physiological significance of expression from an alternative promoter was confirmed using transgenic mice. The overexpression of *PGC-1 $\alpha$* -b and *PGC-1 $\alpha$* -c in skeletal muscle led to the activation of OXPHOS-related genes and the genes regulating fat metabolism [2]. Another study revealed that the overexpression of *PGC-1 $\alpha$* -b in the skeletal muscle of mice induces the expression of *PGC-1 $\alpha$*  target genes, such as cytochrome c oxidase (COX) 2 and 4, genes that regulate fat metabolism (i.e., *CD36*, *MCAD*, and *CPT1*), and the angiogenesis-associated gene *VEGFA*; the activity of citrate synthase (CS), a marker of mitochondrial density, also increases. During an incremental treadmill test, transgenic mice exhibited increased aerobic performance, a higher maximal oxygen consumption rate ( $\dot{V}O_{2max}$ ), an increased percentage of oxidized fat, and a lower accumulation of lactate in blood compared with wild-type animals [53].

The expression of *PGC-1 $\alpha$*  mRNA from different promoters is regulated by different stimuli. The volun-

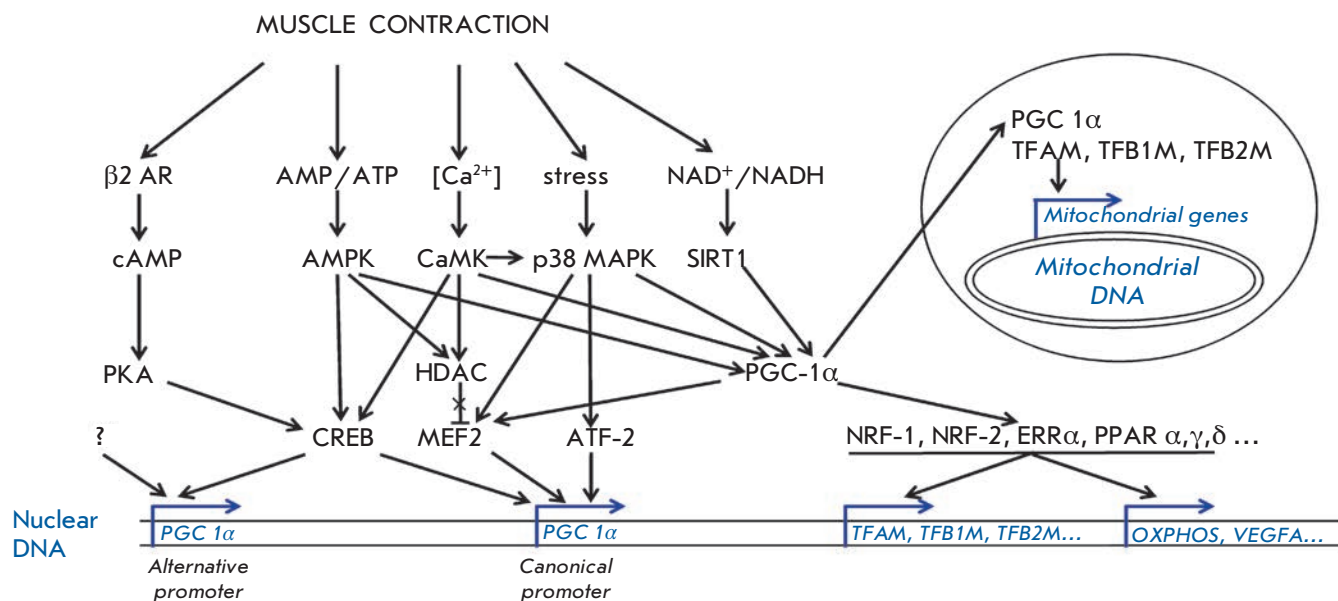


**Fig. 1.** The scheme of PGC-1 $\alpha$  protein activation and regulation of the PGC-1 $\alpha$  gene expression from canonical (proximal) and alternative promoters. AMPK – AMP-activated protein kinase, ATF – activating transcription factor, CaMK – Ca<sup>2+</sup>/calmodulin-dependent protein kinase, CREB – cAMP response element-binding protein, ERR – estrogen-related receptor, HDAC – class IIa histone deacetylase, MEF – myocyte enhancer factor, NRF – nuclear respiratory factor, OXPHOS – oxidative phosphorylation related genes, p38 MAPK – p38 mitogen-activated protein kinases, PGC – peroxisome proliferator-activated receptor gamma, coactivator, PKA – protein kinase A, PPAR – peroxisome proliferator-activated receptor, SIRT1 – NAD-dependent deacetylase sirtuin-1, TFAM – mitochondrial transcription factor A, TFB1M – mitochondrial transcription factor B1, TFB2M – mitochondrial transcription factor B2, VEGFA – vascular endothelial growth factor A,  $\beta$ 2AR –  $\beta$ 2-adrenergic receptor

tary wheel [20] and moderately intensive (15 m/min, 45 min) treadmill [2] running induced a pronounced increase in PGC-1 $\alpha$ -b and PGC-1 $\alpha$ -c mRNA expression in mice skeletal muscle; however, expression of PGC-1 $\alpha$ -a mRNA derived from the canonical promoter remained unchanged. An increase in the running speed up to 20 and 30 m/min led to a proportional 20- and 33-fold increase, respectively, in the PGC-1 $\alpha$ -b mRNA level [48]. Increasing the running speed resulted in only a small rise in the mRNA level of PGC-1 $\alpha$ -a derived from the canonical promoter (1.4- and 1.8-fold increase at running speeds of 20 and 30 m/min, respectively). Following these running sessions, the PGC-1 $\alpha$ -b mRNA level was higher than the PGC-1 $\alpha$ -a mRNA level. A similar ratio was observed between the PGC-1 $\alpha$ -b mRNA level and the PGC-1 $\alpha$ -a mRNA level in human skeletal muscle during recovery after moderately intense exercise (45–90 min) [49,50]. The differences in the regulation of the expression of PGC-1 $\alpha$  isoforms in response to different physiological stimuli were found in other tissues with high metabolic activity. After 21 h of starvation, only the expression of PGC-1 $\alpha$ -a mRNA markedly increased in mouse liver.

After exposure to cold temperatures (4°C) for several hours, only expression of PGC-1 $\alpha$ -b and PGC-1 $\alpha$ -c mRNA increased in the brown adipose tissue of mice [2,54].

The aforementioned studies suggest that the expression derived from the alternative promoter is regulated via activation of a  $\beta$ -adrenergic receptor. This hypothesis was confirmed in the following studies. A clenbuterol injection into the skeletal muscle of mice at rest increased the mRNA levels of PGC-1 $\alpha$ -b and PGC-1 $\alpha$ -c (PGC-1 $\alpha$ -2 and PGC-1 $\alpha$ -3, respectively, in Chinsomboon *et al.*) by several orders of magnitude; however, the mRNA level of PGC-1 $\alpha$ -a (PGC-1 $\alpha$ -1 in Chinsomboon *et al.*) remained unchanged [2,20]. The  $\beta$ -adrenergic receptor inhibitors propranolol and ICI 118551 suppressed the increase in expression from the alternative promoter that is induced by endurance exercise. The pharmacological activation of AMPK was expected to increase the specific expression of PGC-1 $\alpha$  from the canonical promoter. The agent 5-aminoimidazole-4-carboxamide-1 $\beta$ -D-ribofuranoside (AICAR) was used to activate AMPK. However, the injection of AICAR into the skeletal muscle of mice upregulated the

expression from both the canonical promoter (by ~50%) and the alternative promoter (by tenfold) [48]. The authors assumed that the increase in the expression derived from the alternative promoter might be connected to the AICAR-mediated increase in the blood level of catecholamines and stimulation of  $\beta$ -adrenergic receptors in the muscle. In mice, AICAR treatment increased the plasma concentrations of adrenaline and noradrenaline tenfold and by 30%, respectively. The systemic influence of AICAR was excluded in the experiment with isolated rat epitrochlearis muscle. AICAR treatment increased the expression of PGC-1 $\alpha$ -a mRNA by ~50%; however, the expression level of PGC-1 $\alpha$ -b mRNA remained unchanged [48]. This result is in accordance with the findings reported in the previous myoblast study. AICAR treatment did not induce expression from the alternative promoter in C2C12 cells; forskolin, an activator of adenylate cyclase, upregulated expression only from the alternative promoter [44]. Other regulators of expression from the alternative promoter were also revealed. It has been demonstrated that MKK6, a kinase of p38 MAPK, and treatment with calcium ionophore activate expression from the alternative promoter. The constitutively activated forms of the major participants of calcium signaling, CaMKIV and phosphatase calcineurin A, can also upregulate expression from the alternative promoter. The transfection of myoblasts with plasmids containing wild-type or mutant fragments of the alternative promoter confirmed that activation of the alternative promoter depends on the binding of CREB to the CRE site. A similar result was achieved when *m. tibialis anterior* was used to transfect mice [20]. As mentioned above, both the alternative promoter and the canonical promoter contain CRE sites. It remains unclear why phosphorylation of CREB by  $\beta$ -adrenergic receptor signaling induces expression primarily from the alternative promoter [48]. The canonical promoter contains the typical CRE site sequence TGACGTCA (CREB/ATF consensus); the alternative promoter contains a palindromic CRE site with a single nucleotide substitution. This variant of the CRE site can bind CREB and is essential for the initiation of transcription from the alternative promoter. However, the affinity of CREB to a CRE site with a single nucleotide substitution is lower than that of the typical CRE site in the canonical promoter [44,48].

It can be assumed that at rest, even a low concentration of phosphorylated CREB is sufficient to induce high (near maximal) expression from the canonical promoter; the gene expression is induced only slightly as a result of the increased level of phosphorylated CREB. However, a high level of phosphorylated CREB is required to activate transcription from the alternative promoter. Therefore, the alternative promoter might

be more sensitive to changes in CREB activation than the canonical promoter. This fact may explain the differences observed in the expression levels from the canonical and alternative promoters in skeletal muscle at rest and after muscle activity. We cannot ignore the fact that the regulation of transcription from the alternative promoter is sensitive to other CREB-related transcription factors. It has been demonstrated that the transcription factors MyoD and MRF4 can transactivate the alternative promoter through a proximal E-box motif [44].

Through experiments with rodent skeletal muscle, a model of PGC-1 $\alpha$  gene expression under an acute endurance exercise was proposed [20,48]. A low-intensity exercise does not induce AMPK activation; however, exercise of this type increases the activity of the sympathetic nerve system. As a result, the activation of muscle  $\beta$ 2-adrenergic receptors, the accumulation of cAMP, the activation of protein kinase A (PKA), and an increase in the phosphorylation level of CREB<sup>Ser133</sup> occur (Fig. 1). The theoretical AMPK-independent regulation of PGC-1 $\alpha$  gene expression conforms well with the experimental data. In human skeletal muscle, endurance exercise at a moderate intensity does not increase the phosphorylation level of AMPK<sup>Thr172</sup> or the expression level of PGC-1 $\alpha$  from the canonical promoter. Meanwhile, expression of PGC-1 $\alpha$  derived from the alternative promoter is markedly increased [49,50].

An increase in intense endurance exercise above 50–60% of  $\dot{V}O_{2max}$  induces AMPK activation in skeletal muscle [30,31] and increases sympathetic activity. This increase in sympathetic activity activates  $\beta$ -adrenergic receptors in muscle tissue and stimulates expression of the PGC-1 $\alpha$  gene from the alternative promoter. AMPK activation initiates expression from the canonical promoter. AMPK activation occurs only during high-intensity endurance exercise, which results in substantial muscle metabolic perturbations.

We must emphasize that there is no general consensus concerning the mechanisms of PGC-1 $\alpha$  gene regulation in skeletal muscle. Several authors have cast doubt on the PGC-1 $\alpha$  gene regulation model described above. Kim *et al.* investigated the expression of PGC-1 $\alpha$  mRNA and protein in rat tissue 6 and 18 h after clenbutelol and noradrenalin injections [55]. These treatments resulted in a marked increase in PGC-1 $\alpha$  mRNA levels and protein expression in brown adipose tissue; treatment affected neither gene nor protein expression in skeletal muscle. Clenbuterol treatment resulted in an increased phosphorylation level of CREB (Ser<sup>133</sup>) in skeletal muscle. However, the activity of luciferase driven by the PGC-1 $\alpha$  promoter did not change. The authors argued against the above model of PGC-1 $\alpha$  gene regulation. No increase in the PGC-1 $\alpha$  mRNA

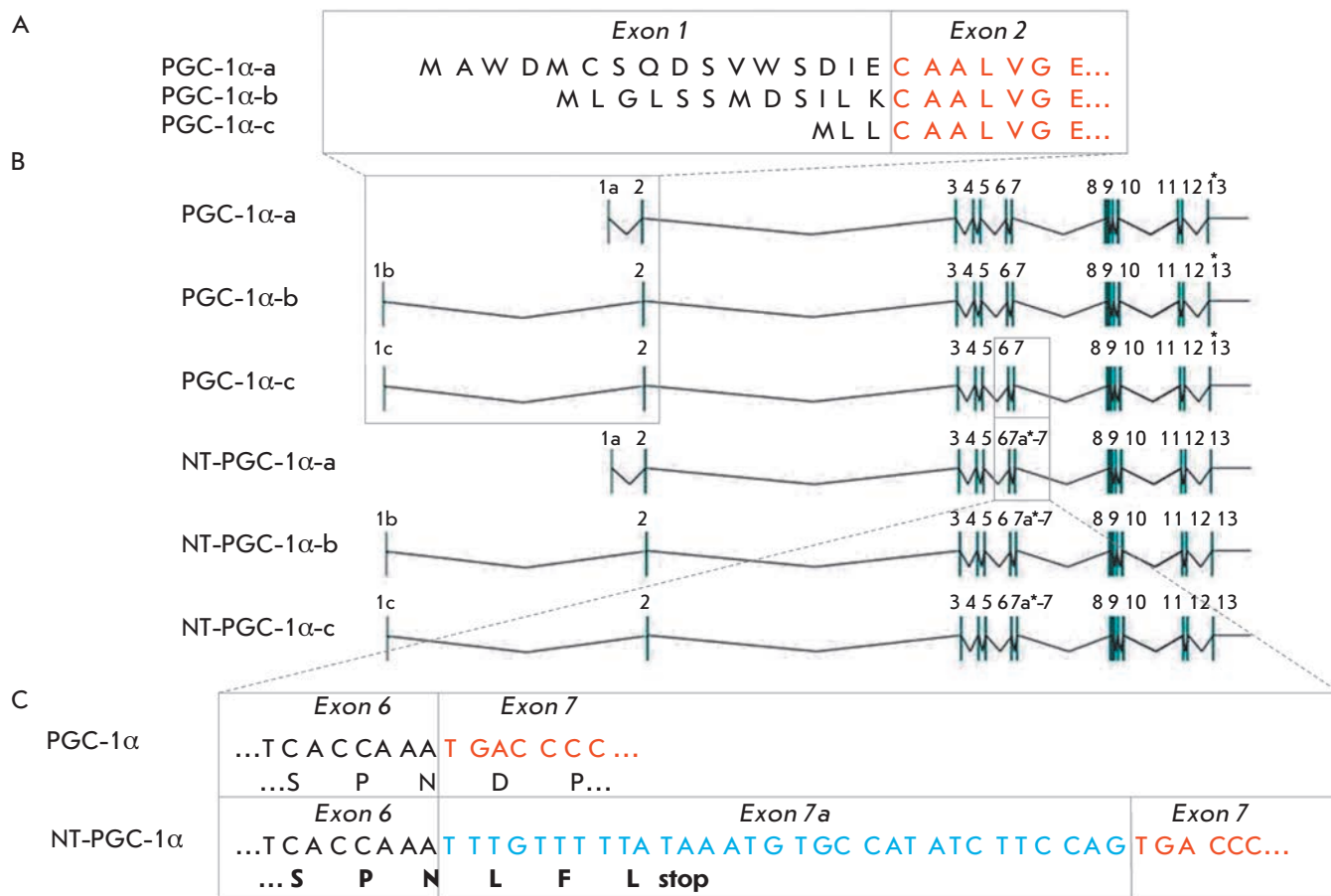


**Fig. 2.** A – Different PGC-1 $\alpha$  mRNA isoforms are expressed from canonical (PGC-1 $\alpha$ -a) and alternative (PGC-1 $\alpha$ -b and PGC-1 $\alpha$ -c) promoters in mice and encode different amino acid sequences in the first exon. B – Scheme of exons (vertical line) of different isoforms and their genomic DNA locations. The asterisk is a stop-codon. C – Nucleotide and amino acid sequences between exons 6 and 7 in the full-length (PGC-1 $\alpha$ ) and truncated (NT-PGC-1 $\alpha$ ) isoforms

level was observed using the primer pair designed to be used in the study. The primers complementary to exon 1a (forward) and 2 (reverse) detected only PGC-1 $\alpha$ -a mRNA derived from the canonical promoter; these primers could not detect changes in expression derived from the alternative promoter. The plasmid used to evaluate luciferase activity contained part of the canonical *PGC-1 $\alpha$*  promoter, which explains why no increase in clenbutelol-mediated transcriptional activity was observed. However, these aspects of the study do not explain the lack of alteration in the PGC-1 $\alpha$  protein expression observed in skeletal muscle; the antibodies used in the study by Kim *et al.* could detect the proteins encoded by transcripts originating from both promoters.

In another article [49], the effects of AICAR and noradrenalin on cultured human myotubes were eval-

uated. Treatment with noradrenalin resulted in an increase only in the PGC-1 $\alpha$ -b mRNA level; this finding is in agreement with the *PGC-1 $\alpha$*  gene regulation model described above. However, AICAR treatment increased both the PGC-1 $\alpha$ -a and PGC-1 $\alpha$ -b mRNA levels. A combined treatment had an additive effect on expression derived from the alternative promoter. The authors concluded that AMPK is the most important regulator of *PGC-1 $\alpha$*  gene expression, since it can regulate expression from both promoters. This finding is in agreement with the result of a recent study in mice [62]. The ability of adrenalin to activate p38 MAPK was demonstrated [56]. This phenomenon could potentially influence *PGC-1 $\alpha$*  gene expression from the canonical promoter.

The activation of *PGC-1 $\alpha$*  gene expression from different promoters may be regulated by the intensity of

the endurance exercise. The aforementioned studies implied that all PGC-1 $\alpha$  isoforms are full-length isoforms containing 13 exons. It was demonstrated later that alternative splicing of other PGC-1 $\alpha$  mRNA isoforms gives rise to a stop-codon between exons 6 and 7 (see below). Most of the studies cited above used a forward primer that was aligned to one of the first exons (1a, 1b or 1c) and reverse primer that was aligned to the second exon (common to all PGC-1 $\alpha$  mRNA isoforms). In most of the studies, PGC-1 $\alpha$  protein abundance was evaluated by immunoblotting at a molecular weight greater than 90 kDa (corresponding to the full-length PGC-1 $\alpha$  protein). Therefore, the evaluated transcripts encoded both full-length and truncated PGC-1 $\alpha$  proteins. These isoforms have different characteristics and functions (see below); many active sites present in full-length PGC-1 $\alpha$  are absent in truncated PGC-1 $\alpha$ .

It remains unclear whether all of the PGC-1 $\alpha$  mRNA isoforms are translated to proteins *in vivo*; the functions of these hypothetical proteins are also unknown. The N-termini of PGC-1 $\alpha$  isoforms differ from each other only by a few amino acids at the beginning of the protein. It is unlikely that such small differences have a substantial influence on the function of these isoforms. The N-terminus often contains sequences related to intracellular transport. Our unpublished data reveal that the N-termini of PGC-1 $\alpha$  isoforms do not contain typical nuclear or mitochondrial localization sequences. The absence of known localization sequences does not disprove the hypothesis that isoforms originating from different promoters have a specific intracellular distribution; however, this distribution becomes less probable. The existence of different *PGC-1 $\alpha$*  promoters indicates that gene expression is regulated by different signaling pathways activated by different physiological stimuli.

### Truncated PGC-1 $\alpha$ isoforms

In their early study, Baar *et al.* investigated the molecular adaptation of rat skeletal muscle to acute endurance exercise. In a Western blot, increased band intensities were observed for full-length PGC-1 $\alpha$  and an additional band at ~34 kDa; it was suggested that this second protein was a smaller form of PGC-1 $\alpha$  [57]. Zhang *et al.* have demonstrated that a short insert might appear between exons 6 and 7 as a result of alternative splicing in brown adipose tissue. This insert (exon 7a) contains a stop-codon and encodes an N-truncated (NT) isoform of PGC-1 $\alpha$  (Fig. 2C). NT-PGC-1 $\alpha$  was detected in a Western blot at ~35–38 kDa. An examination of the NCBI nucleotide database uncovered a variant form of PGC-1 $\alpha$  mRNA in humans (AB061325) and mice (AB061324) [3]; these sequences encoded proteins 271 and 270 a.a. in length, respectively. In theory, transcrip-

tion of the NT-PGC-1 $\alpha$  isoform can occur from both the proximal (1a) and alternative (1b and 1c) promoters [54]; this may explain the existence of several bands between 35 and 38 kDa [3]. NT-PGC-1 $\alpha$  isoforms were found in mice brain tissue and human heart tissue. It is important to note that both the mRNA and protein levels for the full-length and truncated isoforms were comparable [3]. Recent studies have revealed that NT-PGC-1 $\alpha$  isoforms are also expressed in human skeletal muscle [52], where they constitute a significant share of total PGC-1 $\alpha$  mRNA [50,51].

The NT-isoforms retain the following two essential PGC-1 $\alpha$  domains: the N-terminal domain that recruits SRC-1 and CREB-binding proteins and the two LXXLL-like motifs that mediate interactions with nuclear receptors. The NT-isoforms also retain some p38 MAPK, PKA, and AMPK phosphorylation sites. NT-PGC-1 $\alpha$  lacks the C-terminal nuclear localization sequence that regulates nuclear targeting, the ligand-independent PPAR $\gamma$  binding region, the SR-rich and RRM domains, the FOXO1, MEFC2, and the TRAP220 domains, the C-terminal domain involved in the regulation of protein stability, and multiple sites of post-translation regulation and modification (the GSK-3 $\beta$ , AMPK, Akt, p38 MAPK, and PKA phosphorylation sites, arginine methylation sites and lysine acetylation sites) [3,58,59]. These marked differences of the NT-PGC-1 $\alpha$  isoform compared to full-length isoforms confer it unique properties.

### Intracellular localization and stability

The intracellular stability and localization of PGC-1 $\alpha$  were investigated using cardiomyocyte and COS-7 cultures and mutated PGC-1 $\alpha$  proteins lacking various C-terminal fragments [60]. It was demonstrated that the full-length PGC-1 $\alpha$  (1–797 a.a.) protein has a short half-life and is mainly localized in the nucleus. A mutant protein containing the amino acids 1–565 localized in the nucleus and cytoplasm. A mutant containing the amino acids 1–292 was found mainly in the cytoplasm. The ablation of C-terminal fragments improved PGC-1 $\alpha$  protein stability. Apparently, this effect is due to a decrease in the ubiquitination level of the protein [60,61]. These findings are related to the properties of the NT-PGC-1 $\alpha$  isoforms. The lack of a C-terminal fragment increases the stability of NT-PGC-1 $\alpha$  compared to the full-length protein [3,58].

Experiments using a CHO-K1 cell line [3,58] and mice muscle fibers [59] and confocal microscopy have revealed that the NT-isoforms are localized in the cytoplasm (~90%), in contrast to the full-length isoforms, which are localized mainly in the nucleus. A transfection experiment using CHO-K1 demonstrated that the NT-isoforms expressed from both the canonical pro-

moter (NT-PGC-1 $\alpha$ -a) and the alternative promoter (NT-PGC-1 $\alpha$ -b and NT-PGC-1 $\alpha$ -c) are localized in the cytoplasm [54]. These findings confirm that the localization of PGC-1 $\alpha$  isoforms depends on the presence of the C-terminal fragment rather than the amino acid sequences encoded by the first exon.

Different proteins regulate the intracellular localization of the NT-isoforms. In murine muscle fibers [59] and in CHO-K1 cells [58], leptomycin B (a specific inhibitor of exportin 1, which is a regulator of nuclear export) increases the NT-PGC-1 $\alpha$  level in the nucleus. The authors suggested that the low NT-PGC-1 $\alpha$  content in the nucleus depends on the higher rate of exportin 1-mediated nuclear export of NT-PGC-1 $\alpha$  compared to the diffusion rate of NT-PGC-1 $\alpha$  into the nucleus [58] and possible exportin 1-independent nuclear export [59]. The activation of cAMP-dependent signaling induces an increase in the nuclear NT-PGC-1 $\alpha$  content in muscle fibers [59] and in brown adipose tissue [3]. This effect is likely to be regulated by PKA-dependent phosphorylation of NT-PGC-1 $\alpha$  at positions 194, 241, and 256; this phosphorylation decreases exportin 1-mediated nuclear export [58]. Conversely, a p38 MAPK-dependent mechanism for the regulation of NT-PGC-1 $\alpha$  intracellular localization apparently exists. The inhibition of p38 MAPK tempers the increase in nuclear NT-PGC-1 $\alpha$  in brown adipose tissue induced by 8-CPT-cAMP (an analog of cAMP) [3]. However, inhibition of p38 MAPK had only a small negative effect on the increase in nuclear NT-PGC-1 $\alpha$ ; the inhibition of PKA completely eliminated this increase. These findings suggest that activation of muscle  $\beta$ 2-adrenergic receptors regulates intracellular NT-PGC-1 $\alpha$  localization. This fact agrees with the results from mice muscle fibers; AICAR-mediated activation of AMPK and the activation of p38 MAPK by electrical stimulation did not increase nuclear NT-PGC-1 $\alpha$  [59].

### Regulation of NT-PGC-1 $\alpha$ mRNA expression

The NT-isoforms originate due to the alternative splicing of PGC-1 $\alpha$  mRNA, which leads to the formation of a stop-codon between the exons 6 and 7. The expression of the NT-isoforms may be dynamically regulated by different physiological stimuli. Acute endurance exercise initiates comparable increases in the full-length isoform and the NT-isoforms in murine [62] and human skeletal muscle [50,51]. The NT-isoforms can be expressed from the canonical promoter and the alternative promoter [51,62]; the expression magnitude depends on the intensity of the exercise, as observed for full-length isoforms [62].

It can be assumed that expression of both full-length and truncated PGC-1 $\alpha$  mRNA isoforms is induced by activation of AMPK and  $\beta$ 2-adrenergic receptors.

These mechanisms, which regulate mRNA expression, act in the same fashion on both the full-length and truncated isoforms. The expression of both the full-length and truncated PGC-1 $\alpha$  mRNA isoforms is upregulated in AICAR-stimulated muscle myotubes [51]. Injection of AICAR and clenbuterol stimulates the expression of both the full-length and truncated isoforms in the skeletal muscles of mice [62]. Conversely, exposure to cold (4°C, 5 h) activates the expression of both NT-PGC-1 $\alpha$  and full-length PGC-1 $\alpha$  mRNA (~15%) and their corresponding proteins in brown adipose tissue [3]. Under control conditions (22°C), gene expression originates mainly from the canonical promoter (NT-PGC-1 $\alpha$ -a and PGC-1 $\alpha$ -a mRNA); exposure to cold increases expression from the alternative promoter (NT-PGC-1 $\alpha$ -b, NT-PGC-1 $\alpha$ -c, PGC-1 $\alpha$ -b, and PGC-1 $\alpha$ -c mRNA). The latter condition is related to the activation of  $\beta$ 2-adrenergic receptors [3,54].

Thom *et al.* have recently demonstrated that hypoxia may induce splicing of PGC-1 $\alpha$  mRNA between the exons 6 and 7. Hypoxia (0.5% O<sub>2</sub>, 16 h) increases expression of the NT-isoforms in skeletal muscle myocytes and in myocytes with suppressed HIF-1 and -2 activity. These findings suggest that hypoxia induces splicing of PGC-1 $\alpha$  mRNA independent of HIF signaling [63].

The regulation of expression from different promoters and the regulation of splicing between exons 6 and 7 are independent processes; these processes are regulated by different mechanisms. In conclusion, it is unclear whether all of the NT-isoforms can be translated into proteins *in vivo* and whether these hypothetical protein isoforms have different functions.

### Functional roles of NT-isoforms

Different *in vitro* experimental approaches have clearly demonstrated that NT-PGC-1 $\alpha$  is a functionally active protein and can coactivate the following nuclear receptors: PPAR $\alpha$  and PPAR $\gamma$  in CHO-K1 cells [3] and PPAR $\alpha$ , PPAR $\gamma$ , and ERR $\alpha$  in COS-1 cells [54]. Similar to that for full-length isoforms, overexpression of NT-PGC-1 $\alpha$  in brown adipose tissue induces upregulation of UCP1 and CPT-1 $\beta$  mRNA expression and an increased ratio of mitochondrial DNA to nuclear DNA; this ratio serves as a marker of the activation of mitochondrial biogenesis [3].

The function of the NT-isoforms differs significantly from that of the full-length PGC-1 $\alpha$  isoforms. The expression of genes targeted by PGC-1 $\alpha$  and NT-PGC-1 $\alpha$  might differ. Examination of myotubes revealed that overexpression of full-length PGC-1 $\alpha$  (PGC-1 $\alpha$ -1 in the paper by Ruas *et al.*) alters the expression of 2002 genes, while overexpression of NT-PGC-1 $\alpha$ -b (PGC-1 $\alpha$ -4 in paper by Ruas *et al.*) affects the expression of only 519 genes. These isoforms simultaneously influ-

ence the expression of only 98 genes [52]. In brown adipose tissue adipocytes expressing PGC-1 $\alpha$  or NT-PGC-1 $\alpha$ , the expression of the *Cox7al* and *PPAR $\alpha$*  genes increased. However, the increased expression of the *CPT1 $\beta$* , *UCP1*, *ERR $\alpha$* , and *Cox8b* genes are correlated only with the expression of NT-PGC-1 $\alpha$ ; *CytC* expression is associated with PGC-1 $\alpha$  [58,64].

It has recently been demonstrated that the NT-isoforms predominantly activate angiogenesis, whereas the full-length PGC-1 $\alpha$ -a isoforms induce both mitochondrial biogenesis and angiogenesis in skeletal muscle cells [63]. Myotubes derived from *PGC-1 $\alpha$* <sup>-/-</sup> mice myoblasts were infected with an adenovirus encoding NT-PGC-1 $\alpha$ -a or PGC-1 $\alpha$ -a. This led to a comparable increase in the mRNA levels of NT-PGC-1 $\alpha$ -a and PGC-1 $\alpha$ -a; however, the expression of the genes targeted by PGC-1 $\alpha$  and their associated proteins differed. In the myotubes expressing NT-PGC-1 $\alpha$ -a, the expression of OXPHOS-related genes did not change. The content of complex III and V mitochondrial proteins slightly increased in myotubes expressing NT-PGC-1 $\alpha$ -a. In PGC-1 $\alpha$ -a infected cells, a pronounced increase in these indices was observed. The same picture was present in the maximal cell respiration rate: this index increased only after PGC-1 $\alpha$ -a infection. Conversely, NT-PGC-1 $\alpha$ -a induced a more pronounced increase in *VEGFA* gene expression and activation of angiogenesis. Transgenic mice overexpressing the truncated isoform NT-PGC-1 $\alpha$ -b (PGC-1 $\alpha$ 4 in Thom *et al.*) were used to confirm the physiological significance of these findings *in vivo*. In transgenic animals, angiogenesis-related genes (*VEGFA*, *CD31*, *ANGPT2*) were expressed at a higher rate than in wild-type animals; capillary density in *m. tibialis anterior* was also greater in transgenic animals. Angiogenesis induced by NT-isoforms might be due to the retained LXXLL motif; this motif can interact with *ERR $\alpha$* , which is a regulator of *VEGFA* gene expression [20,63].

Obtaining a knockout of the NT-PGC-1 $\alpha$  isoform is a difficult task. Because of this, researchers cannot evaluate the influence of truncated isoforms on the phenotype and function of skeletal muscle and the whole organism. Nevertheless, a few studies [54,65] utilized mice that expressed a mutant PGC-1 $\alpha$ -a protein containing the first 254 a.a. (NT-PGC-1 $\alpha$ <sup>254</sup>) rather than the full-length PGC-1 $\alpha$  protein. The NT-PGC-1 $\alpha$ <sup>254</sup> protein is only a few amino acids shorter than native NT-PGC-1 $\alpha$ -a and is a functional equivalent of NT-PGC-1 $\alpha$ -a [54]. Leon *et al.* [65] showed that the weight of predominantly oxidative *m. soleus* muscle fibers in NT-PGC-1 $\alpha$ <sup>254</sup> mice was slightly lower than that in wild-type animals. However, the weights of predominantly glycolytic *m. tibialis anterior* muscle fibers did not differ between mutant and wild-type mice. A his-

tological examination found no marked changes in the skeletal muscle fibers of NT-PGC-1 $\alpha$ <sup>254</sup> mice. The mitochondrial density, the basal expression of the OXPHOS related genes, the ADP-stimulated maximal respiration rate, the running time to exhaustion during an incremental treadmill test, and the pulmonary  $\dot{V}O_{2max}$  were significantly lower in NT-PGC-1 $\alpha$ <sup>254</sup> mice compared with the wild-type control [65]. Conversely, the decrease in the body temperature of adult NT-PGC-1 $\alpha$ <sup>254</sup> mice was similar to that in the wild-type control after exposure to cold (4°C). In this case, NT-PGC-1 $\alpha$ <sup>254</sup> mice were also able to increase expression of the *UCP1* gene in brown adipose tissue [54,65,66], apparently via the Twist-1-mediated mechanism. It was shown that Twist-1, a negative regulator of full-length PGC-1 $\alpha$ , had no effect on the truncated proteins [64].

It is interesting to compare NT-PGC-1 $\alpha$ <sup>254</sup> mice with mice completely devoid of PGC-1 $\alpha$  activity (the PGC-1 $\alpha$  mRNA sequence was changed after exon 2) in either the whole organism [67,68] or in skeletal muscle [69,70]. Whole-body knockout mice did not show any abnormalities in muscle fiber size, fiber composition, and mitochondrial density compared to wild-type animals. The absence of abnormalities could be partially explained by hyperactivity in the knockout mice due to marked abnormalities in the central nervous system [67,68]. In the mice where the *PGC-1 $\alpha$*  gene was knocked out in the skeletal muscle, the percentage of oxidative fibers (type I) in the red and white muscles was lower compared to the wild-type control [69,70]. Moreover, knockout mice of both types had noticeably lower basal expression of the OXPHOS related genes in mixed (*m. quadriceps femoris*) and white (*m. gastrocnemius*) muscles compared to the wild-type control [67-70]. In contrast to NT-PGC-1 $\alpha$ <sup>254</sup> mice, adult mice completely lacking PGC-1 $\alpha$  activity had a pronounced decrease in body temperature during exposure to cold (4°C) [68]. This effect may be partially explained by the lack of *UCP1* gene expression in brown adipose tissue, which is mediated by PGC-1 $\alpha$  [64]. Taken together, these knockout studies suggest that the functional role of the NT-isoforms differs from that of the full-length isoform.

In this review, the influence of endurance exercise on the regulation of the expression of different PGC-1 $\alpha$  isoforms was analyzed. Most studies focused on the effects of acute endurance exercise, because regular aerobic training activates mitochondrial biogenesis and angiogenesis in skeletal muscle. Therefore, the relationship between endurance exercise and PGC-1 $\alpha$  seems logical. Recently, Ruas and colleagues demonstrated that the truncated PGC-1 $\alpha$  isoform NT-PGC-1 $\alpha$ -b (PGC-1 $\alpha$ 4 in Ruas *et al.*) regulates myogenesis [52]. Myotubes overexpressing NT-PGC-1 $\alpha$ -b showed increased mRNA of the growth factor IGF-1 and the myogenic factors Myf-5

and -6; a lower level of myostatin mRNA was observed in myotubes overexpressing NT-PGC-1 $\alpha$ -b compared with control cells or cells overexpressing PGC-1 $\alpha$ -a. NT-PGC-1 $\alpha$ -b-mediated expression of the OXPHOS-related genes was lower than PGC-1 $\alpha$ -a-mediated expression. The authors revealed that the NT-isoform, as with full-length PGC-1 $\alpha$ , is predominantly localized in the nucleus. This finding does not agree with the previous studies of intracellular localization of NT-PGC-1 $\alpha$  [58,59]. Overexpression of NT-PGC-1 $\alpha$ -b by both adenovirus injection and plasmid electroporation significantly increases the expression of the truncated protein, the area of fiber cross sections, and the weight of mouse muscles compared to those in wild-type animals. Electroporation of the plasmid encoding the truncated isoform (NT-PGC-1 $\alpha$ -a) driven by the canonical promoter increased the NT-PGC-1 $\alpha$ -a mRNA level; however, increased translation of the truncated protein was not observed in a Western blot. The authors concluded that the N-terminal amino acid sequence of NT-PGC-1 $\alpha$ -b allows for the accumulation of this protein in the cell; this sequence is missing in NT-PGC-1 $\alpha$ -a [52]. This finding is not in agreement with the experiment in which the level of the truncated protein increased in myotubes infected with adenovirus-encoded NT-PGC-1 $\alpha$ -a [63]. The physiological significance of NT-PGC-1 $\alpha$ -b overexpression was investigated using transgenic mice. A small increase in mRNA expression of VEGFA, EER $\alpha$ , myoglobin mRNA was observed in transgenic mice; a decrease in myostatin mRNA expression and no changes in the mRNA expression of IGF-1 and other myogenic regulators was also observed compared to wild-type animals [52,63]. The area of muscle fiber cross sections, the muscle weight and force, and the running time to exhaustion during treadmill test were slightly higher in transgenic animals compared to control mice [52]. In the cited study, the effect of acute exercise on the expression of NT-PGC-1 $\alpha$ -b mRNA was not investigated. However, the basal expression level of this transcript in human skeletal muscle was shown to increase after 8 weeks of strength training and to be unchanged after 8 weeks of endurance training. A primer pair aligning to exons 5 (forward) and 7a (reverse) was used to detect NT-PGC-1 $\alpha$ -b mRNA in this study. This primer pair can detect both NT-PGC-1 $\alpha$ -b and NT-PGC-1 $\alpha$ -a transcripts. A recent study has demonstrated that acute strength training and endurance exercise induce the expression of both isoforms in human skeletal muscle [51]. Therefore, it is possible that the strength training that occurred in the Ruas *et al.* study [52] may have induced expression of both NT-PGC-1 $\alpha$ -b and NT-PGC-1 $\alpha$ -a mRNA.

The influence of PGC-1 $\alpha$  isoforms expressed from the canonical promoter on skeletal muscle hypertrophy was

investigated using synergist ablation [71]. An increase in the absolute phosphorylation level of mTORC1 targets, increased IGF-1 mRNA abundance, and a decrease in the myostatin mRNA level in hypertrophied muscle were observed as compared to the control muscle. Moreover, PGC-1 $\alpha$  mRNA expression from the alternative promoter (PGC-1 $\alpha$ -b and NT-PGC-1 $\alpha$ -b, detected using a primer pair aligning to exons 1b and 2) and the canonical promoter (PGC-1 $\alpha$ -a and NT-PGC-1 $\alpha$ -a, detected using a primer pair aligning to exons 1a and 2) decreased; the expression of the OXPHOS related genes and the content and activity of key mitochondrial proteins also decreased. Following synergist ablation, PGC-1 $\alpha$  knockout mice showed a comparable increase in muscle weight, an absolute phosphorylation level of mTORC1 targets, and an IGF-1 mRNA level, as well as a decrease in myostatin mRNA abundance compared to wild-type animals after synergist ablation. The authors draw a conclusion that PGC-1 $\alpha$  is not involved in the chronic overload-induced remodeling of skeletal muscle. This conclusion indirectly supports the hypothesis that the expression of NT-PGC-1 $\alpha$ -b mRNA is regulated by the same stimuli as those that regulate the expression of PGC-1 $\alpha$ -b mRNA; these stimuli are exercise intensity and clenbuterol-mediated activation of  $\beta$ 2-adrenergic receptors [62]. In conclusion, these studies demonstrated that the influence of the PGC-1 $\alpha$  isoforms on the mechanisms of protein synthesis are not fully clear and require further investigation.

## CONCLUSIONS

The coactivator PGC-1 $\alpha$  is a key regulator of mitochondrial biogenesis, fat and carbohydrate metabolism. Both *in vitro* and *in vivo* studies have demonstrated that several isoforms of PGC-1 $\alpha$  mRNA may be expressed in rodent and human skeletal muscle. The expression patterns may markedly differ at rest and after muscle activity. Different signaling pathways are activated by different physiological stimuli that regulate the expression of the PGC-1 $\alpha$  gene from different promoters. Apparently, the expression from the canonical (proximal) promoter is regulated mainly by the activation of AMPK, while expression from an alternative promoter is regulated via the  $\beta$ 2-adrenergic receptor. Most probably, the functional properties of isoforms derived from different promoters do not differ. Therefore, the availability of two signaling pathways regulating the PGC-1 $\alpha$  gene expression provides ample opportunities for a pharmacological influence on the expression of this gene. Those opportunities might be important in treating and preventing various diseases, such as metabolic syndrome and diabetes mellitus.

All transcripts, from both the canonical and alternative promoters, are subject to alternative splicing.

As a result, truncated isoforms that possess different properties are translated. The truncated isoforms are more stable and predominantly activate angiogenesis, whereas full-length isoforms regulate mainly mitochondrial biogenesis. It has recently been shown [52] that in contrast to full-length isoforms, truncated isoforms may regulate myogenesis, but this assumption needs further confirmation. The existence of several isoforms with a broad-spectrum of functions allows the organism to adapt to different physiological stimuli.

The mechanisms of *PGC-1 $\alpha$*  gene expression in human skeletal muscle remain not fully clear. Elucidation

of the regulatory mechanisms of *PGC-1 $\alpha$*  gene expression and their functional role may provide an opportunity to control the expression of different isoforms through exercise and/or pharmacological interventions. This opportunity is important for patients with the metabolic syndrome and diabetes mellitus and perhaps for endurance athletes. ●

*This work was supported by the Russian Science Foundation (grant № 14-15-00768).*

REFERENCES

1. Pedersen B.K., Febbraio M.A. // *Nat. Rev. Endocrinol.* 2012. V. 8. № 8. P. 457–465.
2. Miura S., Kai Y., Kamei Y., Ezaki O. // *Endocrinology.* 2008. V. 149. № 9. P. 4527–4533.
3. Zhang Y., Huypens P., Adamson A.W., Chang J.S., Hengan T.M., Boudreau A., Lenard N.R., Burk D., Klein J., Perwitz N., et al. // *J. Biol. Chem.* 2009. V. 284. № 47. P. 32813–32826.
4. Egan B., Carson B.P., Garcia-Roves P.M., Chibalin A.V., Sarsfield F.M., Barron N., McCaffrey N., Moyna N.M., Zierath J.R., O’Gorman D.J. // *J. Physiol.* 2010. V. 588. № 10. P. 1779–1790.
5. Brenmoehl J., Hoeflich A. // *Mitochondrion.* 2013. V. 13. № 6. P. 755–761.
6. Wright D.C., Han D.H., Garcia-Roves P.M., Geiger P.C., Jones T.E., Holloszy J.O. // *J. Biol. Chem.* 2007. V. 282. № 1. P. 194–199.
7. Safdar A., Little J.P., Stokl A.J., Hettinga B.P., Akhtar M., Tarnopolsky M.A. // *J. Biol. Chem.* 2011. V. 286. № 12. P. 10605–10617.
8. Little J.P., Safdar A., Cermak N., Tarnopolsky M.A., Gibala M.J. // *Am. J. Physiol. Regul. Integr. Comp. Physiol.* 2010. V. 298. № 4. P. R912–R917.
9. Little J.P., Safdar A., Bishop D., Tarnopolsky M.A., Gibala M.J. // *Am. J. Physiol. Regul. Integr. Comp. Physiol.* 2011. V. 300. № 6. P. R1303–R1310.
10. McGee S.L., Howlett K.F., Starkie R.L., Cameron-Smith D., Kemp B.E., Hargreaves M. // *Diabetes.* 2003. V. 52. № 4. P. 926–928.
11. McGee S.L., Hargreaves M. // *Diabetes.* 2004. V. 53. № 5. P. 1208–1214.
12. Handschin C., Rhee J., Lin J., Tarr P.T., Spiegelman B.M. // *Proc. Natl. Acad. Sci. USA.* 2003. V. 100. № 12. P. 7111–7116.
13. Dumke C.L., Mark D.J., Angela M.E., Nieman D.C., Carmichael M.D., Quindry J.C., Travis T.N., Utter A.C., Gross Gowin S.J., Henson D.A., et al. // *Eur. J. Appl. Physiol.* 2009. V. 107. № 4. P. 419–427.
14. Olesen J., Kiilerich K., Pilegaard H. // *Pflugers Arch.* 2010. V. 460. № 1. P. 153–162.
15. Scarpulla R.C. // *Ann. N.Y. Acad. Sci.* 2008. V. 1147. P. 321–334.
16. Litonin D., Sologub M., Shi Y., Savkina M., Anikin M., Falkenberg M., Gustafsson C.M., Temiakov D. // *J. Biol. Chem.* 2010. V. 285. № 24. P. 18129–18133.
17. Smith B.K., Mukai K., Lally J.S., Maher A.C., Gurd B.J., Heigenhauser G.J., Spriet L.L., Holloway G.P. // *J. Physiol.* 2013. V. 591. № 6. P. 1551–1561.
18. Aquilano K., Vigilanza P., Baldelli S., Pagliei B., Rotilio G., Ciriolo M.R. // *J. Biol. Chem.* 2010. V. 285. № 28. P. 21590–21599.
19. Arany Z., Foo S.Y., Ma Y., Ruas J.L., Bommi-Reddy A., Girnun G., Cooper M., Laznik D., Chinsomboon J., Rangwala S.M., et al. // *Nature.* 2008. V. 451. № 7181. P. 1008–1012.
20. Chinsomboon J., Ruas J., Gupta R.K., Thom R., Shoag J., Rowe G.C., Sawada N., Raghuram S., Arany Z. // *Proc. Natl. Acad. Sci. USA.* 2009. V. 106. № 50. P. 21401–21406.
21. Rowe G.C., Raghuram S., Jang C., Nagy J.A., Patten I.S., Goyal A., Chan M.C., Liu L.X., Jiang A., Spokes K.C., et al. // *Circ. Res.* 2014. V. 115. № 5. P. 504–517.
22. Puigserver P., Wu Z., Park C.W., Graves R., Wright M., Spiegelman B.M. // *Cell.* 1998. V. 92. № 6. P. 829–839.
23. Esterbauer H., Oberkofler H., Krempler F., Patsch W. // *Genomics.* 1999. V. 62. № 1. P. 98–102.
24. Czubryt M.P., McAnally J., Fishman G.I., Olson E.N. // *Proc. Natl. Acad. Sci. USA.* 2003. V. 100. № 4. P. 1711–1716.
25. Akimoto T., Li P., Yan Z. // *Am. J. Physiol. Cell Physiol.* 2008. V. 295. № 1. P. C288–C292.
26. Lu J., McKinsey T.A., Nicol R.L., Olson E.N. // *Proc. Natl. Acad. Sci. USA.* 2000. V. 97. № 8. P. 4070–4075.
27. McGee S.L., Fairlie E., Garnham A.P., Hargreaves M. // *J. Physiol.* 2009. V. 587. № 24. P. 5951–5958.
28. Hook S.S., Means A.R. // *Annu. Rev. Pharmacol. Toxicol.* 2001. V. 41. P. 471–505.
29. Corton J.M., Gillespie J.G., Hardie D.G. // *Curr. Biol.* 1994. V. 4. № 4. P. 315–324.
30. Chen Z.P., Stephens T.J., Murthy S., Canny B.J., Hargreaves M., Witters L.A., Kemp B.E., McConell G.K. // *Diabetes.* 2003. V. 52. № 9. P. 2205–2212.
31. Fujii N., Hayashi T., Hirshman M.F., Smith J.T., Habinowski S.A., Kaijser L., Mu J., Ljungqvist O., Birnbaum M.J., Witters L.A., et al. // *Biochem. Biophys. Res. Commun.* 2000. V. 273. № 3. P. 1150–1155.
32. Rose A.J., Kiens B., Richter E.A. // *J. Physiol.* 2006. V. 574. № 3. P. 889–903.
33. Sriwijitkamol A., Coletta D.K., Wajcberg E., Balbontin G.B., Reyna S.M., Barrientes J., Eagan P.A., Jenkinson C.P., Cersosimo E., DeFronzo R.A., et al. // *Diabetes.* 2007. V. 56. № 3. P. 836–848.
34. Rasmussen B.B., Winder W.W. // *J. Appl. Physiol.* 1997. V. 83. № 4. P. 1104–1109.
35. Shaywitz A.J., Greenberg M.E. // *Annu. Rev. Biochem.* 1999. V. 68. P. 821–861.
36. Thomson D.M., Herway S.T., Fillmore N., Kim H., Brown J.D., Barrow J.R., Winder W.W. // *J. Appl. Physiol.* 2008. V. 104. № 2. P. 429–438.

37. Zhang Y., Uguccioni G., Ljubicic V., Irrcher I., Iqbal S., Singh K., Ding S., Hood D.A. // *Physiol. Rep.* 2014. V. 2. e12008.
38. Akimoto T., Pohnert S.C., Li P., Zhang M., Gumbs C., Rosenberg P.B., Williams R.S., Yan Z. // *J. Biol. Chem.* 2005. V. 280. № 20. P. 19587–19593.
39. Wright D.C., Geiger P.C., Han D.H., Jones T.E., Holloszy J.O. // *J. Biol. Chem.* 2007. V. 282. № 26. P. 18793–18799.
40. Widegren U., Jiang X.J., Krook A., Chibalin A.V., Bjornholm M., Tally M., Roth R.A., Henriksson J., Wallberg-Henriksson H., Zierath J.R. // *FASEB J.* 1998. V. 12. № 13. P. 1379–1389.
41. Nordsborg N.B., Lundby C., Leick L., Pilegaard H. // *Med. Sci. Sports Exerc.* 2010. V. 42. № 8. P. 1477–1484.
42. Popov D., Zinovkin R., Karger E., Tarasova O., Vinogradova O. // *J. Sports Med. Phys. Fitness.* 2014. V. 54. P. 362–369.
43. Edgett B.A., Foster W.S., Hankinson P.B., Simpson C.A., Little J.P., Graham R.B., Gurd B.J. // *PLoS One.* 2013. V. 8. № 8. e71623.
44. Yoshioka T., Inagaki K., Noguchi T., Sakai M., Ogawa W., Hosooka T., Iguchi H., Watanabe E., Matsuki Y., Hiramatsu R., et al. // *Biochem. Biophys. Res. Commun.* 2009. V. 381. № 4. P. 537–543.
45. Soyal S.M., Felder T.K., Auer S., Hahne P., Oberkofler H., Witting A., Paulmichl M., Landwehrmeyer G.B., Weydt P., Patsch W. // *Hum. Mol. Genet.* 2012. V. 21. № 15. P. 3461–3473.
46. Felder T.K., Soyal S.M., Oberkofler H., Hahne P., Auer S., Weiss R., Gadermaier G., Miller K., Krempler F., Esterbauer H., et al. // *J. Biol. Chem.* 2011. V. 286. № 50. P. 42923–42936.
47. Miura S., Kawanaka K., Kai Y., Tamura M., Goto M., Shiuchi T., Minokoshi Y., Ezaki O. // *Endocrinology.* 2007. V. 148. № 7. P. 3441–3448.
48. Tadaishi M., Miura S., Kai Y., Kawasaki E., Koshinaka K., Kawanaka K., Nagata J., Oishi Y., Ezaki O. // *Am. J. Physiol. Endocrinol. Metab.* 2011. V. 300. № 2. P. E341–E349.
49. Norrbom J., Sallstedt E.K., Fischer H., Sundberg C.J., Rundqvist H., Gustafsson T. // *Am. J. Physiol. Endocrinol. Metab.* 2011. V. 301. № 6. P. E1092–E1098.
50. Popov D.V., Bachinin A.V., Lysenko E.A., Miller T.F., Vinogradova O.L. // *J. Physiol. Sci.* 2014. V. 64. № 5. P. 317–323.
51. Ydfors M., Fischer H., Mascher H., Blomstrand E., Norrbom J., Gustafsson T. // *Physiol. Rep.* 2013. V. 1. № 6. e00140.
52. Ruas J.L., White J.P., Rao R.R., Kleiner S., Brannan K.T., Harrison B.C., Greene N.P., Wu J., Estall J.L., Irving B.A., et al. // *Cell.* 2012. V. 151. № 6. P. 1319–1331.
53. Tadaishi M., Miura S., Kai Y., Kano Y., Oishi Y., Ezaki O. // *PLoS One.* 2011. V. 6. № 12. e28290.
54. Chang J.S., Fernand V., Zhang Y., Shin J., Jun H.J., Joshi Y., Gettys T.W. // *J. Biol. Chem.* 2012. V. 287. № 12. P. 9100–9111.
55. Kim S.H., Asaka M., Higashida K., Takahashi Y., Holloszy J.O., Han D.H. // *Am. J. Physiol. Endocrinol. Metab.* 2013. V. 304. № 8. P. E844–E852.
56. Frier B.C., Wan Z., Williams D.B., Stefanson A.L., Wright D.C. // *Am. J. Physiol. Cell Physiol.* 2012. V. 302. № 12. P. C1772–C1779.
57. Baar K., Wende A.R., Jones T.E., Marison M., Nolte L.A., Chen M., Kelly D.P., Holloszy J.O. // *FASEB J.* 2002. V. 16. № 14. P. 1879–1886.
58. Chang J.S., Huypens P., Zhang Y., Black C., Kralli A., Gettys T.W. // *J. Biol. Chem.* 2010. V. 285. № 23. P. 18039–18050.
59. Shen T., Liu Y., Schneider M.F. // *J. Biomed. Biotechnol.* 2012. V. 2012. P. 989263.
60. Sano M., Tokudome S., Shimizu N., Yoshikawa N., Ogawa C., Shirakawa K., Endo J., Katayama T., Yuasa S., Ieda M., et al. // *J. Biol. Chem.* 2007. V. 282. № 35. P. 25970–25980.
61. Olson B.L., Hock M.B., Ekholm-Reed S., Wohlschlegel J.A., Dev K.K., Kralli A., Reed S.I. // *Genes Dev.* 2008. V. 22. № 2. P. 252–264.
62. Wen X., Wu J., Chang J.S., Zhang P., Wang J., Zhang Y., Gettys T.W., Zhang Y. // *Biomed. Res. Int.* 2014. V. 2014. e402175.
63. Thom R., Rowe G.C., Jang C., Safdar A., Arany Z. // *J. Biol. Chem.* 2014. V. 289. P. 8810–8817.
64. Jun H.J., Gettys T.W., Chang J.S. // *PPAR. Res.* 2012. V. 2012. e320454.
65. Leone T.C., Lehman J.J., Finck B.N., Schaeffer P.J., Wende A.R., Boudina S., Courtois M., Wozniak D.F., Sambandam N., Bernal-Mizrachi C., et al. // *PLoS Biol.* 2005. V. 3. № 4. e101.
66. Jun H.J., Joshi Y., Patil Y., Noland R.C., Chang J.S. // *Diabetes.* 2014. V. 63. № 11. P. 3615–3625.
67. Arany Z., He H., Lin J., Hoyer K., Handschin C., Toka O., Ahmad F., Matsui T., Chin S., Wu P.H., et al. // *Cell Metab.* 2005. V. 1. № 4. P. 259–271.
68. Lin J., Wu P.H., Tarr P.T., Lindenberg K.S., St-Pierre J., Zhang C.Y., Mootha V.K., Jager S., Vianna C.R., Reznick R.M., et al. // *Cell.* 2004. V. 119. № 1. P. 121–135.
69. Handschin C., Choi C.S., Chin S., Kim S., Kawamori D., Kurpad A.J., Neubauer N., Hu J., Mootha V.K., Kim Y.B., et al. // *J. Clin. Invest.* 2007. V. 117. № 11. P. 3463–3474.
70. Handschin C., Chin S., Li P., Liu F., Maratos-Flier E., LeBrasseur N.K., Yan Z., Spiegelman B.M. // *J. Biol. Chem.* 2007. V. 282. № 41. P. 30014–30021.
71. Perez-Schindler J., Summermatter S., Santos G., Zorzato F., Handschin C. // *Proc. Natl. Acad. Sci. USA.* 2013. V. 110. № 50. P. 20314–20319.

# The Role of Ala198 in the Stability and Coenzyme Specificity of Bacterial Formate Dehydrogenases

A. A. Alekseeva<sup>1,2</sup>, V. V. Fedorchuk<sup>2,3</sup>, S. A. Zarubina<sup>2,3</sup>, E. G. Sadykhov<sup>1</sup>, A. D. Matorin<sup>3</sup>, S. S. Savin<sup>1,2,3</sup>, V. I. Tishkov<sup>1,2,3</sup>

<sup>1</sup>A.N. Bach Institute of Biochemistry, Russian Academy of Sciences, Leninskiy prospect, 33/2, Moscow, 119071, Russia

<sup>2</sup>Innovations and High Technologies MSU Ltd, Tsymlyanskya Str., 16–96, Moscow, 109559, Russia

<sup>3</sup>Department of Chemistry, M.V. Lomonosov Moscow State University; Leninskie gory, 1/3, Moscow, 119991, Russia

\*E-mail: vitishkov@gmail.com

Received 26.11.2014

Copyright © 2015 Park-media, Ltd. This is an open access article distributed under the Creative Commons Attribution License, which permits unrestricted use, distribution, and reproduction in any medium, provided the original work is properly cited.

**ABSTRACT** It has been shown by an X-ray structural analysis that the amino acid residues Ala198, which are located in the coenzyme-binding domain of NAD<sup>+</sup>-dependent formate dehydrogenases (EC 1.2.1.2., FDH) from bacteria *Pseudomonas* sp.101 and *Moraxella* sp. C-1 (PseFDH and MorFDH, respectively), have non-optimal values of the angles  $\psi$  and  $\phi$ . These residues were replaced with Gly by site-directed mutagenesis. The mutants PseFDH A198G and MorFDH A198G were expressed in *E.coli* cells and obtained in active and soluble forms with more than 95% purity. The study of thermal inactivation kinetics showed that the mutation A198G results in a 2.5-fold increase in stability compared to one for the wild-type enzymes. Kinetic experiments indicate that A198G replacement reduces the  $K_M^{\text{NAD}^+}$  value from 60 to 35 and from 80 to 45  $\mu\text{M}$  for PseFDH and MorFDH, respectively, while the  $K_M^{\text{HCOO}^-}$  value remains practically unchanged. Amino acid replacement A198G was also added to the mutant PseFDH D221S with the coenzyme specificity changed from NAD<sup>+</sup> to NADP<sup>+</sup>. In this case, an increase in thermal stability was also observed, but the influence of the mutation on the kinetic parameters was opposite:  $K_M$  increased from 190 to 280  $\mu\text{M}$  and from 43 to 89 mM for NADP<sup>+</sup> and formate, respectively. According to the data obtained, inference could be drawn that earlier formate dehydrogenase from bacterium *Pseudomonas* sp. 101 was specific to NADP<sup>+</sup>, but not to NAD<sup>+</sup>.

**KEYWORDS** site-directed mutagenesis, thermal stability, coenzyme specificity, kinetic parameters.

## INTRODUCTION

A characteristic feature of NAD<sup>+</sup>-dependent dehydrogenases is the presence of the specific sequence (fingerprint) of GxGxxG in their coenzyme-binding domain [1]. In fact, the only exception to this rule is formate dehydrogenase from bacteria and fungi [EC 1.2.1.2] (FDH). In all bacterial FDHs (except for enzymes from symbiotic bacterium *Sinorhizobium meliloti* and bacteria of the genera *Bordetella* and *Staphylococcus*) the GxGxxG sequence contains the Ala, instead of Gly, residue in the first position (*Fig. 1*). A similar pattern was observed for the enzyme from fungi, whereas all known FDHs from various yeasts and plants obey the rule above and possess a classic characteristic sequence.

In our laboratory, a systematic study of FDH from various sources, including methylotrophic bacteria *Pseudomonas* sp. 101 and *Moraxella* sp. C-1 (PseFDH and MorFDH, respectively), was performed. In both enzymes, the non-canonical Ala residue was located at position 198. In collaboration with the laboratory

headed by prof. Vladimir Popov (A.N. Bach Institute of Biochemistry, Russian Academy of Sciences), and groups led by of Dr. Victor Lamzin (EMBL Outstation, Hamburg) and Dr. Konstantin Polyakov (Engelhardt Institute of Molecular Biology, Russian Academy of Sciences), three-dimensional structures of apo-forms of PseFDH and MorFDH and their various complexes were solved [2–5]. In the structures of both enzymes, the Ala198 residue has “forbidden” values for the angles  $\psi$  and  $\phi$ , preventing an optimal orientation of secondary structural elements (*Fig. 2*). Analysis of the X-ray structures of PseFDH MorFDH indicates that the Ala198 residue is located between the  $\beta\text{A}$  strand and  $\alpha\text{B}$  helix (*Fig. 3A*).

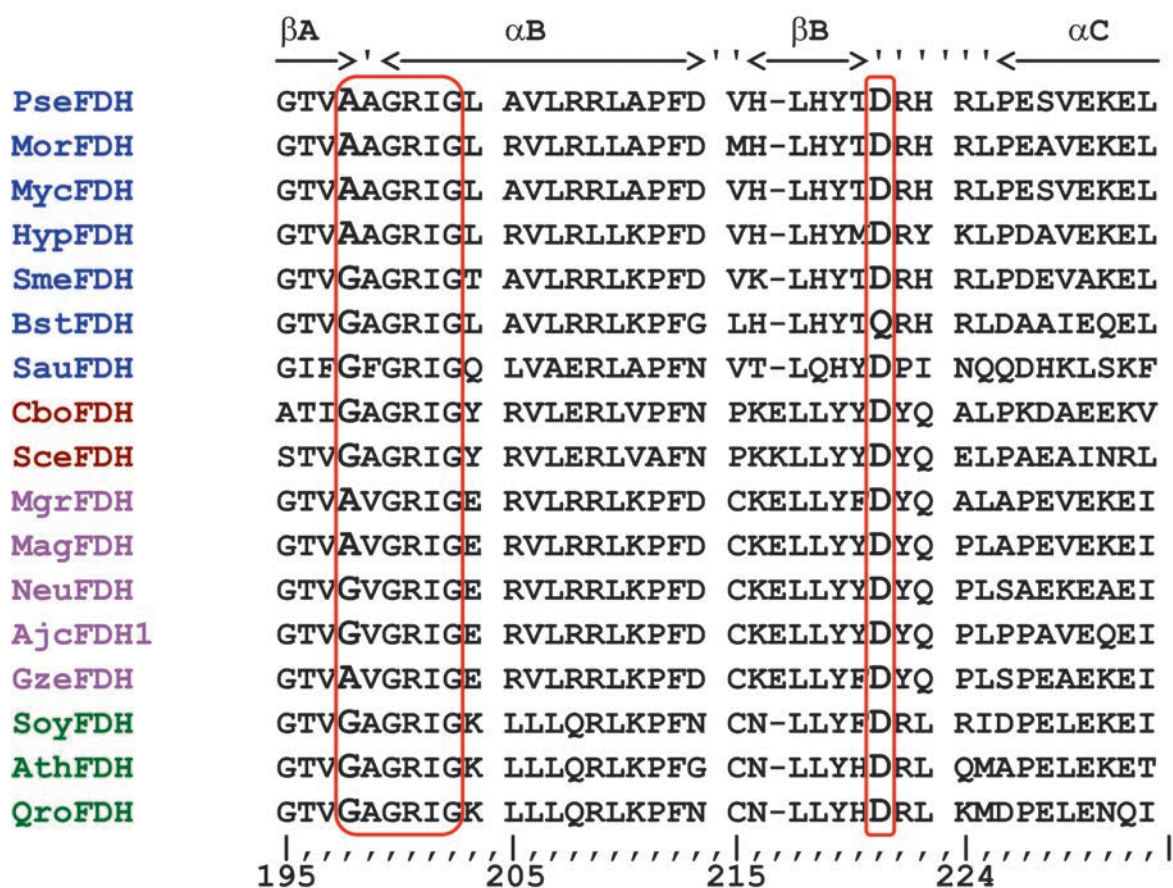
In the present study, Ala198 was replaced with Gly by site-directed mutagenesis in order to decrease conformational tension and elucidate the role of Ala198 in the stability and catalytic properties of PseFDH and MorFDH. Additionally, the Ala198Gly mutation was introduced into PseFDH with the Asp221Ser substi-

tution, which was previously obtained in our laboratory. As a result of the latter substitution, the coenzyme specificity of PseFDH changed from NAD<sup>+</sup> to NADP<sup>+</sup> [6, 7]; therefore, it was important to determine how the removal of conformational tension affects the stability and coenzyme specificity of NADP<sup>+</sup>-specific PseFDH.

### MATERIALS AND METHODS

Molecular Biology Grade reagents were used for the genetic engineering experiments. Bactotryptone, yeast extract and agar (Difco, USA), glycerol (99.9%) and

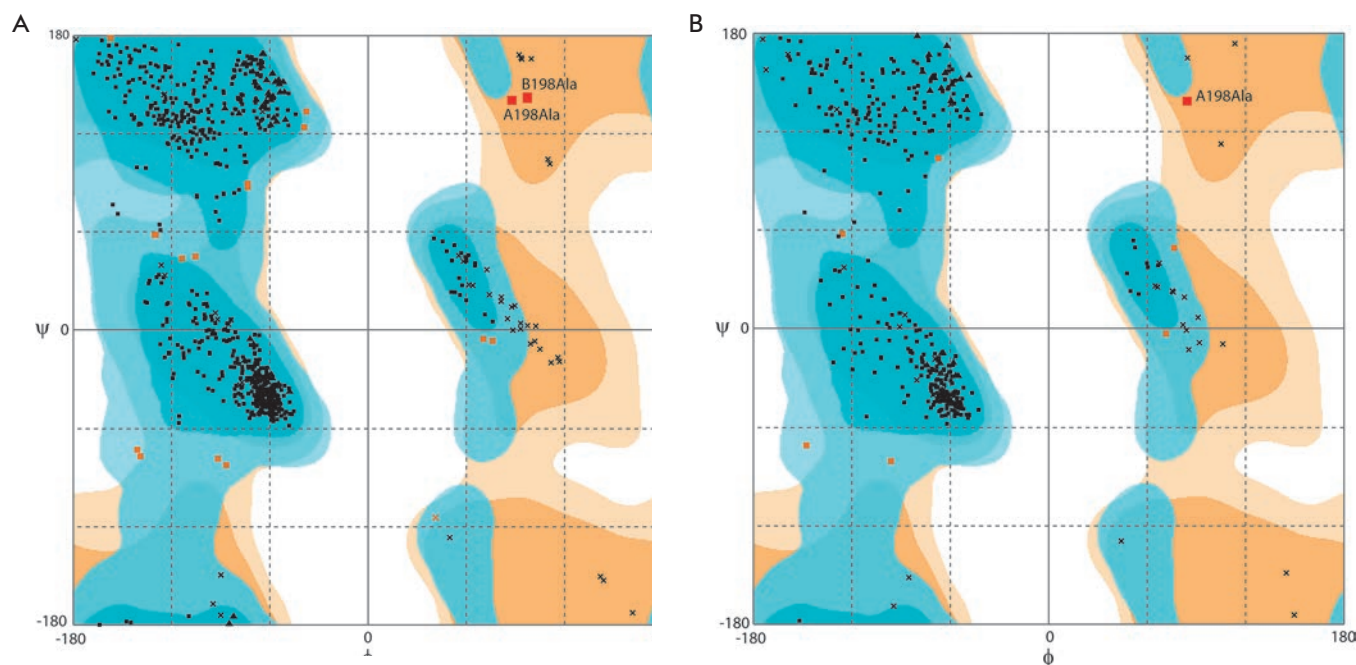
calcium chloride (“ultra pure”), potassium hydrogen phosphate, sodium dihydrogen phosphate (“pure for analysis”), lysozyme (Fluka/BioChemika, Switzerland), lactose (analytical grade), ampicillin and chloramphenicol (Sigma, USA), and sodium chloride (“AR grade”, Helicon, Russia) were used in the microbiological experiments. Restriction endonucleases, DNA ligase of T4 phage, and Pfu-DNA polymerase (Thermo Scientific) were used for cloning DNA fragments and site-directed mutagenesis. Thermo Scientific reagent kits were used to isolate DNA from agarose gel and plasmids



**Fig. 1.** Alignment of amino acid sequences of formate dehydrogenases from different sources in the region of the coenzyme-binding domain. Bacterial FDHs are marked in blue: PseFDH – *Pseudomonas* sp. 101 (UniProtKB/Swiss-Prot: P33160.3), MorFDH – *Moraxella* sp. C-1 (GenBank Accession Y13245), MycFDH – *Mycobacterium vaccae* N10 (GenBank BAB69476), HypFDH – *Hyphomicrobium* strain JC-17 [GenBank BAB55449], SmeFDH – *Sinorhizobium meliloti* 16262453 (GenBank NP\_435497), BstFDH – *Burkholderia stabilis* (GenBank CP000378), SauFDH – *Staphylococcus aureus* (NCBI Reference Sequence: WP\_031923037.1). FDHs from yeasts are marked in brown: CboFDH – *Candida boidinii* (GenBank Accession ABE69165), SceFDH – baker's yeast *S. cerevisiae* (EMBL Z75296). FDHs from fungi are marked in magenta: MgrFDH – *Mycosphaerella graminicola* (*Septoria tritici*) (UniProt Q9Y790), MagFDH – *Magnaporthe grisea* (EMBL AA415108), NeuFDH – *Neurospora crassa* [GenBank Accession XP\_961202.] AjcFDH – *Ajellomyces capsulatus* [GenBank Accession XP\_001539240], GzeFDH – *Gibberella zeae* (GenBank Accession XM\_386303) and FDHs from plants are marked in green: SoyFDH – soybean *Glycine max* (GenBank Accession GB BT094321), AthFDH – *Arabidopsis thaliana* (EMBL AF208029), QroFDH – oak *Quercus robur* (GenBank Accession GB AJ577266)

**Table 1.** Inactivation rate constants and activation parameters of mutant PseFDHs and wild-type enzyme

| Mutant/T, °C        | $k_m, 10^{-5} \text{s}^{-1}$ |               |              |              | $\Delta H^\ddagger$ ,<br>kJ/mol | $\Delta S^\ddagger$ ,<br>J/(mol $\cdot$ K) |
|---------------------|------------------------------|---------------|--------------|--------------|---------------------------------|--|
|                     | 60.1                         | 62.0          | 63.0         | 65.0         |                                 |  |
| wt-PseFDH           | 5.4 $\pm$ 0.2                | 22 $\pm$ 2    | 32 $\pm$ 2   | 140 $\pm$ 12 | 570 $\pm$ 20                    | 1390 $\pm$ 70                              |
| PseFDH A198G        | 2.7 $\pm$ 0.1                | 9.3 $\pm$ 0.5 | 13 $\pm$ 0.8 | 60 $\pm$ 5   | 580 $\pm$ 30                    | 1410 $\pm$ 80                              |
| PseFDH D221S        | 9.2 $\pm$ 0.5                | 32 $\pm$ 4    | 69 $\pm$ 7   | 188 $\pm$ 15 | 570 $\pm$ 40                    | 1410 $\pm$ 100                             |
| PseFDH D221S/ A198G | 2.7 $\pm$ 0.1                | 8.9 $\pm$ 0.4 | 20 $\pm$ 3   | 52 $\pm$ 6   | 580 $\pm$ 30                    | 1380 $\pm$ 110                             |

**Fig. 2.** Ramachandran plot for the structures of the apo-forms of formate dehydrogenases from bacteria *Pseudomonas* sp. 101 (A) (PDB2NAC) and *Moraxella* sp. C-1 (B) (PDB3FN4). Only one pair of angles  $\psi$  and  $\phi$  is shown for MorFDH because the crystallographic cell of the latter enzyme contains only one enzyme subunit

from *E. coli* cells. The oligonucleotides for the polymerase chain reaction (PCR) and sequencing were synthesized by Synthol (Russia). MilliQ (Millipore, USA) purified water was used in these experiments.

All reagents for the electrophoresis of proteins were manufactured by Bio-Rad (USA). Ammonium sulfate (chemically pure, Dia-M, Russia), urea (pure for analysis, Reahim, Russia), NAD<sup>+</sup> and NADP<sup>+</sup> with purity of at least 99% (AppliChem, Germany), EDTA, sodium formate and sodium dihydrogen (pure for analysis, Merck, Germany), sodium azide (Serva, Germany) were used for the purification and characterization of the enzyme.

#### Site-directed mutagenesis

Nucleotide substitutions were introduced using two-step PCR. Plasmids pPseFDH8, pPseFDH8\_D221S, and

pMorFDH2, with the *psefdh* and *morfdh* genes under the control of a strong promoter of T7 RNA polymerase, were used as templates. The mutations were introduced using forward (T7\_For) and reverse (T7\_Rev) primers at the beginning and at the end of the gene, respectively, as well as direct and reverse primers carrying the desired replacements for the *psefdh* gene. The primer sequences are shown below.

```
T7_For      5'-TAATACGACTCACTATAGGG-3'
T7_Rev     5'-GCTAGTTATTGCTCAGCGG-3'
PseFDH_A198G_for 5'-GTCGGCACCGTGGGCGCCGGTGCATCGGT-3'
PseFDH_A198G_rev 5'-CGACCGGCGCCACGGTCCGACATGCATCG-3'
MorFDH_A198G_for 5'-CACCGTGGCCGCGCCGATCGGCTG-3'
MorFDH_A198G_rev 5'-TGGCGCCGCGCGACGGTCCGACATGCATG-3'
```

The reaction mixture for PCR contained 2.5  $\mu$ l of a 10 $\times$  buffer for Pfu-DNA polymerase (200 mM Tris-

HCl (pH 8.8 at 25°C), 100 mM (NH<sub>4</sub>)<sub>2</sub>SO<sub>4</sub>, 100 mM KCl, 1 mg/ml BSA, 1% (v/v) Triton X-100, 20 mM MgSO<sub>4</sub>; 2.5 µl of a dNTP mixture (dATP, dGTP, dTTP, dCTP with the concentration of each component being 2.5 mM); 1 µl of the DNA template (≈10 ng/µL); 2 µl of each primer (10 nM/ml); 0.5 µl of Pfu-DNA polymerase (2.5 U/µl); and deionized water to a total volume of the mixture of 25 µl. PCR was performed in a 0.5-ml thin-walled plastic tube (SSI, USA) using a Tertsik instrument (DNA Technologies, Russia). A total of 30 µl of mineral oil was added to the tube before the PCR to prevent evaporation of the reaction mixture. The tube was heated for 5 min at 95°C, and the PCR reaction was carried out according to the following scheme: denaturation at 95°C, 30 s; primer annealing at 54–58°C; and extension at 72°C, 2 min, a total of 25–35 cycles. After the last cycle, the reaction mixture was further incubated for 10 min at 72°C. The temperature during the second step was 3–5°C below the melting temperature of the duplexes (T<sub>m</sub>) formed by the primers.

For the first two PCR runs, T7\_For/PseFDH\_A198G\_rev (fragment 1) and PseFDH\_A198G\_for/T7\_Rev (fragment 2) primer pairs were used in the case of PseFDH. Fragments T7\_For/MorFDH\_A198G\_rev and MorFDH\_A198G\_for/T7\_Rev (fragments 1 and 2, respectively) were used for MorFDH. The PCR products – fragment 1 and fragment 2 – were purified using electrophoresis in 1% agarose gel. The third uniting PCR was then performed with the T7\_For and T7\_Rev primers, wherein the previously obtained fragments, 1 and 2, were used as the DNA template. The product of the third PCR was purified in a similar way using 1% agarose gel and treated with two restriction endonucleases: XhoI and EcoRI. DNA fragments were purified using electrophoresis in 1% agarose gel, extracted from the gel and ligated with the plasmids pPseFDH8, pPseFDH8\_D221S, and pMorFDH2, treated with the same restriction endonucleases. The ligation mixture was used to transform *E. coli* DH5α cells. The cells were then plated onto Petri dishes with an agar medium containing ampicillin (100 µg/ml) and incubated for 16 h at 37°C. Three colonies of each mutant PseFDH A198G, PseFDH A198G/D221S, and MorFDH A198G were taken from each plate and used to isolate the plasmids. The presence of only the desired mutations was proved by sequencing using the plasmid DNA at the center for the collective use “Genome” (V.A. Engelhardt Institute of Molecular Biology, Russian Academy of Sciences).

#### Expression of FDH mutants in *E. coli* cells

Wild-type PseFDH and MorFDH and their mutant forms were expressed in the *E. coli* cells BL21 (DE3)/pLysS. The cells were transformed using the appropriate plasmid and plated on Petri dishes with an agar

medium containing ampicillin (100 µg/ml) and chloramphenicol (25 µg/ml) in order to obtain a producer strain. A single colony was taken from the plate and cultured for 7–9 h at 30°C and 180 rpm in 5 ml of a 2YT medium (yeast extract 10 g/l, bacto-tryptone 16 g/l, sodium chloride 5 g/l, pH 7.0) in the presence of 100 µg/ml ampicillin and 25 µg/ml chloramphenicol until an absorbance of A<sub>600</sub> ≈ 0.6–0.8 was reached. Then inoculate was transferred into 100 ml of 2YT medium with ampicillin (100 µg/ml) in 1 l baffled conical flasks and cultured at 30°C and 80–90 rpm until an absorbance of A<sub>600</sub> ≈ 0.6–0.8 was reached. Enzyme expression was induced by adding lactose (300 g/l) to the medium to a final concentration of 20 g/l. After induction, the cells were cultivated for 17 h at 120 rpm. The cells were pelleted using a Beckman J-21 (USA) centrifuge (20 min, 7500 rpm, 4°C). The resulting pellet was re-suspended in a 0.1 M sodium phosphate buffer (pH 8.0) in a 1: 4 (wt.) ratio. The resulting suspension was stored at –20°C.

#### Isolation and purification

The enzymes were purified using the previously developed protocol for purifying recombinant wild-type PseFDH [8]. A cell suspension, 20% (w/v) in 0.1 M sodium phosphate buffer (pH 8.0) containing wild-type PseFDH and MorFDH and their mutants, was prepared from the resulting biomass. Final suspensions were subjected to two freeze-thaw cycles, and the cells were disrupted using a sonicator (Branson Sonifier 250, Germany) under continuous cooling. The precipitate was removed by centrifugation using a 5804R Eppendorf centrifuge (11000 rpm, 30 min), and a saturated ammonium sulfate solution was added dropwise to the supernatant to a concentration of 35% of the saturated solution. The resulting solution was incubated for several hours at 4°C. The precipitate was separated by centrifugation using a Beckman J21 centrifuge (20,000 rpm, 30 min, 4°C), and the supernatant was purified on a Phenyl Sepharose Fast Flow (Pharmacia Biotech). The protein was eluted using a linear gradient 35–0% of ammonium sulfate in a 0.1 M sodium phosphate buffer, pH 7.0. Active fractions were collected, and the enzyme solution was concentrated by membrane filtration using a cell with a PM-10 membrane (Amicon). The enzyme preparation was desalted by gel filtration through a Sephadex G-25 column in the same buffer. Preparation purity was monitored by analytical electrophoresis in 12% polyacrylamide gel in the presence of 0.1% sodium dodecyl sulfate on a Mini-Protean III instrument (BioRad).

#### Formate dehydrogenase activity assay

FDH activity was measured spectrophotometrically by monitoring the accumulation of NADH (NADPH)

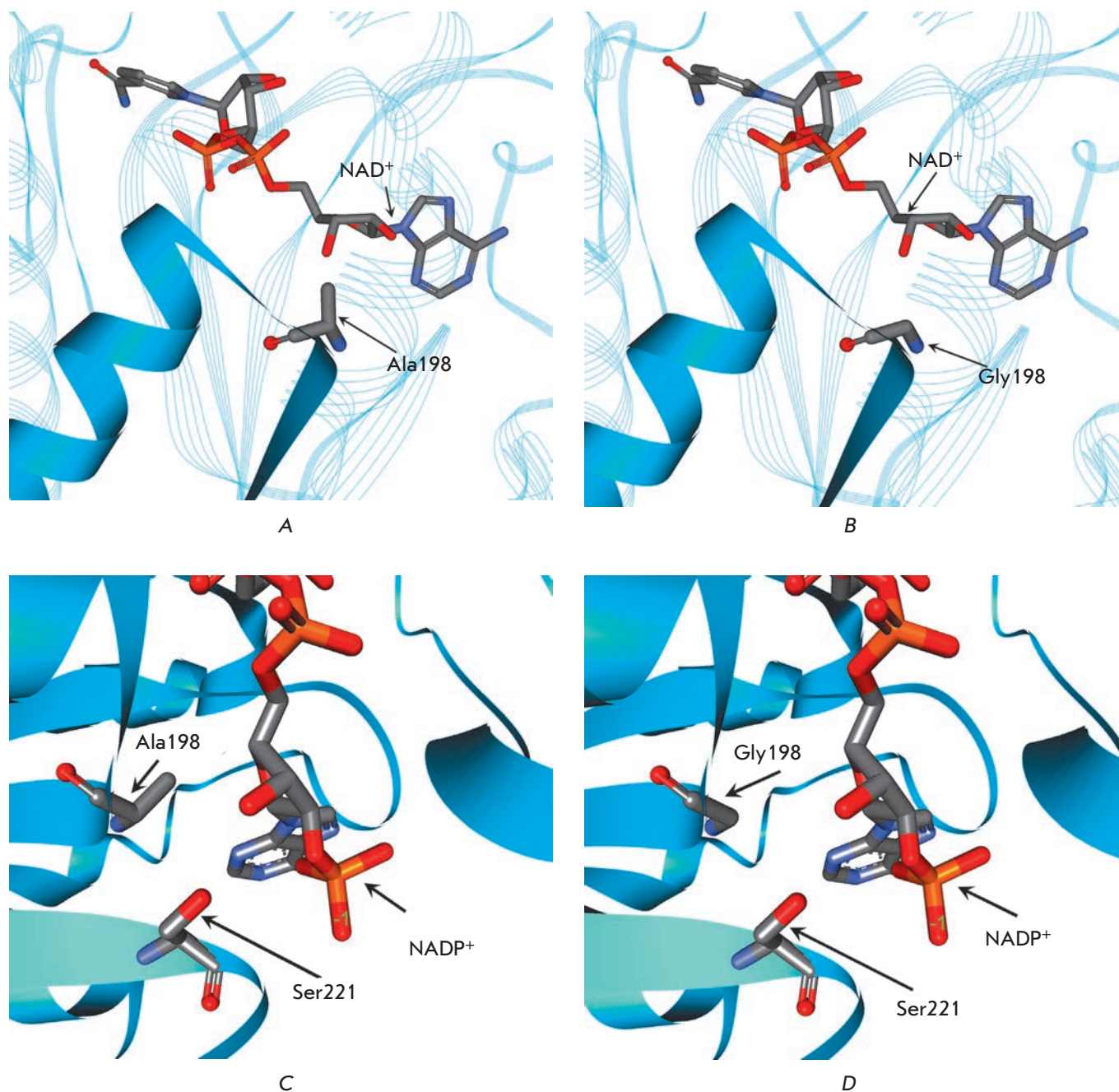


**Fig. 3.** Fragments of the structures of formate dehydrogenase from bacterium *Pseudomonas* sp. 101. A – wild-type enzyme (complex with  $\text{NAD}^+$  and azide – 2NAD), B – model structure of the mutant PseFDH A198G (complex with  $\text{NAD}^+$ ); C and D – model structures of mutant PseFDH D221S and PseFDH A198G/D221S (both – complexes with  $\text{NADP}^+$ ), respectively

at 340 nm ( $\epsilon_{340} = 6220 \text{ M}^{-1} \text{ cm}^{-1}$ ) on a Shimadzu UV 1601PC or UV 1800PC spectrophotometers at 30°C in a 0.1 M sodium-phosphate buffer, pH 7.0.  $\text{NAD(P)}^+$ , and formate concentrations in the cuvette were 0.6 M and 1 mg/ml, respectively.

#### Determination of Michaelis constants

The Michaelis constants ( $K_M$ ) for  $\text{NAD}^+$ ,  $\text{NADP}^+$  and formate were determined from the dependence of the reaction rate on a variable substrate concentration ( $0.4\text{--}6 K_M$ ) at a fixed saturation concentration of the

Table 2. Kinetic parameters of native and mutant formate dehydrogenases

| Enzyme*                         | $K_{M}^{\text{NAD}^+}$ ,<br>$\mu\text{M}$ | $K_{M}^{\text{NADP}^+}$ ,<br>$\mu\text{M}$ | $K_{M}^{\text{HCOO}^-}$ , mM | $k_{cat}$ , $\text{s}^{-1}$ | $k_{cat}/K_{M}^{\text{NAD}^+}$ ,<br>$\text{mM}^{-1}\text{s}^{-1}$ | $k_{cat}/K_{M}^{\text{NADP}^+}$ ,<br>$\text{mM}^{-1}\text{s}^{-1}$ | reference    |
|---------------------------------|---|--|------------------------------|-----------------------------|---|--|--------------|
| Reaction with NAD <sup>+</sup>  |   |  |                              |                             |   |  |              |
| wt-PseFDH                       | 60 ± 5                                    |  | 6.5 ± 0.2                    | 7.3 ± 0.2                   | 122   | 1  | [14]         |
| PseFDH A198G                    | 35 ± 2                                    |  | 7.5 ± 0.2                    | 7.3 ± 0.1                   | 209   | 1.713  | Present work |
| PseFDH D221S                    | 710 ± 45                                  |  | 32 ± 2                       | 5.0 ± 0.3                   | 7.04  | 0.058  | Present work |
| PseFDH D221S/ A198G             | 540 ± 42                                  |  | 53 ± 1                       | 5.0 ± 0.2                   | 9.26  | 0.076  | Present work |
| MorFDH                          | 80 ± 7                                    |  | 7.7 ± 0.3                    | 7.3 ± 0.1                   | 91.3  | 1  | [14]         |
| MorFDH A198G                    | 45 ± 3                                    |  | 8.0 ± 0.5                    | 7.3 ± 0.3                   | 162   | 1.774  | Present work |
| BstFDH                          | 1430                                      |  | ≥ 150                        | 1.7 ± 0.1                   | 1.19  | --   | [15]         |
| wt-CmeFDH                       | 55  |  | NA                           | 1.4                         | 25.5  | --   | [16]         |
| CmeFDH D195S                    | 4700                                      |  | 7.0                          | 1.6                         | 0.34  | --   | [16]         |
| wt-CboFDH                       | 15  |  | 5.9                          | 3.7                         | 246.7   | --   | [17]         |
| CboFDH D195S                    | 1500                                      |  | NA                           | 0.34                        | 0.227   | 9.2*10 <sup>-4</sup>   | [17]         |
| CboFDH D195N                    | 5010                                      |  | NA                           | 0.21                        | 0.04  | 1.7*10 <sup>-4</sup>   | [17]         |
| CboFDH D195A                    | 4800                                      |  | NA                           | 0.76                        | 0.158   | 6.4*10 <sup>-4</sup>   | [17]         |
| CboFDH D195Q                    | 960                                       |  | NA                           | 0.26                        | 0.271   | 0.001  | [17]         |
| SceFDH                          | 36  |  | 5.5                          | 6.5                         | 181   | --   | [18]         |
| SceFDH D196A/Y197R              | 7600                                      |  | 1000                         | 0.095                       | 0.0125  | --   | [18]         |
| Reaction with NADP <sup>+</sup> |   |  |                              |                             |   |  |              |
| wt-PseFDH                       |   | 100000*                                    | NA                           | 1.3 ± 0.1                   | 0.013   | 1  | Present work |
| PseFDH D221S                    |   | 190 ± 30                                   | 43                           | 1.7 ± 0.2                   | 3.04  | 234  | [7]          |
| PseFDH D221S/ A198G             |   | 280 ± 25                                   | 89                           | 1.8 ± 0.2                   | 6.43  | 495  | Present work |
| wt-BstFDH                       |   | 160  | 55.5                         | 4.75                        | 29.7  | --   | [15]         |
| CmeFDH D195S                    |   | > 0.4 M                                    | NA                           | NA                          | NA  | --   | [16]         |
| wt-CboFDH                       |   | > 38000                                    | NA                           | 4*10 <sup>-5</sup>          | 10 <sup>-6</sup>  | --   | [17]         |
| CboFDH D195S                    |   | 6200                                       | NA                           | 0.34                        | 0.055   | 55000  | [17]         |
| CboFDH D195N                    |   | 13200                                      | NA                           | 0.26                        | 0.0196  | 19600  | [17]         |
| CboFDH D195A                    |   | 3300                                       | NA                           | 0.052                       | 0.0157  | 15700  | [17]         |
| CboFDH D195Q                    |   | 4500                                       | NA                           | 0.26                        | 0.058   | 58000  | [17]         |
| SceFDH D196A/Y197R              |   | 4500                                       | 1000                         | 0.13                        | 0.03  | --   | [18]         |

\*PseFDH, MorFDH, BstFDH, CmeFDH, CboFDH, SceFDH – formate dehydrogenases from bacteria *Pseudomonas* sp. 101, *Moraxella* sp. C-1, *Burkholderia stabilis* 15516, yeasts *Candida methylca* and *Candida boidinii*, and baker's yeast *Saccharomyces cerevisiae*, respectively.

second substrate (>15  $K_M$ ). The exact concentrations of the NAD<sup>+</sup> and NADP<sup>+</sup> solutions were determined spectrophotometrically at 260 nm ( $\epsilon_{260} = 17800 \text{ M}^{-1} \text{ cm}^{-1}$ ). The sodium formate solution was prepared by dissolving the required amount of substrate in a 0.1 M sodium phosphate buffer pH 7.0. The solution was adjusted in a volumetric flask.  $K_M$  values were calculated by nonlinear regression using the OriginPro 8.5 software.

### Thermal inactivation study

The thermal stability of the enzymes was studied in a sodium phosphate buffer (0.1 M, pH 7.0) at various temperatures. A number of Eppendorf tubes (0.5 ml) with a 100  $\mu\text{l}$  enzyme solution (0.2 mg/ml) were prepared for each experiment. The tubes were incubated in a wa-

ter bath at different temperatures with a precision of temperature control  $\pm 0.1^\circ\text{C}$ . At fixed time intervals, a tube was transferred from the bath to ice for 5 min. The solution was then centrifuged for 3 min at 12,000 rpm using an Eppendorf 5415D centrifuge. The residual FDH activity was measured as described above. The rate constant of thermal inactivation  $k_{in}$  was calculated from the slope of the linear dependence of remaining activity on time (semi-log coordinates  $\ln(A/A_0) - t$ ) by linear regression using the Origin Pro 8.5 software.

### Computer simulation

The structures of mutant PseFDH and MorFDH were modeled using Insight II (Accelrys), and structures of apo forms of PseFDH (PDB2NAC, resolution 2.05 Å)

and MorFDH (PDB3FN4, resolution 1.96 Å) were used as the template structures. Further optimization of the structure was performed using molecular mechanics (module Discover\_3 in Insight II, a force field CVFF, 1000 cycles), molecular dynamics (5 ps), and again molecular mechanics (1000 cycles). The PseFDH and MorFDH structures were analyzed using the Accelrys Discovery Studio 2.1 software package. The same package was used to obtain images of the protein globule.

## RESULTS AND DISCUSSION

### Selection of amino acid residues for site-directed mutagenesis

Enzymes with the desired properties can be successfully obtained using protein engineering methods. Rational design is one of the widely used approaches. During the first stage, the three-dimensional structure of the target enzyme is analyzed and the sites of directed amino acid substitutions are identified. Multiple alignments of amino acid sequences for the site selected for the substitutions were performed in order to determine the type of introduced residues. The final choice of residues is made after analyzing the model structures of potential mutants. We used the rational design method for two formate dehydrogenases from bacteria *Pseudomonas* sp.101 and *Moraxella* sp. C-1.

The part of the active center binding the adenine portion of the coenzyme is known to have a number of structural features typical of NAD(P)<sup>+</sup>-dependent dehydrogenases. The coenzyme-binding domain consists of two subdomains binding the adenine and nicotinamide portions of the coenzyme in the majority of enzymes of this group. Each of these sub-domains is composed of alternating  $\beta$ -strands and  $\alpha$ -helices. This structure is called the Rossmann fold [9]. The total amount of alternating  $\beta$ -strands and  $\alpha$ -helices can be different. Various folding options were analyzed in [10]. The GxGxxG-conserved motif is located in the site connecting the first strand of the  $\beta$ -sheet to the  $\alpha$ -chain of the Rossmann fold. The first glycine residue, due to its high mobility, provides optimum relative positioning of the secondary structures required for proper orientation of the second glycine residue of this motif. The second Gly residue located in the immediate vicinity of the phosphate moiety of the coenzyme is involved in its binding. It is assumed that at this position the presence of any residue with bulkier side chains would lead to strong steric complications upon binding of the coenzyme. The third residue is important for dense packing of  $\alpha$ A and  $\beta$ B structural elements and their relative orientation.

The alignment of the amino acid sequences of formate dehydrogenase from different organisms in the

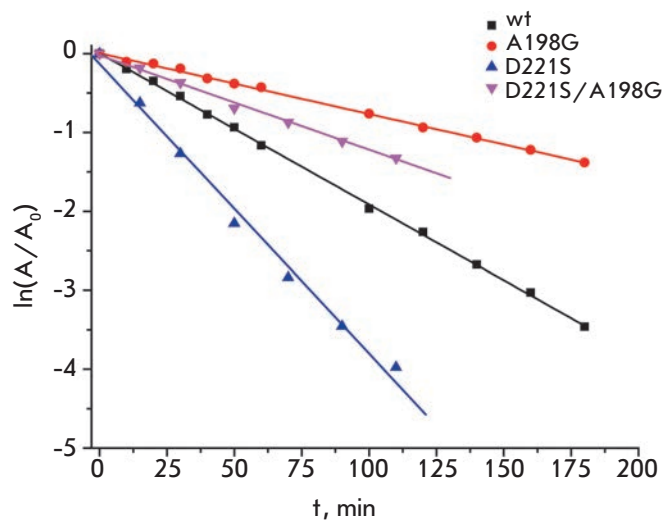


Fig. 4. Residual activity as a function of time for mutant PseFDHs and wild-type enzyme, 0.1 M phosphate buffer, pH 7.0, 63°C

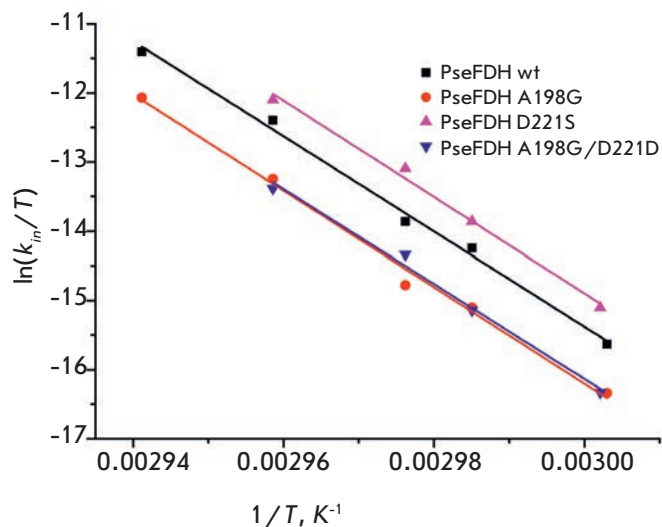


Fig. 5. Temperature dependence of the inactivation rate constant in coordinates  $\ln(k_{in}/T) - 1/T$  for mutant PseFDHs and the wild-type enzyme

site of the coenzyme-binding domain (fragment  $\beta$ - $\alpha$ - $\beta$ ) is shown in Fig. 1. This alignment demonstrates that a significant part of formate dehydrogenases from bacteria and fungi contains Ala residue at the first position instead of Gly. This Ala residue resides at position 198 in FDH from bacteria *Pseudomonas* sp. 101 and *Moraxella* sp. C-1. According to Ramachandran plots, PseFDH and MorFDH apo-forms (2NAC and 3FN4, respective-

ly) possess non-optimal values of the angles  $\psi$  and  $\varphi$  of the Ala198 residue (Fig. 2A, B).

As can be seen from Fig. 3A, the methyl group of the Ala residue is oriented toward the 3'-OH of ribose of adenosine in the ternary complex of PseFDH with NAD<sup>+</sup> and the azide ion (holo form, 2NAD, resolution 1.8 Å, the structure is considered to be an analogue of the transition state). The results of a computer simulation demonstrated that Ala198Gly substitution in PseFDH removes conformational tension (Fig. 3B). The situation is similar for MorFDH (holo form 2GSD structure, not shown in Fig. 3). Based on computer modeling, we decided to obtain mutant PseFDH and MorFDH, where the Ala198 residue is replaced by Gly.

A Ala198Gly substitution was also introduced in a previously obtained PseFDH mutant with the coenzyme specificity changed from NAD<sup>+</sup> to NADP<sup>+</sup>. This effect was achieved by a Asp221Ser substitution (Fig. 3C). The results of a computer simulation showed (Fig. 3C) that steric tension in the structure of the mutant enzyme in complex with NADP<sup>+</sup> is not as strong as that of the wild-type, due to the presence of the Ala198 residue. Nevertheless, an additional pocket, which would more effectively bind the 3'-phosphate group of the coenzyme, should appear as a result of Ala198Gly substitution (Fig. 3D).

### Preparation of mutant enzymes

Three plasmids were isolated after mutagenesis using PCR for each of the three mutants: PseFDH Ala198Gly, PseFDH Ala198Gly/Asp221Ser, and MorFDH Ala198Gly. The sequencing results showed that all plasmids contained only the desired mutations in the *psefdh* and *morfdh* genes, while other nucleotide substitutions were absent. Plasmids with mutations were used to transform *E. coli* BL21 (DE3)/pLysS cells. Both mutant PseFDH and mutant MorFDH were expressed in soluble and active forms. They were isolated according to the method described in the Materials and Methods section. Their purity was at least 95% according to the results of analytical electrophoresis in a polyacrylamide gel in the presence of sodium dodecyl sulfate.

### Study of the thermal stability of mutant formate dehydrogenases

The thermostability of mutant PseFDH and MorFDH was determined based on inactivation kinetics at several temperatures. In wild-type PseFDH and its mutants, the temperature range of measurements was 60–65°C (Table 1). The time course of loss of enzymatic activity fits the first-order reaction kinetics for the entire temperature range (Fig. 4). The thermal inactivation rate constants were determined as the slope of these lines. The observed inactivation rate constant does not

depend on enzyme concentration for the entire temperature range, which means that the inactivation is, in fact, a true monomolecular process. The thermal inactivation rate constants are shown in Table 1. The stability of mutant PseFDH with Ala198Gly substitution at all temperatures was 2–2.5 times higher than the stability of the wild-type enzyme. A similar effect of increased thermal stability was observed for the pair of native and mutant MorFDHA198G, but due to the fact that MorFDH is 25 times less stable than PseFDH [11] the inactivation kinetics were studied at lower temperatures (56–62°C).

Mutant NADP<sup>+</sup>-specific PseFDH Asp221Ser was less stable than the initial NAD<sup>+</sup>-dependent PseFDH (Fig. 4 and Table 1). Ala198Gly substitution in PseFDH Asp221Ser resulted in a significant improvement in thermal stability; the stabilization effect was even slightly higher than that for a similar substitution in the wild-type (Table 1). These data indicate that the methyl group of the Ala198 residue is an important destabilizing factor in this portion of the protein globule. A similar stabilizing effect was observed for Ala198Gly substitution in MorFDH (not shown), which decreased the thermal inactivation rate constant by 2.5 times.

We were interested in establishing which of the two factors, the change in enthalpy or entropy, increased stability of the obtained mutants. For this purpose, we analyzed the temperature dependence of inactivation rate constants. Figure 5 shows the dependence of the first-order inactivation rate constants  $k_{in}$  in coordinates  $\ln(k_{in}/T)$  vs.  $1/T$ , where  $T$  is the absolute temperature in K.

The linear dependence of the secondary plots suggests that the process of thermal inactivation of native and mutant FDHs is described by the temperature dependence of the rate constant according to the transition state theory [12]. This equation can be presented in the following linear form:

$$\ln\left(\frac{k_m}{T}\right) = \ln\left(\frac{k_B}{h}\right) + \frac{\Delta S^\ddagger}{R} - \frac{\Delta H^\ddagger}{RT} = \text{const} - \frac{\Delta H^\ddagger}{R} \frac{1}{T},$$

where  $k_B$  and  $h$  are the Boltzmann and Planck constants, respectively;  $R$  is the universal gas constant;  $\Delta H^\ddagger$  and  $\Delta S^\ddagger$  are activation parameters.

Parallel lines in Fig. 5 indicate that the process of thermal inactivation of wild-type PseFDH and its mutants is characterized by approximately equal  $\Delta H^\ddagger$  values, while the main contribution to increased FDH stability resulting from the introduction of the A198G mutation was determined by the entropy factor. The numerical values of the activation parameters  $\Delta H^\ddagger$  and  $\Delta S^\ddagger$  of the thermal inactivation process are shown in Table 1.

It should be noted that the 2.5-fold increase in enzyme stability resulting from point mutation is a significant effect. Previously, we conducted site-directed mutagenesis experiments with another amino acids residues of the PseFDH globule with non-optimal values of the  $\psi$  and  $\phi$  angles. In these experiments, no increased stability was achieved, since these residues were involved in the formation of hydrogen bonds and the energy of these bonds exceeded the energy of destabilization due to a non-optimal conformation [13].

### Kinetic properties of the mutant enzymes

The kinetic parameters of the obtained mutants are shown in Table 2. For the sake of comparison, the same table shows similar parameters for other known FDHs. As mentioned above, the results of a computer simulation showed that the introduction of Ala198Gly substitution provides higher mobility to the coenzyme-binding  $\alpha$ A-helix domain. As can be seen from Table 2, the introduction of this substitution in NAD<sup>+</sup>-specific wild-type PseFDH and MorFDH improves binding of the coenzyme: in both cases, the Michaelis constant for NAD<sup>+</sup> decreased by almost twofold, while that for formate remained virtually unchanged. The Michaelis constant is typically not an equilibrium constant; however, the reaction catalyzed by PseFDH and MorFDH has a random quasi-equilibrium kinetic mechanism [11, 19, 20]. In this case, the  $K_M$  value for NAD<sup>+</sup> and formate is as an equilibrium constant of substrate binding to the corresponding binary complex.

Asp221Ser substitution deteriorates the enzyme affinity for NAD<sup>+</sup> and increases affinity for NADP<sup>+</sup> (Table 2). This is easily explained by the fact that such a substitution removes the carboxyl group, which provides the specificity to NAD<sup>+</sup> due to the presence of hydrogen bonds with the 2'- and 3'-OH-groups of the ribose present in adenosine, and repulses the negatively charged 2'-phosphate group of NADP<sup>+</sup>.

Ala198Gly substitution in mutant NADP<sup>+</sup>-specific PseFDH Asp221Ser leads, as in the case of the wild-type enzyme, to improved affinity of the enzyme for NAD<sup>+</sup> by approximately 1.5 times, but in the case of NADP<sup>+</sup> affinity for coenzyme decreases by approximately the same value (Table 2). In addition, Ala198Gly substitution in the above-mentioned mutant caused a significant deterioration in the affinity for formate. This was due to the fact that the major structural changes in FDH protein globules required for the formation of the ternary enzyme-substrate complex and the transition state of enzymatic reactions occur at the stage of coenzyme binding. Therefore, the conformation of the double complex (FDH-coenzyme) is critical

for efficient binding of formate. It is known that even small changes in the active site of FDH lead to significant changes in the affinity for formate. Data for FDH from bacterium *Burkholderia stabilis* are shown in Table 2. It can be seen that the substitution at position 221 of PseFDH allows one to approach the values of the constants for this natural NADP<sup>+</sup>-dependent enzyme.

Our data allow us to propose a hypothesis explaining the presence of the “non-canonical” Ala residue in the first position of the highly conserved “canonical” sequence GxGxxG for the coenzyme binding domain of PseFDH. Apparently, this enzyme is an intermediate product of formate dehydrogenase evolution from NADP<sup>+</sup>- to a NAD<sup>+</sup>-specific enzyme. During the early stages of development of living systems, when aerobic processes were the main metabolic pathways, FDH was probably an NADP<sup>+</sup>-dependent enzyme and was responsible for the production of NADPH for the biosynthesis of various compounds. The presence of the Ala residue at position 198 in NADP<sup>+</sup>-dependent enzymes provided 10 times more efficient binding of formate than in the case of Gly198. In this enzyme, an uncharged amino acid resided at position 221 and a positively charged Arg residue, required to neutralize the negative charge of the phosphate groups of NADP<sup>+</sup>, was at position 222. An enzyme effectively using NAD<sup>+</sup> rather than NADP<sup>+</sup> was required in the course of evolution when methylophilic microorganisms appeared. The first stage of the evolutionary process was the emergence of the Asp residue at position 221, providing NAD<sup>+</sup> specificity. FDH from bacterium *Pseudomonas* sp. 101 is probably the product of this evolution stage. This enzyme has an Asp residue responsible for NAD<sup>+</sup> specificity, while containing a positively charged Arg222 residue involved in the binding of NADP<sup>+</sup>, and Ala at position 198 as “rudiments.” FDH of methylophilic yeast appeared at the later stages of evolution. These enzymes have lost their “rudimentary” residues and possess absolute specificity for NAD<sup>+</sup> (Table 2). Over the course of evolution, the “non-canonical” Ala residue at position 198 in yeast formate dehydrogenases was replaced by “canonical” Gly and the residue corresponding to Arg222 in PseFDH was substituted by the Tyr residue, as was clearly shown in our experiments studying the changes in coenzyme specificity from NAD<sup>+</sup> to NADP<sup>+</sup> in FDH from baker's yeast [18]. The experiments of changes in FDH coenzyme specificity are described in more detail in [7]. ●

*This study was supported by the grant of a President of Russian Federation for State support of young Russian scientists (MK-2304.2014.4).*

## REFERENCES

1. Wierenga R.W., Hol W.G.J. // *Nature*. 1983. V. 302. № 5911. P. 842–844.
2. Lamzin V.S., Dauter Z., Popov V.O., Harutyunyan E.H., Wilson K.S. // *J. Mol. Biol.* 1994. V. 236. № 3. P. 759–785.
3. Filippova E.V., Polyakov K.M., Tikhonova T.V., Stekhanova T.N., Boiko K.M., Sadykhov E.G., Tishkov V.I., Popov, V.O., Labrou, N. // *Crystallography Reports*. 2006. V. 51. № 4. P. 627–631.
4. Shabalin I.G., Filippova E.V., Polyakov K.M., Sadykhov E.G., Safonova T.N., Tikhonova T.V., Tishkov V.I., Popov V.O. // *Acta Crystallogr. D Biol. Crystallogr.* 2009. V. 65. № 12. P. 1315–1325.
5. Shabalin I.G., Polyakov K.M., Tishkov V.I., Popov V.O. // *Acta Naturae*. 2009. V. 1. № 3. P. 89–93.
6. Matorin A.D. Mechanism of substrate and coenzyme specificity of bacterial formate dehydrogenase. Ph.D. Thesis. M.V.Lomonosov Moscow State University, Moscow, 2000, 127 pages.
7. Alekseeva A.A., Dolina I.A., Zarubina S.A., Matorin A.D., Sadykhov E.G., Savin S.S., Tishkov V.I. // *Biochimie*. 2015. submitted for publication.
8. Rojkova A.M., Galkin A.G., Kulakova L.B., Serov A.E., Savitsky P.A., Fedorchuk V.V., Tishkov V.I. // *FEBS Lett.* 1999. V. 445. № 1. P. 183–188.
9. Rao S.T., Rossmann M.G. // *J. Mol. Biol.* 1973. V. 76. № 2. P. 241–256.
10. Lesk A.M. // *Curr. Opin. Struct. Biol.* 1995. V. 5. № 6. P. 775–783.
11. Tishkov V.I., Popov V.O. // *Biomol. Eng.* 2006. V. 23. № 1. P. 89–110.
12. Cornish-Bowden A. *Fundamentals of Enzyme Kinetics*. 4th Ed. Wiley-Blackwell, 2012. 510 p.
13. Serov A.E., Odintzeva E.R., Uporov I.V., Tishkov V.I. // *Biochemistry (Moscow)*. 2005. V. 70. № 4. P. 804–808.
14. Tishkov V.I., Popov V.O. // *Biochemistry (Moscow)*. 2004. V. 69. № 11. P. 1252–1267.
15. Hatrongjit R., Packdibamrung K. // *Enz. Microbial Technol.* 2010. V. 46. № 7. P. 557–561.
16. Gul-Karaguler N., Sessions R.B., Clarke A.R., Holbrook J.J. // *Biotechnol. Lett.* 2001. V. 23. № 4. P. 283–287.
17. Andreadeli A., Platis D., Tishkov V., Popov V., Labrou N.E. // *FEBS J.* 2008. V. 275. № 15. P. 3859–3869.
18. Serov A.E., Popova A.S., Fedorchuk V.V., Tishkov V.I. // *Biochem. J.* 2002. V. 367. № 3. P. 841–847.
19. Tishkov V.I., Galkin A.G., Egorov A.M. // *Biochimie*. 1989. V. 71. № 4. P. 551–557.
20. Serov A.E., Popova A.S., Tishkov V.I. // *Dokl. Biochem. Biophys.* 2002. V. 382. № 1–3. P. 26–30.

# Reconstruction of Rabbit Urethral Epithelium with Skin Keratinocytes

O. S. Rogovaya<sup>1,2\*</sup>, A. K. Fayzulin<sup>3</sup>, A. V. Vasiliev<sup>1</sup>, A. V. Kononov<sup>4</sup>, V. V. Terskikh<sup>1</sup>

<sup>1</sup>N.K. Koltsov Institute of Developmental Biology, Russian Academy of Sciences, Vavilova Str., 26, Moscow, 119334, Russia

<sup>2</sup>N.I. Pirogov Russian National Research Medical University, Ministry of Healthcare of the Russian Federation, Ostrovityanova Str., 1, Moscow, 117997, Russia

<sup>3</sup>Morozov Children's Clinical Hospital, Moscow Department of Health Care, 4<sup>th</sup> Dobryninsky Per., 1, Moscow, 119049, Russia

<sup>4</sup>A.I. Evdokimov State University of Medicine and Dentistry, Ministry of Healthcare of the Russian Federation, Delegatskaya Str., 20/1, Moscow, 127473, Russia

E-mail: Rogovaya26f@gmail.com

Received: 24.06.2014

Copyright © 2015 Park-media, Ltd. This is an open access article distributed under the Creative Commons Attribution License, which permits unrestricted use, distribution, and reproduction in any medium, provided the original work is properly cited.

**ABSTRACT** We have investigated the living skin equivalent (LSE) as an alternative source of plastic material for closing full-thickness epithelial-stromal urethral injuries. The possibility of transdifferentiation of epidermal keratinocytes, a component of 3D tissue constructs, was investigated *in vivo* in a model of the recovery of urethral injuries in laboratory rabbits. Autologous grafting of LSE in de-epithelialized urethra showed that skin keratinocytes placed in a specific *in vivo* microenvironment can be incorporated into the damaged area and function as urothelium. The use of EGFP transfected keratinocytes allowed us to identify transplanted cells. The reconstructed urethral tubes did not develop strictures or fistulas at the site of the grafted LSE. Immunohistochemical studies of neo-urothelium revealed EGFP-positive cells expressing the urothelial markers K7 and UP3. **KEYWORDS** epidermal stem cells, keratinocytes, urothelium, cell plasticity, transdifferentiation, tissue engineering.

## INTRODUCTION

According to the current concept of the cellular mechanisms of regeneration, the nature and mechanisms of regeneration are defined by the types of tissue-specific stem and early progenitor cells involved in the process [1–3]. There is a significant amount of data demonstrating that under certain conditions tissue-specific stem cells can exhibit considerable phenotypic plasticity, which suggests a possibility of their transdifferentiation. Transdifferentiation has been successfully demonstrated in a number of models, including those for restoration of epithelial tissue in cornea, bladder, intestine, etc. [4, 5]. We believe that this phenomenon can be used in tissue engineering and cell technologies as an approach to create the cells and cell constructs required for the restoration of structures and/or functions of tissues and organs. Advances in this area of regenerative medicine will resolve the pressing issue of the shortage of a patient's own tissues, which is implicated in a significant portion of reconstructive surgeries failures today [6, 7]. Another equally important aspect is the *in vitro* development of histotypic tissue constructs suitable for modeling morphogenetic processes, including those featuring tissue-specific stem cells [8–11].

In addition to direct incorporation into the damaged tissue structure, stem cells and cellular constructs can participate in repair and regeneration through induction [12, 13]. The effect may vary in its intensity and specificity. The induction can explain such phenomena as tissue recovery after transplantation of allogeneic tissue-engineering histotypic constructs containing stem/progenitor cells.

Taking this into account, the present study investigated the possibility of using the living skin equivalent (LSE) as an alternative source of plastic material for closing full-thickness epithelial-stromal urethral injuries. An *in vivo* model of the recovery of urethral injuries in laboratory rabbits was used to study the possibility of transdifferentiation of epidermal keratinocytes in 3D tissue constructs.

## MATERIALS AND METHODS

A total of 20 male chinchilla rabbits weighing no more than 2 kg were used in the experiments. All procedures were performed according to the rules established by the Bioethics Commission of the Institute of Developmental Biology, Russian Academy of Sciences. Animal experiments were conducted in accordance with Or-

der № 267 of the Ministry of Healthcare of the Russian Federation issued June 19, 2003 “On the Approval of Laboratory Practice Rules.” The study group consisted of 14 animals; the control group, of six animals.

#### **Isolation and growth of rabbit keratinocytes**

All experimental animals had been assigned serial numbers prior to the start of the study. A tag with the number was attached to the cage in which the rabbit was kept for the duration of the study. The number was registered in the laboratory journal and subsequently assigned to the keratinocyte culture obtained from the rabbit.

At the first stage, skin samples were collected from the interior of a rabbit’s ear; the thickness of a biopsy slice was ca. 0.3 mm.

Immediately after the collection, the skin flaps were placed in a M199 medium with 4 mg/mL gentamicin. If necessary, the skin flaps were stored for 24 h at 4°C. All experiments were conducted under sterile conditions. Prior to storage, all skin samples were thoroughly washed with Hanks’ solution and placed in M199 or Eagle’s medium supplemented with antibiotics. Prior to cell isolation, the biopsy samples were washed with Hanks’ solution containing gentamicin (0.4 mg/mL) or 2000 U/mL penicillin and 1 mg/mL streptomycin. The skin flaps were cut into 3×10 mm strips, washed with PBS, and incubated in 0.125% dispase solution (Sigma) for 16–24 h at 4°C or in 2% dispase solution for 1 h at 37°C. The epidermis was subsequently separated from the dermis along the basal layer with forceps. Pieces of the epidermis separated from the underlying dermis were washed with PBS and placed into PBS + 0.25% trypsin (1:1) solution. Following 10–15 min of incubation at 36°C, trypsin was inhibited by bovine or horse serum solution and a suspension of epidermal rabbit keratinocytes was obtained by pipetting. The suspension was then filtered through a 100 µm nylon mesh and centrifuged at 100g for 10 min. The supernatant was discarded, and the pellet was re-suspended in a keratinocyte growth medium. The keratinocyte suspension was seeded into plastic Costar cell culture flasks pre-coated with a collagen solution at a concentration of 200,000 cells/mL.

A liquid type 1 collagen (0.1 mg/mL) solution in 0.1% acetic acid was used to treat the working surface of the cell culture flasks. The procedure was performed as follows: 2–3 mL of the collagen solution was poured onto the bottom (25 cm<sup>2</sup>) of the flask and was kept at 37°C for 20 min. The collagen was then discarded, and the flask was thoroughly washed with Hanks’ solution supplemented with phenol red, until the disappearance of acid reaction.

For the first 3 days, rabbit keratinocytes were grown in a DMEM/F-12 (2:1) medium containing 10% fetal bo-

vine serum (FBS), 5 µg/mL insulin (Sigma), 10<sup>-6</sup> M isoproterenol (Sigma), and 5 µg/mL transferrin (Sigma). The cells were then switched to DMEM/F-12 medium (2:1) containing 5% FBS, 10 ng/mL epidermal growth factor (EGF), and other additives (see above) and cultivated in a CO<sub>2</sub> incubator; the medium was replaced regularly.

#### **Destratification of keratinocyte culture layers**

Keratinocyte cultures were destratified after a multilayered sheet had been formed. The medium in the cell culture flasks was replaced with a Ca<sup>2+</sup>-free KBE medium, and the flasks were kept for 1–3 days until complete destratification of all cell layers, except for the basal one. After stripping, the keratinocyte cultures were switched to a normal growth medium and after 24 h were plated on the surface of the LSE. The keratinocytes were plated by removing them from the surface of the cell culture flasks with trypsin/EDTA (1:1) solution.

#### **Preparation of autologous rabbit keratinocytes and fibroblast-based LSE to be transplanted into urethral injury**

A Spongostan™ sponge package was opened under sterile conditions and a piece with a size and shape corresponding to those of a Petri dish was cut out with scissors and washed once with Hanks’ solution. Collagen gel containing postnatal human or rabbit fibroblasts at a concentration of 25–30 thousands cells per mL of the gel was prepared as described above and poured into the Petri dishes with Spongostan™ sponges. 1.5 mL of gel was poured into each Petri dish (Ø 3.5 cm).

Fibroblasts in collagen gel were cultivated on the sponge surface for 24 h in a CO<sub>2</sub> incubator. This construct was then used as a connective tissue equivalent to prepare a LSE with fibroblasts in collagen gel and rabbit skin keratinocytes on its surface, according to the aforescribed standard protocol. To observe the autologous grafting principle at all subsequent stages, the cell culture flasks with keratinocytes and LSE were marked with an adhesive label containing the number assigned to an experimental animal.

#### **Cell labeling with a tracer**

At the initial stage, the autologous keratinocytes were labeled with a 0.00001% solution of the DiI membrane tracer in a serum-free culture medium; the cells ready for transplantation were incubated in this medium for 1 h.

#### **Lentiviral transfection of the keratinocyte culture**

Transfection of cells with an enhanced green fluorescent protein (EGFP) was performed using the lentiviral

construct (Evrogen; the virus is supplied in DMEM medium in the amount of  $1.5 \times 10^6$  virus particles/mL). The transfection was performed by introducing the amount recommended by the manufacturer (10 copies per cell).

For transfection,  $1.5 \times 10^5$  keratinocytes were plated on a Petri dish ( $\varnothing$  3.5 cm). After complete cell adhesion, the medium in the dish was replaced with the virus-containing DMEM medium. In order to increase the permeability of the cell membrane, polybrene at a concentration of 5 mg/mL was added simultaneously and the mixture was incubated for 24 h. After transfection, the cells were switched to the standard culture medium. EGFP expression was observed after 72 h.

## HISTOLOGICAL STUDIES

### Preparation of paraffin sections

4% of paraformaldehyde in PBS (pH 7.4) was used for fixation. The tissue was fixed for 24 h and subsequently washed with PBS. The tissue was dehydrated through a series of alcohol baths according to the standard protocol. Xylene was used for further histological processing. The samples were then embedded in paraffin. The sections of paraffin blocks were prepared using a Carl Zeiss MICROM microtome. 5- $\mu$ m-thick serial paraffin sections were prepared and transferred onto the glass. After deparaffinization, the sections were stained with hematoxylin and eosin.

### Preparation of cryosections

Pieces larger than  $0.5 \times 1.0$  cm were fixed for 1 h at room temperature in 4% paraformaldehyde solution, washed with PBS, and placed into 20% sucrose solution for infiltration for 8–12 h until full immersion. The materials thus prepared were frozen in nitrogen vapor and stored at  $-70^\circ\text{C}$ . The 15- to 20- $\mu$ m-thick sections were prepared using a Leica DM IL cryostat (Germany).

### Immunohistochemical studies of the preparations

The expression of various proteins was measured using monoclonal antibodies to detect skin (K14) and urothelium (K7 and K18) keratins (NovoCastra), uroplakin 3(UP3) (UsBioLogical), and EGFP (Evrogen). The immunofluorescence method was used for antigen detection.

The following staining protocol was used for immunofluorescence studies: primary antibodies were diluted in a blocking solution (5% bovine serum albumin + 0.1% Triton X-100 in PBS) at the concentrations recommended by the antibody manufacturers and applied to the sections washed in 0.1% PBS. The samples were incubated for 12–16 h at  $4^\circ\text{C}$ . The material was subsequently washed 4–5 times with 0.1% PBS and incubated in Alexa-488 secondary antibody solution (Molecular

probes) in PBS for 40 min in the dark at room temperature. To prepare temporary preparations, the samples were embedded in glycerol.

### Reconstruction of the experimental urethral injuries in rabbits

The surgery was performed under general anesthesia as described above. Additional novocaine blockade of the penis was performed simultaneously by introducing 0.5 mL of novocaine into the operating theater area. The surgery began with a circumferential incision around the glans penis followed by a longitudinal skin incision on the ventral side of the penis towards its root. Shaft skin was mobilized up to the root of the penis; the muscle was cut on the ventral side towards the urethral lumen. The epithelial lining of the urethra was then separated by forceps along the basal membrane for 1–1.5 cm up to the prostate section at the root of the rabbit's penis. The rectangular collagen-based LSE, with a length equal to that of the urethral tube injury and a width equal to the circumference of the urethra being constructed, was stitched into a tube (*Fig. 1*). At the next stage, the proximal section of the urethra was anastomosed on a catheter to the remnants of the urothelium, stitching it to the tube, which was positioned between the distal de-epithelialized section of the urethra “end to end,” and to the top of the glans penis. In conclusion, the wound defect was sutured with local tissues. An 8 Ch. urethral catheter was sutured to the skin of the glans penis using atraumatic thread PDS 5/0. A compression bandage with glycerol was applied as the final stage. The urethral catheter was removed on day 7.

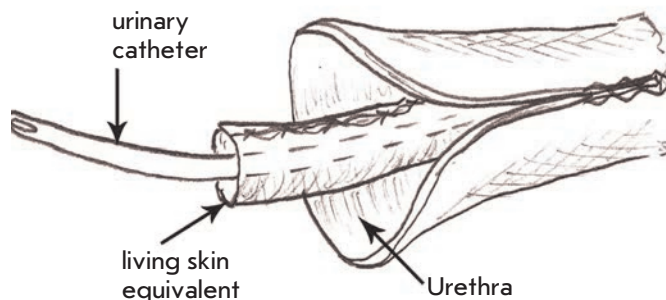


**Fig. 1.** The scheme for LSE transplantation into de-epithelialized urethra

### Reagents and solutions used in the study

M199<sup>x10</sup> medium, DMEM/F-12 medium, Hanks' solution, EDTA solution, PBS (PanEco LLC), fetal bovine serum (HyClon, USA); epidermal growth factor (Sigma), insulin (Sigma), isoproterenol (Sigma), hydrocortisone (Sigma), transferrin (PanEco LLC), HEPES (Sigma), antibiotics: gentamicin, penicillin, streptomycin (Ferein, Moscow), DiI Red membrane tracer (Sigma), lentiviral construct with *e-gfp* (Evrogen LLC, Moscow); trypsin solution (Biolot LLC, St. Petersburg), dispase (Sigma); plastic cell culture flasks (Costar, USA), Spongostan<sup>™</sup> gelatin medical sponge (Johnson & Johnson, USA). An inverted microscope Leica DM IL (Germany) and Kayensa conductive light microscope (Japan) were used for microscopy experiments.

Specific antibodies to keratins of epidermal basal layer cells K14 and differentiation markers of urothelium K7 and K18 (NovoCastra) and UP3 (UsBioLogical).

### RESULTS AND DISCUSSION

LSE were transplanted into de-epithelialized urethra of laboratory rabbits in order to study the plasticity of keratinocytes and analyze their behavior in the new microenvironment. One of the main prerequisites for potential incorporation of a graft into a damaged area is the absence of graft-versus-host reaction, which governed our choice of autologous skin cells for transplantation.

At the first stage a model of LSE transplantation into de-epithelialized rabbit urethra was developed (see the Materials and Methods section). The animals that had undergone surgery were capable of unassisted urination three weeks after the transplantation, whereby indicating the restoration of the urothelium function.

The epithelium of the restored urethra differed significantly from the normal urothelium; its morphology matched that of flat multilayered epithelium (Fig. 2). This can be attributed to the choice of rabbit ear skin epithelium as a source of keratinocytes for construction of the LSE; nonetheless, the neoepithelium successfully functioned as the urothelium (unassisted urination, lack of fistulas). Since the objective of the first experiment was to develop a technology of graft preparation and surgery techniques, the behavior of the graft was monitored for 21 days.

In subsequent experiments, we used LSEs with labeled keratinocytes, which could be identified in the urethra. A total of 17 adult rabbits (6–12 months old) were used. Two groups of animals were used as a control: one group consisted of three animals with de-epithelialized urethra with no transplantation of the LSE, and the other one, of three animals that received a cell-free Spongostan<sup>™</sup> gelatin sponge as a graft. The experimental group consisted of 11 animals grafted with LSE

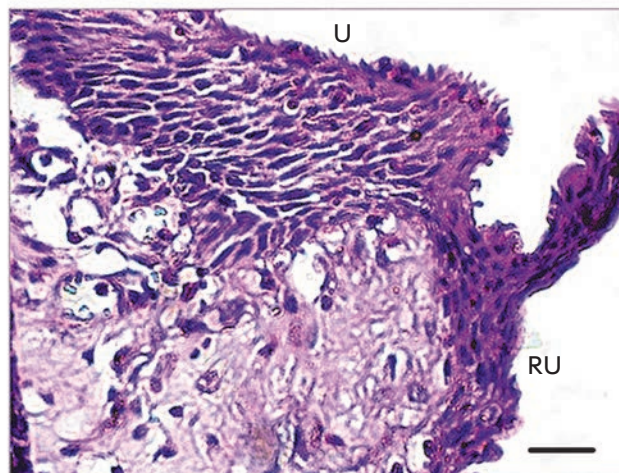


**Fig. 2.** A section of the reconstructed portion of rabbit urethra 21 days after the transplantation. The site of the anastomosis between the host urethra (U, indicated by an arrow, upper part) and the restored urethra (RU). Stained with hematoxylin and eosin; scale bar length 20 $\mu$ m

with the labeled cells. Within 2 weeks after surgery, all animals in the control groups developed complications, such as fistulas and a severe inflammatory response. After the catheter had been removed, four out of six control animals were incapable of unassisted urination. Therefore, the control group animals were sacrificed 2 weeks after the start of the experiment. All rabbits in the experimental group were capable of unassisted urination already on day 4–7 after the transplantation of the LSE. Neither urethral strictures nor narrowing of the tubes was observed.

The autologous cells were labeled with a DiI membrane tracer prior to transplantation. The resulting constructs were implanted into an experimental urethral injury site in seven rabbits. The outcome was evaluated 14, 30, 45 days, and 3 months after the implantation.

The animals' urothelium had not been fully restored by day 14 after the LSE implantation. Small areas of epithelialization and cell clustering were detected, which contained DiI-labeled cells and cells positive for K14, a marker of skin epidermis basal keratinocytes. No cells positive for the urothelial markers K18 and K7 were observed.

Thirty days after transplantation, the histological sections revealed the presence of reconstituted epithelium, represented by one to three layers of cells. Virtually all its cells contained the membrane tracer and were positive for the urothelium differentiation marker K7 and basal epidermal keratinocyte marker K14.

Keratin 18 was not expressed at this stage of urothelium restoration.

The complete recovery of urothelium in rabbits, evident from the presence of a multilayer transitional epithelium, was observed 45 days after the transplantation (*Fig. 3*). The samples contained some labeled cells. Since the membrane tracer used for labeling in this experiment was diluted with every cell division, it had certain inherent limitations in terms of its detection in cells over time. By this point, all cells of the restored urothelium expressed K18 and K7. The presence of K14 in cells was weakly manifested. Therefore, the restored urethral epithelium matched the normal urothelium in rabbits in terms of keratin expression 45 days after the transplantation. The results obtained allowed us to conclude that the autologous skin keratinocytes grown in the LSE remain alive in rabbit urethra 1.5 months after the transplantation. The LSE transplantation allows one to restore the urothelium structure and function. In contrast to Atala [14], who used bladder biopsy samples as a source of cells, we used autologous epidermal keratinocytes, because the collection of autologous urinary tract epithelial cells significantly expands the operative field (biopsy of the bladder). This technology allowed us to resolve the issue of shortage of plastic material. Furthermore, it helps avoid the use of urethroplasty of skin containing hair follicles, which is often used by surgeons today.

The autologous epidermal cells used for transplantation can be incorporated into an injured area. The replacement of the missing tissue may be due to the compartment of the stem and transient cells that constitute the equivalent. Lehrer *et al.* [15] found that epidermal regeneration mainly occurs due to the basal layer stem cell compartment and transient cells. The rate of basal cell maturation and differentiation can be reduced. Li *et al.* [16] have shown that after the transplantation of keratinocytes grown in culture formations, the reconstruction of epidermis involves not only stem cells, but also some transient cells, including those that have already been committed to differentiation. Our findings and analysis of the published data suggest that when introduced into an urothelium microenvironment, stem cells and transient cells of the epidermis that are present in the LSE both perform urothelium functions and exhibit plasticity, thus acquiring the properties of urothelial cells.

In order to monitor the expansion of cell clones in the animal and to observe phenotypic plasticity under the influence of the microenvironment, we obtained cultures of epidermal skin keratinocytes from four rabbits and transfected them with a *e-GFP* lentiviral construct. A week after the transfection, 90% of the cells contained GFP and were strongly fluorescent in

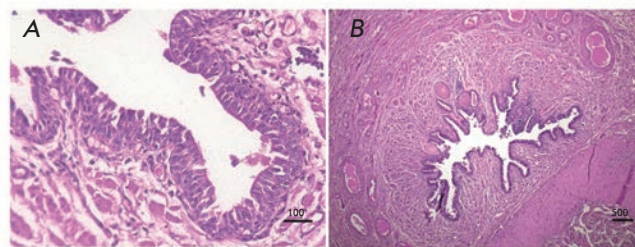


**Fig. 3.** A section of the restored rabbit urethra 45 days after the transplantation. Stained with hematoxylin and eosin

the green spectrum. The transfected keratinocytes were used to create LSE and were cultivated for one week.

The resulting graft with autologous cells was used to create the neourethra in rabbits as described above. Histological and immunohistochemical studies were performed 21, 45, and 90 days after transplantation. We used anti-EGFP antibodies to amplify the EGFP signal. In addition, the preparations were stained with antibodies against keratin 14 and 7, as well as the urothelial differentiation marker uroplakin III (UP3).

Twenty-one days after transplantation, a newly formed epithelium consisting of one to four cell layers was detected in the rabbit urethra. The epithelium was positive for EGFP in immunohistochemical experiments. This fact most likely indicated that we had detected the EGFP containing implanted skin keratinocytes in the urethral lumen. No UP3 was present in the restored urothelium at the time.

Forty-five days after the transplantation, the urethral epithelium consisted of transitional epithelium which was three to seven layers thick. The EGFP-labeled cells were found in all layers of the urethral epithelium (*Fig. 4*), some of which also expressed keratin 14 (*Fig. 4A, B*).

Other urothelial markers, K7 and UP3, have also been detected. High-magnification examination of the distribution of markers and EGFP expression in the neourethra strongly indicates colocalization of the green protein and the markers of differentiated urothelial cells (*Figs. 4C–F*).

The restored urothelium preparations made three months after the transplantation had a fully formed urothelium with a normal structure and large proportion of top layer cells expressing UP3 (*Fig. 5*). EGFP-containing cells were also detected (*Fig. 5, 6*). The localization of label-containing cells can be explained by the fact that the regeneration rate in animals, in particular in rabbits, is rather high, and, therefore, the marginal migration of urothelial cells from the up-

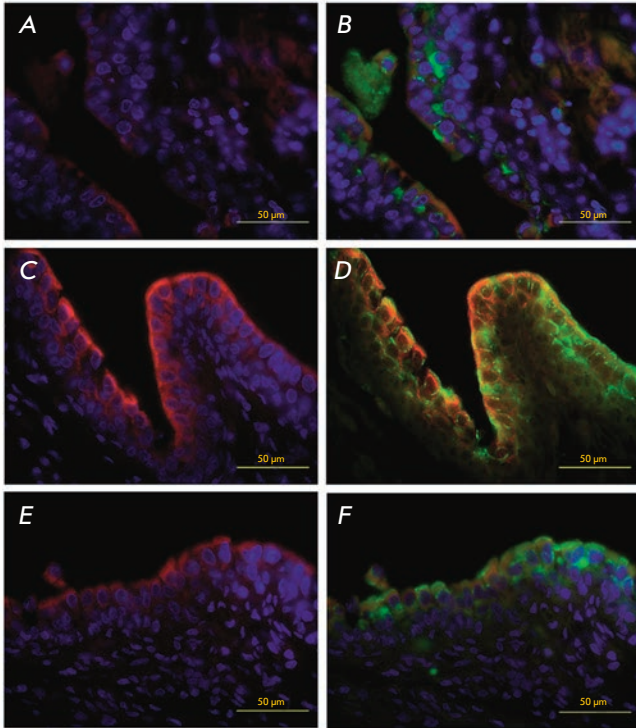


**Fig. 4.** A cross-section of the restored rabbit urethra 45 days after the transplantation. A portion of the restored urothelium (immunofluorescent detection of urothelial markers). Colocalization of the EGFP genetic tag (B, D and F, green) and urothelial markers K 14 (A and C, red), K7 (C and D, red), and UP3 (E and F, red). Nuclear staining with DAPI (blue)

per part of the urethra and proliferation of individual urothelial cells, which most likely remained in the site of the experimental injury, occurred in parallel with the widening of epithelialization islets of the transplanted keratinocytes. Identically to the previous experiments, all neurothelium layers expressed keratin 7 (Fig. 6).

The transplantation of autologous EGFP-containing rabbit skin keratinocytes into the urethral tube revealed that skin keratinocytes fully restore the urothelium within 3 months after their transplantation into the urethra. Urethral cells change their phenotype under the influence of the specific microenvironment, acquiring such features as expression of keratin 7 and UP3.

After being transplanted into an urothelial injury region, autologous skin keratinocytes incorporate into the urethra, restoring its integrity, and acquire the specific phenotypic traits of urothelial cells under the influence of the microenvironment.

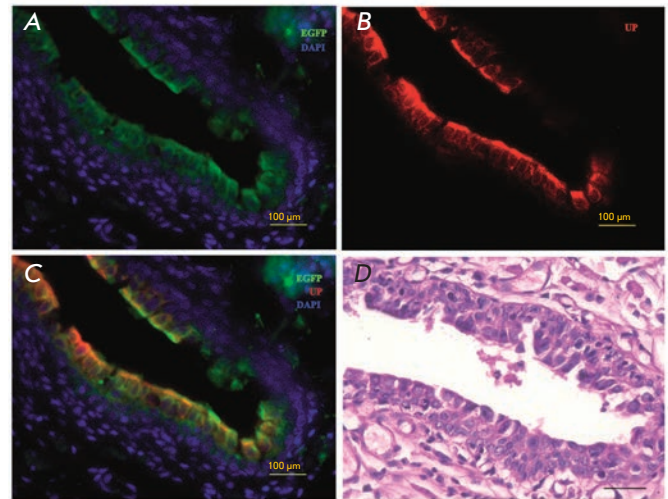


**Fig. 5.** A cross-section of the reconstructed rabbit urethra 3 months after the transplantation. The restored urothelium (immunofluorescent detection of urothelial markers). Colocalization of the EGFP genetic tag (A and C, green) and urothelial marker UP3 (B and C, red). Nuclear staining with DAPI (blue). Stained with hematoxylin and eosin

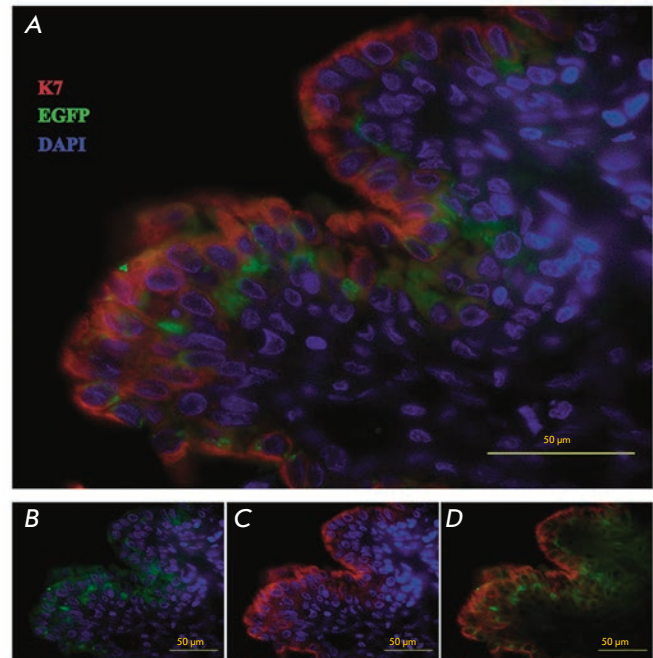


**Fig. 6.** A cross-section of the reconstructed rabbit urethra 3 months after the transplantation. The restored urothelium (immunofluorescent detection of urothelial markers). Colocalization of the EGFP genetic tag (A, C and E, green) and urothelial marker K7 (A, C and D, red). Nuclear staining with DAPI (blue)

The data suggest that adult skin keratinocytes grown *in vitro* and transplanted into the urethra can exhibit plasticity. This assumption is consistent with the data on the plasticity of adult stem/progenitor cells. In particular, it has been shown that epidermal keratinocytes exhibit plasticity under certain conditions. Under the influence of the seminal vesicles mesoderm of newborn rats, the differentiated cells of adult human urothelium start to express new non-specific markers of functional and morphological differentiation [17]. There is data showing that corneal cells can transdifferentiate into epidermal cells when exposed to fetal dermis signals [18]. Plasticity of epidermal keratinocytes has also been observed in experiments in cell transplantation into corneas. In [5], the authors investigated the phenotypic changes in genetically labeled cells and observed the transdifferentiation effect, which involved changes in the epidermal keratinocyte expression profile from K14 to K3/12 typical of the corneal epithelium.

The signals produced by the microenvironment determine the behavior and properties of stem cells. In particular, mesenchymal signals play a crucial role in maintaining their status. Ferraris *et al.* performed interspecies cross transplantations [19] and found that the signals from the embryonic mouse dermis can be recognized by adult rabbit corneal epithelium when it is transplanted under a renal capsule. Moreover, the corneal epithelium transdifferentiates into hair follicle-containing epidermis. The influence of urothelial-like cells on the phenotype of transplanted skin keratinocytes is also an important factor affecting the direction of their differentiation. In particular, this effect has been described *in vitro* for hair follicular keratinocyte cells grown in a medium conditioned by urothelial-like cells. As early as after 2 weeks of cultivation, skin cells cease to express K15 and begin expressing the urethral epithelium-specific keratins 7 and 18 [20].

These findings are both of theoretical and practical interest. The shortage of plastic material leads to

a number of issues in reconstructive surgery of the genitourinary system. Atala [14] described a method for *de novo* creation of the urethra using bladder cells grown on a collagen substrate. The success rate of these surgeries suggests that tissue-engineering approaches to urethral reconstruction are very promising. However, this method has certain disadvantages, such as shortage of original plastic material and the invasive procedure of biopsy material collection from the bladder cavity. Many years of experience in using the skin (e.g. scrotum skin) as a readily available plastic material to create an artificial urethra have demonstrated that skin cells can take root in an aggressive environment (adapting to the effect of the urine) and function as urothelium [21, 22]. However, the method can lead to complications such as hair growth in the urethral lumen during puberty. We propose a construction created from keratinocytes which have already passed the final step of cultivation and, therefore, no longer form hair follicles.

## CONCLUSIONS

We have developed an approach for urethral reconstruction using a collagen substrate and skin cells that have passed the final stage of cultivation. This urethra equivalent does not contain hair follicles and can be used in case of a shortage of plastic material. Autologous skin keratinocytes exhibit phenotypic and functional plasticity in a urothelial-specific microenvironment, acquiring the functions of urothelium.

Transplantation of the LSE with autologous skin keratinocytes into the site of a urethral tube epithelial injury in rabbits results in complete restoration of both the urothelium structure and the urethra function.

Transplantation of the LSE into the site of a urethral injury in rabbits leads to phenotypic changes in autologous epidermal keratinocytes, which acquire characteristics typical of urethral epithelium (K7 synthesis and UP3), whereby indicating the plasticity of adult epidermal stem cells. ●

## REFERENCES

- Phinney D.G., Prockop D.J. // *Stem Cells*. 2007. V. 25. № 11. P. 2896–2902.
- Bais M.V., Shabin Z.M., Young M., Einhorn T.A., Kotton D.N., Gerstnefeld L.C. // *Biochem. Biophys. Res. Commun.* 2012. V. 417. № 1. P. 211–216.
- Baker R.E., Murray P.J. // *Curr. Opin. Genet. Dev.* 2012. V. 22. № 6. P. 607–612.
- De Coppi P., Callegari A., Chiavegato A., Gasparotto L., Piccoli M., Taiani J., Pozzobon M., Boldrin L., Okabe M., Cozzi E., et al. // *J. Urol.* 2007. V. 177. № 1. P. 369–376.
- Meyer-Blazejewski E.A., Call M.K., Yamanaka O., Liu H., Schlötzer-Schrehardt U., Kruse F.E., Kao W.W. // *Stem Cells*. 2011. V. 29. № 1. P. 57–66.
- Mhashilkar A., Atala A. // *Curr. Stem Cell Res. Ther.* 2012. V. 7. № 1. P. 1.
- Fisher M.B., Mauck R.L. // *Tissue Eng. Part B Rev.* 2013. V. 19. № 1. P. 1–13.
- Grinnell F. // *Trends Cell Biol.* 2000. V. 10. № 9. P. 362–365.
- Palmiero C., Imparato G., Urciuolo F., Netti P. // *Acta Biomater.* 2010. V. 6. № 7. P. 2548–2553.
- Tuan R.S. // *Int. J. Oral Maxillofac. Implants.* 2011. V. 26. P. 50–62.
- Peterbauer-Scherb A.I., Danzer M., Gabriel C., van Griensven M., Redl H., Wolbank S. // *J. Tissue Eng. Regen. Med.* 2012. V. 6. № 6. P. 434–442.

## RESEARCH ARTICLES

12. Vasiliev A.V., Vorotelyak E.A., Kisilev I.V., Terskikh V.V. // *Vestn. Ros. acad. med. nauk* 2008. № 2. P. 45–53.
13. Kim J.H., Kong W.H., Kim J.G., Kim H.J., Seo S.W. // *Artif. Organs*. 2011. V. 35. № 2. P. 122–130.
14. Atala A. // *J. Endourol.* 2000. V. 14. № 1. P. 49–57.
15. Lehrer M.S., Sun T.-T., Lavker R.M. // *J. Cell Sci.* 1988 V. 111. P. 2867–2875.
16. Li A., Pouliot N., Redvers R., Kaur P. // *J. Clin. Invest.* 2004. V. 113. P. 390–400.
17. Aboseif S., El-Sakka A., Young P., Cunha G. // *Differentiation*. 1999. V. 65. P. 113–118.
18. Pearton D.J., Yang Y., Dhouailly D. // *Proc. Natl. Acad. Sci. USA*. 2005. V. 102. P. 3714–3719.
19. Ferraris C., Chevalier G., Favier B., Jahoda C.A., Dhouailly D. // *Development*. 2000. V. 127. № 24. P. 5487–5495.
20. Drewa T., Joachimiak R., Bajek A., Gagat M., Grzanka A., Bodnar M., Marszalek A., Dębski R., Chłosta P. // *Int. J. Urol.* 2013. V. 20. № 5. P. 537–542.
21. Fayzulin A.K., Kovarskiy S.L. // *Andrologia i genitalnaya khirurgia* 2002. № 2. P. 84–85.
22. Fayzulin A.K., Demin N.V. // *Andrologia i genitalnaya khirurgia* 2009. № 4. P. 31–35.

# Influence of Drug Resistance Mutations on the Activity of HIV-1 Subtypes A and B Integrases: a Comparative Study

O. A. Shadrina<sup>1</sup>, T. S. Zatsepin<sup>2,3</sup>, Yu. Yu. Agapkina<sup>3</sup>, M. G. Isaguliants<sup>4,5</sup>, M. B. Gottikh<sup>2,3\*</sup>

<sup>1</sup>Faculty of Bioengineering and Bioinformatics, Lomonosov Moscow State University, Leninskie gory, Moscow, 119991, Russia

<sup>2</sup>Belozersky Institute of Physical-Chemical Biology, Lomonosov Moscow State University, Leninskie gory, Moscow, Russia; 119991

<sup>3</sup>Chemistry Department, Lomonosov Moscow State University, Leninskie gory, Moscow, 119991, Russia

<sup>4</sup>Ivanovsky Institute of Virology, Gamaleya Str., Moscow, 123098, Russia

<sup>5</sup>Department of Microbiology, Tumor and Cell Biology, Karolinska Institutet, Stockholm, 17177, Sweden

\*E-mail: gottikh@belozersky.msu.ru

Received: 22.10.2014

Copyright © 2015 Park-media, Ltd. This is an open access article distributed under the Creative Commons Attribution License, which permits unrestricted use, distribution, and reproduction in any medium, provided the original work is properly cited.

**ABSTRACT** Integration of human immunodeficiency virus (HIV-1) DNA into the genome of an infected cell is one of the key steps in the viral replication cycle. The viral enzyme integrase (IN), which catalyzes the integration, is an attractive target for the development of new antiviral drugs. However, the HIV-1 therapy often results in the IN gene mutations inducing viral resistance to integration inhibitors. To assess the impact of drug resistance mutations on the activity of IN of HIV-1 subtype A strain FSU-A, which is dominant in Russia, variants of the consensus IN of this subtype containing the primary resistance mutations G118R and Q148K and secondary compensatory substitutions E138K and G140S were prepared and characterized. Comparative study of these enzymes with the corresponding mutants of IN of HIV-1 subtype B strains HXB-2 was performed. The mutation Q148K almost equally reduced the activity of integrases of both subtypes. Its negative effect was partially compensated by the secondary mutations E138K and G140S. Primary substitution G118R had different influence on the activity of proteins of the subtypes A and B, and the compensatory effect of the secondary substitution E138K also depended on the viral subtype. Comparison of the mutants resistance to the known strand transfer inhibitors raltegravir and elvitegravir, and a new inhibitor XZ-259 (a dihydro-1H-isoindol derivative), showed that integrases of both subtypes with the Q148K mutation were insensitive to raltegravir and elvitegravir but were effectively inhibited by XZ-259. The substitution G118R slightly reduced the efficiency of IN inhibition by raltegravir and elvitegravir and caused no resistance to XZ\_259.

**KEYWORDS** integrase, HIV-1 subtype A, strain FSU-A, strand transfer inhibitor, drug resistance mutations.

**ABBREVIATIONS** HIV-1 – human immunodeficiency virus type 1; IN – integrase; IN<sub>A</sub> – integrase of HIV-1 subtype A strain FSU-A; IN<sub>B</sub> – integrase of HIV-1 subtype B strain HXB-2; RAL – raltegravir; EVG – elvitegravir; DTG – dolutegravir; IC<sub>50</sub> – inhibitor concentration causing 50% decrease in enzymatic activity; FC – fold change in IC<sub>50</sub> of a mutant protein compared to that of wild-type integrase, wt – wild-type integrase; PAAG – polyacrylamide gel; DTT – dithiothreitol, EDTA – ethylenediaminetetraacetic acid, TBE – tris-borate-EDTA buffer.

## INTRODUCTION

Integrase (IN) is one of the key enzymes of human immunodeficiency virus type 1 (HIV-1) required for its replication. IN catalyzes the insertion of a DNA copy of the viral genomic RNA into the host DNA in two consecutive reactions. The first reaction is the 3'-processing, consisting in the GpT dinucleotide cleavage from both 3'-ends of the viral DNA. The second reaction is

the strand transfer, in which the viral DNA is inserted into the host cell's DNA.

Since IN homologues within human cells have not been described, IN is an attractive target for developing new antiviral drugs. Three strand transfer inhibitors are currently used as components of highly active antiretroviral therapy: raltegravir (RAL), elvitegravir (EVG), and dolutegravir (DTG). However, strand transfer inhibitors

cause drug resistance mutations in the IN gene both in patients and in a HIV-infected cell culture [1]. The virus rapidly develops resistance, including cross-resistance, to the first generation of strand transfer inhibitors – RAL and EVG. One of the common reasons for the high resistance to both inhibitors is a primary mutation at the Q148 residue [2–6]. In most cases, this mutation occurs in combination with secondary mutations, most frequently G140S/A and E138K/A [2–7]. The results of *in vitro* and *in vivo* studies have demonstrated that secondary mutations partially restore the viral replication ability reduced by primary substitutions and may also increase drug resistance [7–11].

DTG is a second-generation drug active against most RAL- and EVG-resistant virus strains [9, 12, 13]. However, investigation of the DTG effect on HIV-1 isolates from patients insensitive to RAL and EVG showed that Q148H/K/R substitutions in the integrase structure lead to some resistance to DTG. Secondary and tertiary mutations (G140A/C/S, L74I and E138A/K/T) further enhance the resistance [14, 15]. Variants containing a number of amino acid substitutions in IN (H51Y, L101I, G118R, T124A, S153F/Y, R263K) were found during selection of HIV-1 strains resistant to DTG in a lymphocytes culture [13, 16]. However, only two substitutions, G118R and R263K, proved to be responsible for the virus resistance to DTG [15, 17].

HIV-1 is represented by different subtypes and recombinant strains, and among them subtype B is prevalent in the United States, Australia, Japan, and Western Europe. Mutations Q148H/R/K lead to RAL- and EVG-resistance in different HIV-1 subtypes. Mutations associated with DTG-resistance are more specific. Thus, *in vitro* selection of DTG-resistant strains of HIV-1 subtypes B, C, and A/G demonstrated that only the R263K substitution was common to all subtypes; the G118R substitution was found only in the subtypes A/G and C [16]. In subtype C, this mutation was found also by *in vitro*-selection with the second-generation strand transfer inhibitor MK-2048 [18]. The same study demonstrated that the E138K mutation was a secondary compensatory substitution for G118R. The fact that the G118R mutation is associated with the lack of sensitivity to RAL in patients infected with the CRF02\_A/G strain has recently been demonstrated [19]. It is important to note that this virus isolate, containing the G118R substitution in the IN gene, was resistant not only to RAL, but also to EVG and DTG [15]. All these data suggest that the G118R substitution is most characteristic for non-B subtypes of HIV-1 and that the presence of this substitution can lead to patient insensitivity to all IN inhibitors approved for therapeutic use.

HIV subtype A (FSU-A) dominates within the territory of the former Soviet Union, and IN of this viral

subtype has not been fully characterized [20]. In particular, information on resistance mutations caused by IN inhibitors in HIV-1 strain FSU-A is limited. To assess the impact of drug resistance mutations on the enzymatic properties of IN of HIV-1 subtype A, we prepared a consensus IN of the FSU-A strain, where RAL- and EVG-resistance mutations were introduced by site-directed mutagenesis [21, 22]. The consensus IN sequence of HIV-1 strain FSU-A (IN<sub>A</sub>) differs from the sequence of the best studied IN of HIV-1 subtype B (HXB-2) by substitutions of 16 amino acid residues, nine of which are located in the catalytic domain. We characterized the catalytic activity of IN<sub>A</sub> and its variants containing two major combinations of RAL- and EVG-resistance mutations: E92Q, V151I, N155H, G163R, L74M (mutant 1), and Q148K, E138K, G140S (mutant 2) [22]. The consensus enzyme was significantly more active than IN of subtype B (IN<sub>B</sub>) in 3'-processing and strand transfer reactions. The introduction of these mutations significantly increased IN<sub>A</sub> resistance to RAL and EVG but dramatically reduced its catalytic activity in both reactions [22].

In this study we continued the investigation of the role of drug resistance mutations and meticulously compared the effect of the primary mutation Q148K and the secondary mutations E138K and G140S on the activity of IN<sub>A</sub> and IN<sub>B</sub>. We also described the activity of the IN<sub>A</sub> mutants containing the primary G118R substitution and compensatory E138K substitution for the first time. The Q148K mutation dramatically decreased the activity of enzymes of both viral subtypes in both reactions: 3'-processing and strand transfer. This decrease was partially restored by the secondary mutations E138K and G140S. The G118R substitution reduced the efficiency of 3'-processing for both integrases by 5 times, but it differently affected the enzymes of different strains in the strand transfer reaction: IN<sub>A</sub> activity decreased more significantly than IN<sub>B</sub> activity. Moreover, the secondary substitution E138K had a compensatory effect on IN<sub>B</sub> only. We also compared the resistance of all the mutants to RAL, EVG, and the new strand transfer inhibitor XZ-259 [23]. XZ-259 effectively inhibited the RAL- and EVG-resistant IN forms containing substitution Q148K. Substitution G118R slightly reduced the efficiency of IN inhibition by RAL and EVG, this effect was more pronounced in the case of IN<sub>B</sub>, and did not affect the sensitivity of INs to XZ-259.

## MATERIALS AND METHODS

### Enzymes

Plasmid vector pET-15b (Novagen, USA) was used for expression of recombinant INs (wt and mutants)

of both HIV-1 subtypes with N-terminal His6-tag. Protein samples were isolated from cells of the Rosetta (DE3) *Escherichia coli* producer strain and purified without adding a detergent as per [24]. Genetic constructs encoding IN mutant forms were obtained by site-directed mutagenesis of a plasmid encoding corresponding wild-type IN using a QuikChange II Site-Directed Mutagenesis kit (Agilent Technologies, USA). All procedures were performed in accordance with the manufacturer's instructions. Preparations were analyzed by electrophoresis in 12% SDS-PAGE according to Laemmli, followed by staining with SimplyBlue™ SafeStain (Invitrogen, USA) according to the manufacturer's instruction. The purity of the IN preparations was not lower than 90%.

### Oligodeoxyribonucleotides

All oligodeoxyribonucleotides were synthesized using the phosphoramidite method on an ABI 3400 DNA synthesizer (Applied Biosystems, USA) in accordance with the standard operating procedures using commercially available reagents (Glen Research, USA).

The radioactive <sup>32</sup>P-label was introduced at the 5'-end of the oligonucleotides. To achieve this, 10 pmol of the oligonucleotide was incubated with T4-poly-nucleotide kinase (Fermentas, Lithuania) and 50 μCi (16 pmol) [ $\gamma$ -<sup>32</sup>P]ATP (3000 Ci/mmol), in 10 μl of a buffer containing 50 mM Tris-HCl, pH 7.5, 10 mM MgCl<sub>2</sub>, 5 mM DTT, 0.1 mM spermidine, 0.1 mM EDTA, for 1 h at 37°C. Then, the kinase was inactivated by adding 2 μl of 250 mM aqueous EDTA and heating to 65°C for 10 min. An equimolar amount of the complementary oligonucleotide was added, and a duplex was formed by heating the oligonucleotide mixture to 95°C followed by slow cooling to room temperature. The duplex was purified from the excess [ $\gamma$ -<sup>32</sup>P]ATP and salts on a MicroSpin G-25 column (Amersham Biosciences, USA) according to the manufacturer's instructions.

### HIV-1 IN catalytic activity assays

Duplex U5B/U5A consisting of 21-mer oligonucleotides U5B (5'-GTGTGGAAAATCTCTAGCAGT-3') and U5A (5'-ACTGCTAGAGATTTTCACAC-3') and mimicking the end of the HIV-1 U5 LTR was used as a substrate for the 3'-processing. For this reaction, 3 nM duplex U5B/U5A (with <sup>32</sup>P-labeled U5B-chain) was incubated with 100 nM IN in 20 μl of a buffer (20 mM HEPES, pH 7.2, 7.5 mM MgCl<sub>2</sub>, 1 mM DTT) at 37°C. The incubation time varied from 1 to 2,000 min. The reaction was stopped by adding 80 μl of the buffer containing 7 mM EDTA, 0.4 M sodium acetate, 10 mM Tris-HCl, pH 8, and 0.1 g/l glycogen (stop solution). The IN protein was extracted with phenol: chloroform: iso-amyl alcohol = 25: 24: 1, the DNA duplex

was precipitated with ethanol (250 μl). The reaction products were separated by electrophoresis in a 20% polyacrylamide/7 M urea gel in the TBE buffer. Autoradiographic data analysis was performed using a GE Typhoon FLA 9500 scanner; densitometry was performed using the ImageQuant 5.0 software. The efficiency of 3'-processing was determined as the intensity ratio of the bands corresponding to the U5B substrate and the reaction product U5B-2 truncated by two residues using the ImageQuant™ 5.0 software. The statistical analysis was performed using the GnuPlot version 4.6.

For the homologous strand transfer reaction, the U5B-2/U5A duplex was used as both a DNA substrate and a target. The reaction was carried out in the buffer used for 3'-processing with the 10 nM U5B-2/U5A duplex (with <sup>32</sup>P-labeled U5B-2 chain) and 100 nM IN at 37°C; aliquots were taken after 2, 4, and 6 h.

For the heterologous strand transfer reaction, U5B-2/U5A and 36-bp duplex DNA (5'-ACAAAAT-TCCATGACAATTGTGGTGGGAATGCCACTA-3', 5'TAGTGGCATTCCACCACAATTGTCATGGAAT-TTTGT-3') were used as a DNA substrate and a target respectively. The U5B-2/U5A substrate (2 nM, <sup>32</sup>P-labeled U5B-2chain) was first incubated in the buffer for 3'-processing with 100 nM IN at 25°C for 30 min; the target DNA (8 nM) was then added, and the mixture was incubated for 2 h at 37°C. The reaction products were isolated and analyzed as described above.

### Inhibition of the strand transfer reaction

The resistance of INs to inhibitors, RAL, EVG (Santa Cruz Biotechnology Inc., USA) and XZ-259 (kindly provided by Dr. Xue Zhi Zhao from NIH, USA), was investigated in the homologous strand transfer reaction carried out as described above for 2 h in the presence of increasing inhibitor concentrations. Using the results of three independent determinations, IC<sub>50</sub> values were determined for each inhibitor. Data for the reaction efficiency were approximated by the exponential decay function; the concentration value corresponding to 50% of inhibition was calculated.

### RESULTS AND DISCUSSION

Fourteen mutant proteins (seven for each IN: Q148K, G140S, E138K, G118R, Q148K/E138K, Q148K/G140S, and G118R/E138K) were prepared by site-directed mutagenesis for the comparative analysis of the effect of drug resistance mutations on the catalytic activity of INs of FSU-A (IN<sub>A</sub>) and HXB-2 (IN<sub>B</sub>) strains. Enzymatic activities were determined in 3'-processing and strand transfer reactions using synthetic DNA duplexes corresponding to the end of the U5 region of the viral cDNA long terminal repeat.

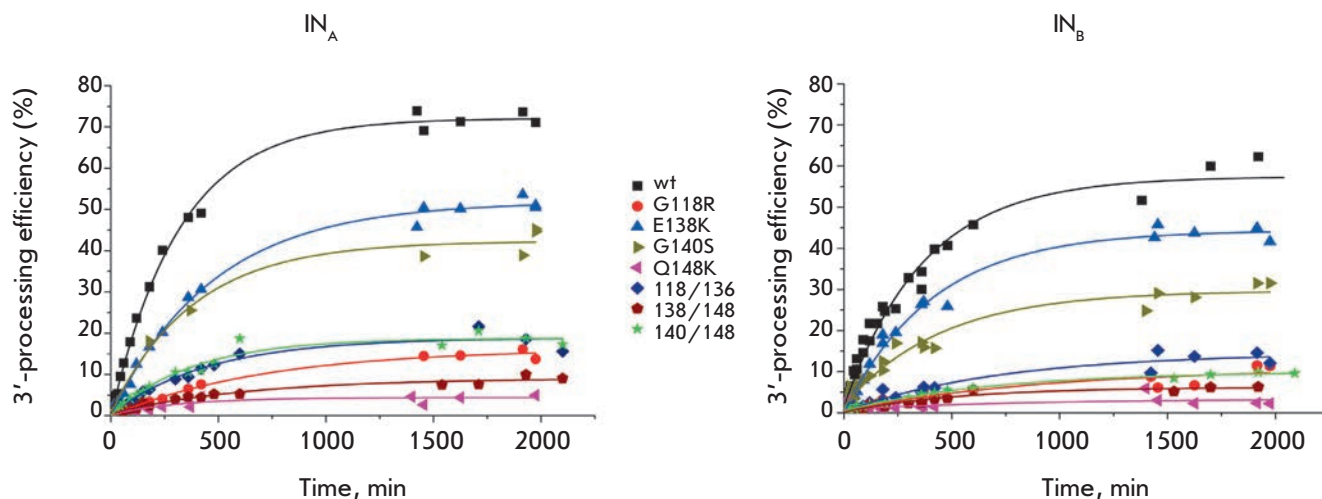


**Fig. 1.** The kinetics of 3'-processing product accumulation catalyzed by consensus IN of HIV-1 subtype A strain FSU-A ( $IN_A$ ) and IN of HIV-1 subtype B strain HXB-2 ( $IN_B$ ) and their mutants. The reaction was carried out at 37°C using 100 nM  $IN_A$  and 3 nM U5 substrate. The average values of at least three independent measurements with a standard error of less than 12% are shown

#### Mutations influence on the catalytic activity of $IN_A$ and $IN_B$ in the 3'-processing reaction

We used a 21-mer DNA duplex U5B/U5A mimicking the U5 region of HIV-1 DNA (U5-substrate) and the conditions (enzyme and DNA concentrations, buffer composition) described earlier for the analysis of catalytic activities of  $IN_A$  and  $IN_B$  [22] in the 3'-processing reaction.

We evaluated the dependence of the 3'-processing efficiency on time and plotted kinetic curves for product accumulation (Fig. 1). The initial rates of the 3'-processing reaction ( $V_0$ ) were calculated from the linear part of the curve (first 60 min) (Table 1).

As we demonstrated earlier [22],  $IN_A$  was more active than  $IN_B$  in the 3'-processing reaction. All  $IN_A$  mutants were also characterized by a higher efficiency of product accumulation than the corresponding  $IN_B$  mutants (Fig. 1). However, the initial reaction rates for mutant forms of both INs were not significantly different (Table 1).

All mutations introduced into INs of both subtypes reduced both the 3'-processing rate and the efficiency of product accumulation (Fig. 1, Table 1). The most significant decrease was detected for proteins with the Q148K substitution; this finding is in good agreement with the previous results for  $IN_B$  [25].

As we expected based on published data [7–11, 13], the negative effect of the primary mutation Q148K was partially recompensed by the G140S substitution (Fig. 1, Table 1). The compensatory effect of G140S was stronger for  $IN_A$ : the difference in the 3'-processing efficiency and initial rate for mutants  $IN_A^{G140S/Q148K}$  and

**Table 1.** Initial rates and efficiencies of 3'-processing catalyzed by  $IN_A$  and  $IN_B$  and their mutants

| Mutation    | $V_0$ , pM/min*  |                 | Relative reaction efficiency, %** |        |
|-------------|------------------|-----------------|-----------------------------------|--------|
|             | $IN_A$           | $IN_B$          | $IN_A$                            | $IN_B$ |
| Wild type   | $10.1 \pm 0.29$  | $6.4 \pm 0.19$  | 100                               | 100    |
| G118R       | $0.98 \pm 0.074$ | $0.79 \pm 0.15$ | 21                                | 20     |
| E138K       | $4.8 \pm 0.24$   | $4.6 \pm 0.9$   | 69                                | 76     |
| G118R/E138K | $2.6 \pm 0.37$   | $1.4 \pm 0.18$  | 24                                | 24     |
| G140S       | $4.3 \pm 0.21$   | $4.8 \pm 0.75$  | 58                                | 51     |
| Q148K       | $0.90 \pm 0.16$  | $0.65 \pm 0.35$ | 6                                 | 13     |
| E138K/Q148K | $1.2 \pm 0.31$   | $0.7 \pm 0.61$  | 13                                | 11     |
| G140S/Q148K | $2.62 \pm 0.11$  | $1.3 \pm 0.23$  | 25                                | 15     |

\*Mean values of at least three independent experiments with standard deviations are shown.

\*\*Relative reaction efficiency after 1,500 min of incubation is shown; efficiency of the reaction catalyzed by wt IN is 100%.

$IN_A^{Q148K}$  was more pronounced than that for the corresponding pair of subtype B (Fig. 1, Table 1). However, it should be noted that the compensatory effect of G140S on the Q148K mutation observed for  $IN_A^{Q148K}$  and  $IN_B^{Q148K}$  was not as significant as on the Q148H substitution in  $IN_B$  [8]. This may be explained by the stronger negative impact of the Q148K mutation on the IN activity. The difference in the activities of IN with the primary mutations Q148K and Q148N correlated with

the differences in the integration capacity of viruses carrying these mutations [7, 10, 11].

A compensatory effect of E138K on the catalytic activity of both INs with the primary Q148K substitution was also detected (*Fig. 1, Table 1*). However, both double mutants  $IN_A^{E138K/Q148K}$  and  $IN_B^{E138K/Q148K}$  were less active than the double mutants carrying the G140S/Q148K substitutions. This finding is consistent with a decrease in the replication and integration activity of HIV-1 subtype B mutants in the series: Q148K < Q148K/E138K < Q148K/G140S [7]. Interestingly, activity of  $IN_A$  with triple mutation E138K/G140S/Q148K was slightly higher than that of the enzymes with two substitutions: 1,500 min after initiation of the reaction, the 3'-processing efficiency for the triple mutant was about 30% of that for the wt  $IN_A$  [22], while for the most active double mutant  $IN_A^{G140S/Q148K}$  it was not higher than 20% (Table 1). Thus, the compensatory effect of the combination of two mutations, E138K and G140S, was slightly higher than that of the individual secondary substitution, G140S or E138K. A similar observation was made earlier for HIV-1 subtype B: the addition of the E138K mutation to the Q148K/G140S substitutions improved viral replication while not affecting viral sensitivity to strand transfer inhibitors [11].

Finally, we found that the G118R substitution strongly decreased the activities of both  $IN_A$  and  $IN_B$  (*Fig. 1, Table 1*). This result contradicts the data reported in [17], which demonstrated that the efficiency of 3'-processing catalyzed by recombinant  $IN_B$  with the G118R substitution was slightly reduced, whereas the double mutants G118R/E138K and G118R/H51Y were somewhat more active than the wt enzyme. Under our conditions, the introduction of the secondary E138K substitution also led to increased activities of both the  $IN_A^{G118R}$  and  $IN_B^{G118R}$  mutants; however, the activities of all enzymes with the G118R substitution were significantly lower than those of wt  $IN_A$  and  $IN_B$  (*Fig. 1, Table 1*). This contradiction can be explained by the different 3'-processing conditions; in particular, by the length of the DNA substrate: we used a standard 21-mer DNA duplex, while a 32-mer substrate was used in [17].

### Effect of mutations on the catalytic activities of $IN_A$ and $IN_B$ in the strand transfer reaction

We also investigated the mutations effect on the second reaction catalyzed by IN, which is the strand transfer. In *in vitro* reaction, the 3'-processed DNA substrate may be inserted by IN into itself (homologous strand transfer) or into any random DNA duplex or plasmid (heterologous strand transfer). The U5B-2/U5A duplex was used as a DNA substrate. A synthetic 36-mer

oligonucleotide duplex was used as a target for heterologous strand transfer. Since the sites of the substrate insertion do not depend on the DNA target sequence, reaction products with different lengths were detected (*Fig. 2*).

As we established earlier [22],  $IN_A$  activity was slightly higher than that of  $IN_B$  in the strand transfer reaction (*Fig. 2*). A difference in the profiles of the integration products for the homologous (*Fig. 2A*) and heterologous strand transfer (*Fig. 2B*) catalyzed by  $IN_A$  and  $IN_B$  can be observed.

INs of both subtypes carrying the Q148K substitution were the least active in the strand transfer reaction, identically to 3'-processing. For these mutants, the efficiency of homologous strand transfer was reduced to approximately 5% of that of the wt enzymes. Surprisingly, the G140S substitution significantly decreased the reaction efficiency, too (*Fig. 2A, C*). This effect was observed for the enzymes of both subtypes,  $IN_A^{G140S}$  and  $IN_B^{G140S}$ , though no data on a G140S negative effect on the activity of recombinant IN have been published, and only a slight decrease in the integration and replication capabilities was demonstrated for HIV-1 subtype B with this substitution [7, 8]. Despite the negative effect of the G140S substitution, its combination with the Q148K mutation increased the reaction efficiency and the double mutants  $IN_A^{G140S/Q148K}$  and  $IN_B^{G140S/Q148K}$  were more active than  $IN_A^{Q148K}$  and  $IN_B^{Q148K}$  (*Fig. 2C*). Some compensatory effect was also produced by the E138K mutation. Moreover, the compensatory effect of G140S was somewhat stronger for  $IN_A$ , while the compensatory effect of E138K was stronger for  $IN_B$  (*Fig. 2C*). It is interesting to note that a single E138K substitution significantly increased the reaction efficiency for INs of both subtypes (*Fig. 2C*). In general, the primary mutation Q148K and its compensatory substitutions G140S and E138K equally affected the activities of  $IN_A$  and  $IN_B$  during 3'-processing and strand transfer reactions. Thus, the differences in the primary structure of  $IN_A$  and  $IN_B$  did not affect the enzymatic properties of this group of mutants *in vitro*.

It is important that another group of mutations, G118R and G118R/E138K, exhibited a different effect on the activity of INs of different subtypes in strand transfer reactions.  $IN_A$  was more sensitive to the G118R substitution than  $IN_B$ : the reaction efficiency was strongly reduced for the  $IN_A^{G118R}$  enzyme, while it was not changed significantly for  $IN_B^{G118R}$  (*Fig. 2A, C*). It should also be noted that in the case of  $IN_A$ , the G118R mutation resulted in a changed integration profile, and only two predominant products were detected for  $IN_A^{G118R}$  instead of the large set of products found for wt  $IN_A$  (*Fig. 2A*). The addition of the compensatory mutation E138K had virtually no effect on the activity of the

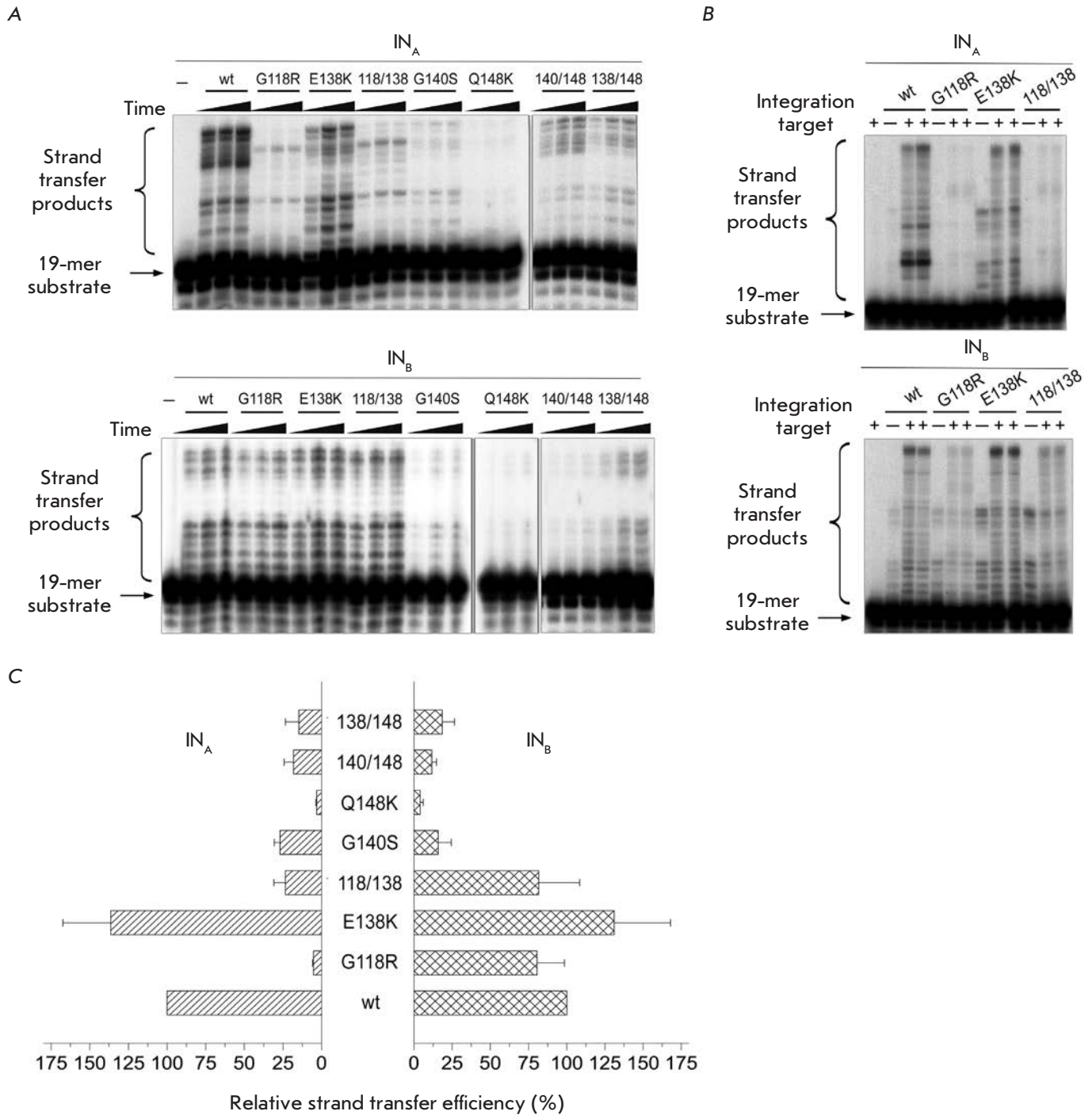


**Fig. 2.** The catalytic activity of the mutant INs of HIV-1 subtypes A and B in the strand transfer reaction. All products were resolved by electrophoresis in 20% PAAG under denaturing conditions. **A.** Reaction of homologous strand transfer was performed at 37°C for 2, 4, 6 h using 100 nM IN and 10 nM substrate U5B-2/U5A. **B.** Reaction of heterologous strand transfer was performed using 100 nM IN, 2 nM substrate U5B-2/U5A (pre-incubated for 30 min at 25°C) and 8 nM 36-mer DNA target for 2 h at 37°C. **C.** Relative efficiency of homologous strand transfer catalyzed by the mutant INs: the reaction efficiency for wt IN<sub>A</sub> and IN<sub>B</sub> is considered to be 100%. The average values of at least three independent measurements with the standard error are shown

$IN_B^{G118R}$  mutant, while the double mutant  $IN_A^{G118R/E138K}$  was more active than  $IN_A^{G118R}$  carrying a single substitution. However, the efficiency of the homologous strand transfer catalyzed by  $IN_A^{G118R/E138K}$  was only 23% of the reaction catalyzed by the wt  $IN_A$  (Fig. 2C).

It was shown previously that G118R substitution in  $IN_B$  significantly (over 90%) reduces its activity in the heterologous strand transfer reaction [17]. The double mutation G118R/E138K resulted in partial recovery of the activity, but it failed to achieve even 50% of the wt  $IN$  activity [17]. Similar effects were observed for HIV-1 subtype B containing these mutations: G118R substitution caused a significant decrease in the viral replication and integration, and the addition of the E138K mutation led to their partial recovery [18]. Our study of the G118R effect on the ability of  $IN_A$  and  $IN_B$  to catalyze the heterologous strand transfer showed that, identically to the homologous strand transfer, the effect of this substitution on the enzymes of different HIV-1 subtypes is different (Fig. 2B). The G118R mutation decreased  $IN_B$  activity by approximately 50%, while the corresponding  $IN_A^{G118R}$  mutant was virtually inactive. The secondary substitution E138K had a compensatory effect only on  $IN_B$ : the activity of the  $IN_B^{G118R/E138K}$  double mutant was somewhat higher than that of the  $IN_B^{G118R}$  mutant (Fig. 2B). These results are consistent with data [17], and the difference in the activities of  $IN_B$  mutant forms (in our work and [17]) can be explained by differences in the reaction conditions. As for subtype A  $IN$  mutants,  $IN_A^{G118R}$  and  $IN_A^{G118R/E138K}$ , they demonstrated equally low activities, although the substitution E138K alone resulted in increased efficiency of heterologous strand transfer catalyzed by  $IN$ s of both subtypes (Fig. 2B).

The reduced integration activity of the subtype B mutant  $IN_B^{G118R}$  had been explained by the reduced ability of the complex of this mutant with its DNA substrate to bind the DNA target [17]. As a result of natural polymorphism,  $IN_B$  contains Ser at position 119 and  $IN_A$  contains Pro [21]. It should be noted that Ser119 is likewise present in drug-resistant strains of HIV-1 subtype C, which most often contain the G118R mutation [16, 18]. The proline residue increases the rigidity of the  $IN$  spatial structure in the vicinity of the active site (Asp116 is a component of the catalytic triad). The Pro119 and G118R mutations obviously affect the ability of  $IN_A$  to interact with the DNA target to a higher extent than a combination of Ser119 and G118R. As a result,  $IN_A$  containing a G118R substitution is significantly less active in the strand transfer reaction than the corresponding  $IN_B$  mutant.

### The effects of mutations on the sensitivity of $IN_A$ and $IN_B$ to strand transfer inhibitors

We have studied the influence of the selected drug re-

sistance mutations on the  $IN$  sensitivity to three strand transfer inhibitors: RAL, EVG, and the new inhibitor XZ-259, a dihydro-1H-isoindole derivative, with biochemical and antiviral activities comparable to RAL [23]. We determined the concentration of the inhibitor required to reduce  $IN$  activity by 50% ( $IC_{50}$ ) in the homologous strand transfer reaction (Table 2; increased  $IC_{50}$  shows a decreased sensitivity of the enzyme to the inhibitor).

Our results demonstrate that  $IC_{50}$  values for RAL and EVG were comparable for  $IN$ s of both subtypes, but the average  $IN_A$  sensitivity to both inhibitors was somewhat higher; this finding correlates with the data obtained previously [22].  $IN_A$  sensitivity to the new inhibitor XZ-259 was also slightly higher than that of  $IN_B$ ; the  $IC_{50}$  value for  $IN_B$  (65 nM, Table 2) is in good agreement with [23] (77 nM).

It is convenient to use the FC values indicating by how much the  $IC_{50}$  value for a particular mutant has changed compared to the wild-type (i.e., a higher resistance of mutants to inhibitors in comparison with the wt enzyme) to analyze  $IN$  sensitivity to inhibitors. FC analysis of the protein family containing the primary substitution Q148K ( $IN^{Q148K}$ ,  $IN^{E138K/Q148K}$  and  $IN^{G140S/Q148K}$ ) showed that the resistance of the mutant  $IN$ s of both subtypes to EVG increased in a similar manner (Table 2). RAL inhibited  $IN_A$  carrying the Q148K and G140S/Q148K substitutions twice more effectively than the corresponding  $IN_B$  variants. A compensatory E138K mutation decreased the resistance of  $IN_B^{Q148K}$  to RAL and EVG almost twofold, without a significant effect on the resistance of the  $IN_A^{Q148K}$  mutant. It should also be noted that the sensitivity of both Q148K mutants to XZ-259 was significantly higher than the sensitivity to EVG and especially to RAL; these results were in agreement with the results obtained earlier for  $IN_B$  [23]. It is interesting to note that the secondary E138K substitution increased the sensitivity of the  $IN_A^{Q148K}$  and  $IN_B^{Q148K}$  mutants to XZ-259, while G140S reduced their sensitivity (Table 2).

The FC analysis of the protein family with G118R and G118R/E138K substitutions showed a slight decrease in the sensitivity of both subtypes  $IN$ s to RAL and EVG (Table 2). A single G118R mutation reduced the  $IN_B$  sensitivity more significantly (Table 2). Interestingly, the compensatory E138K substitution reduced the emerging resistance (Table 2). It is also important to note that resistance to XZ-259 did not occur. In general, our results correlate well with previously published data. Thus, the HIV-1 subtype CRF02\_A/G isolate carrying a G118R substitution in the  $IN$  gene was resistant (FC>100) to all  $IN$  inhibitors approved for therapeutic use: RAL, EVG, and DTG [15]. Meanwhile, the HIV-1 subtype B (clone pNL4-3) carrying this mu-

**Table 2.** Inhibition of the activity of IN<sub>B</sub>, IN<sub>A</sub> and their mutants in the reaction of homologous strand transfer by RAL, EVG, and XZ-259

| Mutation    | Inhibitory activity, IC <sub>50</sub> * (nM), and ratio of IC <sub>50</sub> for mutants over wt (FC) |     |                  |     |                  |      |                  |     |                  |     |                  |     |
|-------------|--|-----|------------------|-----|------------------|------|------------------|-----|------------------|-----|------------------|-----|
|             | IN <sub>A</sub>  |     |                  |     |                  |      | IN <sub>B</sub>  |     |                  |     |                  |     |
|             | RAL  |     | EVG              |     | XZ-259           |      | RAL              |     | EVG              |     | XZ-259           |     |
|             | IC <sub>50</sub>   | FC  | IC <sub>50</sub> | FC  | IC <sub>50</sub> | FC   | IC <sub>50</sub> | FC  | IC <sub>50</sub> | FC  | IC <sub>50</sub> | FC  |
| Wild type   | 5 ± 2  | 1   | 17 ± 5           | 1   | 40 ± 15          | 1    | 7 ± 3            | 1   | 25 ± 10          | 1   | 65 ± 10          | 1   |
| G118R       | 12 ± 5   | 2.4 | 45 ± 10          | 2.6 | 40 ± 10          | 1    | 30 ± 10          | 4.3 | 90 ± 30          | 3.6 | 80 ± 20          | 1.2 |
| E138K       | 7 ± 3  | 1.4 | 35 ± 5           | 2   | 50 ± 15          | 1.25 | 7 ± 5            | 1   | 20 ± 8           | 0.8 | 70 ± 10          | 1   |
| G118R/E138K | 7 ± 3  | 1.4 | 40 ± 10          | 2.4 | 30 ± 10          | 0.75 | 25 ± 8           | 3.6 | 50 ± 15          | 2   | 80 ± 15          | 1.2 |
| G140S       | 15 ± 5   | 3   | 300 ± 50         | 18  | 150 ± 50         | 3.8  | 35 ± 15          | 5   | 200 ± 80         | 8   | 150 ± 50         | 2.3 |
| Q148K       | 400 ± 100  | 80  | 700 ± 80         | 41  | 350 ± 100        | 8.8  | 1100 ± 250       | 157 | 1000 ± 200       | 40  | 600 ± 100        | 9.2 |
| E138K/Q148K | 350 ± 80   | 70  | 650 ± 100        | 38  | 200 ± 50         | 5    | 500 ± 150        | 71  | 600 ± 150        | 24  | 500 ± 200        | 7.7 |
| G140S/Q148K | 400 ± 150  | 80  | 450 ± 150        | 26  | 600 ± 150        | 15   | 1000 ± 200       | 200 | 850 ± 200        | 34  | 850 ± 100        | 13  |

\*Values are the average results of at least three independent determinations ± standard deviation.

tation showed negligible resistance to these inhibitors (FC = 3.1 for EVG, 8.2 for RAL and 10 for DTG) [15]. Thus, our study confirms the heterogenic effect of the primary G118R mutation on the drug resistance of different HIV-1 subtypes.

## CONCLUSIONS

We have carried out the first systematic study of the enzymatic properties of consensus IN of HIV-1 subtype A strain FSU-A, which is dominant in the territory of the former Soviet Union, containing mutations G118R and Q148K causing HIV-1 resistance to strand transfer inhibitors. We have demonstrated that the sensitivity of IN<sub>A</sub> to the inhibitors approved for therapeutic use, RAL and EVG, as well as to the novel inhibitor XZ-259, is somewhat higher than the sensitivity of IN<sub>B</sub>. The primary mutation Q148K associated with resistance to RAL and EVG caused a sharp decrease in IN<sub>A</sub> activity, which is partially restored by the secondary mutations E138K and G140S. A similar dependence was observed for IN<sub>B</sub>. At the same time, the primary mutation G118R reduced the integration activity of IN<sub>A</sub> much more significantly than the activity of IN<sub>B</sub>. This may be due to the IN natural polymorphism, and in

particular to the presence of Pro119 in IN<sub>A</sub> instead of Ser119 in IN<sub>B</sub>. We can assume that the Ser119Pro substitution, which leads to a more rigid conformation of the IN<sub>A</sub> active site, confers higher enzyme activity but reduces the ability to adapt its active site to the G118R mutation. Recombinant IN activity reduced by drug resistant mutations usually corresponds to a reduced replicative capacity of the mutant virus; therefore, we can expect the emergence and fixation of drug-resistant variants of HIV-1 FSU-A carrying the primary mutation Q148K and compensatory mutations E138K and/or G140S, while the emergence and fixation of drug-resistant variants of FSU-A with the G118R substitution are unlikely. ●

*We thank Xue Zhi Zhao (Chemical Biology Laboratory, Center for Cancer Research, Frederick National Laboratory, NIH, USA) for providing the XZ-259 inhibitor. This work was supported by the Russian Foundation for Basic Research (grants 13-04-91440-NIZ, 13-04-01523a, 14-04-00833\_a, 14-04-32086\_mol-a) and by the Development Program of Lomonosov Moscow State University (PNR 5.13).*

## REFERENCES

- Quashie P.K., Mesplède T., Wainberg M.A. // *Curr. Opin. Infect. Dis.* 2013. V. 26. № 1. P. 43-49.
- Malet I., Delelis O., Valantin M.A., Montes B., Soulie C., Wiriden M., Tchertanov L., Peytavin G., Reynes J., Mouscadet J-F., et al. // *Antimicrob. Agents. Chemother.* 2008. V. 52. № 4. P. 1351-1358.
- Charpentier C., Karmochkine M., Laureillard D., Tisserand P., Bélec L., Weiss L., Si-Mohamed A., Piketty C. // *HIV Med.* 2008. V. 9. № 9. P. 765-770.
- Cooper D.A., Steigbigel R.T., Gatell J.M., Rockstroh J.K., Katlama C., Yeni P., Lazzarin A., Clotet B., Kumar P.N., Eron J.E., BENCHMRK Study Teams, et al. // *N. Engl. J. Med.* 2008. V. 359. № 4. P. 355-365.
- Goethals O., Clayton R., Van Ginderen M., Vereycken I., Wagemans E., Geluykens P., Dockx K., Strijbos R., Smits V., Vos A., et al. // *J. Virol.* 2008. V. 82. № 21. P. 10366-10374.
- Stanford HIV Drug Resistance Database // <http://hivdb.stanford.edu/DR/INIResiNote.html>

## RESEARCH ARTICLES

7. Nakahara K., Wakasa-Morimoto C., Kobayashi M., Miki S., Noshi T., Seki T., Kanamori-Koyama M., Kawauchi S., Suyama A., Fujishita T., et al. // *Antiviral Res.* 2009. V. 81. № 2. P. 141-146.
8. Delelis O., Malet I., Na L., Tchertanov L., Calvez V., Marcelin A.G., Subra F., Deprez E., Mouscadet J-F. // *Nucleic Acids Res.* 2009. V. 37. № 4. P. 1193-1201.
9. Abram M.E., Hluhanich R.M., Goodman D.D., Andreatta K.N., Margot N.A., Ye L., Niedziela-Majka A., Barnes T.L., Novikov N., Chen X., et al. // *Antimicrob. Agents. Chemother.* 2013. V. 57. № 6. P. 2654-2663.
10. Franssen S., Gupta S., Danovich R., Hazuda D., Miller M., Witmer M., Petropoulos C.J., Huang W. // *J. Virol.* 2009. V. 83. № 22. P. 11440-11446.
11. Goethals O., Vos A., Van Ginderen M., Geluykens P., Smits V., Schols D., Hertogs K., Clayton R. // *Virology.* 2010. V. 402. № 2. P. 338-346.
12. Canducci F., Ceresola E.R., Boeri E., Spagnuolo V., Cossarini F., Castagna A., Lazzarin A., Clementi M. // *J. Infect. Dis.* 2011. V. 204. № 11. P. 1811-1815.
13. Underwood M.R., Johns B.A., Sato A., Martin J.N., Deeks S.G., Fujiwara T. // *J. Acquir. Immune. Defic. Syndr.* 2012. V. 61. № 3. P. 297-301.
14. Kobayashi M., Yoshinaga T., Seki T., Wakasa-Morimoto C., Brown K.W., Ferris R., Foster S.A., Hazen R.J., Miki S., Suyama-Kagitani A., et al. // *Antimicrob. Agents. Chemother.* 2011 V. 55. № 2. P. 813-821.
15. Malet I., Gimferrer Arriaga L., Artese A., Costa G., Parrotta L., Alcaro S., Delelis O., Tmeizeh A., Katlama C., Valantin M.A. // *J. Antimicrob. Chemother.* 2014. V. 69. № 8. P. 2118-2122.
16. Quashie P.K., Mesplède T., Han Y.S., Oliveira M., Singhroy D.N., Fujiwara T., Underwood M.R., Wainberg M.A. // *J. Virol.* 2012. V. 86. № 5. P. 2696-2705.
17. Quashie P.K., Mesplède T., Han Y.S., Veres T., Osman N., Hassounah S., Sloan R.D., Xu H.T., Wainberg M.A. // *Antimicrob. Agents. Chemother.* 2013. V. 57. № 12. P. 6223-6235.
18. Bar-Magen T., Sloan R.D., Donahue D.A., Kuhl B.D., Zabeida A., Xu H., Oliveira M., Hazuda D.J., Wainberg M.A. // *J. Virol.* 2010. V. 84. № 18. P. 9210-9216.
19. Malet I., Fourati S., Charpentier C., Morand-Joubert L., Armenia D., Wirdein M., Sayon S., Van Houtte M., Ceccherini-Silberstein F., Brun-Vézinet F., Perno et al. // *J. Antimicrob. Chemother.* 2011. V. 66. № 12. P. 2827-2830.
20. Lapovok I.A., Laga V.Yu., Vasil'ev A.V., Salamov G.G., Kazennova Ye.V., Matkovsky I.A., Mokhniy G.A., Melnik T.A., Bobkova M.P. // *HIV-infection and immunosuppression.* 2012. V. 4. № 2. P. 73-81. (Russian)
21. Krotova O., Starodubova E., Petkov S., Kostic L., Agapkina J., Hallengård D., Viklund A., Latyshev O., Gelius E., Dillenbeck T., et al. // *PLoS One.* 2013. V. 8. № 5. P. e62720.
22. Shadrina O., Krotova O., Agapkina J., Knyazhanskaya E., Korolev S., Starodubova E., Viklund A., Lukashov V., Magnani M., Medstrand P., et al. // *Biochimie.* 2014. V. 102. P. 92-101.
23. Métifiot M., Maddali K., Johnson B.C., Hare S., Smith S.J., Zhao X.Z., Marchand C., Burke T.R. Jr, Hughes S.H., Cherepanov P., et al. // *ACS Chem. Biol.* 2013. V. 8. № 1. P. 209-217.
24. Leh H., Brodin P., Bischerour J., Deprez E., Tauc P., Brochon J.C., LeCam E., Coulaud D., Auclair C., Mouscadet J.F. // *Biochemistry.* 2000. V. 39 P. 9285-9294.
25. Marinello J., Marchand C., Mott B.T., Bain A., Thomas C.J., Pommier Y. // *Biochemistry.* 2009. V. 47. № 36. P. 9345-9354.

# The Role of HCV E2 Protein Glycosylation in Functioning of Virus Envelope Proteins in Insect and Mammalian Cells

O. V. Orlova<sup>1</sup>, V. L. Druitsa<sup>2</sup>, P. V. Spirin<sup>1</sup>, V. S. Prasolov<sup>1</sup>, P. M. Rubtsov<sup>1</sup>, S. N. Kochetkov<sup>1</sup>, S. N. Beljelarskaya<sup>1\*</sup>

<sup>1</sup>Engelhardt Institute of Molecular Biology, Russian Academy of Sciences, Vavilova Str., 32, 119991, Moscow, Russia

<sup>2</sup>Chemical Department of Moscow State University, Leninskie Gory, 1, Bld. 3, 119899, Moscow, Russia

E-mail: belj@eimb.ru

Copyright © 2015 Park-media, Ltd. This is an open access article distributed under the Creative Commons Attribution License, which permits unrestricted use, distribution, and reproduction in any medium, provided the original work is properly cited.

**ABSTRACT** The hepatitis C virus (HCV) envelope proteins E1 and E2, being virion components, are involved in the formation of infectious particles in infected cells. The detailed structure of the infectious particle of HCV remains poorly understood. Moreover, the virion assembly and release of virions by the cell are the least understood processes. It is believed that virion properties depend on glycosylation of the virus envelope proteins in a cell, while glycans at several glycosylation sites of these proteins play a pivotal role in protein functioning and the HCV life cycle. N-glycans of glycoproteins can influence viral particle formation, virus binding to cell surface, and HCV pathogenesis. We studied the effect of glycans on the folding of the E2 glycoprotein, formation of functional glycoprotein complexes and virus particles in insect and mammalian cells. In order to investigate these processes, point mutations of the N-glycosylation sites of HCV protein E2 (genotype 1b strain 274933RU) were generated and the mutant proteins were further analyzed in the baculovirus expression system. Elimination of the single glycosylation sites of the E2 glycoprotein, except for the N6 site, did not affect its synthesis efficiency in Sf9 insect cells, while the electrophoretic mobility of mutant proteins increased in proportion to the decrease in the number of glycosylation sites. The level of synthesis of HCV glycoprotein E2 in human HEK293T cells depended on the presence of glycans at the N1 and N8 glycosylation sites in contrast to Sf9 cells. At the same time, elimination of glycans at the N1, N2, and N10 sites led to the accumulation of unproductive E1E2 dimers as aggregates and productive assembly suppression of virus-like particles both in insect and mammalian cells. In addition, elimination of single glycosylation sites of HCV E2 had no impact on the RNA synthesis of structural proteins and formation of virus-like particles in insect and mammalian cells.

**KEYWORDS** baculovirus expression vector system, hepatitis C virus envelope proteins E1 and E2, virus-like particles, N-linked protein glycosylation, Sf9 insect cells, mammalian HEK293T and Huh7.0 cells, oligonucleotide-directed mutagenesis.

**ABBREVIATIONS** CFU – colony forming units; HCV – hepatitis C virus; VLPs – virus-like particles; ER – endoplasmic reticulum.

## INTRODUCTION

Hepatitis C virus is one of the most nefarious pathogens causing severe liver diseases, including cirrhosis and hepatocellular carcinoma. The range of drugs for the HCV infection is rather limited, while immunoprophylaxis of the HCV infection is not yet available. The high replication activity of HCV with the lack of proofreading ability of the viral RNA-dependent RNA polymerase results in a high genetic variability of the virus. As a consequence, HCV circulates in the serum of an infected person as a population of quasi species differing in their genomes by 1–5%. Distinct strains of the same HCV subtype can differ in their nucleotide sequence by

5–15%; subtypes, by 10–30%; and different genotypes, by 30–50% [1]. Some strains have higher virulence; yet, definite molecular determinants for such phenotype still remain unknown. Hepatocytes are the main cellular target of HCV. Binding of a virus particle to the cell surface remains poorly studied. Furthermore, not all receptors, including HCV-specific ones, are known.

Virus envelope glycoproteins affect the binding of a viral particle to hepatocyte receptors and its absorption by a cell. The mechanism of assembly of viral structural proteins and RNA into new viral particles, along with the routes of virus transmission into a cell, remains poorly studied [2]. HCV is the only member of the ge-

nus *Hepacivirus* and belongs to the *Flaviviridae* family. Its genome encodes a single polyprotein precursor. Structural and nonstructural viral proteins are formed under the effect of cellular and viral proteases [3–5]. The capsid protein C and envelope proteins E1 and E2 are structural proteins. Envelope proteins undergo post-translational modification such as N-glycosylation, wherein the unbranched oligosaccharide chain consisting of nine mannose residues (Man) and three glucose residues (Glc) are bound to a specific asparagine residue as a part of the Asn-X-Ser or Asn-X-Thr sequence (where X is any amino acid except proline) [6, 7]. The glycoproteins of the viral envelope are heavily glycosylated. The degree of conservation of the glycosylation sites 9–11 in E2 and 4–5 in E1 is high, which is an indication that they play an important role in the functioning of these proteins in the life cycle of HCV [8]. It should be noted that it still remains unknown what the actual number of glycosylation sites of proteins is; exactly which sites participate in protein modification; and whether all potential sites undergo glycosylation *in vivo*.

The nature of glycoprotein glycosylation plays an important role in its functioning. Thus, glycoprotein E2 can be the receptor binding subunit of the HCV envelope. It has been shown that, depending on the HCV strain, a number of E2 glycans can determine the possibility of penetration of the virus into a cell, allowing the E2 glycoprotein to interact with cellular receptors. Certain E2 glycans are involved in the modulation of the immune response. It is thought that the glycans associated with the viral envelope influence protein folding, with the involvement of the chaperones of the endoplasmic reticulum (ER) and the productive assembly of the viral particles that are able to penetrate and infect another cell. Oligosaccharide attachment to a protein is related to its folding, while the glycoprotein penetrates the calnexin/calreticulin cycle interacting specifically with the endoplasmic reticulum chaperones that ensure its partial folding. Binding of glycoproteins to chaperones and their dissociation are followed by the detachment (trimming) of abundant glucose and mannose residues and reglycosylation of N-linked glycans.

Envelope protein E2 accumulates in the ER lumen both as a properly folded glycoprotein and aggregates of misfolded proteins. A portion of E2 remains unglycosylated in the cytosol and is degraded via the ubiquitin–proteasome pathway after ubiquitination. The calnexin protein interacts with noncovalently bound E1E2 complexes, while calreticulin interacts with aggregates of the misfolded proteins [9]. The first type of proteins provides binding of the virus to cellular receptors and penetration of the viral particle into a cell; it

also influences the formation of its antigenic composition and probably plays an essential role in viral pathogenesis [10]. The formation of misfolded glycoproteins aggregates can lead to the emergence of defective viral particles incapable of binding to new cells [11–13]. The HCV envelope proteins can also influence each other's folding. Thus, E2 acts as a chaperone during E1 folding and the formation of functional heterodimers, although the E1 protein also assists the productive folding of E2 [14, 15]. Assembly of HCV virions remains insufficiently studied due to the absence of appropriate cell models that would allow one to obtain infectious virus particles. The role of glycans in the functioning of virus envelope proteins of different genotypes in an infected cell also remains poorly investigated.

In this study, we investigated the influence of N-glycans of the E2 protein of HCV (genotype 1b strain 274933RU [16]) on the synthesis of structural proteins and formation of virus particles in Sf9 insect cells and HEK293T human cells transfected with baculovirus vectors directing the gene expression of HCV structural proteins [17].

## MATERIALS AND METHODS

### Bacterial strains, cells, and plasmids

*Escherichia coli*, *Spodoptera frugiperda* Sf9 cells, and mammalian HEK293T and Huh7.0 cells were used. *Escherichia coli* cells of the DH5a and DH10Bac strains were transformed with the plasmid DNA according to the manufacturer's recommendation (Amersham, USA). Isolation and purification of plasmids, restriction enzyme digestion, ligation, agarose gel electrophoresis of DNA, and other genetic engineering experiments were carried out using the standard protocols [18].

Sf9 insect cells were cultured at 27°C in a Sf-900 II medium supplemented with 10% fetal bovine serum following the basic procedures that were previously discussed and described in the protocol [19]. To assess virus titer, amplification of recombinant virus, infection of Sf9 cells with recombinant baculovirus, and viral gene expression using the same protocol were used.

Human embryonic kidney cells (HEK293T cell line) were cultured at 37°C and 5% CO<sub>2</sub> in DMEM media supplemented with 10% fetal bovine serum, 4 mM L-glutamine, 1 mM sodium pyruvate, and streptomycin/penicillin at concentrations of 100 mg/ml and 100 IU/ml, respectively.

Recombinant constructs for the corresponding cDNA fragments of the genes of HCV structural proteins, recombinant bacmids, as well as recombinant baculovirus bv-CE1E2, were obtained and analyzed according to the previously discussed procedures [20].

### Site-directed mutagenesis

The DNA fragment corresponding to cDNA of the gene encoding HCV glycoprotein E2 was cloned into plasmid pFastBacHTb at NcoI–EcoRI restriction sites according to the standard protocol [20]. Oligonucleotide primers were constructed to obtain a series of recombinant plasmids bearing cDNA of the E2 protein with mutations of glycosylation sites (*table*). Each primer consisted of 25–30 nucleotides and contained the sequence encoding the *N*-glycosylation site: Asn-X-Thr/Ser (X<sup>1</sup>Pro), in which the triplet encoding Asn was substituted with the triplet encoding Gln.

The method described by Drutsaet *al.* was used for mutagenesis [21]. PCR was performed on a CycloTemp 107 programmable thermocycler (ResursPribor, Russia). Predetermined base substitutions were verified by sequencing.

### Analysis of total cellular DNA

The total cellular DNA was isolated from insect cells 72 h after infection with recombinant baculoviruses bv-CE1E2, bv-E2mut, bv-E1E2mut, bv-CE1E2mut (multiplicity of infection being 5 CFU per cell) [20]. The presence of cDNA genes of HCV structural proteins in the total cellular DNA was assessed by PCR using the baculovirus primers of vector pFastBacHT (the forward 5'-GTGGTTGGCTACGTATACTCC-3' and reverse 5'-CCTCTACAAATGTGGTATGGC-3').

### Analysis of HCV RNA using RT-PCR

Sf9 cells were infected with recombinant baculoviruses bv-CE1E2mut (5 CFU per cell) and incubated at 27°C for 72 h. After 72 h, the medium was eliminated and cell debris was removed by low-speed centrifugation. The supernatant was centrifuged over a cushion of 30% sucrose at 23,000 *g* for 16 h at 4°C (Becman Coulter Optima L-100XP centrifuge, 80Ti rotor). RNA extraction

with TRIzol (Invitrogen) was performed according to the manufacturer's recommendations, and RNA was then treated with DNase I (Promega). Reverse transcription was carried out using a Phusion RT-PCR Kit (Thermo Scientific). The obtained cDNA was amplified using PCR with primers of the genes of structural and non-structural HCV proteins. The total cellular RNA was obtained from Sf9 cells infected with recombinant baculoviruses bv-CE1E2mut (5 CFU per cell) that was incubated at 27°C for 72 h and then washed three times with phosphate buffered saline (PBS). RNA isolation, reverse transcription, and amplification were performed using the previously mentioned protocols.

HEK283T cells were transfected with recombinant plasmids BacMamCE1E2mut-GFP (5 CFU per cell) and incubated at 37°C for 48 h. The medium was removed, RNA was isolated, and reverse transcription and amplification were performed using the previously mentioned protocols.

### Anti-HCV Antibodies

Mouse monoclonal antibodies to the HCV E1 (Hep C E1 1879: sc-65459) and HCV E2 (Hep C E2 BDI167: sc-57769) (SantaCruz Biotechnology, USA) proteins, as well as monoclonal antibodies to calnexin (AF18) and calreticulin (FMC75) (Abcam, UK), were used. Polyclonal rabbit antibodies to the structural protein C were kindly provided by M.G. Isagulyants (Ivanovsky Institute of Virology, Russian Academy of Sciences, Moscow). Anti-mouse IgG antibodies (AB6706-1EA) conjugated to horseradish peroxidase (Sigma, USA) were used as secondary antibodies.

### Western blotting and immunoprecipitation

After 72 h of infection with the recombinant baculoviruses bv-E2mut, bv-E1E2mut, bv-CE1E2mut (multiplicity of infection of 5 CFU per cell), Sf9 cells

### Primers used

| Primer    | Orientation | Nucleotide sequence 5' → 3'                               |
|-----------|-------------|---|
| 28-E2N1m  | –           | TG AAT ACC CAA GGC AGC TGG CAC AT                         |
| 30-E2N2m  | –           | TGG CAC ATC CAA AGT ACT GCC CTA AAT TGC                   |
| 30-E2N3m  | –           | GCCCTAAATTGCCAAGACTCCCTCCAAACT                            |
| 30-E2N4m  | –           | GCA CAC AAG TTC CAA TCG TCC GGG TGC CCG                   |
| 25-E2N6m  | –           | TGG GGG GAG CAA GAG ACA GAC GTG A                         |
| 30-E2N7m  | –           | GTG ATG CTC CTC CAA AAC ACG CGT CCG CCA                   |
| 30-E2N8m  | –           | TGT ACA TGG ATG CAA AGT ACT GGG TTC ACT                   |
| 27-E2N9m  | –           | GGGGTCCGGTCAACGCACCTTGATTTGC                              |
| 30-E2N10m | –           | TAC CCC TGC ACT CTC CAA TTT TTC CAT CAT                   |
| 27-E2N11m | –           | GCCGCATGCCAATGGACTCGAGGAGAGCGC                            |
| E2 for    | +           | AGGTCTAGAATGTTATGATTGTTTTGCTAC                            |
| E2 Back   | +           | CT ATA GTG TCA CCT AAA TCC GAA AGC TTC GGC CTC AGC TTG AG |

were harvested, washed three times with PBS (1.47 mM  $\text{KH}_2\text{PO}_4$ , 4.29 mM  $\text{Na}_2\text{HPO}_4 \cdot 7\text{H}_2\text{O}$ , 137 mM NaCl, 2.68 mM KCl), resuspended in a TNC lysis buffer containing 0.25% digitonin, and disrupted using ultrasonic vibrations. Cell debris was removed by centrifugation (15,000 *g*, 15 min, 4°C). Cell lysate was loaded into a 12% denaturing gel (each sample contained 10 µg of the protein). After electrophoresis, the proteins were transferred onto a Hybond-ECL nitrocellulose membrane (Amersham Biosciences, USA) using semi-dry electrophoretic transfer. The membranes were washed with PBS containing 5% nonfat dry milk, incubated with primary antibodies to the structural HCV proteins E1 or E2 (dilution 1 : 1500 for E1 and 1 : 2000 for E2), to calnexin or calreticulin (dilutions 1 : 1000 and 1 : 2000, respectively), and then to secondary antibodies (dilution 1 : 20,000). Protein complexes on immunoblots were detected using ECL and ECL Plus chemiluminescent reagents (Western blotting detection reagents and analysis systems, Amersham Biosciences) according to the manufacturer's recommendations.

For immunoprecipitation, the cells infected with recombinant baculoviruses bv-E2mut, bv-E1E2mut, and bv-CE1E2mut were harvested after 72 h of infection; the cells were lysed, and subsequently cell debris and nuclei were removed. The structural proteins and their complexes were precipitated by monoclonal antibodies to HCV E1 and HCV E2, calnexin and calreticulin in dilution 1 : 1000 (according to the manufacturer's recommendations). The precipitated proteins were separated using PAGE (12% denaturing gel), transferred onto a nitrocellulose membrane, and incubated with primary antibodies in the previously mentioned dilutions; the membranes were treated with secondary antibodies.

#### **Analysis of glycosylation by treatment with endoglycosidase H (Endo H)**

The proteins of the cell lysate were incubated with the corresponding monoclonal antibodies at 4°C. The obtained complex was precipitated by protein G sepharose (BioVision, USA). 1 µl of a 10× denaturing buffer (5% SDS, 0.4 M DTT) was added to the precipitated protein, the mixture volume was then diluted with water to 10 µl, and the mixture was boiled for 10 min. Next, the mixture volume was diluted to 20 µl by adding 2 µl of a 10× G5 reaction buffer (50 mM sodium citrate), 3 µl of water, and 5 µl of a Endo H solution (5 units) (P0702S BioLabs Inc., UK). The mixture was incubated for 15 min at 37°C and analyzed by PAGE (12% denaturing gel).

#### **Preparation and purification of virus-like particles (VLPs)**

A cell monolayer cultured at 27°C was infected with recombinant baculovirus bv-CE1E2 (10 CFU per cell).

After 72 h, the cells ( $2 \times 10^8$ ) were harvested, washed three times with PBS, re-suspended in a TNC lysis buffer (10 mM Tris-HCl, pH 7.5, 150 mM NaCl, 1 mM  $\text{CaCl}_2$ , 1 mM PMSF, protease inhibitors cocktail II (Calbiochem, USA) (1 : 200) containing 0.25% digitonin, and disrupted using ultrasonic vibrations. Cell debris was removed from the VLPs extracted from homogenized lysates by low-speed centrifugation (1,200 *g*, 15 min, 4°C). After purification, VLPs were concentrated by centrifugation over a cushion of 30% sucrose at 23,000 *g* for 16 h at 4°C. The VLPs precipitate was re-suspended in a TNC buffer containing 1 mM PMSF, protease inhibitors (1 : 200), and analyzed using centrifugation in a sucrose gradient.

#### **Centrifugation in sucrose gradient**

The VLPs precipitate re-suspended in a 100 µl TNC buffer containing 1 mM PMSF and protease inhibitors (1 : 200) was placed layer after layer on sucrose solutions of different concentrations (from 10 to 60% in 50 mM Tris-HCl, 100 mM NaCl, pH 7.4) and centrifuged at 200,000 *g* for 2.5 h at 4°C (Beckman Coulter Optima L-100XP centrifuge, 80Ti rotor). Ten 1 ml fractions were collected, and each fraction was concentrated by high-speed ultracentrifugation at 230,000 *g* for 16 h at 4°C. The precipitate was dissolved in a 100 µl TNC buffer containing 1 mM PMSF and protease inhibitors (1 : 200) and analyzed using Western blotting [18, 22].

#### **Analysis of VLP binding to CD81 receptor**

Huh7.0 cells were incubated in the presence of VLPs obtained in Sf9 cells for 1 h at 4°C. Huh7.0 cells pre-incubated with anti-CD81 antibodies (20 µg/ml, 1 h at 4°C) to block the CD81 receptor were used as a control. The cells were harvested, washed twice with PBS to remove unbound VLPs, and analyzed using Western blotting with anti-E2 antibodies.

#### **Fluorescent microscopy and flow cytometry**

HEK293T cells were trypsinized after 48 h of transfection with the recombinant plasmids BacMam-CE1E2mutGFP. The cells were collected, washed twice with PBS, and analyzed using flow cytometry (Beckman Coulter EPICS, USA) and Western blotting.

## **RESULTS AND DISCUSSION**

#### **Preparation of genetic engineering constructs and site-directed mutagenesis**

We had previously studied the influence of *N*-glycans of HCV protein E1 on its folding and productive heterodimer assembly of E1E2 in insect and mammalian cells. We have revealed that glycans linked to the N1

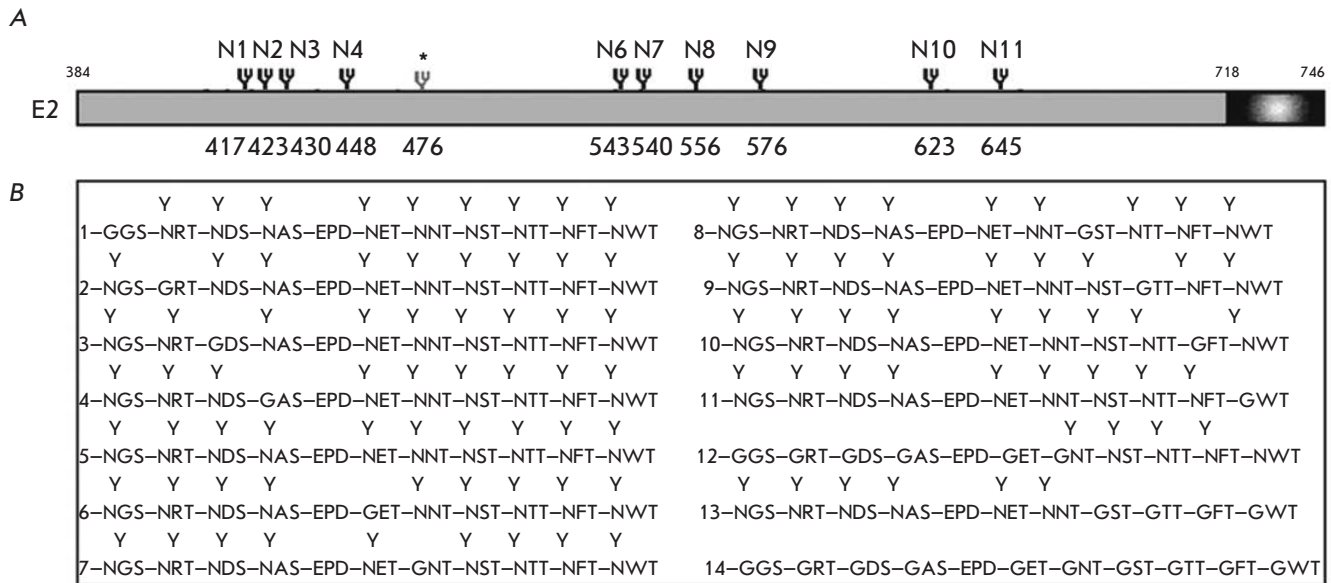


**Fig. 1.** N-glycosylation sites of the HCV E2 structural protein and its mutant variants. **A** – Positions of N1–N11 glycosylation sites in the polypeptide chain of E2. **B** – Mutant variants of glycoprotein E2 with modified (disrupted) glycosylation sites: 1, N1; 2, N2; 3, N3; 4, N4; 5, wild-type E2; 6, N6; 7, N7; 8, N8; 9, N9; 10, N10; 11, N11; 12, N1–N7(mL); 13, N8–N11(mR); 14, N1–N11( $\Sigma$ N). Glycosylation sites are marked with “Y”

and N5 sites of the E1 protein play the most significant role in the proper folding of these proteins [23]. In this study, we have investigated the involvement of glycans of the HCV glycoprotein E2 (genotype 1b strain 274933RU [16]) in the glycoprotein folding and formation of functional glycoprotein complexes and virus particles in insect and mammalian cells. For this purpose, we generated single-point mutations in the E2 at N-glycosylation sites and expressed the genes of mutant proteins in insect and mammalian cells using the baculovirus expression system [17, 20].

The DNA fragment corresponding to the cDNA sequence of the gene encoding the HCV glycoprotein E2 was cloned into the pFastBacHTb plasmid at NcoI–EcoRI using the standard protocol [20]. Oligonucleotide primers were constructed according to Drutsa *et al.* to obtain a series of recombinant plasmids bearing cDNA of the E2 protein with point mutations at glycosylation sites [20, 21] (*see* Materials and Methods section). The presence of all predetermined base substitutions was verified by sequencing. As a result, we obtained vector DNA pFastBacHTbE2mut containing E2 genes with the generated mutations, which were subsequently used to construct the pFastBacHTbE1E2mut, pFastBacHTbCE1E2mut, and BacMamCE1E2mutGFP vectors. The scheme of potential positions of N-glycosylation sites in the HCV E2 protein and the constructed mutant variant of E2 are shown in *Fig. 1*.

#### INVESTIGATION OF THE ROLE OF THE GLYCOSYLATION OF HCV PROTEIN E2 IN THE FUNCTIONING OF VIRUS ENVELOPE PROTEINS IN INSECT AND MAMMALIAN CELLS

##### Influence of N-glycans of HCV glycoprotein E2 on the expression of the genes of mutant HCV proteins E2 in insect and mammalian cells

We have previously shown that effective posttranslational glycosylation of HCV envelope proteins occurs in insect cells [22]. We have also revealed that disruption of the glycosylation sites of HCV glycoprotein E1 in various combinations does not influence its synthesis in Sf9 cells, although the absence of carbohydrate chains at the N1 and N5 E1 sites drastically reduces the level of its expression in HEK293T mammalian cells [23]. An analysis of the gene expression of mutant E2 proteins in Sf9 insect cells revealed that disruption of glycosylation sites in various combinations does not influence E2 synthesis, while electrophoretic mobility of mutant proteins increases in proportion to the decrease in the number of glycosylation sites (*Fig. 2*).

The intensity of the synthesis of HCV E2 in mammalian cells was found to depend on the presence of glycans at the specific glycosylation sites. To analyze the influence of N-glycans of HCV glycoprotein E2 on the efficiency of the expression of HCV envelope proteins in mammalian cells, plasmids pFastBacMam1GFP based on a baculovirus vector with expression cassettes

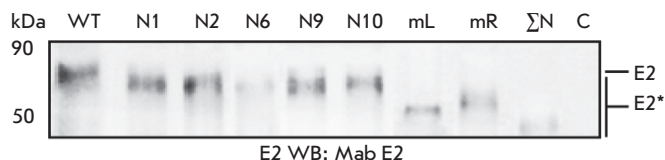


**Fig. 2.** Analysis of the gene expression of the mutant E2 proteins of HCV in Sf9 cells. Western blotting using anti-E2 antibodies following PAGE in 12% denaturing gel. Lysates of cells infected with recombinant baculoviruses: wild-type E2 (WT) and E2 with mutations of the glycosylation sites N1; N2; N6; N9; N10; N1–N7(mL); N8–N11 (mR); N1–N11(ΣN; mutations of all sites); C – negative control (Hsp90). Here and in Figs. 3–9, numbers on the left side are the protein molecular weight marker, kDa. Mutant proteins are marked as E2\*

under the control of the cytomegalovirus promoter (CMV) carrying the cDNA of mutant E2 were constructed. Human cells HEK293T were transfected with the resulting vector DNA pFastBacMam-CE1E2mut-GFP encoding E2 with point mutations at the glycosylation sites N1, N2, N4, N8, N10, mL(N1–N7), mR(N8–N11), and ΣN(N1–N11). Expression of the genes of mutant E2 proteins of HCV and the efficiency of their glycosylation in cells were assessed according to the level of synthesis of polypeptides CE1E2mutGFP using flow cytometry and PAGE, followed by immunoblotting (Fig. 3A, 3B).

According to flow cytometry data, the absence of N1 and N8 glycosylation sites in HCV E2 significantly reduces GFP fluorescence, which attests to a decreased E2 synthesis in CE1E2mutGFP polypeptides in HEK293T cells compared to the control cells. The mutation at the N10 site leads to an insignificant decrease in the synthesis of E2 glycoprotein. PAGE followed by immunoblotting revealed that mutant E2 variants were synthesized in mammalian cells and that the intensity of their synthesis depends on the presence of glycans at specific glycosylation sites of a protein. In addition, electrophoretic mobility of the proteins increased in proportion to the decrease in the number of glycosylation sites.

An analysis of the expression of the genes of mutant E2 proteins of HCV in E1E2 has revealed that the absence of glycans at any site except for N6 does not influence their synthesis in Sf9 cells (Fig. 4).

Treatment of mutant HCV glycoproteins E2 with endoglycosidase H (Endo H) followed by Western blotting has shown that mutant variants of the glycoprotein are sensitive to endoglycosidase activity (data are not presented), while glycosylation of the synthesized mutant glycoproteins occurs in insect cells.

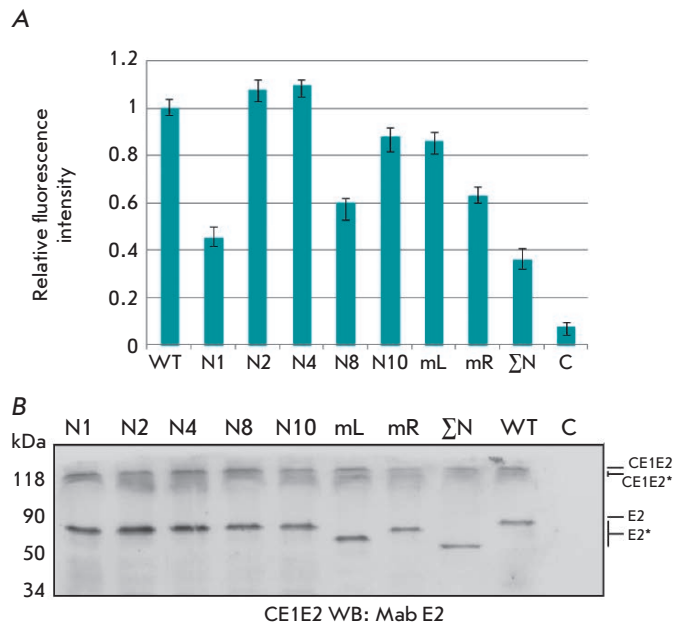


**Fig. 3.** Analysis of the gene expression of mutant E2 proteins within the HCV CE1E2 polypeptide in mammalian cells. A – Flow cytometry of HEK293T cells transfected with the pFastBacMam CE1E2mutGFP plasmid. Relative values of fluorescence intensity are plotted on the Y axis, and E2 variants with mutations at the glycosylation sites N1, N2, N4, N8, N10, mL(N1–N7), mR(N8–N11), and ΣN(N1–N11) are indicated along the X axis; (B) PAGE in 8% denaturing gel and Western blotting of lysates of HEK293T cells transfected with pFastBacMamCE1E2GFP and synthesizing the following variants of E2: wild-type E2 (WT) and E2 with mutations of N1, N2, N4, N8, N10, N1–N7(mL), N8–N11 (mR), and N1–N11(ΣN, mutations of all E2 glycosylation sites) glycosylation sites using anti-E2 antibodies; C – negative control (Hsp90). Mutant proteins are marked as E2\*

### Influence of N-glycans of HCV glycoprotein E2 on the formation of a productive E1E2 complex in insect cells

We have shown that the assembly of HCV glycoprotein complexes E1E2 in insect cells depends on the disorder of the N1 and N5 glycosylation sites of glycoprotein E1, while mutations in other sites do not influence the assembly [23]. In this study, the influence of the disorder of glycosylation sites in E2 on its folding and formation of E1E2 heterodimers in insect cells, identically to the case of mutant glycoprotein E1, was estimated by their interaction with calnexin and calreticulin (Fig. 5A–5C).

An analysis of the expression of the genes of mutant HCV proteins E2 in the glycoprotein complexes E1E2 in Sf9 insect cells has revealed that the noncovalently bound E1E2 complex is formed as in the case of the

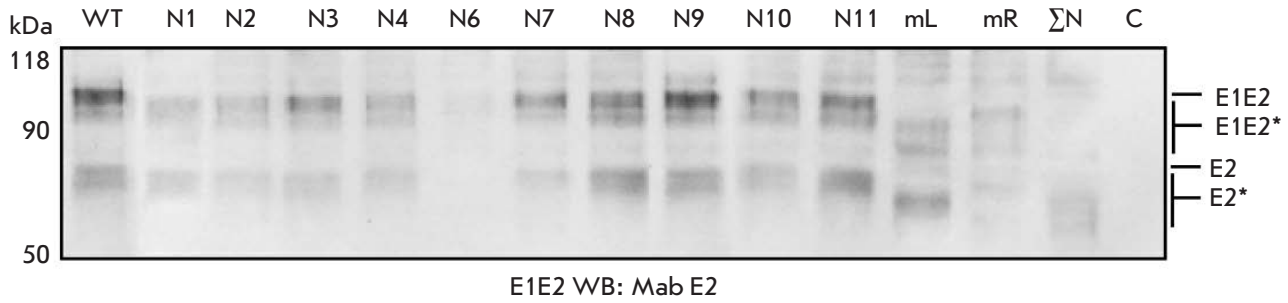


**Fig. 4.** Analysis of the gene expression of mutant E2 proteins as part of the HCV E1E2 polypeptide in Sf9 cells. Western Blotting using anti-E2 antibodies following PAGE in 10% denaturing gel. Lysates of cells infected with recombinant baculovirus synthesizing E2 as part of E1E2: wild-type E2 (WT) and E2 with mutations of the glycosylation sites N1; N2; N3; N4; N6; N7; N8; N9; N10; N11; N1–N7(mL); N8–N11(mR); N1–N11(ΣN; mutations of all glycosylation sites); C – negative control (Hsp90). Mutant proteins are marked as E2\*

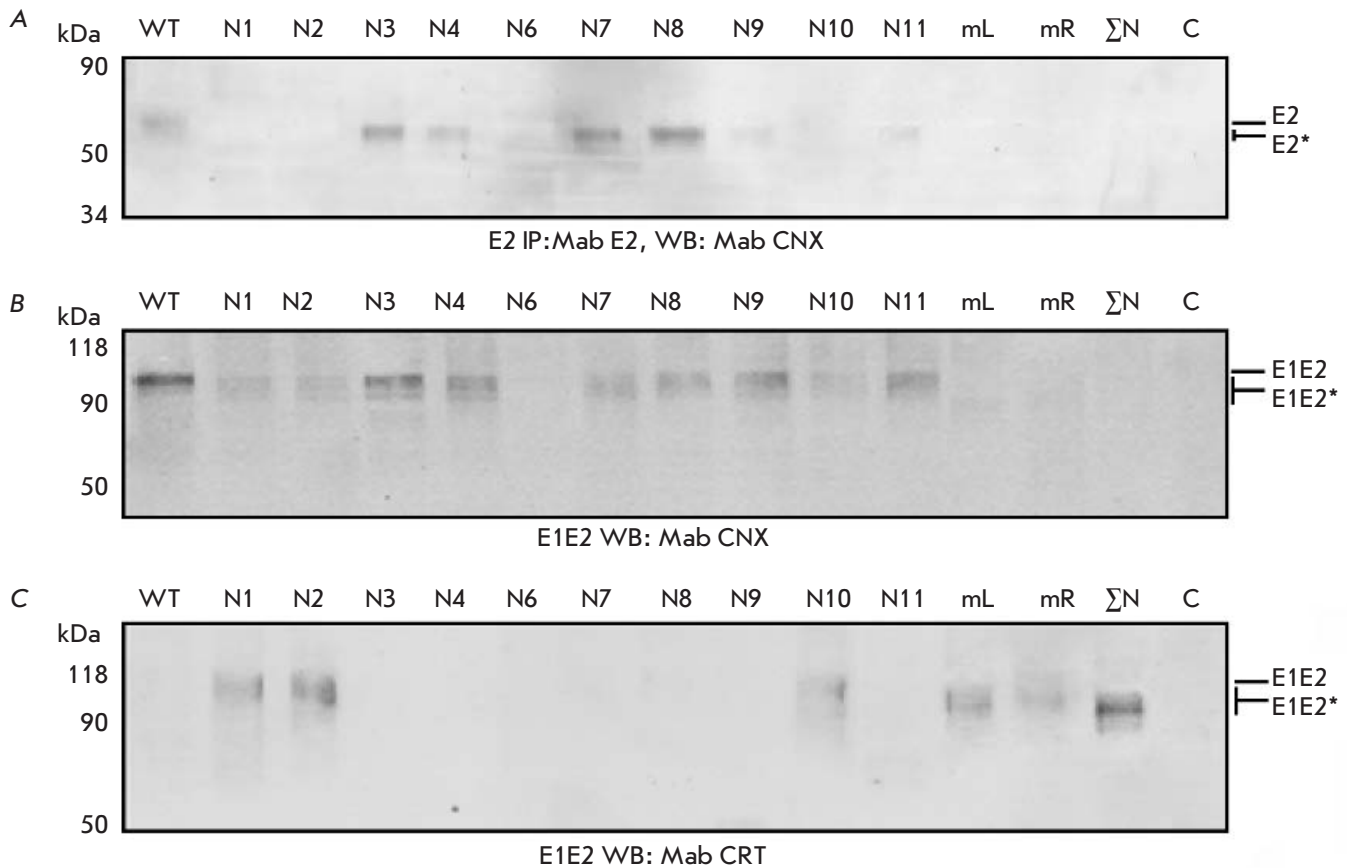


**Fig. 5.** Analysis of the gene expression of mutant E2 proteins in Sf9 cells. A – Western blotting with anti-calnexin antibodies following PAGE in 12% denaturing gel after preliminary immunoprecipitation with anti-E2 antibodies. Lysates of cells infected with recombinant baculovirus producing wild-type E2 (WT) and E2 with mutations of the glycosylation sites N1; N2; N3; N4; N6; N7; N8; N9; N10; N11; N1–N7(mL); N8–N11 (mR); N1–N11(ΣN; mutations of all E2 glycosylation sites). Western blotting using antibodies to (B) calnexin and (C) calreticulin following PAGE in 10% denaturing gel. Lysates of cells infected with recombinant baculovirus synthesizing mutant E2 as part of E1E2. C –negative control (Hsp90). Mutant proteins are marked as E2\*

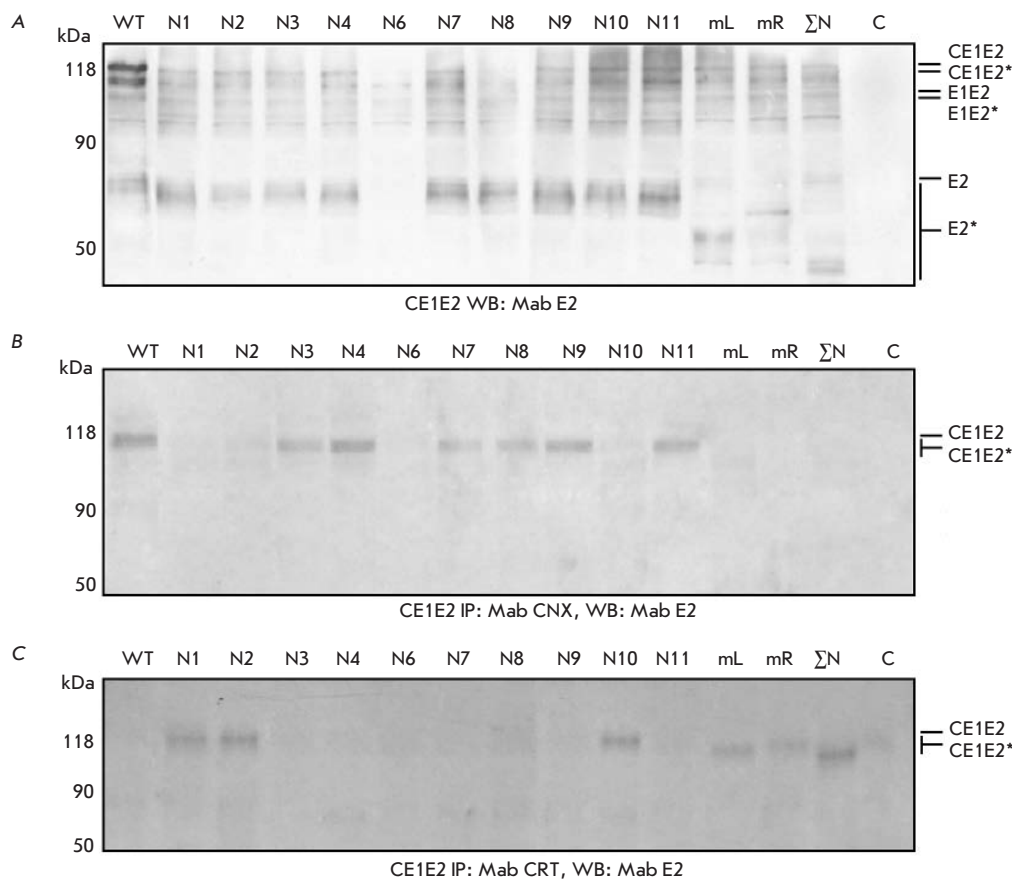


**Fig. 6.** Analysis of the gene expression of mutant E2 proteins as part of HCV CE1E2 in Sf9 cells. PAGE in 12% denaturing gel followed by Western blotting using anti-E2 antibodies (A) and anti-E2 antibodies after preliminary immunoprecipitation with antibodies to calnexin (B) and calreticulin (C). Lysates of cells infected with recombinant baculovirus synthesizing E2 as part of HCV CE1E2: wild-type E2 (WT) and E2 with mutations at the glycosylation sites N1; N2; N3; N4; N6; N7; N8; N9; N10; N11; N1–N7(mL); N8–N11 (mR); N1–N11 (ΣN; mutations of all E2 glycosylation sites). C –negative control (Hsp90). Mutant proteins are marked as E2\*

expression of wild-type E2 if one of the glycosylation sites is disrupted (N3, N4, N7, or N8). Mutant E2 containing neither the N9 nor N10 site have a moderate effect on the assembly of HCV envelope glycoproteins. The interaction between heterodimers and calnexins enhanced, and the assembly of the productive E1E2 complex is disrupted as the number of damaged sites (N1–N7(mL) and N8–N11(mR)) decreases. Aggregates of misfolded E1E2 dimers formed by the E2 protein with mutations at all glycosylation sites do not interact with calnexin. Interestingly, the assembly of the non-covalently bound E1E2 complex is also disrupted when one of the sites (N1, N2, or N10) is damaged. Mutations at these glycosylation sites in E2 apparently interfere with the formation of a proper conformation of the proteins forming the functional E1E2 complex.

#### **Influence of N-glycans of HCV glycoprotein E2 on the formation of virus-like particles in Sf9 and HEK293T cells**

It was shown that the synthesis of the structural proteins C (core), E1, and E2 of HCV in insect cells is accompanied by the formation of virus-like particles. We have previously shown that the recombinant structural proteins of HCV (including mutant E1 protein)

synthesized in insect cells are incorporated into the ER membranes where their folding, generation of E1E2, and formation of VLPs occur. Formation of VLPs in microsomal fractions with Sf9 insect cells infected with recombinant baculoviruses having been removed was detected using electron microscopy [20]. We revealed that the absence of glycans at the glycosylation sites of the E1 protein does not influence the formation of VLPs in insect cells [23]. An analysis of the expression of the genes of mutant E2 proteins of HCV as part of CE1E2 in Sf9 insect cells showed that disruption of glycosylation sites in various combinations (except for the N6 site) has no effect on their synthesis, while the electrophoretic mobility of mutant proteins increases in proportion to the reduction in the number of glycosylation sites (*Fig. 6A*).

Mutations introduced at the N3, N4, N7, N8, N9, N11 glycosylation sites of E2 do not interfere with glycoprotein folding as part of HCV CE1E2 in Sf9 cells. Meanwhile, the modification of the N1, N2, and N10 sites disrupts the assembly, leading to the formation of unproductive E1E2 heterodimers and their misfolding in VLPs (*Fig. 6B, 6C*). The formation of misfolded glycoprotein aggregates does not interfere with the formation of HCV VLPs in insect cells, but apparently it leads to the

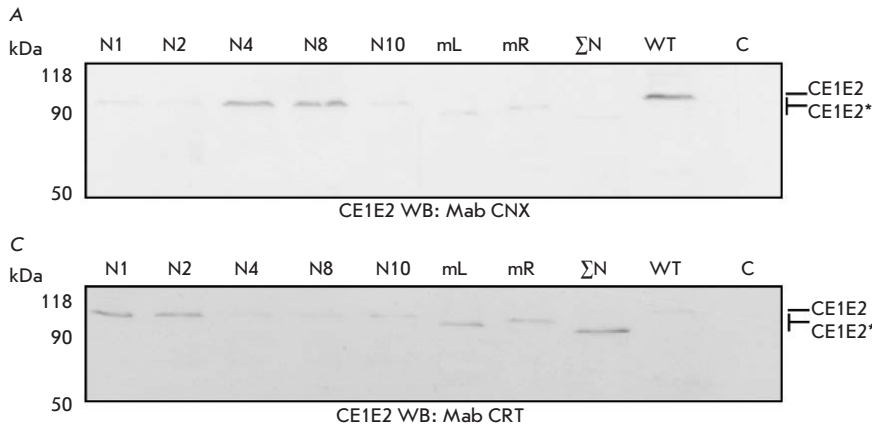


**Fig. 7.** Analysis of the gene expression of mutant E2 proteins as part of HCV CE1E2 in mammalian HEK293T cells. Western blotting using antibodies to calnexin (A) and calreticulin (B) following PAGE in 10% denaturing gel. Lysates of cells infected with recombinant plasmid DNA pFastBacMam CE1E2GFP synthesizing E2 with mutations at the glycosylation sites N1; N2; N4; N8; N10; N1–N7 (mL); N8–N11 (mR); and N1–N11 ( $\Sigma$ N; mutations of all E2 glycosylation sites). WT – wild-type E2; C – negative control (Hsp90). Mutant proteins are marked as E2\*

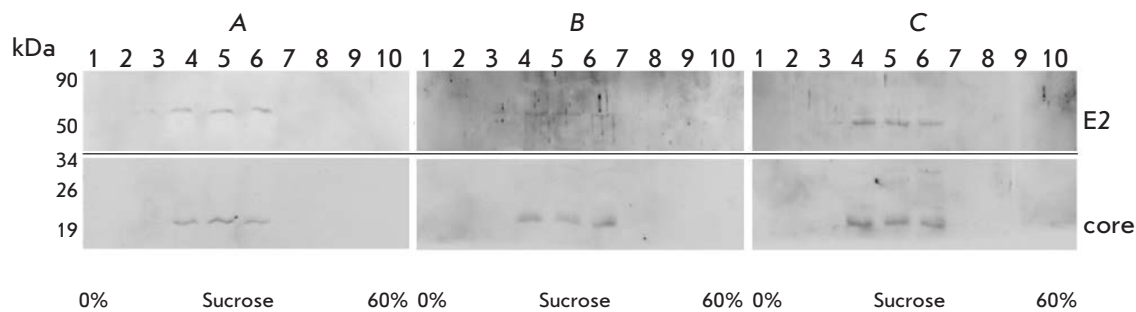


**Fig. 8.** Analysis of HCV-like particles isolated from HEK293T cells by centrifugation in sucrose gradient. Western blotting of ten VLP fractions, top-to-bottom, with antibodies to HCV core and E2 proteins following PAGE in 10% denaturing gel. HEK293T cells were transfected with recombinant DNA pFastBacMamCE1E2-GFP: intact DNA (A) and DNA with mutations at the glycosylation site N1 of E2 (B) or in all E2 glycosylation sites (C)

formation of defective virus particles that differ from natural ones. An analysis of the expression of the genes of HCV mutant E2 proteins in CE1E2 in both HEK293T and Sf9 cells showed that proper folding of glycoproteins in HCV CE1E2 is not disrupted upon formation of the E2 protein without either the N4 or N8 glycosylation site. In addition, the interaction between the resulting heterodimers and calnexin decreases, while the interaction with calreticulin increases with a rising number of damaged N1–N7 (mL) or N8–N11 (mR) glycosylation sites in E2. The dimers formed by E2 with mutations at all glycosylation sites ( $\Sigma$ N) interact with calreticulin. Interestingly, the assembly of the productive E1E2 complex and its folding in VLPs are disrupted as a result of the damage to the E2 N1, N2, and partially N10 glycosylation sites both in mammalian and insect cells (Fig. 7A, 7B).

The absence of carbohydrate chains at the N1, N2 sites and, to a smaller extent, at the N10 site of the E2 glycoprotein seems to play an essential role in the misfolding of the proteins of the HCV VLP functional complex, thus impeding the formation of mature virus particles [24].

We have previously demonstrated the formation of HCV VLPs in insect cells using Western blotting with anti-HCV antibodies and electron microscopy. To determine the biophysical characteristics of HCV VLPs obtained in mammalian cells, VLPs were purified and concentrated by centrifugation over a cushion of 30% sucrose at 23,000 g. The VLP precipitate was then analyzed by sucrose gradient centrifugation as described in the *Materials and Methods* section. The collected fractions were analyzed by Western blotting using antibodies to the structural proteins (Fig. 8A–8C).

Immunoblotting using antibodies to the proteins C and E2 revealed that VLPs are contained in all fractions at a density of 1.14–1.16 g/cm<sup>3</sup>. This fact can be an indication that RNA fragments are present in VLPs [25].

RT-PCR on total RNA isolated from insect cells infected with recombinant baculovirus bv-CE1E2mut with primers for the genes of the HCV proteins C and E2 revealed fragments of structural proteins (data are not presented). Similar results were obtained for HEK293T cells. Thus, N-glycans of HCV glycoprotein

E2 do not influence the synthesis of RNA of structural proteins in insect and mammalian cells and probably do not affect the incorporation of these RNA into virus-like particles.

### Influence of CD81 receptor on binding of recombinant HCV VLPs to Huh7.0 hepatoma cells

We have studied binding of HCV VLPs carrying mutant E2 proteins to Huh7.0 cells. Huh7.0 cells treated and untreated with specific anti-CD81 antibodies were incubated with VLPs derived from insect cells. After incubation with antibodies, binding of mutant E2 proteins to the cells was analyzed using Western blotting (Fig. 9). The working concentration of Ab CD81 was preliminarily determined (20 µg/ml) [26].

It was shown that HCV VLPs formed in insect cells and containing mutants of the E2 protein are bound to Huh7.0 cells regardless of whether the CD81 receptor is present on their surface or not. Helleet *al.* [26] have demonstrated that mutant E2 proteins as part of virus particles bind to HepG2, Huh7.0 cells in a CD81-dependent manner. It is understood that the influence of the CD81 receptor on the binding HCV virus particles to different cell types (HepG2, Huh7.0, NKNT-3, Molt-4) manifests itself in different ways [27].

### CONCLUSIONS

Glycosylation of viral envelope proteins in an infected cell is the crucial stage in the morphogenesis of the hepatitis C virus, determining proper virion assembly. We have demonstrated that HCV envelope proteins synthesized in insect and mammalian cells, and in particular the E2 protein containing mutations at the glycosylation sites, are incorporated into the ER membranes, where their folding, formation of the E1E2 complex, and virus-like particles take place. Investigation of the role of the glycosylation of envelope proteins in the morphogenesis of the hepatitis C virus (genotype 1b strain 274933RU) revealed that disruption of the single glycosylation sites N1 and N8 of HCV protein E2 (as well as the N1 and N5 sites of HCV protein E1) enhances the expression of these proteins in mammalian cells in contrast to expression in insect cells. It was revealed for the first time that disruption of the N1, N2, and N10 glycosylation sites of the E2 protein (as well as the N1 and N5 sites of HCV protein E1) influences the formation of functional E1E2 heterodimers. Unproductive dimers are predominantly

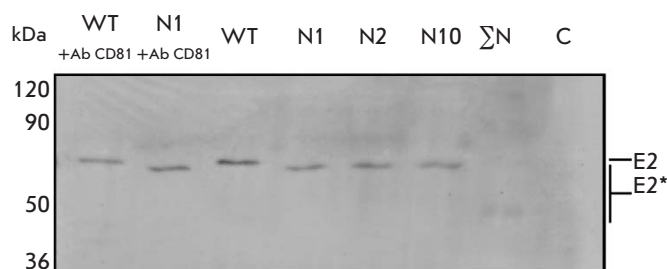


**Fig. 9.** Binding of mutant E2 proteins within recombinant HCV-like particles to Huh-7 cells, either treated with anti-CD81 antibodies or not. Western blotting of mutant E2 proteins using anti-E2 antibodies following PAGE in 10% denaturing gel. Lysates of Huh-7 cells after incubation with VLPs isolated from Sf9 insect cells after being infected with recombinant baculoviruses synthesizing E2 as part of CE1E2: wild-type E2 (WT) and E2 with mutations of the glycosylation sites N1; N2; N10; N1–N11 ( $\Sigma$ N; mutations of all E2 glycosylation sites); WT+Ab CD81 and N1+Ab CD81, Huh-7 cells after pre-incubation with Ab CD81; C – negative control (Huh-7). Mutant proteins are marked as E2\*

formed at these sites in the absence of glycans, while it does not impede the formation of HCV VLPs both in Sf9 insect and HEK293T human cells. We have put forward a hypothesis that the resulting virus-like particles with misfolded glycoproteins are defective and incapable of infecting target cells. These findings show that RNA-containing virus-like particles are formed with a density of 1.14–1.16 g/cm<sup>3</sup> in Sf9 and HEK293T cells. It has been demonstrated that N-glycans of HCV glycoproteins have no effect on the synthesis of RNA structural proteins in insect and mammalian cells and perhaps on their incorporation into virus-like particles. We have shown that HCV virus-like particles synthesized in insect cells are bound to Huh7.0 hepatoma cells through the CD81-independent route. ●

*This work was supported  
by the Russian Foundation for Basic*

*Research (grants № 07-04-12136, 08-04-00281,  
011-04-00231) and the Ministry of Education and  
Science of the Russian Federation  
(project № 16.512.11.2266).*

### REFERENCES

- Hnatyszyn H.J. // *Antivir. Ther.* 2005. V. 10. P. 1–11.
- Baumert T.F., Ito S., Wong D.T., Liang T.J. // *J. Virol.* 1998. V. 72. P. 3827–3836.
- Reed K.E., Rice C.M. // *Curr. Top. Microbiol. Immunol.* 2000. V. 242. P. 55–84.
- Ivanov A.V., Kuzyakin A.O., Kochetkov C.N., // *Uspehi biokhimii.* (Advances Biochemistry). 2005. V. 45. P. 37–86.

## RESEARCH ARTICLES

5. Choo Q.L., Kuo G., Weiner A.J., Overby L.R., Bradley D.W., Houghton M. // *Science*. 1989. V. 244. P. 359–362.
6. Burda P., Aebi M. // *Biochim. Biophys. Acta*. 1999. V. 1426. P. 239–257.
7. Choukhi A., Ung S., Wychowski C., Dubuisson J. // *J. Virol.* 1998. V. 72. P. 3851–3858.
8. Goffard A., Dubuisson J. // *Biochimie*. 2003. V. 85. P. 295–301.
9. Op de Beeck A., Cocquerel L., Dubuisson J. // *J. Gen. Virol.* 2001. V. 82. P. 2589–2595.
10. Montreuil J., Vliegenthart J.F., Schachter H. // *Glycoproteins*. Elsevier. 1995. P. 1–12.
11. Chapel C., Garcia C., Roingeard Ph. // *J. Gen. Virol.* 2006. V. 87. P. 861–871.
12. Helle F., Goffard A., Morel V., Duverlie G., McKeating J., Keck Z.Y., Fong S., Penin F., Dubuisson J., Voisset C. // *J. Virol.* 2007. V. 81. P. 8101–8111.
13. Xiang J., Wunschmann S., George S.L., Klinzman D., Schmidt W.N., LaBrecque D.R., Stapleton J.T. // *J. Med. Virol.* 2002. V. 68. P. 537–543.
14. Brazzoli M., Helenius A., Fong S.K., Houghton M., Abrignani S., Merola M. // *Virol.* 2005. V. 332. P. 438–453.
15. Cocquerel L., Meunier J.C., Op de Beeck A., Bonte D., Wychowski C., Dubuisson J. // *J. Gen. Virol.* 2001. V. 82. P. 1629–1635.
16. Mohonov V.V., Novikov E.I., Samohvalov E.I. // *Voprosy virusologii. (Problems of Virology)*. 2002. V. 47. P. 9–12.
17. Jones D.M., McLauchlan J. // *J. Biol. Chem.* 2010. V. 285. P. 22733–22739.
18. Maniatis T., Fritsch E.F., Sambrook J. *Molecular cloning. A Laboratory Manual*. Cold Spring Harbor, N.Y.: Cold Spring Harbor Lab. Press, 1982.
19. Bac-to-Bac Baculovirus Expression System. *Instruction Manual*. St. Louis, MO: Life Technologies, Inc., Monsanto Corp. Res. 1993.
20. Beljelarskaya S.N., Koroleva N.N., Popenko V.I., Drutsa V.L., Orlova O.V., Rubtsov P.M., Kochetkov S.N. // *Molekulyar. biologiya. (Molecular biology)*. 2010. V. 44. P. 107–119.
21. Drutsa V.L., Kaberdin V.R., Koroleva O.N., Shilov I.O. // *Bioorgan. khimiya. (Bioorganic chemistry)*. 1991. V. 17. P. 1487–1493.
22. Timohova A.V., Bakinovskii L.V., Zinin A.I., Popenko V.I., Ivanov A.V., Rubtsov P.M., Kochetkov S.N., Beljelarskaya S.N. // *Molekulyar. biologiya. (Molecular biology)*. 2012. V. 46. P. 644–653.
23. Orlova O.V., Drutsa V.L., Spirin P.V., Popenko V.I., Prasolov V.S., Rubtsov P.M., Kochetkov S.N., Beljelarskaya S.N. // *Molekulyar. biologiya. (Molecular biology)*. 2013. V. 47. P. 147–156.
24. Clayton R.F., Owsianka A., Aitken J., Graham S., Bhella D., Patel A.H. // *J. Virol.* 2002. V. 76. P. 7672–7682.
25. McEwen C.R. // *Anal. Biochem.* 1967. V. 20. P. 114–149.
26. Helle F., Vieyres G., Elkrief L., Popescu C.I., Wychowski C., Descamps V., Castelain S., Roingeard P., Duverlie G., Dubuisson J. // *J. Virol.* 2010. V. 84. P. 11905–11915.
27. Tryatni M., Saunier B., Maruvada P., Davis A.R., Ulianich L., Heller T., Patel A., Kohn L.D., Liang T.J. // *J. Virol.* 2002. V. 76. P. 9335–9344.

# New Nanobiocomposite Materials for Bioelectronic Devices

D. V. Pankratov<sup>1,2,3</sup>, E. González-Arribas<sup>3</sup>, Yu. M. Parunova<sup>1</sup>, M. A. Gorbacheva<sup>1,2</sup>,  
Yu. S. Zeyfman<sup>1</sup>, S. V. Kuznetsov<sup>4</sup>, A. V. Lipkin<sup>1</sup>, S. V. Shleev<sup>1,2,3\*</sup>

<sup>1</sup>National Research Center "Kurchatov Institute", Akademika Kurchatova Sq., 1, Moscow, 123182, Russia

<sup>2</sup>A.N. Bach Institute of Biochemistry, Russian Academy of Sciences, Leninsky prospect, 33, building 2, Moscow, 119071, Russia

<sup>3</sup>Malmö University, Jan Waldenströms gata, 25, Malmö, 21428, Sweden

<sup>4</sup>I.G. Petrovsky Bryansk State University, Bezhitskaya Str., 14, Bryansk, 241036, Russia

E-mail: shleev@inbi.ras.ru

Received: 12.11.2014

Copyright © 2015 Park-media, Ltd. This is an open access article distributed under the Creative Commons Attribution License, which permits unrestricted use, distribution, and reproduction in any medium, provided the original work is properly cited.

**ABSTRACT** We have developed and synthesized nanobiocomposite materials based on graphene, poly(3,4-ethylenedioxythiophene), and glucose oxidase immobilized on the surface of various nanomaterials (gold nanoparticles and multi-walled carbon nanotubes) of different sizes (carbon nanotubes of different diameters). Comparative studies of the possible influence of the nanomaterial's nature on the bioelectrocatalytic characteristics of glucose-oxidizing bioanodes in a neutral phosphate buffer solution demonstrated that the bioelectrocatalytic current densities of nanocomposite-based bioanodes are only weakly dependent on the size of the nanomaterial and are primarily defined by its nature. The developed nanobiocomposites are promising materials for new bioelectronic devices due to the ease in adjusting their capacitive and bioelectrocatalytic characteristics, which allows one to use them for the production of dual-function electrodes: i.e., electrodes which are capable of generating and storing electric power simultaneously.

**KEYWORDS** glucose oxidase, graphene, conducting organic polymer, carbon nanotubes, nanobiocomposite/double function electrode.

**ABBREVIATIONS** ACN – acetonitrile; GE – gelatin; EDOT – 3,4-ethylenedioxythiophene; PEDOT – poly(3,4-ethylenedioxythiophene); PEG – polyethylene glycol; GA – glutaraldehyde; TTF – tetrathiafulvalene; TCNQ – 7,7,8,8-tetracyanoquinodimethane; THF – tetrahydrofuran; GOx – glucose oxidase; AuNP – gold nanoparticles; GR – graphene; CNT – carbon nanotubes; SCE – saturated calomel electrode; SEM – scanning electron microscopy; Au – gold electrode; CTC – charge transfer complex; PB – phosphate buffer;  $j$  – bioelectrocatalytic current density; CV – cyclic voltammogram.

## INTRODUCTION

Nanobiocomposite materials are increasingly in use in various fields of science and technology, including new biomedical technologies [1]. Modern bioelectronic nanocomposite-based devices (biosensors, biofuel elements, biobatteries, etc.) can be used for continuous monitoring of an organism's state, for targeting organs and tissues, as well as for spot delivery of drugs. Comparative studies of the particular features of the performance of nanobiocomposites in buffer solutions and complex human physiological fluids provide the foundation for the development of highly efficient and stable bioelectronics for biomedical applications. This work discusses the production of novel nanobiocomposite materials based on graphene, poly(3,4-ethylenedioxythiophene), and glucose oxidase immobilized on the surface of na-

nomaterials of different nature (gold nanoparticles and multi-walled carbon nanotubes) and sizes (carbon nanotubes of different diameters) and examines their properties under near-physiological conditions.

## MATERIALS AND METHODS

### Materials and Methods

$\text{Na}_2\text{HPO}_4 \cdot 2\text{H}_2\text{O}$ ,  $\text{NaH}_2\text{PO}_4 \cdot \text{H}_2\text{O}$ , NaCl,  $\text{HAuCl}_4 \cdot 3\text{H}_2\text{O}$ ,  $\text{H}_2\text{SO}_4$ ,  $\text{LiClO}_4$ , sodium citrate, acetonitrile ( $\geq 99.9\%$ , ACN), toluene ( $\geq 99.8\%$ ), gelatin (GE), *D*-glucose, 3,4-ethylenedioxythiophene (EDOT), polyethylene glycol (PEG), 25% glutaraldehyde solution (GA), tetrathiafulvalene (TTF), 7,7,8,8-tetracyanoquinodimethane (TCNQ), tetrahydrofuran (THF), and glucose oxidase (GOx) from *Aspergillus niger* were purchased

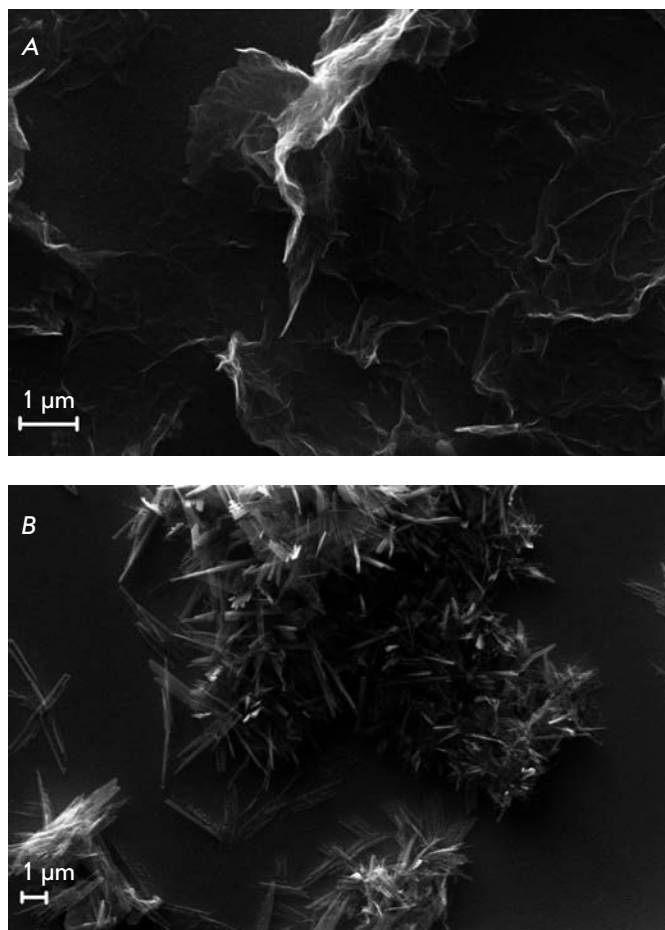


**Fig. 1.** SEM images of the surfaces of (A) Au|PEDOT/GR and (B) Au|PEDOT/GR|TCNQ/TTF electrodes

from Sigma-Aldrich (USA) and used without further purification. Ethanol (95%) and argon were purchased from Kemetyl AB (Sweden) and AGA Gas AB (Sweden), respectively. All solutions were prepared using deionized water (18 MΩ·cm) produced using a PURE-LAB UHQ II system from ELGA Labwater (UK).

Nanobiocomposites were synthesized using gold nanoparticles (AuNP) with a diameter of 20 nm and three types of carbon nanomaterials: graphene (GR, 1.6 nm thick, less than three carbon monolayers) and two types of multi-walled carbon nanotubes (CNT): CNT<sub>1</sub> (outer diameter of 10–15 nm, inner diameter of 2–6 nm, length of 0.1–10 μm) and CNT<sub>2</sub> (outer diameter of 20–30 nm, inner diameter of 1–2 nm, length of 0.5–2 μm). GR was purchased from Graphene Supermarket (USA); CNT, from Sigma-Aldrich (USA). AuNP were synthesized by the method described in [2], using sodium citrate as a reductant. 50 mL of a 250 μM HAuCl<sub>4</sub> solution was brought to a boil under constant stirring, and 750 μL of an aqueous 1 wt. % sodium citrate solu-

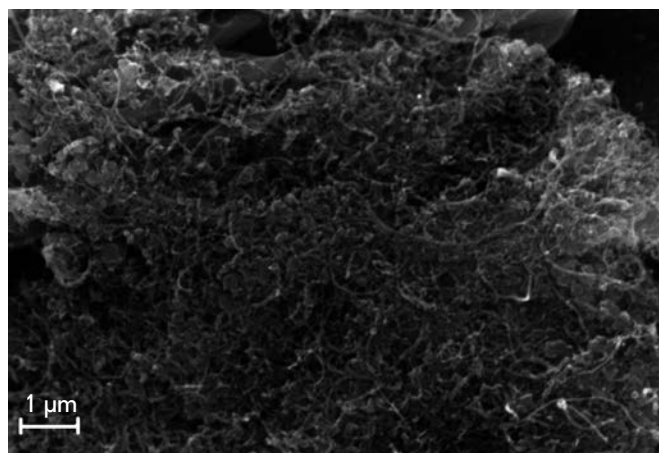


**Fig. 2.** SEM image of the surface of the Au|PEDOT/GR|TCNQ/TTF|CNT<sub>1</sub>/GOx electrode

tion was added. After the addition of sodium citrate, the mixture was incubated for 10 min under constant stirring without heating. The resultant AuNP suspension was cooled to room temperature and concentrated (50-fold) by centrifugation at 10,000 g for 30 min [3]; 98% of the supernatant was removed, and the AuNP precipitate was re-suspended using sonication.

Electrochemical measurements were performed using a μAutolab Type III/FRA2 potentiostat/galvanostat (Metrohm Autolab BV, Netherlands) using a three-electrode circuit with a saturated calomel reference electrode (242 mV vs. normal hydrogen electrode, NHE) and a platinum wire as an auxiliary electrode. All potentials are reported with respect to SCE, unless specified otherwise.

Sonication was performed on an Ultrasonic Cleaner XB2 bath (VWR International Ltd., UK). Scanning electron microscopy (SEM) images were obtained using a EVO LS 10 high-resolution scanning electron microscope from Zeiss (Germany).

#### **Production of nanobiocomposite material-based electrodes**

Polycrystalline gold disc electrodes from Bioanalytical Systems (USA) with a geometric surface area of 0.031 cm<sup>2</sup> were mechanically cleaned through polishing with Microcloth paper (Buehler, UK) in an aluminum oxide suspension with a particle size of 0.1 μm (Struers, Denmark). The electrodes were further washed with deionized water, sonicated in ethanol for 5 min to remove residual aluminum oxide particles, and electrochemically cleaned through cycling in 0.5 M H<sub>2</sub>SO<sub>4</sub> using a range of potentials from –0.2 to +1.7 V for 20 cycles at a scan rate of 0.1 V/s, washed with water, and dried in an airflow.

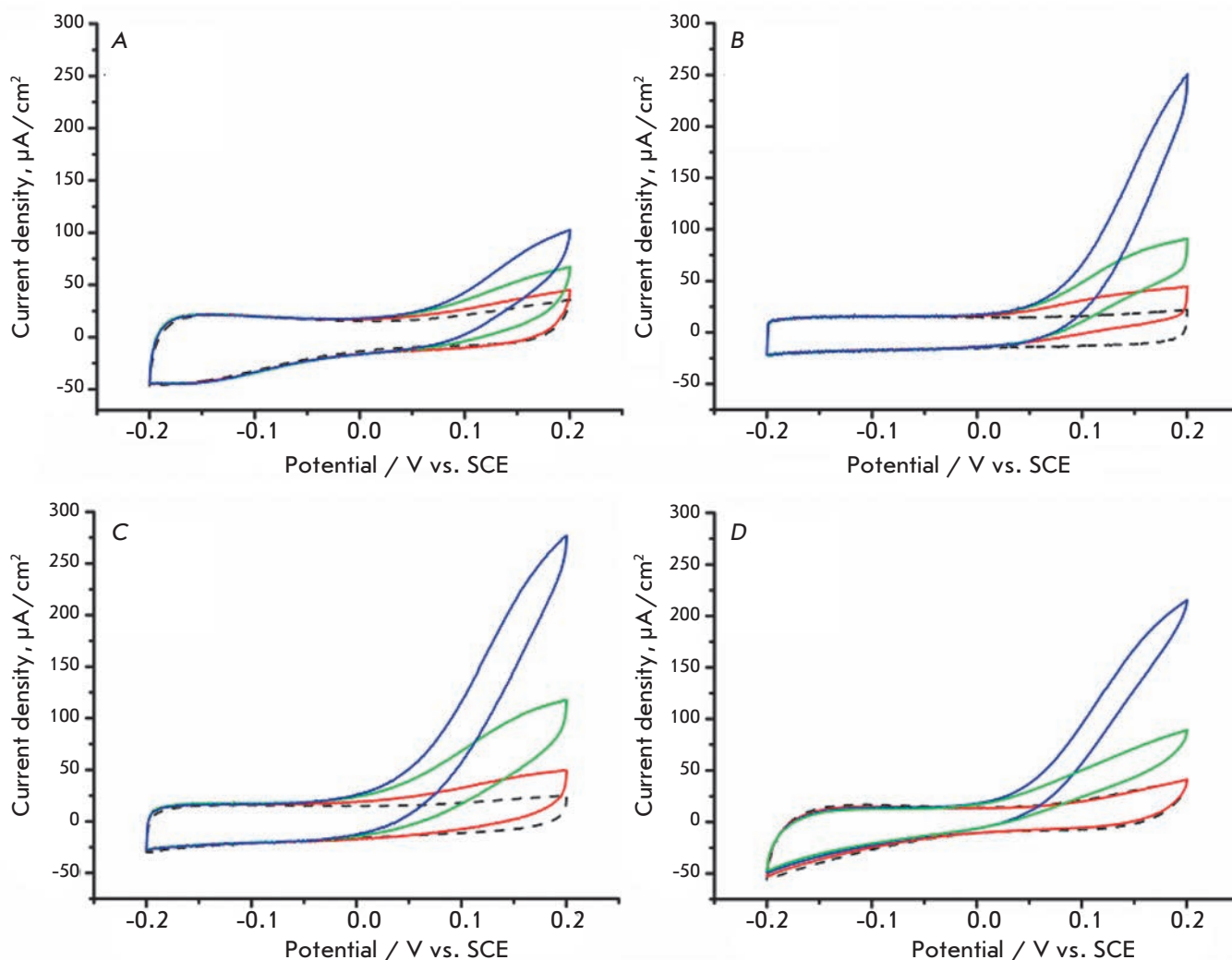


**Fig. 3.** CVs of bioanodes submerged in PBS. Au|PEDOT/GR|TCNQ/TTF|GOx|GE (A), Au|PEDOT/GR|TCNQ/TTF|Nanomaterial/GOx|GE (B-D), PB without glucose (dashed line), and PB with glucose (solid line), mmol L<sup>-1</sup>. 0.05 (red), 5 (green) and 50 (blue). Nanomaterial: CNT<sub>1</sub> (B), CNT<sub>2</sub> (B), AuNP (D)

Poly(3,4-ethylenedioxythiophene)/graphite (PEDOT/GR) nanocomposite was synthesized on Au surface by potentiodynamic cycling in a range of potentials from 200 to 1,300 mV (1 cycle at 100 mV/s) in 0.1 M phosphate buffered saline (PBS, pH 7.4) containing 20 mM EDOT, 1 mM PEG, 0.1 M LiClO<sub>4</sub> and GR at a GR : EDOT weight ratio of 1:5 [4]. Prior to electropolymerization, the mixture was sonicated for 1 h to obtain a stable suspension and then purged with argon for 20 min to remove oxygen. The resulting layer of PEDOT/GR was sufficiently homogeneous with only minor defects filled with polymer (*Fig. 1A*).

The charge-transfer complex (CTC) TCNQ/TTF, a known mediator to ensure contact between the electrode and the immobilized GOx (see below), was syn-

thesized on the surface of the composite PEDOT/GR material [4]. TCNQ and TTF were dissolved in THF and ACN, respectively, to obtain solutions with a concentration of 1.2 mg/mL. The TCNQ (1 μL) and TTF (2 μL) solutions were mixed on the surface of the PEDOT/GR composite; the excess unreacted TTF was washed away with ACN after the CTC crystallization process had been completed. The resulting CTC crystals had a characteristic needle-like shape, which is in accordance with the data in [5], but were rather unevenly distributed over the electrode surface, forming islands corresponding to the crystallization centers (*Fig. 1B*).

2 μL of nanomaterial suspension (CNT or AuNP) was applied to the surface of the TCNQ/TTF complex. To obtain a stable suspension, 1 mg of CNT was mixed

with 1 mL of toluene; the AuNP concentrate was 10-fold diluted with deionized water; the mixtures obtained were sonicated for 20 min.

To perform biomodification of the resulting nanobiocomposites, PEDOT/GR|TCNQ/TTF|CNT and PEDOT/GR|TCNQ/TTF|AuNP, 2  $\mu$ L of a GOx solution (10 mg/mL in PBS) was applied to the electrode surface and kept at +4 °C for 1 h. To evaluate the influence of the nanomaterial on the biocatalytic properties of the electrode, a PEDOT/GR|TCNQ/TTF|GOx biocomposite was produced with the enzyme immobilized directly on the CTC surface. The SEM image of the PEDOT/GR|TCNQ/TTF|CNT<sub>1</sub>/GOx nanobiocomposite surface is shown in Fig. 2. Remarkably, the surface is well developed and the CNT<sub>1</sub>/GOx layer is sufficiently homogeneous and evenly coats the CTC.

2 mL of a gelatin solution in water (2.5 wt. %) was applied to the electrode surface to stabilize the resultant structure, followed by drying for 1 h at room temperature. The electrodes were subsequently immersed in an aqueous GA solution (5 wt. %) for 60 s and washed with water.

## RESULTS AND DISCUSSION

The biocatalytic properties of the designed electrodes were studied in 0.1 M PB in a range of potentials from -0.2 to 0.2 V relative to the SCE at a scan rate of 10 mV/s. The cyclic voltammograms (CV) of the bioanodes with different structures are shown in Fig. 3.

The capacity of the produced electrodes is independent of the presence of nanocomposite and ranges from 1.5 to 2.5 mF/cm<sup>2</sup> for all types of structures. It should be noted that it is easy to modify the capacity of the nanobiocomposites both during the PEDOT/GR synthesis (the number of electropolymerization cycles) and when designing nanobiocomposites. This feature allows one to use the developed materials to design and optimize hybrid bioelectrodes with dual functions: generation and storage of electrical power [6].

The data show that a pronounced bioelectrocatalytic response with an initial potential of glucose electroox-

idation ca. 0 V, increasing with the glucose concentration rising to 50 mM, was recorded for all electrodes in glucose-containing PBS, which is consistent with the published data for CTC/GOx systems [7].

The biocatalytic current density ( $j$ ) of Au|PEDOT/GR|TCNQ/TTF|GOx|GE electrodes was low compared to the samples containing nanomaterial, which can be attributed to the uneven distribution of CTC over the electrode surface (Fig. 1B). Enzyme adsorption on the CTC surface blocks the mediating electron transfer for the GOx molecules adsorbed onto the PEDOT/GR nanocomposite and, therefore, reduces the proportion of the bioelectrochemically active enzyme.

In the case of Au|PEDOT/GR|TTF/TCNQ|nanomaterial/GOx|GE electrodes, the experimental value of  $j$  was  $229 \pm 13$  and  $251 \pm 15$   $\mu$ A/cm<sup>2</sup> for CNT<sub>1</sub> and CNT<sub>2</sub> as a nanomaterial, respectively, and  $175 \pm 8$   $\mu$ A/cm<sup>2</sup> for AuNP, under conditions similar to those for bioanodes containing no nanomaterials. The  $j$  value was ca. 10% higher for CNT<sub>2</sub>-based electrodes than for those based on CNT<sub>1</sub>, which is in agreement with the difference in the capacity of Au|PEDOT/GR|TCNQ/TTF|CNT<sub>1</sub>/GOx|GE and Au|PEDOT/GR|TCNQ/TTF|CNT<sub>2</sub>/GOx|GE ( $1.63 \pm 0.05$  and  $1.85 \pm 0.05$  mF/cm<sup>2</sup>, respectively). The higher  $j$  values in the case of CNT<sub>2</sub> can be attributed to a larger specific surface area rather than to better conditions for enzyme immobilization. This fact is consistent with the data obtained previously for bilirubin oxidase adsorbed onto the surface of modified AuNP with different diameters exceeding the enzyme size [8].

## CONCLUSIONS

Our research resulted in the development of multi-component nanobiocomposites with the possibility of controlled regulation of their capacitive and bioelectrocatalytic parameters. The material obtained can be used to create modern bioelectronic devices which are fully operational under near-physiological conditions. ●

*This study was supported by a Russian Science Foundation grant (project № 14-14-00530).*

## REFERENCES

1. Nanocomposites /Ed. C. S. S. R. Kumar. Weinheim: Wiley-VCH, 2010. V. 8. 466 p.
2. Haiss W., Thanh N.T.K., Aveyard J., Fernig D.G. // *Anal. Chem.* 2007. V. 79. № 11. P. 4215-4221.
3. Wang X.J., Falk M., Ortiz R., Matsumura H., Bobacka J., Ludwig R., Bergelin M., Gorton L., Shleev S. // *Biosens. Bioelectron.* 2012. V. 31. № 1. P. 219-225.
4. Xiao X.X., Wang M.E., Li H., Si P.C. // *Talanta.* 2013. № 116. P. 1054-1059.
5. Sugimoto T., Tanaka H., de Caro D., Valade L. // *Materials.* 2010. V. 3. № 3. P. 1640-1673.
6. Pankratov D., Blum Z., Suyatin D.B., Popov V.O., Shleev S. // *ChemElectroChem.* 2014. V. 1. № 2. P. 343-346.
7. Khan G.F., Ohwa M., Wernet W. // *Anal. Chem.* 1996. V. 68. № 17. P. 2939-2945.
8. Pankratov D.V., Zeifman Y.S., Dudareva A.V., Pankratova G.K., Khlupova M.E., Parunova Y.M., Zajtsev D.N., Bashirova N.F., Popov V.O., Shleev S.V. // *Acta Naturae.* 2014. V. 6. № 1. P. 102-106.

# Selective Protective Potency of *Yersinia pestis* $\Delta nlpD$ Mutants

S. V. Dentovskaya<sup>1</sup>, S. A. Ivanov<sup>1</sup>, P. Kh. Kopylov<sup>1</sup>, R. Z. Shaikhutdinova<sup>1</sup>, M. E. Platonov<sup>1</sup>,  
T. I. Kombarova<sup>1</sup>, T. V. Gapel'chenkova<sup>1</sup>, S. V. Balakhonov<sup>2</sup>, A. P. Anisimov<sup>1\*</sup>

<sup>1</sup>State Research Center for Applied Microbiology, Obolensk, Moscow Region, 142279, Russia

<sup>2</sup>Irkutsk Antiplague Research Institute of Siberia and Far East, Trilissera Str., 78, 664047, Irkutsk, Russia

\*E-mail: anisimov@obolensk.org, a-p-anisimov@yandex.ru

Received: 12.06.2014

Copyright © 2015 Park-media, Ltd. This is an open access article distributed under the Creative Commons Attribution License, which permits unrestricted use, distribution, and reproduction in any medium, provided the original work is properly cited.

**ABSTRACT** It has recently been shown that the NlpD lipoprotein is essential to *Yersinia pestis* virulence and that subcutaneous administration of the *nlpD* mutant could protect mice against bubonic and pneumonic plague better than the EV vaccine strain [PLoS One 2009. V. 4. № 9. e7023]. In this study, similar  $\Delta nlpD$  mutants were generated on the basis of other *Y. pestis* parent strains, including strains from the subspecies *microtus*, which is avirulent to guinea pigs and humans. Comparative testing confirmed that immunization of mice with  $\Delta nlpD$  mutants induces immunity  $10^5$  times more potent than the one induced by the administration of the EV vaccine strain. At the same time, NlpD<sup>-</sup> bacteria failed to protect guinea pigs in the case of a subcutaneous challenge with *Y. pestis*, inducing a  $10^6$  times less potent protection compared with that conferred by immunization with the EV vaccine strain. The possible causes of the observed phenomena are discussed.

**KEYWORDS** *Yersinia pestis*,  $\Delta nlpD$  mutant, selectivity of protective potency, live plague vaccine.

**ABBREVIATIONS** SCPM-Obolensk – State Collection of Pathogenic Microbes and Cell Cultures on the base of State Research Center for Applied Microbiology and Biotechnology; SRCAMB – State Research Center for Applied Microbiology and Biotechnology; II – index of immunity; ELISA – enzyme-linked immunosorbent assay; CFU – colony-forming unit; LPS – lipopolysaccharide; CS – current study; CCIARISFE – Culture Collection of Irkutsk Antiplague Research Institute of Siberia and Far East; PHAT – passive hemagglutination test; DCL (LD<sub>100</sub>) – absolutely lethal dose (*dosis certa letalis*); ImD<sub>50</sub> – immunizing dose protecting 50% of infected animals from death; LB – Luria-Bertani broth; LD<sub>50</sub> – dose lethal for 50 % of infected animals.

## INTRODUCTION

Live vaccines stimulate not only humoral, but also cell-mediated immunity, which, in some species, plays the leading role in the immunogenesis of plague [1–8]. Furthermore, live vaccines constructed on the basis of attenuated strains contain not merely one or two immunodominant antigens, but a whole range of complex (protein complexes with lipopolysaccharides (LPS), etc.) conformationally labile and minor antigens, which ensure induction of a “heterogeneous” immune response after a single immunization. This immune response can protect different species of animals against bacterial pathogens, including bacteria with partially altered antigenic specificity, in case of both subcutaneous and aerosol administrations [3, 7–11]. However, a commercial live plague vaccine created on the basis of the *Yersinia pestis* EV strain can cause local and systemic adverse reactions of varying severity in 5–29% of subjects with a normal immune status, regardless of route of administration [1, 2, 12, 13]. Therefore, studies aimed at creating live plague vaccines based on pre-

cisely attenuated strains of *Y. pestis* with superior immunogenicity and reduced reactogenicity compared to those of the commercial EV vaccine strain remain relevant [2, 8, 14–19].

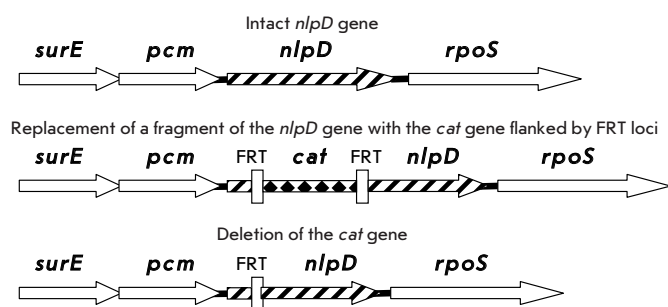
Potential target genes for the attenuation of virulent strains are either selected (i) by random mutagenesis with individually labeled transposons [20], (ii) using reverse vaccinology techniques [21–23] or (iii) chosen by investigating analogs of genes from other bacterial pathogens, whose mutations had been previously shown to reduce virulence [24]. For example, a relationship has been established in the past decade between the expression of the *nlpD/lppB* (novel lipoprotein D/lipoprotein B) family of genes and survival of some gram-negative bacteria in a stressful environment, as well as their pathogenicity [18, 25, 26]. It has been shown [14] that lipoprotein NlpD is essential for virulence of the plague pathogen *Y. pestis* in case of subcutaneous and aerosol administration. Moreover, immunization of mice by  $10^5$  CFU of  $\Delta nlpD$ -mutant of *Y. pestis* Kimberley53 strain, followed by administra-

tion of  $10^5$  LD<sub>50</sub> of the wild-type Kimberley53 strain (1 LD<sub>50</sub> = 1–3 CFU) resulted in a 100% survival rate, whereas the EV vaccine strain protected only 10% of the animals against death.

The purpose of this study was to construct  $\Delta nlpD$  mutants of other parental *Y. pestis* strains, including strains of subsp. *microtus*, which are avirulent for guinea pigs and humans, and to evaluate their protective potency in mice and guinea pigs.

## MATERIALS AND METHODS

**Bacterial strains** used in the study and their characteristics are listed in Table 1. Strains of *Y. pestis* and *Escherichia coli* were grown in liquid or solid Hottinger culture media (various batches prepared in the SRCAMB) and LB (1% tryptone, 0.5% yeast extract, 1% sodium chloride)



Construction of *Y. pestis*  $\Delta nlpD$  mutants. Detailed description of the strategy is given in [30, 31]

at pH 7.2. Selection of cells containing recombinant plasmids was carried out in the media supplemented with antibiotics ampicillin (100  $\mu$ g/mL), chloramphenicol (10  $\mu$ g/mL), and polymyxin B (100  $\mu$ g/mL). Strains of *Y. pestis* for the immunization and infection of animals were grown at 28 °C for 48 h.

## Mutagenesis

*Y. pestis* mutants were constructed by homologous recombination with a recombinant plasmid pCVD442- $\Delta nlpD::cat$  based on the suicide vector pCVD442 [30], in which a portion of the cloned coding sequence of the *nlpD* gene (nucleotides 112–318) was replaced with the *cat* gene from pKD3 plasmid [31] (Figure).

pCVD442- $\Delta nlpD::cat$  plasmid from a donor *E. coli* S17-1  $\lambda pir$  strain was transferred into a recipient wild type *Y. pestis* strain (231, I-3455 or I-2359) by conjugation. Elimination of the suicide vector and selection of *Y. pestis* clones were performed in the presence of 5% sucrose and chloramphenicol [30]. The chloramphenicol resistance gene was removed using pCP20 plasmid [31] (Figure). pCP20 plasmid was removed by culturing bacteria at 40°C in a medium containing 2.5 mM of calcium chloride overnight. Clones that had lost resistance to the both ampicillin (100  $\mu$ g/mL) and chloramphenicol (20  $\mu$ g/mL) were selected. The accuracy of recombination was monitored by a polymerase chain reaction.

## Microscopic studies and bacteriological assays

Microscopic studies, the rates of growth and lysis of cultures by plague bacteriophage L-413C, fibrinolytic

**Table 1.** Characteristics of the microorganism strains used in the study

| Strain                     | Characteristics   | Source of the strain and/or reference* |
|----------------------------|---|--|
| <i>Y. pestis</i>           |   |  |
| EV NIEG line               | pFra <sup>+</sup> pCad <sup>+</sup> pPst <sup>+</sup> $\Delta pgm$ (subsp. <i>pestis</i> bv. <i>orientalis</i> ), vaccine strain  | SCPM-Obolensk                          |
| 231                        | pFra <sup>+</sup> pCad <sup>+</sup> pPst <sup>+</sup> Pgm <sup>+</sup> (subsp. <i>pestis</i> bv. <i>antiqua</i> ), wild type  | SCPM-Obolensk                          |
| 231 $\Delta nlpD$          | $\Delta nlpD$ mutant of 231   | CS                                     |
| I-3455                     | pFra <sup>+</sup> pCad <sup>+</sup> pPst <sup>+</sup> Pgm <sup>+</sup> (subsp. <i>microtus</i> , bv. <i>altaica</i> )**, wild type  | CCIARISFE                              |
| I-3455 $\Delta nlpD$       | $\Delta nlpD$ mutant of I-3455  | CS                                     |
| I-2359                     | pFra <sup>+</sup> pCad <sup>+</sup> pPst <sup>+</sup> Pgm <sup>+</sup> (subsp. <i>microtus</i> , bv. <i>altaica</i> ), wild type  | CCIARISFE                              |
| I-2359 $\Delta nlpD$       | $\Delta nlpD$ mutant of I-2359  | CS                                     |
| <i>E. coli</i>             |   |  |
| DH5 $\alpha$ $\lambda pir$ | F <sup>-</sup> , $\lambda$ , <i>recA1</i> , <i>endA1</i> , <i>gyrA96</i> , <i>thi-1</i> , <i>hsdR17</i> ( <i>r<sub>K</sub></i> <sup>-</sup> , <i>m<sub>K</sub></i> <sup>+</sup> ), <i>supE44</i> , <i>recA1</i> | [27]                                   |
| S17-1 $\lambda pir$        | <i>thi pro hsdR hsdM<sup>+</sup> recA</i> RP4 2-Tc::Mu-Km::Tn7(Tp <sup>R</sup> Sm <sup>R</sup> Pm <sup>S</sup> )  | [28]                                   |

\* SCPM-Obolensk, State Collection of Pathogenic Microorganisms and Cell Cultures of the State Research Center for Applied Microbiology and Biotechnology (Rospotrebnadzor); CCIARISFE, Culture Collection of the Irkutsk Antiplague Research Institute of Siberia and Far East (Rospotrebnadzor).

\*\* Names of *Y. pestis* subspecies and biovars as proposed in [29].

and plasma-coagulase activities, pigmentation phenotype, and plasmid profile were assayed as described in [14, 32–34].

### Immunochemical studies

F1 titers in *Y. pestis* strains under study were determined by a passive hemagglutination test as described in [35].

Antibody titers against F1 and LcrV antigens in the sera of animals immunized for evaluation of the immunity index (see below) were determined by indirect ELISA on day 21 after subcutaneous administration of the constructed and control strains. Antibody titers were determined individually in five randomly selected animals in each group of 40 animals immunized with one of the constructed or control strains, followed by calculation of the mean titer in the group. The titer value was defined as the highest dilution of specific antisera that corresponded to the optical density of the substrate solution at a wavelength of 492 nm, which was 0.1 higher than the value observed for the same dilution of the control [36]. The difference between the theoretical and experimental values of  $A_{492}$  was calculated and plotted versus appropriate dilutions of antisera, which were fitted by a polynomial function.

### Safety of *Y. pestis* strains

The safety of the constructed *Y. pestis* strains in BALB/c mice and guinea pigs was assessed as described in [35]. Cultures of *Y. pestis* strains under study were administered subcutaneously to mice (18–20 g) at a dose of  $10^2$ ,  $10^3$ ,  $10^5$  and  $10^7$  CFU (10 mice per dose) and five guinea pigs (180–200 g) at a dose of  $1.5 \times 10^{10}$  CFU.

### Evaluation of immunogenic potency of vaccine candidates

was performed in accordance with the Methodological Guidelines [35]. The immunogenicity of the constructed strains was assessed by their  $\text{ImD}_{50}$  values. Guinea pigs (10 animals per group) were immunized subcutaneously in the upper third of the right femur by two-day-old agar cultures of the strains under study at doses of  $4 \times 10$ ,  $2 \times 10^2$ ,  $1 \times 10^3$  and  $5 \times 10^3$  CFU in a total volume of 0.5 mL. BALB/c mice (10 animals per group) were immunized subcutaneously with  $2 \times 10^2$ ,  $1 \times 10^3$ ,  $5 \times 10^3$  and  $2.5 \times 10^4$  CFU in a total volume of 0.2 mL. The animals were challenged in the upper third of the left femur on day 21 after subcutaneous immunization at a dose corresponding to 200 DCL ( $\text{LD}_{100}$ ) of a virulent *Y. pestis* strain (in our experiments, 1 DCL was equal to 10 CFU in mice and 100 CFU in guinea pigs). Infected animals were kept under observation for 20 days. Animals that succumbed to infection were sacrificed and examined bacteriologically.

**The intensity of immunity (immunity index)**, i.e., the vaccine's ability to protect animals against death after administration of high doses of virulent strains on day 21 after the immunization, was calculated using the following formula:

$$\text{II} = \frac{\text{LD}_{50\text{imm}}}{\text{LD}_{50\text{nai}}}, \quad (1)$$

where II is the immunity index;  $\text{LD}_{50\text{imm}}$  is  $\text{LD}_{50}$  for animals immunized with a strain under study, CFU; and  $\text{LD}_{50\text{nai}}$  is  $\text{LD}_{50}$  for naïve animals, CFU [35].

To determine the immunity index, the animals were immunized subcutaneously with two-day-old agar cultures of the constructed and control strains (40 guinea pigs and 40 mice per strain): guinea pigs at a dose of  $5 \times 10^3$  CFU in 0.5 mL, BALB/c mice at a dose of  $10^4$  CFU in 0.2 mL. On day 21 after the immunization, the animals were infected with a virulent *Y. pestis* 231 strain at four doses:  $10^2$ ,  $10^4$ ,  $10^6$ , and  $10^8$  CFU (guinea pigs in a volume of 0.5 ml, mice in a volume of 0.2 mL). Naïve (control) animals were simultaneously infected at doses of 1, 5, 25, and 125 CFU in the same volume as the immunized ones. Infected animals were kept under observation for 20 days. Animals that succumbed to infection were sacrificed and examined bacteriologically.

### Statistical methods

$\text{ImD}_{50}$  values of *nlpD* strains and  $\text{LD}_{50}$  of the virulent strain for immunized and naïve animals, as well as the corresponding confidence intervals (95% level of confidence), were calculated using the Kärber method [37].

## RESULTS

### Construction and characterization of *NlpD* variants of virulent *Y. pestis* strains

$231\Delta nlpD$ ,  $I-2359\Delta nlpD$ , and  $I-3455\Delta nlpD$  mutants without antibiotic resistance genes were obtained by site-directed mutagenesis of the *nlpD* gene in *Y. pestis* subsp. *pestis* strain 231 and two subsp. *microtus* bv. altaica strains I-2359 and I-3455, respectively, followed by deletion of the chloramphenicol resistance marker.

Microscope analyses of Gram-stained smears prepared from  $231\Delta nlpD$ ,  $I-2359\Delta nlpD$ , and  $I-3455\Delta nlpD$  strains revealed that culturing of the mutant strains at  $28^\circ\text{C}$  results in the formation of undivided chains containing an average of  $8.2 \pm 3.6$  cells/chain as opposed to aggregative morphology of cultures of the parent *Y. pestis* 231, I-2359, and I-3455 strains. Elevation of the culturing temperature to  $37^\circ\text{C}$  reduced the mean number of mutant cells per chain to  $4 \pm 2.5$  for  $\Delta nlpD$  mutants. The morphology of cells and cell clusters of the wild-type strains was temperature-independent. The

**Table 2.** Antibody response to administration of *Y. pestis* strains based on ELISA data

| Strains | Mean IgG titers (inverse values) |                      |                      |                    |
|---------|----------------------------------|----------------------|----------------------|--------------------|
|         | 231 $\Delta$ nlpD                | I-3455 $\Delta$ nlpD | I-2359 $\Delta$ nlpD | EV NIEG            |
|         | Guinea pigs                      |                      |                      |                    |
| Antigen |                                  |                      |                      |                    |
| F1      | 4435 $\pm$ 1625                  | 2650 $\pm$ 1045      | 130 $\pm$ 80         | 127630 $\pm$ 52830 |
| LcrV    | 1555 $\pm$ 840                   | 710 $\pm$ 260        | 920 $\pm$ 630        | 94390 $\pm$ 49290  |
|         | Mice                             |                      |                      |                    |
| Antigen |                                  |                      |                      |                    |
| F1      | 942560 $\pm$ 16620               | 9140 $\pm$ 1590      | 550 $\pm$ 95         | 310 $\pm$ 140      |
| LcrV    | 2465 $\pm$ 970                   | 6715 $\pm$ 1620      | 1580 $\pm$ 850       | 235 $\pm$ 85       |

growth rate of *Y. pestis* 231 $\Delta$ nlpD was identical to that of the parent strain at both 28 and 37°C.

The constructed  $\Delta$ nlpD mutants were lysed by the plague diagnostic bacteriophage L-413C. Based on the data of the passive hemagglutination test, the level of F1 capsular antigen in the mutants was 4–16 times higher than that in the culture of *Y. pestis* vaccine strain EV line NIEG grown under similar conditions (1–4  $\mu$ g/10<sup>9</sup> CFU and 0.25  $\mu$ g/10<sup>9</sup> CFU, respectively). These  $\Delta$ nlpD-mutants were not inferior to the EV strain in terms of their fibrinolytic and plasma coagulase activities. They contained the same three pFra, pCad, and pPst plasmids as the vaccine strain; however, they differed from the EV strain in their ability to absorb pigments.

#### Determination of safety of the strains

All strains of *Y. pestis* defective in the nlpD gene, 231 $\Delta$ nlpD, I-3455 $\Delta$ nlpD, and I-2359 $\Delta$ nlpD, as well as *Y. pestis* EV vaccine strain, were avirulent in mice upon subcutaneous administration to BALB/c mice (100% survived the infection at a dose of 10<sup>2</sup>, 10<sup>3</sup>, 10<sup>5</sup> and 10<sup>7</sup> CFU), and in guinea pigs (100% survival rate at a dose of 1.5 $\times$ 10<sup>10</sup> CFU). The animals were kept under observation for 50 days.

#### Antibody response to vaccine candidates

Levels of antibodies against *Y. pestis* F1 and LcrV in the blood of BALB/c mice were evaluated on day 21 after subcutaneous immunization with *Y. pestis* strain under study at a dose of 10<sup>4</sup> CFU (Table 2). Mean antibody titers against F1 and LcrV in the mouse sera after vaccination with cultures of *Y. pestis* 231 $\Delta$ nlpD and I-3455 $\Delta$ nlpD exceeded those obtained for *Y. pestis* I-2359 $\Delta$ nlpD and EV vaccine strain ( $p < 0.05$ ).

Titers of anti-F1- and anti-LcrV-antibodies in the blood of the vaccinated and control guinea pigs were determined on day 21 after subcutaneous immunization with *Y. pestis* strain under study at a dose of 5 $\times$ 10<sup>4</sup>

CFU (Table 2). According to our data, mean antibody titers against F1 and LcrV in the sera of guinea pigs after administration of the EV vaccine strain were two–three orders of magnitude higher than the values for the strains 231 $\Delta$ nlpD, I-3455 $\Delta$ nlpD, and I-2359 $\Delta$ nlpD ( $p < 0.05$ ). Antibody response to *Y. pestis* F1 and LcrV in guinea pigs after administration of the vaccine and constructed strains varied; in mice, the response was more uniform.

The levels of circulating anti-F1 and anti-LcrV antibodies in the blood of mice immunized with the vaccine-candidate strains *Y. pestis* 231 $\Delta$ nlpD and I-3455 $\Delta$ nlpD were significantly higher than those for guinea pigs immunized with the same strains.

In the control group, no antibodies against *Y. pestis* F1 and LcrV were detected after administration of an isotonic sodium chloride solution.

#### The protective efficacy of vaccine candidate strains

The indicators of immunogenic potency and immunity indices for BALB/c mice after a single immunization are presented in Table 3. For laboratory animals of this species, ImD<sub>50</sub> of *Y. pestis* 231 $\Delta$ nlpD and I-3455 $\Delta$ nlpD strains was 58 and 26 times lower than that of the EV vaccine strain, respectively; however, the value was 1.5 times higher for I-2359 $\Delta$ nlpD strain. The immunity indices for *Y. pestis* 231 $\Delta$ nlpD and I-3455 $\Delta$ nlpD were five orders of magnitude higher than that of the EV vaccine strain, but they were only 2.5 times higher for I-2359 $\Delta$ nlpD.

The opposite was observed for guinea pig models in immunogenic potency and immunity index experiments (Table 4). ImD<sub>50</sub> was 140, 66, and 1692 times higher for *Y. pestis* 231 $\Delta$ nlpD, I-3455 $\Delta$ nlpD, and I-2359 $\Delta$ nlpD strains, respectively, than for the EV vaccine strain. The immunity index of the EV vaccine strain was six orders of magnitude higher than that of the strains 231 $\Delta$ nlpD and I-3455 $\Delta$ nlpD and seven orders of magnitude higher than that of the strain I-2359 $\Delta$ nlpD.

**Table 3.** Indicators of immunogenic potency and intensity of immunity in BALB/c mice vaccinated with *nlpD* mutants of *Y. pestis* strains 231, I-3455, and I-2359

| Immunizing strain of <i>Y. pestis</i> | ImD <sub>50</sub> , CFU   | Immunity index  |                       |
|---------------------------------------|---|---|-----------------------|
|                                       |   | LD <sub>50</sub> upon challenging with <i>Y. pestis</i> 231, CFU          | II                    |
| 231Δ <i>nlpD</i>                      | 1.3 × 10 <sup>2</sup><br>(5.3 × 10 ÷ 3.4 × 10 <sup>2</sup> )              | 3.9 × 10 <sup>8</sup><br>(too large)                                      | 7.1 × 10 <sup>7</sup> |
| I-3455Δ <i>nlpD</i>                   | 2.9 × 10 <sup>2</sup><br>(1.2 × 10 <sup>2</sup> ÷ 7.5 × 10 <sup>2</sup> ) | 2.5 × 10 <sup>7</sup><br>(1 × 10 <sup>7</sup> ÷ 3.9 × 10 <sup>8</sup> )   | 4.5 × 10 <sup>7</sup> |
| I-2359Δ <i>nlpD</i>                   | 1.1 × 10 <sup>4</sup><br>(4.4 × 10 <sup>3</sup> ÷ 2.8 × 10 <sup>4</sup> ) | 2.5 × 10 <sup>3</sup><br>(6.3 × 10 <sup>2</sup> ÷ 3.9 × 10 <sup>3</sup> ) | 4.5 × 10 <sup>2</sup> |
| EV NIEG                               | 7.5 × 10 <sup>3</sup><br>(2.4 × 10 <sup>3</sup> ÷ 5.9 × 10 <sup>4</sup> ) | 1.0 × 10 <sup>3</sup><br>(2.5 × 10 <sup>2</sup> ÷ 3.9 × 10 <sup>3</sup> ) | 1.8 × 10 <sup>2</sup> |

**Table 4.** Indicators of immunogenic potency and intensity of immunity in guinea pigs vaccinated with *nlpD*-mutants of *Y. pestis* strains 231, I-3455, and I-2359

| Immunizing strain of <i>Y. pestis</i> | ImD <sub>50</sub> , CFU                   | Immunity index   |                       |
|---------------------------------------|---|--|-----------------------|
|                                       |   | LD <sub>50</sub> upon challenging with <i>Y. pestis</i> 231, CFU | II                    |
| 231Δ <i>nlpD</i>                      | 9.1 × 10 <sup>3</sup><br>(too large)      | 63<br>(1.6 × 10 ÷ 2.5 × 10 <sup>2</sup> )                        | 3.7                   |
| I-3455Δ <i>nlpD</i>                   | 4.3 × 10 <sup>3</sup><br>(too large)      | 158<br>(4.0 × 10 ÷ 6.3 × 10 <sup>2</sup> )                       | 9.3                   |
| I-2359Δ <i>nlpD</i>                   | 1.1 × 10 <sup>5</sup><br>(too large)      | 10<br>(3 ÷ 4.0 × 10)   | 0.59                  |
| EV NIEG                               | 65<br>(1.6 × 10 ÷ 2.6 × 10 <sup>2</sup> ) | 1.6 × 10 <sup>8</sup><br>(too large)                             | 9.4 × 10 <sup>6</sup> |

## DISCUSSION

To evaluate the universal applicability of a combination of attenuation and high immunogenicity of *Y. pestis* Δ*nlpD* mutants, site-directed mutagenesis was performed in three wild-type *Y. pestis* strains: one subsp. *pestis* bv. *antiqua* strain 231 and two subsp. *microtus* bv. *altaica* strains I-3455 and I-2359. Subsp. *microtus* strains, which include biovar *altaica* [29], are known to be virulent for mice, but avirulent for guinea pigs, rabbits, and humans [38, 39]. It is believed [40] that subsp. *microtus* strains possessing all protective antigens are avirulent for humans and can be used to design live plague vaccines. Furthermore, one of the strains used in our study, bv. *altaica* I-3455, produces LcrV with increased immunogenic/protective activity (due to the replacement of tryptophan at position 113 with glycine) [41].

In the Russian Federation all trials of attenuated *Y. pestis* vaccine candidate strains are conducted by comparing them to the reference *Y. pestis* vaccine strain EV line NIEG. According to [35], “the strain, proposed

as a vaccine, must match or surpass the reference vaccine strain in immunogenicity, match the control strain in safety and reactogenicity or be safer; however, some non-essential characteristics that define it as a member of *Y. pestis* species may be different from the reference strain.” “Non-essential characteristics” mean that “an experimental vaccine candidate strain must:

- be susceptible to the plague diagnostic bacteriophage L-413C;
- have typical culture-morphological properties;
- have F1 titer not lower than that obtained for the culture of the control *Y. pestis* EV strain, grown under similar conditions;
- have less than 0.3% calcium-independent mutants in the population of plague microbe cultures, which has been passaged through laboratory animals and exposed to neither long-term storage nor physical impact;
- at least match the fibrinolytic and plasma coagulase activities of the control strain;
- constructed and control strains must have pigmentation-negative phenotype; and

– the vaccine strains under study must have the same electrophoregram pattern as the reference EV strain: three bands of DNA plasmids corresponding to pFra (60 MD), pCad (47 MD), and pPst (6 MD)”. The first of the plasmids encodes the main *Y. pestis* immunogen, its capsular F1 antigen. The second one encodes a system that allows extracellularly located bacteria to neutralize the host cells involved in the immune response, Yop virulon, and the second immunodominant antigen LcrV involved in the virulon system; the third plasmid encodes the plasminogen activator responsible for dissemination of the plague microbe in host tissues [13].

The constructed *Y. pestis*  $\Delta nlpD$  mutants met most of the requirements for non-essential indicators of plague microbe vaccine strains [35]. They were susceptible to L-413C bacteriophage, the production of F1 in the mutant strains was 2–4 times higher than that in the EV strain, fibrinolytic and plasma coagulase activity in all strains were at the same level, and all strains contained a full set of the three classic *Y. pestis* plasmids.

The culture-morphological properties of  $\Delta nlpD$  mutants of the 231, I-3455, and I-2359 strains, such as their filamentous morphology, distinguish them from wild-type bacteria and the EV vaccine strain, which is in agreement with data [14] indicating that *Y. pestis* NlpD lipoprotein plays an important role in cell separation. Particular features of cell separation may be the main cause of attenuation in  $\Delta nlpD$  mutants.

The constructed strains preserved their ability to absorb pigments at the level of the wild-type strains, since their attenuation did not result from deletion of the *pgm* locus, but rather that of the *nlpD* structural gene.

In terms of compliance of  $\Delta nlpD$  mutants with the main selection criteria for *Y. pestis* vaccine strains, the degree of attenuation (safety) of NlpD<sup>-</sup> strains was not inferior to that of the EV strain in mice and guinea pigs. However, the second criterion, immunogenicity, was more ambiguous. This parameter was evaluated in two animal species in three independent tests: titers of antibodies against F1 and LcrV, determination of immunizing doses, which protect 50% of infected animals against death, and immunity indices.

Even though the antibody levels are only partially correlated with the protective efficacy of plague vaccines, the humoral immunity plays an important role in protection against the disease [42]. The data obtained demonstrate the development of an effective immune response in mice after administration of attenuated *Y. pestis* cultures; the  $\Delta nlpD$  strains were statistically sig-

nificantly superior to the EV vaccine strain. The opposite was observed in the experiments on guinea pigs; the vaccine strain was superior to  $\Delta nlpD$  mutants in its ability to induce an antibody response.

In a mouse model, *Y. pestis* strains 231 $\Delta nlpD$  and I-3455 $\Delta nlpD$  were statistically significantly superior to the EV strain in terms of ImD<sub>50</sub> and, especially, II values. In experiments on guinea pigs, the constructed strains were inferior to the vaccine strain and the immunity index in animals immunized with  $\Delta nlpD$  mutants was close to 1; i.e., it almost did not differ from this index in naïve animals.

The results of our experiments confirm the findings of other researchers showing that different animal species have different reactions to the same antigen/vaccine formulations [12, 43–48]. The differences in the protective efficacy of *Y. pestis* NlpD<sup>-</sup> mutants in guinea pigs and mice may be attributed to the peculiarities of immunogenesis in these biological models [2]. The lack of protective efficacy of  $\Delta nlpD$  mutants in guinea pigs can have at least two possible explanations.

On the one hand, attenuation by mutation in the *nlpD* gene may result in an excessive decrease in residual virulence [12, 49], and, therefore, the mutants are unable to replicate in the guinea pigs for a period of time long enough to induce immunity.

On the other hand, it is possible that NlpD lipoprotein of the plague pathogen is the insoluble “residual” antigen R or one of its constituents and that it induces potent long-term protection against the plague in guinea pigs [50–52]. Consequently, its absence in the cultures used for immunization may be the main reason for the weak protective properties of  $\Delta nlpD$  mutants.

We are currently conducting experiments to test these two hypotheses.

## CONCLUSIONS

To sum up the data obtained in this study, without additional modifications that would increase their immunogenicity in guinea pigs,  $\Delta nlpD$  mutants are not promising candidates for live plague vaccines due to the selectivity of their protective potency in different animal species. ●

*This research was conducted in the Laboratory for Plague Microbiology of the State Research Center for Applied Microbiology and Biotechnology as a part of government contracts No. 40-D of 30.05.2012, No. 34-D of 08.08.2013 within the framework of FTP “National System of Chemical and Biological Safety of the Russian Federation (2009-2014).”*

## REFERENCES

1. Naumov A.V., Ledvanov M.Yu., Drozdov I.G. *Immunologiya chumy* (Plague immunology). Saratov: Russian Research Anti-Plague Institute "Microbe", 1992. 172 p.
2. Dentovskaya S.V., Kopylov P.Kh., Ivanov S.A., Ageev S.A., Anisimov A.P. // *Mol. Genet. Microbiol. Virol.* 2013. V. 28. P. 87–98.
3. Feodorova V.A., Corbel M.J. *Expert Rev. Vaccines.* 2009. V. 8. P. 1721–1738.
4. Firstova V.V., Tyurin E.A., Kravchenko T.B., Zyrina E.V., Biketov S.F., Dyatlov I.A. // *Adv. Exp. Med. Biol.* 2012. V. 954. P. 173–177.
5. Li B., Du C., Zhou L., Bi Y., Wang X., Wen L., Guo Z., Song Z., Yang R. *Clin. Vaccine Immunol.* 2012. V. 19. P. 228–234.
6. Smiley S.T. // *Adv. Exp. Med. Biol.* 2007. V. 603. P. 376–386.
7. Smiley S.T. // *Immunol. Rev.* 2008. V. 225. P. 256–271.
8. Sun W., Roland K.L., Curtiss R. 3<sup>rd</sup>. *J. Infect. Dev. Ctries.* 2011. V. 5. P. 614–627.
9. Anisimov A.P., Molecular genetic mechanisms of formation and functional significance of *Yersinia pestis* capsule. Saratov: Russian Research Anti-Plague Institute "Microbe", Obolensk: State Research Center for Applied Microbiology, 1999.
10. Korobkova E.I. *Zhivaya protivochumnaya vaksina* (Live antiplague vaccine). Moscow: Medgiz, 1956. 208 p.
11. Girard G. // *Biol. Med. (Paris).* 1963. V. 52. P. 631–731.
12. Meyer K.F., Smith G., Foster L., Brookman M., Sung M. // *J. Infect. Dis.* 1974. V. 129 (Suppl. 1). P. S85–S120.
13. Perry R.D., Fetherston J.D. // *Clin. Microbiol. Rev.* 1997. V. 10. P. 35–66.
14. Tidhar A., Flashner Y., Cohen S., Levi Y., Zauberman A., Gur D., Aftallon M., Elhanany E., Zvi A., Shafferman A., Mamroud E. // *PLoS One.* 2009. V. 4: e7023.
15. Braciale V.L., Nash M., Sinha N., Zudina I.V., Motin V.L. Correlates of Immunity Elicited by Live *Yersinia pestis* Vaccine. *National Institute of Allergy and Infectious Diseases, NIH. Volume 1, Frontiers in Research.* Edited by: Vassil St. Georgiev. Totowa, NJ: Humana Press Inc., 2007: 473–480.
16. Derbise A., Cerdà Marín A., Ave P., Blisnick T., Huerre M., Carniel E., Demeure C.E. // *PLoS Negl Trop Dis.* 2012. V. 6: e1528.
17. Rosenzweig J.A., Chopra A.K. // *Expert Rev. Vaccines.* 2012. V. 11 P. 659–661.
18. Sha J., Agar S.L., Baze W.B., Olano J.P., Fadl A.A., Erova T.E., Wang S., Foltz S.M., Suarez G., Motin V.L., et al. // *Infect Immun.* 2008. V. 76. P. 1390–1409.
19. Zhang X., Qi Z., Du Z., Bi Y., Zhang Q., Tan Y., Yang H., Xin Y., Yang R., Wang X. // *Vaccine.* 2013. V. 31. P. 2539–2542.
20. Flashner Y., Mamroud E., Tidhar A., Ber R., Aftalion M., Gur D., Lazar S., Zvi A., Bino T., Ariel N., et al. // *Infect. Immun.* 2004. V. 72. P. 908–915.
21. Garbom S., Forsberg A., Wolf-Watz H., Kihlberg B.M. // *Infect. Immun.* 2004. V. 72. P. 1333–1340.
22. Rappuoli R. // *Curr. Opin. Microbiol.* 2000. V. 3. P. 445–450.
23. Sun W., Roland K.L., Branger C.G., Kuang X., Curtiss R. // *PLoS One.* 2009. V. 4: e6720.
24. Oyston P.C., Mellado-Sanchez G., Pasetti M.F., Nataro J.P., Titball R.W., Atkins H.S. // *Microb. Pathog.* 2010. V. 48. P. 191–195.
25. Padmalayam I., Kelly T., Baumstark B., Massung R. // *Infect. Immun.* 2000. V. 68. P. 4972–4979.
26. Sha J., Kirtley M.L., van Lier C.J., Wang S., Erova T.E., Kozlova E.V., Cao A., Cong Y., Fitts E.C., Rosenzweig J.A., Chopra A.K. // *Infect Immun.* 2013. V. 81. P. 815–828.
27. Woodcock D., Crowther P., Doherty J., Jefferson S., De Cruz E., Noyer-Weidner M., Smith S., Michael M., Graham M. // *Nucleic Acids Res.* 1989. V. 17. P. 3469–3478.
28. Simon R., Priefer U., Pulher A. // *Biotechnology.* 1983. V. 1. P. 784–791.
29. Platonov M.E., Evseeva V.V., Dentovskaya S.V., Anisimov A.P. // *Mol. Genet. Microbiol. Virol.* 2013. V. 28 P. 41–45.
30. Datsenko K., Wanner B. // *Proc. Natl. Acad. Sci. USA.* 2000. V. 97. P. 6641–6645.
31. Donnenberg M.S., Kaper J.B. // *Infect. Immun.* 1991. V. 59. P. 4310–4317.
32. Filippov A.A., Solodovnikov N.S., Kookleva L.M., Prot-senko O.A. // *FEMS Microbiol Lett.* 1990. V. 55. P. 45–48.
33. Filippov A.A., Sergueev K.V., He Y., Huang X.Z., Gnade B.T., Mueller A.J., Fernandez-Prada C.M., Nikolich M.P. // *PLoS One.* 2011. V. 6: e25486.
34. Bahmanyar M., Cavanaugh D.C. *Plague manual.* Geneva: WHO, 1976. 78 p.
35. Anisimova T.I., Sayapina L.V., Sergeeva G.M., Isupov I.V., Beloborodov R.A., Samoilova L.V., Anisimov A.P., Ledvanov M.Y., Shvedun G.P., Zadumina S.Y. et al. Main requirements for vaccine strains of the plague pathogen: Methodological Guidelines MU 3.3.1.1113-02 (approved by the Main State Health Officer of Russian Federation on 02.03.2002). Moscow, 2002. 69 p.
36. Qiu Y., Liu Y., Qi Z., Wong W., Kou Z., Zhang Q., Liu G., Yang X., Xin Y., Li C. et al. *Scandinavian Journal of Immunology.* 2010. V. 72. P. 425–433.
37. Finney D.J. *Statistical method in biological assay*, 3<sup>rd</sup> Ed. London: Charles Griffin, 1978. 508 p.
38. Anisimov A.P., Lindler L.E., Pier G.B. Intraspecific diversity of *Yersinia pestis* Clin. Microbiol. Rev. 2004. V. 17. P. 434–464.
39. Song Y., Tong Z., Wang J., Wang L., Guo Z., Han Y., Zhang J., Pei D., Zhou D., Qin H. et al. *DNA Res.* 2004. V. 11. P. 179–197.
40. Zhou D., Tong Z., Song Y., Han Y., Pei D., Pang X., Zhai J., Li M., Cui B., Qi Z. et al. // *J. Bacteriol.* 2004. V. 186. P. 5147–5152.
41. Kopylov P.Kh., Bakhteeva I.V., Anisimov A.P., Dentovskaya S.V., Ivanov S.A., Kiseleva N.V., Levchuk V.P., Panfertsev E.A., Platonov M.E., Svetoch T.E. et al. Russian patent RUS 2439155 C1, C12N15/10, C07H21/00, C12N15/70, C12N1/21, C12P21/00, C12R1/19, 2010.
42. Bashaw J., Norris S., Weeks S., Trevino S., Adamov-icz J.J., Welkos S. // *Clin. Vaccine Immunol.* 2007. V. 14. P. 605–616.
43. Byvalov A.A., Pautov V.N., Chicherin Iu.V., Lebedinskiĭ V.A., Evstigneev V.I. // *Zh. Mikrobiol. Epidemiol. Immunobiol.* 1984. № 4. P. 74–76.
44. Burrows T.W. // *Nature.* 1957. V. 179. P. 1246–1247.
45. Hallett A.F., Issacson M., Meyer K.F. // *Infect. Immun.* 1973. V. 8. P. 876–881.
46. Jones S.M., Griffin K.F., Hodgson I., Williamson E.D. // *Vaccine.* 2003. V. 21. P. 3912–3918.
47. Von Metz E., Eisler D.M., Hottle G.A. // *Appl. Microbiol.* 1971. V. 22. P. 84–88.
48. Welkos S., Pitt M.L.M., Martinez M. Friedlander A., Vogel P., Tammariello R. // *Vaccine.* 2002. V. 20. P. 2206–2214.
49. Miranda K.L., Poester F.P., Minharro S., Dorneles E.M., Stynen A.P., Lage A.P. // *Vaccine.* 2013. V. 31. P. 3014–3018.
50. Brubaker R.R. // *Curr. Top. Microbiol. Immunol.* 1972. V. 57. P. 111–158.
51. Meyer K.F. // *J. Immunol.* 1950. V. 64. P. 139–163.
52. Schütze H. // *Br. J. Exp. Pathol.* 1939. V. 19. P. 293–298.

# Interaction with Serum Albumin As a Factor of the Photodynamic Efficacy of Novel Bacteriopurpurinimide Derivatives

A. V. Akimova<sup>1\*</sup>, G. N. Rychkov<sup>2,3</sup>, M. A. Grin<sup>4</sup>, N. A. Filippova<sup>5</sup>, G. V. Golovina<sup>1</sup>, N. A. Durandin<sup>1</sup>, A. M. Vinogradov<sup>1</sup>, T. A. Kokrashvili<sup>6</sup>, A. F. Mironov<sup>4</sup>, A. A. Shtil<sup>5</sup>, V. A. Kuzmin<sup>1</sup>

<sup>1</sup>N.M. Emanuel Institute of Biochemical Physics, Kosygina Str., 4, Moscow, 119334, Russia

<sup>2</sup>Petersburg Nuclear Physics Institute, Orlova Roscha, Gatchina, Leningrad district, 188300, Russia

<sup>3</sup>St.Petersburg State Polytechnical University, Politekhnicheskaya Str., 29, St. Petersburg, 195251, Russia

<sup>4</sup>M.V. Lomonosov Moscow State University of Fine Chemical Technologies, Prospekt Vernadskogo, 86, Moscow, 119571, Russia

<sup>5</sup>N.N. Blokhin Russian Cancer Research Center, Kashirskoe Shosse, 24, Moscow, 115478, Russia

<sup>6</sup>Georgian Technical University, Kostava Str., 77, Tbilisi, 0175, Georgia

\*E-mail: alexa\_karpenko@mail.ru

Received 21.02.2014

Copyright © 2015 Park-media, Ltd. This is an open access article distributed under the Creative Commons Attribution License, which permits unrestricted use, distribution, and reproduction in any medium, provided the original work is properly cited.

**ABSTRACT** Optimization of the chemical structure of antitumor photosensitizers (PSs) is aimed at increasing their affinity to a transport protein, albumin and irreversible light-induced tumor cell damage. Bacteriopurpurinimide derivatives are promising PSs thanks to their ability to absorb light in the near infrared spectral region. Using spectrophotometry, we show that two new bacteriopurpurinimide derivatives with different substituents at the N atoms of the imide exocycle and the pyrrole ring A are capable of forming non-covalent complexes with human serum albumin (HSA). The association constant (calculated with the Benesi-Hildebrand equation) for N-ethoxybacteriopurpurinimide ethyloxime (compound 1) is higher than that for the methyl ether of methoxybacteriopurpurinimide (compound 2) ( $1.18 \times 10^5 \text{ M}^{-1}$  vs.  $1.26 \times 10^4 \text{ M}^{-1}$ , respectively). Molecular modeling provides details of the atomic interactions between 1 and 2 and amino acid residues in the FA1 binding site of HSA. The ethoxy group stabilizes the position of 1 within this site due to hydrophobic interaction with the protein. The higher affinity of 1 for HSA makes this compound more potent than 2 in photodynamic therapy for cultured human colon carcinoma cells. Photoactivation of 1 and 2 in cells induces rapid (within a few minutes of irradiation) necrosis. This mechanism of cell death may be efficient for eliminating tumors resistant to other therapies.

**KEYWORDS** photosensitizers, albumin, association constant, photodynamic therapy, cancer, necrosis.

**ABBREVIATIONS** DMSO – dimethyl sulfoxide; PB – phosphate buffer; PDT – photodynamic therapy; PS – photosensitizer; HSA – human serum albumin.

## INTRODUCTION

The biological effect of exogenous photoactivatable chemical compounds on the cells of prokaryotes and eukaryotes is determined by the formation of reactive species and induction of numerous processes, finally resulting in cell death [1, 2]. This mechanism is used in photodynamic therapy (PDT) for tumors and non-neoplastic and infectious diseases [3–5]. Compounds containing tetrapyrrole macrocycles: porphyrins and their hydrogenated analogues, such as chlorins and bacteriochlorins, are the most frequently used photosensitizers (PSs) in PDT [3].

Structural optimization of PSs, aimed at improving their clinical efficacy, includes the following directions. First, photodamage of deep tissue layers

in the lesion should be achieved. For this purpose, bacteriochlorophyll *a* derivatives that absorb light in the longer wavelength range (near the infrared region) of the spectrum are, in particular, used [6–9]. Second, PS should interact with transport proteins, mainly albumins (human serum albumin, HSA), to be efficiently delivered to the pathologic nidus. Increasing the binding affinity can be achieved by introduction of metal cations into the macrocycle and modification of peripheral substituents [10–15]. In addition to the transport function, complexes of HSA with Pd-containing bacteriochlorin act as photocatalytic oxidoreductases, significantly increasing the yield of active oxygen species and the photodynamic effect [2].

Finally, the ability of PSs to cause irreversible photodamage (death) to cells that are resistant to other therapeutic modalities is important. This ability is particularly important in cases where application of other treatment methods is impossible (impossibility of radical surgical treatment, residual tumor after combination therapy, etc.). Photoinduced cell death can occur via the necrotic mechanism. A distinctive feature of this mechanism is primary irreversible damage of the plasma membrane and membrane organelles [5].

The aim of this study was to explore the quantitative parameters characterizing binding of HSA with two bacteriopurpurinimide derivatives that differ from each other by peripheral substituents. These parameters are considered as an efficacy factor of induction of tumor cell photo necrosis.

## EXPERIMENTAL

Bacteriopurpurinimide derivatives with various substituents at the nitrogen atom in the imide exocycle (**1** – ethoxy group and **2** – methoxy group) and the pyrrole ring A (**1** – N-ethoxy group, and **2** – N-hydroxy group) (Fig. 1) were studied. The compounds were prepared by treating bacteriopurpurine with ethoxy amine (**1**) [16] and hydroxylamine (**2**), followed by methylation with diazomethane [17], dissolved in dimethyl sulfoxide (DMSO; Marbiopharm, Russia) to a concentration of 10 mM, and stored at 4 °C. The concentrations of **1** and **2** were determined based on the known extinction coefficients for chloroform [16, 17].

To study the association, HSA (Sigma Aldrich, USA) was dissolved in a 20 mM phosphate buffer (PB), pH 7.0. The concentrations of **1** and **2** were  $1 \times 10^{-5}$  M, and the concentration of HSA was  $0 - 5 \times 10^{-4}$  M. Stock solutions of compounds **1** and **2** in dimethyl sulfoxide (DMSO) were added to PB. The final concentration of DMSO in the tested samples was 1%.

The absorption spectra of the tested solutions were measured on a Shimadzu UVVIS3101PC (Japan) spectrophotometer, using quartz cells ( $0.4 \times 1.0$  cm) with an optical path length of 1 cm (spectral slit width was 1 nm). The absorption spectra of the dyes in the presence of HSA were recorded in the range of 380–950 nm.

The binding constants of **1** and **2** and HSA were determined based on the change in optical density at the Q-band maximum of a dye associated with HSA, by adding the protein to a solution of **1** or **2**. The required parameters were calculated with the Benesi-Hildebrand equation [18]:

$$\frac{1}{dD} = \frac{1}{\Delta\epsilon[l]} + \frac{1}{K_c(\Delta\epsilon[l])} \cdot \frac{1}{[HSA]}, \quad (1)$$

where  $dD$  is the change in the solution optical density without and with HSA, measured at the absorption

peak of the protein complex;  $\Delta\epsilon$  is the change in the molar extinction coefficient value in the absence and presence of HSA;  $K_c$  is the binding constant;  $[l]$  is the concentration of a ligand **1** or **2**; and  $[HSA]$  is the HSA concentration.

The photosensitizing activity of **1** and **2** was studied in the HCT116 (human colon cancer) cell line. Cells were cultured in Dulbecco's modified Eagle's medium supplemented with 5% fetal calf serum, 2 mM L-glutamine, 100 µg/mL streptomycin, and 100 U/mL penicillin (PanEco, Russia) at 37 °C in a humidified atmosphere of 5% CO<sub>2</sub>. Cells were plated in 35 mm Petri dishes ( $2 \times 10^4$  cells in 3 mL of culture medium). After 16 h, compound **1** or **2** (final concentrations are provided in the Results section) was added and incubation was continued at 37 °C for 30 min. The culture medium was removed, and the cell monolayer was washed out with PB and irradiated with the red light through the 1 cm water filter (saturated aqueous solution of NaNO<sub>2</sub>). A tungsten lamp was used as a light source. The irradiation period was up to 20 min. Cultures irradiated in the absence of **1** or **2**, as well as cells loaded with these compounds but not subjected to irradiation (dark exposure), were used as the control. The integrity of the cells was evaluated by the trypan blue exclusion test.

For the purpose of an electron microscopy analysis, HCT116 line cells were plated onto 60-mm Petri dishes ( $10^5$  cells in 5 mL of culture medium). Addition of **1** or **2** and irradiation of the cells were carried out by the method described above. Next, the cells were detached from the substrate using versene and trypsin and fixed with a 1% glutaraldehyde solution in PB. Samples were analyzed with a Shimadzu electronic microscope (Japan).

Rough spatial molecular models of **1** and **2** were generated using the Molsoft ICM version 3.7 [19] and Avogadro [20] software, based on the structure of purpurin *a* taken from the ChemSpider database (www.chemspider.com) (record number: 16736724 of 08.15.2013). Optimization of their structures was carried out using the Gamess US program [21]. The electronic state multiplicity of molecules was taken equal to 1, and molecular charge was neutral. The structure was optimized according to a standard protocol using the quadratic approximation and Huzinaga's minimal basis set [22]. Self-consistent field wave functions were calculated using the restricted Hartree-Fock method [23].

The spatial structure 1N5U [24] deposited in the Protein Data Bank was used as an initial model of HSA. Molecules of myristic acid, protoporphyrin IX, and water were removed from the structure of HSA prior to flexible docking, and each atom of **1** and **2** was charged according to *ab initio* calculations following geometry

optimization. Flexible docking was performed using the Molsoft ICM Pro 3.7 package according to the protocol described in detail by the software developers [19, 25, 26]. Docking was run three times, starting from different initial positions and conformations of **1** and **2** and HSA. The resulting ensemble of conformations was used to calculate an average binding free energy ( $E_c$ ) according to the Gibbs-Boltzmann formula:

$$E_c = \sum_n E_n \frac{e^{-\frac{E_n}{kT}}}{Z}, \quad (2)$$

where  $Z$  is the partition function for the binding free energy of ligands  $E_n$  from the ensemble at temperature  $T = 300$  K. Only the contributions of electrostatic and hydrophobic components, as well as the entropy contribution of the amino acid side chains of the protein, were taken into account upon calculation of the binding free energy. The electrostatic component was calculated using the REBEL method [27]. According to the recommendations of the software developers, the dielectric constants of HSA, **1**, **2**, and the complexes were set equal to 12.7; the dielectric constant of implicit solvent, was set equal to 78.5. The hydrophobic component of each atom was estimated based on an assumption of its linear proportionality to the atom's solvent accessible surface area. The atomic solvation parameter was set equal to 0.012 kcal/(mol  $\times$   $\text{\AA}^2$ ). The loss of configurational entropy of protein amino acid side chains upon binding to **1** or **2** was determined using maximal possible entropy read from the program's residue library [28].

## RESULTS

### Spectrophotometry

Figure 2 demonstrates the absorption spectra of bacteriopurpurinimide derivatives **1** and **2** in the absence and presence of HSA. The absorption bands of **1** in PB correspond to 539 and 899 nm. The lack of a band at 899 nm in ethanol and chloroform (data not shown) indicates that this band corresponds to the J-aggregate [28]. Compound **2** in PB is characterized by absorption bands at 421, 550, and 800 nm. The absence of additional bands relative to ethanol and chloroform indicates that compound **2** does not form J-aggregates in PB.

Transformation of the main absorption bands of both compounds was observed upon addition of HSA. In the case of **1**, this was reflected in the reduction in the intensity of the band at 899 nm, increase in the intensity of the band at 539 nm, and appearance of bands at 419 and 802 nm; the latter probably corresponds to the monomer of **1** (Fig. 2A). These results suggest the formation of molecular complexes between **1** and HSA. The spectra intersect at the isobestic point, indicating

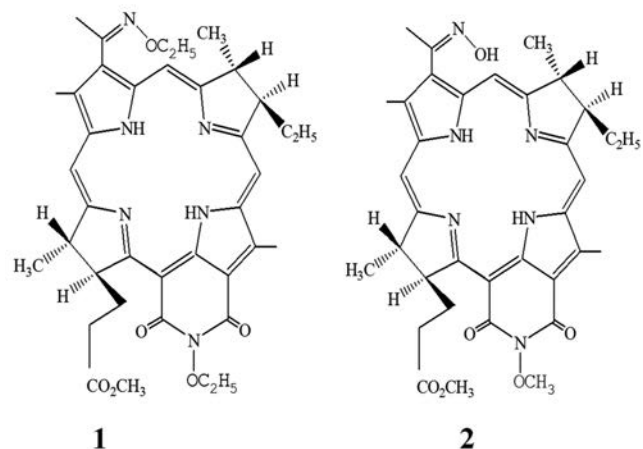


Fig. 1. Structures of compounds **1** and **2**

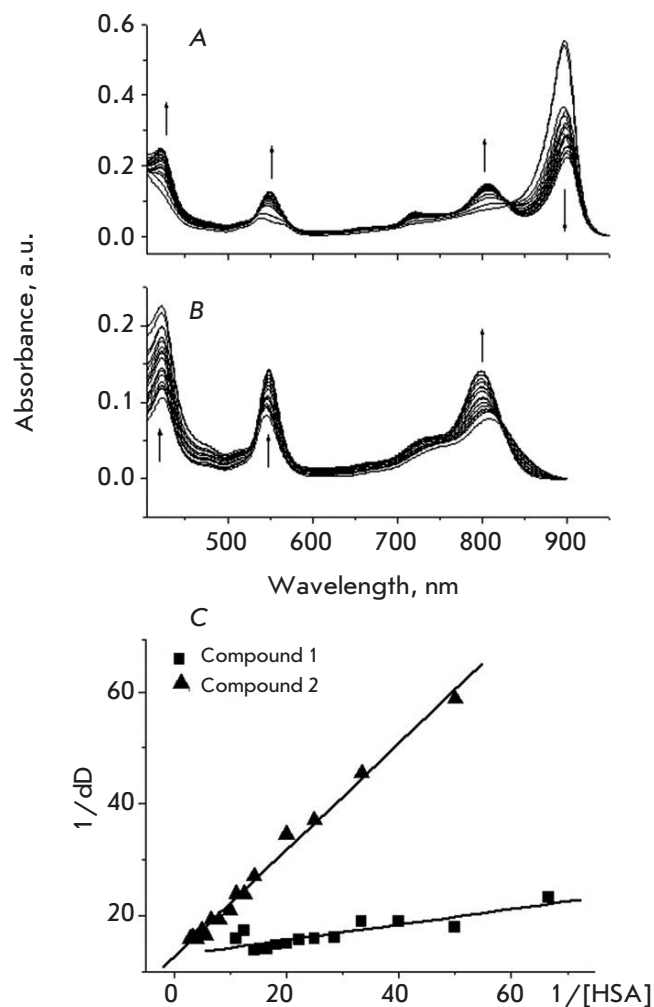
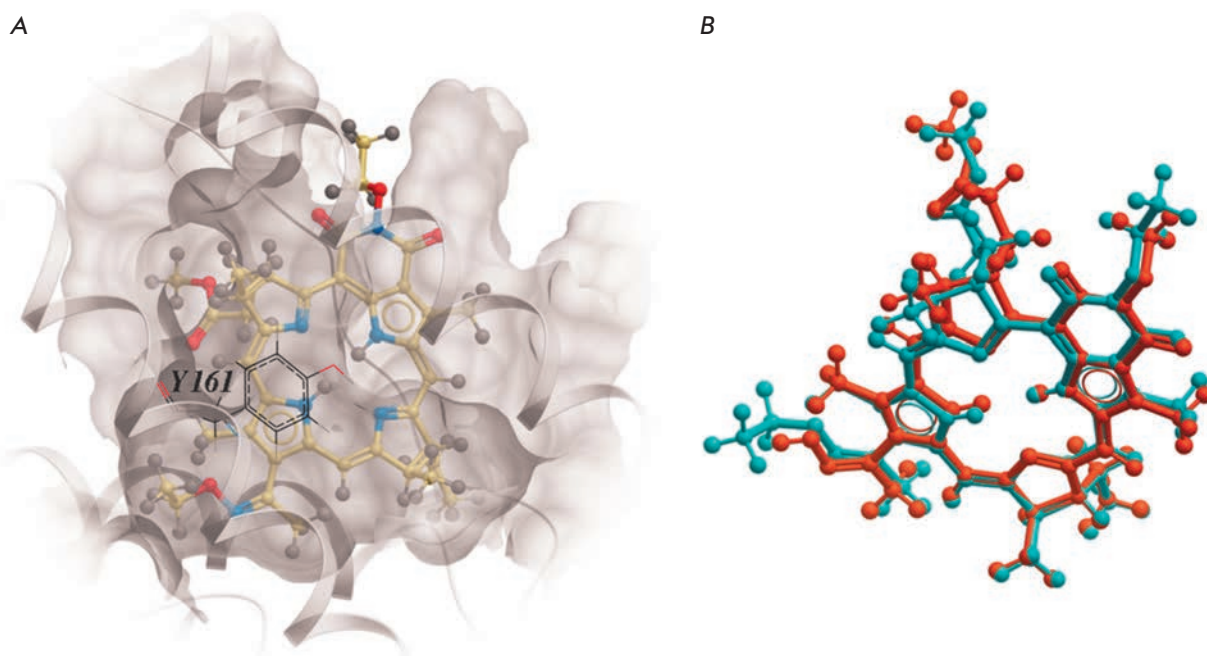


Fig. 2. Absorption spectra of compounds **1** (A) and **2** (B) at different HSA concentrations (20 mM PB, pH 7.0). The Benesi-Hilbedrand plots for complexes of **1** or **2** with HSA (C). Arrows indicate the direction of spectral changes upon HSA addition



**Fig. 3.** (A) The most probable pose of **1** in the FA1 binding site of HSA determined by flexible molecular docking. The position of Tyr161 is depicted in the foreground. (B) The most probable conformations of **1** and **2** in the binding site are shown. Compound **1** is shown in blue-green and **2** in orange. The macrocycles of both compounds have the same spatial arrangement

equilibrium in the monomer-aggregate system. Therefore, the monomer-aggregate equilibrium shifts towards the monomer as the protein concentration is increased. The obtained result is consistent with the data on the dissociation of aggregates upon complexation of porphyrin derivatives with albumin [29].

Figure 2B shows the absorption spectra of **2** in the presence of HSA. The optical density of the peaks at 422, 545, and 808 nm increases as the protein concentration rises. A 10-nm hypsochromic shift of the long wavelength maximum is observed. The band with a maximum at 545 nm undergoes a 3.5-nm bathochromic shift to 548.5 nm. The changes in the absorption spectra in the presence of HSA suggest its association with **2**, and the isosbestic point at 835 nm indicates one equilibrium in the monomer-albumin complex and the formation of a stable complex between monomer **2** and HSA.

The Benesi-Hildebrand plots for **1** and **2** and HSA are presented in Figure 2C. The association constant for compound **1** and HSA is  $1.18 \times 10^5 \text{ M}^{-1}$ , whereas this parameter for **2** is significantly lower,  $1.26 \times 10^4 \text{ M}^{-1}$ ; i.e., the affinity of compound **1** to HSA is an order of magnitude higher than that to the complex formed by **2** and HSA.

### Molecular modeling

HSA binding site for heme-like molecules (FA1) is a narrow and quite deep hollow on the surface of the

subdomain 1B, formed mainly by hydrophobic amino acid residues [30]. According to the results of flexible docking, compounds **1** and **2** are located within the FA1 site in poses similar to that of protoporphyrin IX in the 1N5U crystal structure (Protein Data Bank) (Fig. 3A). As these poses have the lowest free energy of binding,  $E_C$ , they are the most probable ones. The macrocycle of both compounds effectively “hides” the surface of its hydrophobic groups within the hollow. The hydroxyl group of Tyr161 is located near the macrocycle’s center. However, the macrocycle is shifted by approximately 1 Å towards the entrance to the binding site compared to protoporphyrin IX. The results of molecular modeling demonstrate that unlike **1** the conformational diversity of **2** in the FA1 binding site of HSA is wider. However, the conformations of both compounds having the highest value of the scoring function are almost match (Fig. 3B).

Importantly, in this conformation, the hydroxyl group of the pyrrole ring A of compound **2** occurs in the hydrophobic environment formed by Leu135, Leu139, and Ala168 residues and an aliphatic part of Tyr161 within the binding site (Fig. 4B), losing the energetically favorable hydrogen bond. Therefore, it is unlikely that this conformation will be realized in the interaction between **2** and HSA. In turn, the ethoxy group of the pyrrole ring of **1** forms an energetically favorable tight hydrophobic contact with HSA in this locus (Fig. 4A).

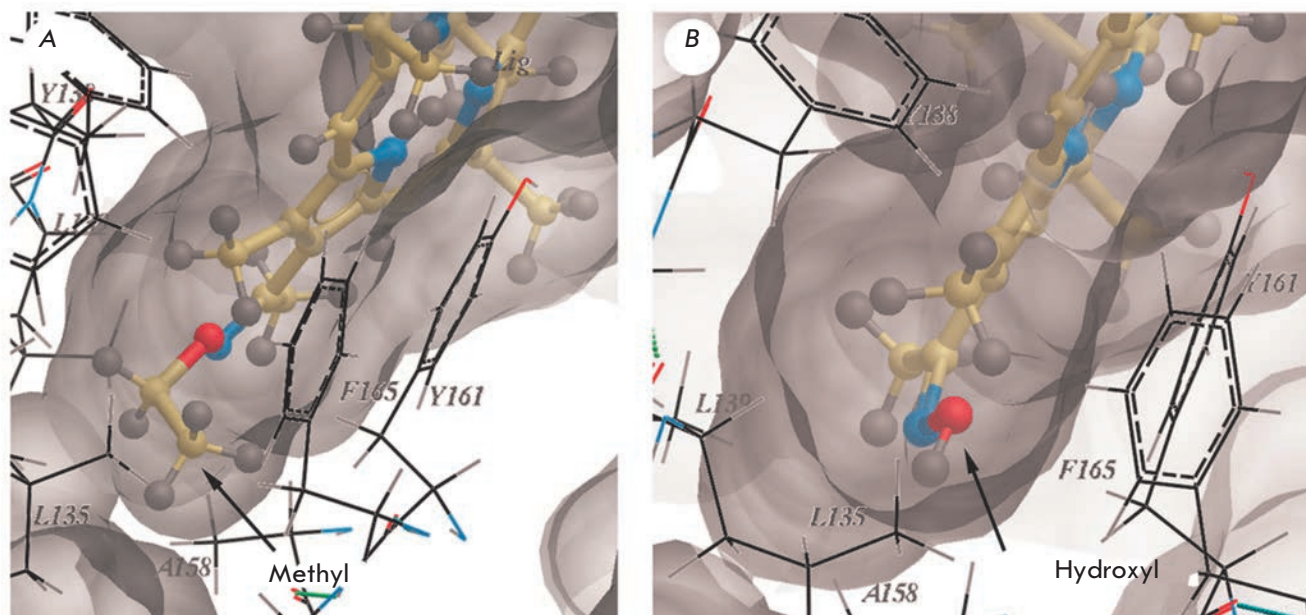


**Fig. 4.** Poses of **1** and **2** in the FA1 binding site. The poses of compounds with the maximum scoring function value are shown. The FA1 binding site is displayed as a grey molecular surface. The compounds are presented as a ball-and-stick model. Carbons are shown in beige, hydrogens in grey, nitrogens in blue, and oxygens in red. The non-polar methyl group of **1** (A) and the polar hydroxyl group of **2** (B) occur in the hydrophobic microenvironment

The average binding free energy to HSA is  $-10.5$  kcal/mol for compound **1** and  $-9.3$  kcal/mol for compound **2** (excluding the indicated conformations). These values correlate well with the association constants obtained experimentally for compounds **1**, **2** and HSA (Fig. 2).

#### Photodynamic activity in cell culture

Without irradiation, compounds **1** and **2** at concentrations of up to  $50$   $\mu\text{M}$  caused no death of HCT116 line cells under continuous exposure for 72 h. On the contrary, the photosensitizing ability of **1** and **2** was high: the micromolar concentrations of **1** or **2** were sufficient to induce cell damage. After 15 min of irradiation of cells treated with either of the two tested compounds, the fraction of damaged cells amounted to 100% for **1** and 57.8% for **2** (Fig. 5A). After incubation with  $1$   $\mu\text{M}$  of each PS, the fraction of dead cells increased as the irradiation time was elongated up to 20 min (for **1**), whereas the percentage of dead cells in the case of compound **2** did not increase after irradiation for 10–15 min (Fig. 5B). Almost complete loss of the culture was observed after 10 min of exposure to light after incubation of the cells with  $5$   $\mu\text{M}$  of compound **1** (Fig. 5C).

#### Electron microscopy

For the purpose of a detailed investigation of the cell death mechanism, we analyzed the ultrastructure of

dying cells by transmission electron microscopy. Figure 6A–C presents the results of electron microscopy of HCT116 cells irradiated in the absence of PS (control) or after incubation with **1**. In the control cells (Fig. 6A), the cell membranes formed microvilli, which are typical of the intestinal epithelium, at the free surfaces. Mitochondria, cisterns of the endoplasmic reticulum, ribosomes, and vesicles of the Golgi complex were observed in the cytoplasm. Chromatin was diffusely distributed over the nucleus, with denser clusters located mainly on the periphery. The nuclei were round with shallow invaginations of the nuclear membrane.

After 10 min of irradiation of cells loaded with compound **1**, swelling of mitochondria and a reduction in their matrix density were observed (Fig. 6B). Mitochondria with damaged cristae and a “washed out” matrix, lipid droplets, and a small expansion of the endoplasmic reticulum cisternae appeared there. Most cells had an irregular shape due outgrowths on the cell membranes. The integrity of the cell membranes was retained. The amount of chromatin in the nuclei was decreased, and the regions of dense fibrillar component in the nucleoli were increased. After 20 min of irradiation, the number of lysosomes and lipid inclusions in the cytoplasm was increased and the amount of chromatin in the nuclei was decreased. A significant number of cells were destroyed (Fig. 6C).

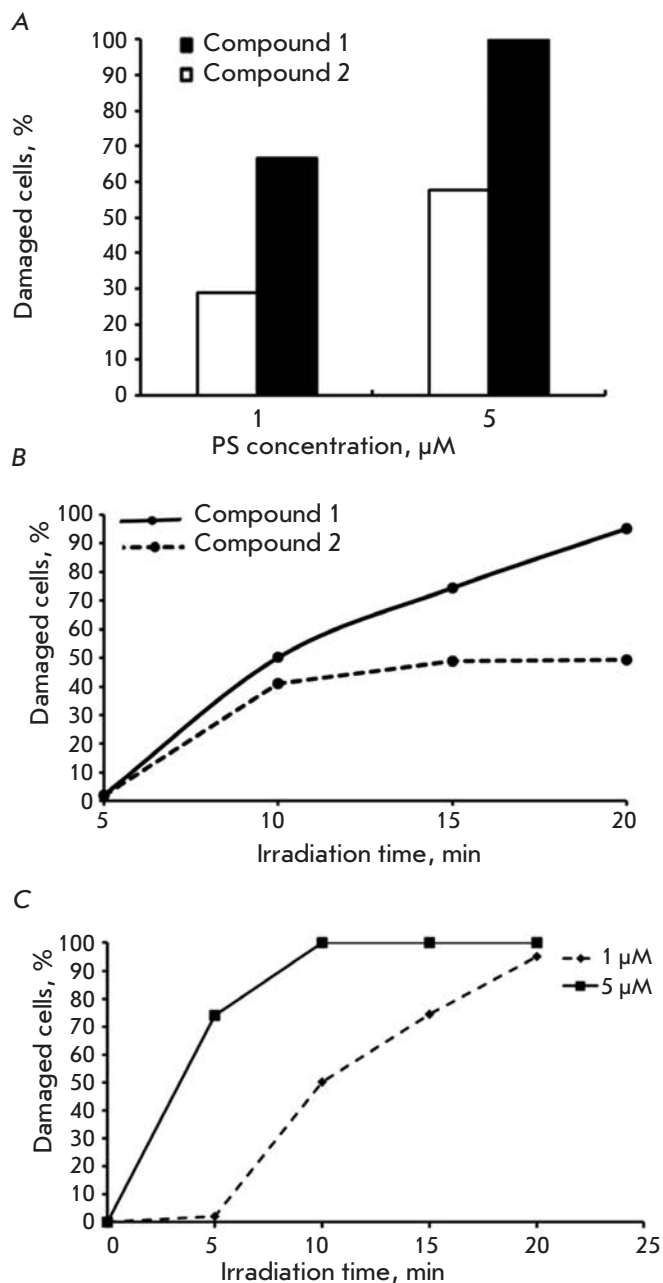


**Fig. 5.** Dependence of HCT116 cell photodamage on the PS concentration and irradiation time. (A) 15 min irradiation; (B) 1  $\mu\text{M}$  **1** or **2**; (C) compound **1**

## DISCUSSION

The modification of peripheral substituents in the bacteriopurpurinimide molecule was found to alter significantly the photodynamic efficacy of PS. The bacteriopurpurinimide derivative with ethoxy groups at nitrogen atoms in the exocycle and pyrrole ring A (compound **1**) forms stronger complexes with the transport protein HSA. These results were obtained

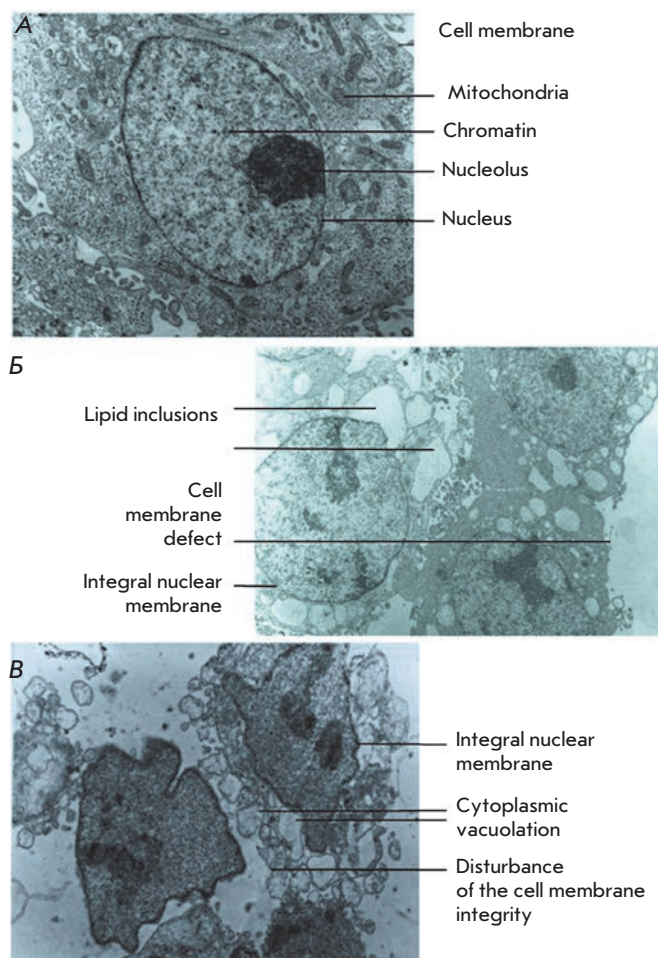


**Fig. 6.** Ultrastructural signs of HCT116 cell photodamage. (A) control cells (irradiated in the absence of **1**); (B) 10 min irradiation; (C) 20 min irradiation. In (B) and (C) cases, cells were loaded with 1  $\mu\text{M}$  **1** prior to irradiation. 5,000 $\times$  magnification

experimentally and confirmed by molecular modeling of the PS-HSA complexes. Reduced affinity of compound **2** for HSA is caused by occurrence of its oxime hydroxyl group in the hydrophobic environment upon binding within the FA1 site. In this case the energetically favorable hydrogen bond with water is lost, which weakens binding to the protein. Conversely, the ethoxy group of compound **1** promotes stronger binding to the protein due to hydrophobic interactions.

Compounds **1** and **2** appear to be highly active PSs: micromolar concentrations and brief incubation were sufficient to induce cell death. It is important that a higher association constant for compound **1** and HSA corresponded to a higher photoactivity of this PS in the cell culture. The effect of peripheral substituents

on photoactivity parameters such as accumulation and distribution of PS in cells, the ability to generate reactive species (yield of singlet oxygen or oxygen radicals) should be evaluated.

We suppose that the increased affinity of **1** for HSA leads to a high yield of active oxygen species during photoactivation. These are the key metabolites for the processes of photodamage to biomacromolecules. The non-covalent **1**-HSA complex can act as a light-activated oxidoreductase and repeatedly catalyze electron transfer from a PS molecule in the triplet state to molecular O<sub>2</sub>, boosting the formation of active oxygen species. The mechanism according to which PS in the excited triplet state can directly interact with a substrate and/or solvent through electron or proton transfer, was described previously [2].

The high photoactivity of **1** and **2** results in necrosis of tumor cells – primary damage to the cell membrane. Photo necrosis was detected in the first few minutes of exposure to light and accompanied by pronounced and irreversible damage to cell structures. Such a damage was identified in the cytoplasm, whereas the nucleus retained its structure. A similar photo necrosis pattern was observed upon activation of the membrane-active boronated chlorin derivative e<sub>8</sub> [5]. These features differentiate **1** and **2** from other PSs that cause photo-induced cell death through other mechanisms (apoptosis and autophagy) [31–34]. We believe that rapid death of tumor cells as a result of PDT is desirable in clinical

situations, especially in order to eliminate tumors with primary or acquired drug resistance. However, it is necessary to assess the significance of possible immunological reactions in response to necrosis-inducing PDT.

In this work, the necessity to optimize long wavelength (infrared) PSs for PDT is demonstrated. The optimization criteria includes increased affinity to the transport protein HSA and the ability to provoke photo necrosis. Indeed, the chemical modification of bacteriopurpurinimide enables the production of a compound with increased affinity for HSA and the ability to cause irreversible photodamage to tumor cells. These features, as well as the lack of dark cytotoxicity and sufficient solubility in aqueous media (at least in the range of concentrations required to induce photo necrosis), make new bacteriopurpurine derivatives promising for further research. ●

*G.N. Rychkov acknowledge the Committee on Science and Higher Education of the Administration of St. Petersburg for support.*

*This work was supported by the Russian Foundation for Basic Research (grant №11-03-00620) and the Federal Target Program “Research and Development in Priority Areas of Scientific and Technological Complex of Russia for 2007–2013” (state contract № 14.512.11.0016).*

## REFERENCES

- Phillips D. // *Int. Rev. J.* 1997. V. 22, № 3/4. P. 3–50.
- Ashur I., Goldschmidt R., Pinkas I., Salomon I., Szewczyk G., Sarna T., Scherz A. // *J. Phys. Chem. A.* 2009. V.113. P. 8027–8037.
- Josefsen L.B., Boyle R.W. // *Theranostics.* 2012. V. 3, № 9. P. 916–966.
- Chen Y., Li G., Pandey R.K. // *Curr. Org. Chem.* 2004. № 8. P. 1105–1134.
- Moisenovich M.M., Ol’shevskaya V.A., Rokitskaya T.I., Ramonova A.A., Nikitina R.G., Savchenko A.N., Tatarskiy V.V., Kaplan M.A., Kalinin V.N., Kotova E.A., et al. // *PLoS ONE.* 2010. V. 5, № 9. P. e12717.
- Grin M.A., Mironov A.F., Shtil A.A. // *Anti-Cancer Agents Med. Chem.* 2008. V. 8. № 6. P. 683–697.
- Oertel M.I., Schastak S.I., Tannapfel A., Hermann R., Tannapfel A., Hermann R., Sack U., Mossner J., Berr F. // *J. Photochem. Photobiol. B: Biology.* 2003. V. 71. P. 1–10.
- Dąbrowski J.M., Arnaut L.G., Pereira M.M., Urbańska K., Simões S., Stochel G., Cortes L. // *Free Rad. Biol. Med.* 2012. V. 52. P. 1188–1200.
- Meerovich I.G., Grin M.A., Tsiprovskiy A.G., Meerovich G.A., Oborotova N.A., Loschenov V.B., Baryshnikov A.Y., Mironov A.F. // *Russian Biotherapeutic J.* 2007. V. 6. № 1. P. 22.
- Ol’shevskaya V.A., Nikitina R.G., Guiul’malieva M.A., Zaitsev A.V., Luzgina V.N., Kononova E.G., Ivanov O.G., Burmistrova N.V., Kaplan M.F., Kalinin V.N., et. al. // *Org. Biomol. Chem.* 2006. V. 4. P. 3815–3821.
- Ol’shevskaya V.A., Nikitina R.G., Savchenko A.N., Malshakova M.V., Vinogradov A.M., Golovina G.V., Belykh D. V., Kutchin A.V., Kaplan M.A., Kalinin V.N., et. al. // *Bioorg. Med. Chem.* 2009. V. 17. № 3. P. 1297–1306.
- Ol’shevskaya V.A., Savchenko A.N., Zaitsev A. V., Kononova E. G., Petrovskii P.V., Ramonova A.A., Tatarskiy V.V. Jr., Moisenovich M.M., Kalinin V.N., Shtil A.A. // *J. Organometal. Chem.* 2009. V. 694. № 11. P. 1632–1637.
- Pshenkina N.N. // *Med. Academ. J.* 2011. V. 11. № 3. P. 3–15.
- Sharman W.M., van Lier J.E., Allen C.M. // *Adv. Drug Delivery Rev.* 2004. V. 56. P. 53–76.
- Tsuchida T., Zheng G., Pandey R.K., Potter W.R., Bellnier D.A., Henderson B.W., Kato H., Dougherty T.J. // *Photochem. Photobiol.* 1997. V. 66. № 2. P. 224–228.
- Mironov A.F., Grin M.A., Tsiprovskiy A.G., Meerovich G.A., Meerovich I.G., Oborotova N.A., Treshalina E.M., Loschenov V.B., Baryshnikov A.Y., Tsiganov A.A. // *Patent of Russia № 2411943. Bull. № 29.* 2011.
- Mironov A.F., Grin M.A., Tsiprovskiy A.G. // *J. Porph. Phthalocyan.* 2002. V. 6. N. 5. P. 358–361.
- Benesi H.A., Hildebrandt J.H. // *J. Am. Chem. Soc.* 1949. V. 71. P. 2703–2707.
- Abagyan R., Totrov M., Kuznetsov D. // *J. Comput. Chem.* 1994. V. 15. P. 488–506.

## RESEARCH ARTICLES

20. Hanwell M.D., Curtis D.E., Lonie D.C., Vandermeersch T., Zurek E., Hutchison G.R. // *J. Chem. Inform.* 2012. V. 4. № 1. P. 17.
21. Schmidt M.W., Baldrige K.K., Boatz J.A., Elbert S.T., Gordon M.S., Jensen J.H., Koseki S., Matsunaga N., Nguyen K.A., Su S., Windus T.L., Dupuis M., Montgomery J.A. // *J. Comput. Chem.* 1993. V. 14. № 11. P. 1347–1363.
22. Huzinaga S., Andzelm J., Klobukowski M., Radzio-Andzelm E., Sakai Y., Tatewaki H. *Gaussian Basis Sets for Molecular Calculations* // Amsterdam: Elsevier, 1984, 240 P.
23. Roothaan C.C.J. // *Rev. Modern Phys.* 1951. V. 23. № 2. P. 69.
24. Wardell M., Wang Z., Ho J.X., Robert J., Ruker F., Ruble J., Carter D.C. // *Biochem. Biophys. Res. Commun.* 2002. V. 291. № 4. P. 813–819.
25. Fernández-Recio J., Totrov M., Abagyan R. // *Proteins: Structure, Function, and Bioinformatics.* 2003. V. 52. № 1. P. 113–117.
26. Totrov M. and Abagyan R. // *Proteins.* 1997. Suppl 1. P. 215–220.
27. Totrov M. and Abagyan R. // *Peptide Sci.* 2001. V. 60. № 2. P. 124–133.
28. Eisfeld A., Briggs J.S. // *Chem. Phys.* 2006. № 324. P. 376–384.
29. Yao-Bing Y., Wang Y.-N., Ma J.-B. // *Spectrochim. Acta Part A.* 2006. V. 64. P. 1032–1038.
30. Ascenzi P. and Fasano M. // *IUBMB Life.* 2009. V. 61. № 12. P. 1118–1122.
31. Garg A.D., Bose M., Ahmed M.I., Bonass W.A., Wood S.R. // *PLoS ONE.* 2012. V. 7. № 4. P. e34475.
32. Chin W.W., Heng P.W., Bhuvanewari R., Lau W.K., Olivo M. // *Photochem. Photobiol. Sci.* 2006. № 5. P. 1031–1037.
33. Calin M.A., Paraska S.V. // *J. Optoelectron. Adv. Mat.* 2006. V. 8. № 3. P. 1173–1179.
34. Evans C.L., Abu-Yousif Adnan O., Jin P. Yong, Klein O.J., Celli J.P., Rizvi I., Zheng X., Hasan T. // *PLoS ONE.* 2011. V. 6. № 8. P. e23434.

# Recombinant $\alpha$ -N-Acetylgalactosaminidase from Marine Bacterium-Modifying A Erythrocyte Antigens

L. A. Balabanova<sup>1,2\*</sup>, V. A. Golotin<sup>1</sup>, I. Y. Bakunina<sup>1</sup>, L. V. Slepchenko<sup>1</sup>, V. V. Isakov<sup>1</sup>, A. B. Podvolotskaya<sup>2</sup>, V. A. Rasskazov<sup>1</sup>

<sup>1</sup>G.B. Elyakov Pacific Institute of Bioorganic Chemistry, Far Eastern Branch, Russian Academy of Sciences, 100-letiya Vladivostoka Ave., 159, 690022, Vladivostok, Russia

<sup>2</sup>Far Eastern Federal University, Sukhanova Str., 8, 690950, Vladivostok, Russia

\*E-mail: balaban@piboc.dvo.ru

Received 14.11.2014

Copyright © 2015 Park-media, Ltd. This is an open access article distributed under the Creative Commons Attribution License, which permits unrestricted use, distribution, and reproduction in any medium, provided the original work is properly cited.

**ABSTRACT** A plasmid based on pET-40b was constructed to synthesize recombinant  $\alpha$ -N-acetylgalactosaminidase of the marine bacterium *Arenibacter latericius* KMM 426<sup>T</sup> ( $\alpha$ -AlNaGal) in *Escherichia coli* cells. The yield of  $\alpha$ -AlNaGal attains 10 mg/ml with activity of  $49.7 \pm 1.3$  U at 16°C, concentration of inducer 2 mM, and cultivation for 12 h. Techniques such as anion exchange, metal affinity and gel filtration chromatography to purify  $\alpha$ -AlNaGal were applied.  $\alpha$ -AlNaGal is a homodimer with a molecular weight of 164 kDa. This enzyme is stable at up to 50°C with a temperature range optimum activity of 20–37°C. Furthermore, its activity is independent of the presence of metal ions in the incubation medium. <sup>1</sup>H NMR spectroscopy revealed that  $\alpha$ -AlNaGal catalyzes the hydrolysis of the O-glycosidic bond with retention of anomeric stereochemistry and possesses a mechanism of action identical to that of other glycoside hydrolases of the 109 family.  $\alpha$ -AlNaGal reduces the serological activity of A erythrocytes at pH 7.3. This property of  $\alpha$ -AlNaGal can potentially be used for enzymatic conversion of A and AB erythrocytes to blood group O erythrocytes.

**KEYWORDS** glycoside hydrolase GH109; *Arenibacter latericius*; <sup>1</sup>H NMR spectroscopy; conversion of A erythrocytes.

## INTRODUCTION

$\alpha$ -N-Acetylgalactosaminidases (EC 3.2.1.49) catalyze the removal of 2-acetamido-2-deoxy-D-glucopyranosyl residues bound via the  $\alpha$ -O-glycosidic bond (GalNAc $\alpha$ ) from the non-reducing ends of oligosaccharides and glycoconjugates: in particular agglutinogens of the human blood groups A and AB.  $\alpha$ -N-Acetylgalactosaminidases can be used to study the structure of natural compounds and synthesize new oligosaccharides [1]. The study of  $\alpha$ -N-acetylgalactosaminidases is also associated with their involvement in the catabolism of complex oligosaccharides in the human body [2]. The practical interest in the enzyme has stemmed from the fact that it can potentially be used for enzymatic conversion of the blood groups A and AB to the universal blood group O via deglycosylation of antigenic determinants [3]. For this purpose, glycoside hydrolases of family 27 (GH27) from chicken liver and family 36 (GH36) from *Clostridium perfringens* bacterium were isolated [4, 5]. These enzymes have a number of disadvantages for biotechnological application, such as an

unphysiological pH optimum and inefficiency in converting erythrocytes of subtype A<sub>1</sub>.

$\alpha$ -N-Acetylgalactosaminidase of *Arenibacter latericius* KMM 426<sup>T</sup>, which effectively inactivates the serological activity of the A<sub>1</sub> and A<sub>2</sub> antigens of erythrocytes at neutral pH, was discovered by screening 3,000 strains of marine bacteria [6, 7]. Based on the classification of structural homology,  $\alpha$ -N-acetylgalactosaminidase of *Arenibacter latericius* KMM 426<sup>T</sup> is classified as belonging to the glycoside hydrolase family 109 (GH109) [8, 9].

A method for synthesizing recombinant  $\alpha$ -N-acetylgalactosaminidase ( $\alpha$ -AlNaGal) to study its enzymatic properties is suggested in this work.

The nucleotide sequence of the  $\alpha$ -AlNaGal gene was amplified from the genomic DNA of marine bacterium *A. latericius* type strain KMM 426<sup>T</sup> using primers: Nac40\_NcoF (5'-TTAACCATGGAAAATCTTTAT-TTTCAGGGTGGGGCTAAGTACATGGGCG-GTTTTTCTGCT-3') and Nac40\_SalIR (5'-TTAAGTCGACACCCTGAAAATAAAGATTTTCGCTTA-

CAATATCTAATGGTGCAGTGTT-3') (Eurogene). PCR amplification was performed in an Eppendorf amplifier using the following program: 95°C for 2 min and 35 cycles of 95°C for 15 s, 72°C for 1 min. The  $\alpha$ -A/NaGal gene was cloned into vector pET-40b(+) (Novagen) at the NcoI–SalI restriction sites after the DsbC sequence and His-tag. Recombinant plasmids were obtained in *Escherichia coli* DH5 $\alpha$  cells. The  $\alpha$ -A/NaGal-producing strain was obtained by transformation of plasmid into *E. coli* Rosetta(DE3). An overnight culture of the producing strain was grown in a 1-l flask with a liquid LB medium (pH 7.7) containing 25 mg/ml of kanamycin at 37°C and shaking at 200 rpm. When the culture reached the OD<sub>600</sub> of 0.6–0.8, it was induced with 0.2 mM isopropyl- $\beta$ -D-1-thiogalactopyranoside (IPTG) and incubated at 16°C for 12 h.

Activity of  $\alpha$ -A/NaGal was determined according to the cleavage of *p*-nitrophenyl- $\alpha$ -N-acetylgalactosaminide. The reaction mixture (400  $\mu$ l) contained 10 mM NaH<sub>2</sub>PO<sub>4</sub>, pH 7.2, 3 mM substrate, and the enzyme. After 20 min of incubation at 20°C, the reaction was terminated by adding 0.6 ml of 1-M Na<sub>2</sub>CO<sub>3</sub>. Absorbance at 400 nm was used to calculate the amount of the released product. One unit of activity (U) was defined as the amount of enzyme catalyzing the formation of 1  $\mu$ M of *p*-nitrophenol per minute. Specific activity was estimated as units of enzyme activity per milligram of the protein. Protein concentration was determined according to the Bradford method. The yield of the total enzyme activity was 49.7  $\pm$  1.3 U per 1 l of culture broth.

Purification of  $\alpha$ -A/NaGal was carried out at +6°C. *E. coli* cells were centrifuged at 5,000 rpm for 10 min, re-suspended in 200  $\mu$ l of buffer A (0.01 M NaH<sub>2</sub>PO<sub>4</sub>, pH 7.8, 0.01% NaN<sub>3</sub>), and sonicated using a UZDN 2-T ultrasonic disperser (USSR). The solution was centrifuged (25 min, 11,000 rpm) and added to the column (2.5  $\times$  37 cm) containing a DEAE-MacroPrep ion exchange resin (Bio-Rad) equilibrated with buffer A. Elution was performed with a linear gradient of 0–0.25 M NaCl in buffer A. The active fractions were collected and loaded onto a column (1  $\times$  2 cm) with Ni-agarose (Qiagen). The protein was eluted using 50 mM EDTA. The eluate was loaded onto a Sephacryl S-200HR (Sigma) gel filtration column equilibrated with buffer A. Homogeneity of  $\alpha$ -A/NaGal was confirmed using a 12% polyacrylamide gel in the presence of sodium dodecyl sulfate (SDS-PAGE) (Fig. 1). The results of gel filtration revealed that  $\alpha$ -A/NaGal is a homodimer with a molecular weight of 164 kDa (96 kDa after DsbC plasmid sequence at the site of enterokinase (Novagen) had been removed). The enzyme is stable at up to 50°C with a temperature range of optimum activity of 20–37°C, while its activity is independent of the

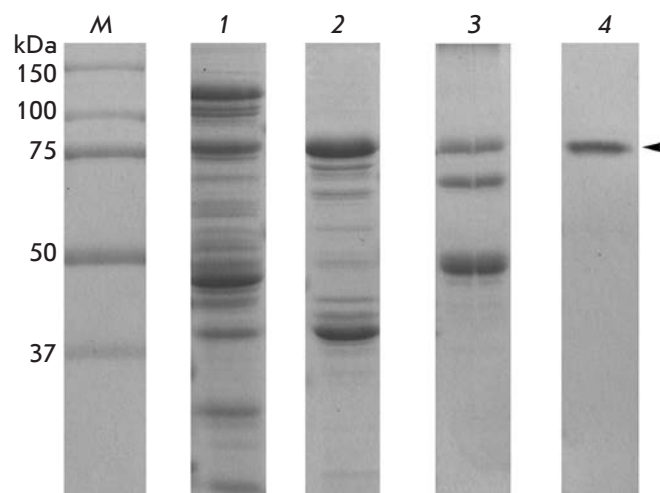


**Fig. 1.** The expression and purification of  $\alpha$ -A/NaGal (12% SDS-PAGE): **M** – protein molecular weight marker (Bio-Rad); **1** – whole-cell extract; **2** – DEAE-MacroPrep; **3** – Ni-agarose; **4** – Sephacryl S-200HR. Migration of  $\alpha$ -A/NaGal is marked with an arrow

presence of metal ions in the incubation medium. The additional amino acid residues have no influence on the enzymatic properties; therefore, their removal can be neglected. The optimum pH was determined in 20 mM Na<sup>+</sup>-phosphate and glycine-NaOH buffers at intervals of pH 5.4–8.2 and 8.0–10.0 (Fig. 2A). The study of the  $\alpha$ -A/NaGal properties revealed a possibility of usage to deglycosylate blood group A erythrocyte determinants (blood transfusion station, Vladivostok) at neutral pH. Blood group A erythrocytes were washed with a normal saline solution and then diluted with a Na<sup>+</sup>-phosphate isotonic buffer to a final concentration of 20%. 0.02 ml of the obtained suspension was mixed with 0.08 ml of the  $\alpha$ -A/NaGal solution (0.004 U) in the same buffer. After 24 h of incubation at 26°C, erythrocytes were washed three times using the same buffer (pH 7.3) with gentle shaking. A 1% suspension was prepared and then mixed with an anti-A serum (Mediclone, Russia) in a series of double-dilution steps in 96-well plates (Costar). After 1 h of incubation at room temperature, agglutination titer was measured (Fig. 2B). The results of an immunological analysis showed that the serological activity of A antigens of erythrocytes treated with  $\alpha$ -A/NaGal decreases as a result of their enzymatic transformation to H antigens, because no agglutination was observed up to a titer of 1/16.  $\alpha$ -A/NaGal causes neither nonspecific aggregation of erythrocytes nor their hemolysis.

The enzyme of marine bacterium *Arenibacter latericus* type strain KMM 426<sup>T</sup> can fully inactivate the se-

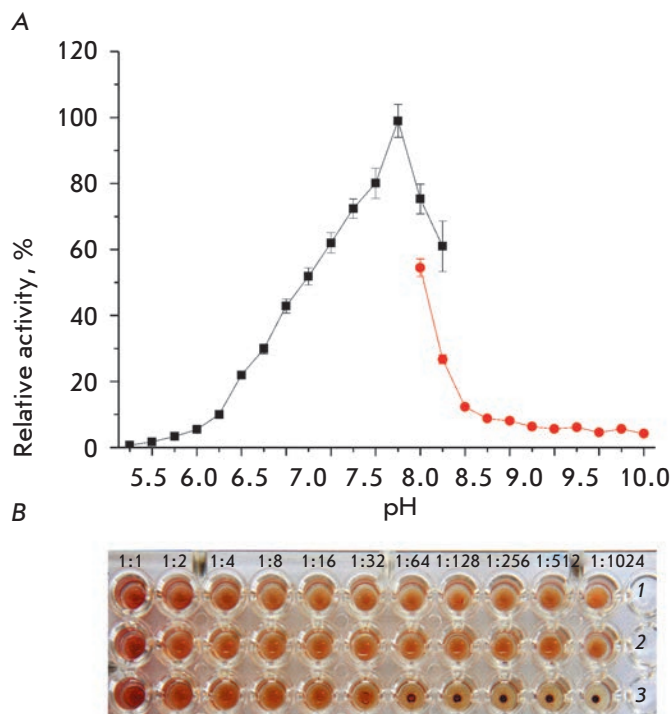


**Fig. 2.** Enzymatic properties of  $\alpha$ -A/NaGal: **A** – optimum pH of  $\alpha$ -A/NaGal; **B** – 1% suspension of A erythrocytes mixed with anti-A serum in a series of double-dilution steps in: **1** – 20 mM  $\text{Na}^+$ -phosphate buffer, **2** – 20 mM glycine-NaOH buffer, **3** – 20 mM  $\text{Na}^+$ -phosphate buffer after treatment with  $\alpha$ -A/NaGal

rological activity of A erythrocytes at neutral pH and compares favorably with  $\alpha$ -N-acetylgalactosaminidases from chicken liver and *C. perfringens*, which affect only the  $A_2$  subgroup of erythrocytes [5, 6]. Being classical hydrolases, the GH27 and GH36 enzymes catalyze the hydrolysis of the O-glycosidic bond of their substrate via the double displacement mechanism with retention of the stereochemistry of the anomeric center of the substrate [10]. More recently, an enzyme of a new GH109 family has been isolated from pathogenic bacterium *Elizabethkingia meningoseptica*. This enzyme had properties similar to those of  $\alpha$ -N-acetylgalactosaminidase of the *A. latericius* type strain KMM 426<sup>T</sup> and a different mechanism of hydrolysis of the classical hydrolases [8]. The mechanism includes stages of elimination of the O-glycosidic bond and proton exchange at C2 of N-acetylgalactosamine with retention of anomeric stereochemistry.

The configuration of the anomeric center of the hydrolysis products of  $\alpha$ -A/NaGal was directly examined using  $^1\text{H}$  NMR spectroscopy. The experiment was carried out at 20°C using a DRX-500 NMR spectrometer

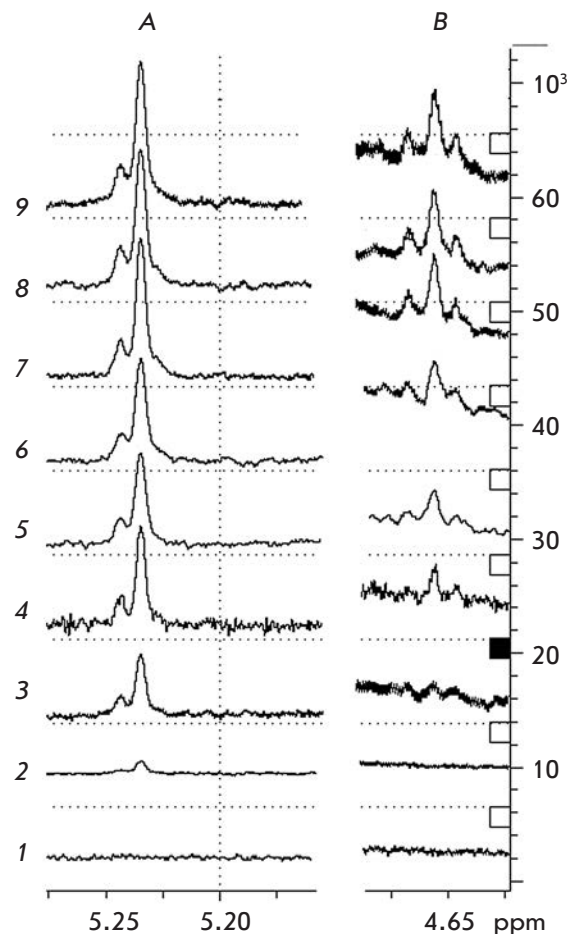


**Fig. 3.** The resonance regions  $\Delta\delta=5.30\text{--}5.20$  ppm (**A**) and  $\Delta\delta=4.75\text{--}4.10$  ppm (**B**) of  $^1\text{H}$  NMR spectrum of  $\alpha$ - and  $\beta$ -anomeric atoms of N-acetylgalactosamine as a product of  $\alpha$ -A/NaGal hydrolysis for 0 min (1), 10 min (2), 20 min (3), 30 min (4), 40 min (5), 50 min (6), 80 min (7), 90 min (8), 100 min (9)

(Bruker).  $^1\text{H}$  NMR spectra were acquired using a spectral width of 5,000 Hz over 32,000 data points. Prior to the analysis, 0.6 ml of a 50 mM  $\text{Na}^+$ -phosphate solution (pH 7.5) containing 6.0 mM *p*-nitrophenyl- $\alpha$ -N-acetylgalactosaminide substrate was evaporated and dissolved in 0.6 ml of  $\text{D}_2\text{O}$ . The deuterium-exchanged  $\alpha$ -A/NaGal was obtained using Vivaspin turbo 10 k MWCO columns (Sartorius). Chemical shifts in spectra were referenced to acetone ( $\delta = 2.22$  ppm) in  $\text{D}_2\text{O}$  used as an external standard. After measuring the initial spectra of the substrate at  $t = 0$  min, 0.1 ml of the deuterium-exchanged  $\alpha$ -A/NaGal, containing 0.98 U, was added to 6.0 mM of the deuterium-exchanged *p*-nitrophenyl- $\alpha$ -N-acetylgalactosaminide in 0.6 ml  $\text{D}_2\text{O}$  to initiate the reaction. The  $^1\text{H}$  NMR spectra were

automatically recorded at 10 min intervals for 180 min after the onset of the reaction. *Figure 3* shows the resonance regions  $\Delta\delta=5.30\text{--}5.20$  ppm and  $\Delta\delta=4.75\text{--}4.10$  ppm of the  $^1\text{H}$  NMR spectrum of the reaction products. The product, with a resonance signal at 5.22 ppm, is formed during the first minutes after enzyme addition (*Fig. 3A*). This signal corresponds to the proton of the anomeric center of unbound N-acetylgalactosamine (GalNAc $\alpha$ ). Signal intensity increases during the following 10 min of the reaction. The signal of the  $\beta$ -anomer of GalNAc $\alpha$  with the chemical shift at 4.64 ppm as a result of mutarotation appears only after 20 min of the reaction's onset (*Fig. 3B*). The spectra of  $\alpha$ - and  $\beta$ -anomers of unbound GalNAc $\alpha$  show that the signals are observed as doublets with SSCC of 3.8 and 7.8 Hz, and a singlet. These observations indicate that proton–deuterium substitution takes place at C2. Such a catalytic mechanism is typical of glycoside hydrolases GH109 [8, 11].

## CONCLUSIONS

The recombinant protein  $\alpha$ -AlNaGal with a molecular weight of 164 kDa, with the properties of  $\alpha$ -N-acetylgalactosaminidase of marine bacterium *A. latericius* type strain KMM 426<sup>T</sup>, was synthesized.  $\alpha$ -AlNaGal catalyzes the hydrolysis of the  $\alpha$ -O-glycosidic bond with retention of the stereochemistry of the anomeric center of the substrate and proton exchange to deuterium of the solvent at C2 via a mechanism typical of glycoside hydrolases of the GH109 family.  $\alpha$ -AlNaGal deglycosylates A antigens of the blood at pH 7.5. This property demonstrates that  $\alpha$ -AlNaGal can be used to obtain blood group O erythrocytes. ●

*This work was supported  
by the Russian Foundation for Basic  
Research (grant № 13-04-00806) and the Scientific  
Foundation of the Far Eastern Federal University  
(14-08-06-10\_i).*

## REFERENCES

- Vallée F., Karaveg K., Herscovics A., Moremen K.W., Howell P.L. // *J. Biol. Chem.* 2000. V. 275. № 52. P. 41287–41298.
- Keulemans J.L.M., Reuser A.J.J., Kroos M.A., Willemsen R., Hermans M.M.P., van den Ouweland A.M.W., de Jong J.G.N., Wevers R.A., Renier W.O., Schindler D., et al. // *J. Med. Genet.* 1996. V. 33. № 6. P. 458–464.
- Olsson M.L., Hill C.A., de laVega H., Liu Q.P., Stroud M.R., Valdinocci J., Moon S., Clausen H., Kruskall M.S. // *Transfus. Clin. Biol.* 2004. V. 11. № 1. P. 33–39.
- Hata J., Dhar M., Mitra M., Harmata M., Haibach P., Sun P., Smith D. // *Biochem. Int.* 1992. V. 28. № 1. P. 77–86.
- Hsieh H.Y., Smith D. // *Biotechnol. Appl. Biochem.* 2003. V. 37. № 2. P. 157–163.
- Ivanova E.P., Bakunina I.Y., Nedashkovskaya O.I., Gorshkova N.M., Mikhailov V.V., Elyakova L.A. // *Marine Biology* (Russian). 1998. V. 24. № 6. P. 351–358.
- Bakunina I.Y., Kulman R.A., Likhosherstov L.M., Martynova M.D., Nedashkovskaya O.I., Mikhailov V.V., Elyakova L.A. // *Biochemistry* (Russian). 2002. V. 67. № 6. P. 830–837.
- Liu Q.P., Sulzenbacher G., Yuan H., Bennett E.P., Pietz G., Saunders K., Spence J., Nudelman E., Levery S.B., White T., et al. // *Nat. Biotechnol.* 2007. V. 25. № 4. P. 454–464.
- Bakunina I., Nedashkovskaya O., Balabanova L., Zvyagintseva T., Rasskazov V., Mikhailov V. // *Mar. Drugs.* 2013. V. 11. P. 1977–1998.
- Comfort D.A., Bobrov K.S., Ivanen D.R., Shabalin K.A., Harris J.M., Kulminskaya A.A., Brumer H., Kelly R.M. // *Biochemistry.* 2007. V. 46. № 11. P. 3319–3330.
- Chakladar S., Abadib S.S.K., Bennet A.J. // *Med. Chem. Commun.* 2014. V. 5. P. 1188.

## GENERAL RULES

*Acta Naturae* publishes experimental articles and reviews, as well as articles on topical issues, short reviews, and reports on the subjects of basic and applied life sciences and biotechnology.

The journal is published by the Park Media publishing house in both Russian and English.

The journal *Acta Naturae* is on the list of the leading periodicals of the Higher Attestation Commission of the Russian Ministry of Education and Science

The editors of *Acta Naturae* ask of the authors that they follow certain guidelines listed below. Articles which fail to conform to these guidelines will be rejected without review. The editors will not consider articles whose results have already been published or are being considered by other publications.

The maximum length of a review, together with tables and references, cannot exceed 60,000 symbols (approximately 40 pages, A4 format, 1.5 spacing, Times New Roman font, size 12) and cannot contain more than 16 figures.

Experimental articles should not exceed 30,000 symbols (20 pages in A4 format, including tables and references). They should contain no more than ten figures. Lengthier articles can only be accepted with the preliminary consent of the editors.

A short report must include the study's rationale, experimental material, and conclusions. A short report should not exceed 12,000 symbols (8 pages in A4 format including no more than 12 references). It should contain no more than four figures.

The manuscript should be sent to the editors in electronic form: the text should be in Windows Microsoft Word 2003 format, and the figures should be in TIFF format with each image in a separate file. In a separate file there should be a translation in English of: the article's title, the names and initials of the authors, the full name of the scientific organization and its departmental affiliation, the abstract, the references, and figure captions.

## MANUSCRIPT FORMATTING

The manuscript should be formatted in the following manner:

- Article title. Bold font. The title should not be too long or too short and must be informative. The title should not exceed 100 characters. It should reflect the major result, the essence, and uniqueness of the work, names and initials of the authors.
- The corresponding author, who will also be working with the proofs, should be marked with a footnote \*.
- Full name of the scientific organization and its departmental affiliation. If there are two or more scientific organizations involved, they should be linked by digital superscripts with the authors' names. Abstract. The structure of the abstract should be very clear and must reflect the following: it should introduce the reader to the main issue and describe the experimental approach, the possibility of practical use, and the possibility of further research in the field. The average length of an abstract is 20 lines

(1,500 characters).

- Keywords (3 – 6). These should include the field of research, methods, experimental subject, and the specifics of the work. List of abbreviations.

- INTRODUCTION
- EXPERIMENTAL PROCEDURES
- RESULTS AND DISCUSSION
- CONCLUSION

The organizations that funded the work should be listed at the end of this section with grant numbers in parenthesis.

- REFERENCES

The in-text references should be in brackets, such as [1].

## RECOMMENDATIONS ON THE TYPING AND FORMATTING OF THE TEXT

- We recommend the use of Microsoft Word 2003 for Windows text editing software.
- The Times New Roman font should be used. Standard font size is 12.
- The space between the lines is 1.5.
- Using more than one whole space between words is not recommended.
- We do not accept articles with automatic referencing; automatic word hyphenation; or automatic prohibition of hyphenation, listing, automatic indentation, etc.
- We recommend that tables be created using Word software options (Table → Insert Table) or MS Excel. Tables that were created manually (using lots of spaces without boxes) cannot be accepted.
- Initials and last names should always be separated by a whole space; for example, A. A. Ivanov.
- Throughout the text, all dates should appear in the “day.month.year” format, for example 02.05.1991, 26.12.1874, etc.
- There should be no periods after the title of the article, the authors' names, headings and subheadings, figure captions, units (s – second, g – gram, min – minute, h – hour, d – day, deg – degree).
- Periods should be used after footnotes (including those in tables), table comments, abstracts, and abbreviations (mon. – months, y. – years, m. temp. – melting temperature); however, they should not be used in subscripted indexes ( $T_m$  – melting temperature;  $T_{p.t}$  – temperature of phase transition). One exception is mln – million, which should be used without a period.
- Decimal numbers should always contain a period and not a comma (0.25 and not 0,25).
- The hyphen (“-”) is surrounded by two whole spaces, while the “minus,” “interval,” or “chemical bond” symbols do not require a space.
- The only symbol used for multiplication is “×”; the “×” symbol can only be used if it has a number to its right. The “·” symbol is used for denoting complex compounds in chemical formulas and also noncovalent complexes (such as DNA·RNA, etc.).
- Formulas must use the letter of the Latin and Greek alphabets.

# GUIDELINES FOR AUTHORS

- Latin genera and species' names should be in italics, while the taxa of higher orders should be in regular font.
- Gene names (except for yeast genes) should be italicized, while names of proteins should be in regular font.
- Names of nucleotides (A, T, G, C, U), amino acids (Arg, Ile, Val, etc.), and phosphonucleotides (ATP, AMP, etc.) should be written with Latin letters in regular font.
- Numeration of bases in nucleic acids and amino acid residues should not be hyphenated (T34, Ala89).
- When choosing units of measurement, SI units are to be used.
- Molecular mass should be in Daltons (Da, KDa, MDa).
- The number of nucleotide pairs should be abbreviated (bp, kbp).
- The number of amino acids should be abbreviated to aa.
- Biochemical terms, such as the names of enzymes, should conform to IUPAC standards.
- The number of term and name abbreviations in the text should be kept to a minimum.
- Repeating the same data in the text, tables, and graphs is not allowed.

## GUIDENESS FOR ILLUSTRATIONS

- Figures should be supplied in separate files. Only TIFF is accepted.
- Figures should have a resolution of no less than 300 dpi for color and half-tone images and no less than 500 dpi.
- Files should not have any additional layers.

## REVIEW AND PREPARATION OF THE MANUSCRIPT FOR PRINT AND PUBLICATION

Articles are published on a first-come, first-served basis. The publication order is established by the date of acceptance of the article. The members of the editorial board have the right to recommend the expedited publishing of articles which are deemed to be a priority and have received good reviews.

Articles which have been received by the editorial board are assessed by the board members and then sent for external review, if needed. The choice of reviewers is up to the editorial board. The manuscript is sent on to reviewers who are experts in this field of research, and the editorial board makes its decisions based on the reviews of these experts. The article may be accepted as is, sent back for improvements, or rejected.

The editorial board can decide to reject an article if it does not conform to the guidelines set above.

A manuscript which has been sent back to the authors for improvements requested by the editors and/or reviewers is reviewed again, after which the editorial board makes another decision on whether the article can be accepted for publication. The published article has the submission and publication acceptance dates set at the beginning.

The return of an article to the authors for improve-

ment does not mean that the article has been accepted for publication. After the revised text has been received, a decision is made by the editorial board. The author must return the improved text, together with the original text and responses to all comments. The date of acceptance is the day on which the final version of the article was received by the publisher.

A revised manuscript must be sent back to the publisher a week after the authors have received the comments; if not, the article is considered a resubmission.

E-mail is used at all the stages of communication between the author, editors, publishers, and reviewers, so it is of vital importance that the authors monitor the address that they list in the article and inform the publisher of any changes in due time.

After the layout for the relevant issue of the journal is ready, the publisher sends out PDF files to the authors for a final review.

Changes other than simple corrections in the text, figures, or tables are not allowed at the final review stage. If this is necessary, the issue is resolved by the editorial board.

## FORMAT OF REFERENCES

The journal uses a numeric reference system, which means that references are denoted as numbers in the text (in brackets) which refer to the number in the reference list.

*For books:* the last name and initials of the author, full title of the book, location of publisher, publisher, year in which the work was published, and the volume or issue and the number of pages in the book.

*For periodicals:* the last name and initials of the author, title of the journal, year in which the work was published, volume, issue, first and last page of the article. Must specify the name of the first 10 authors. Ross M.T., Grafham D.V., Coffey A.J., Scherer S., McLay K., Muzny D., Platzer M., Howell G.R., Burrows C., Bird C.P., et al. // Nature. 2005. V. 434. № 7031. P. 325–337.

References to books which have Russian translations should be accompanied with references to the original material listing the required data.

References to doctoral thesis abstracts must include the last name and initials of the author, the title of the thesis, the location in which the work was performed, and the year of completion.

References to patents must include the last names and initials of the authors, the type of the patent document (the author's rights or patent), the patent number, the name of the country that issued the document, the international invention classification index, and the year of patent issue.

The list of references should be on a separate page. The tables should be on a separate page, and figure captions should also be on a separate page.

**The following e-mail addresses can be used to contact the editorial staff: vera.knorre@gmail.com, actanaturae@gmail.com, tel.: (495) 727-38-60, (495) 930-87-07**

# ActaNaturae

SUBSCRIPTION TO

*Acta Naturae* journal focuses upon interdisciplinary research and developments at the intersection of various spheres of biology, such as molecular biology, biochemistry, molecular genetics, and biological medicine.

*Acta Naturae* journal is published in Russian and English by Park Media company. It has been included in the list of scientific journals recommended by the State Commission for Academic Degrees and Titles of the Ministry of Education and Science of the Russian Federation and the Pubmed abstracts database.

## SUBSCRIBE AT THE EDITORIAL OFFICE

Leninskie Gory, 1-75G, Moscow, 119234 Russia  
Telephone: +7 (495) 930-87-07, 930-88-51  
Bio-mail: [podpiska@biorf.ru](mailto:podpiska@biorf.ru)  
Web site: [www.actanaturae.ru](http://www.actanaturae.ru)

## SUBSCRIBE USING THE CATALOGUES OR VIA THE INTERNET:

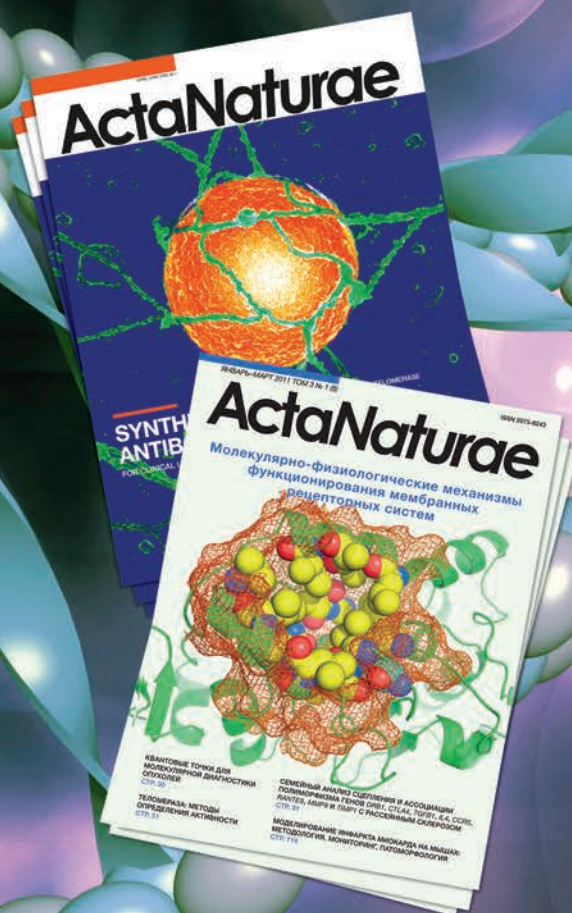
ROSPECHAT (The Russian Press)  
Indices: 37283, 59881  
[www.pressa.rosp.ru](http://www.pressa.rosp.ru)

INFORMNAUKA  
Index: 59881  
[www.informnauka.com](http://www.informnauka.com)

INTER-POCHTA  
17510  
[www.interpochta.ru](http://www.interpochta.ru)

### INFORMATION FOR AUTHORS:

If you would like to get your research paper published in *Acta Naturae* journal, please contact us at [journal@biorf.ru](mailto:journal@biorf.ru) or call +7 (495) 930-87-07.





# Russian NanoTechnologies journal turns 10 this year

Volume 9, Numbers 7–8  
July–August 2014

ISSN: 1995-0780

## NANOTECHNOLOGIES IN RUSSIA

English Translation of *Rossiiskie Nanotekhnologii*

Editor-in-Chief  
Mikhail V. Alfimov

<http://www.mnk.ru>  
<http://www.springerlink.com>



Distributed by Springer